KINETICS OF IRON CARBONATE AND IRON SULFIDE SCALE FORMATION IN CO_2/H_2S CORROSION

A dissertation presented to

the faculty of

the Russ College of Engineering and Technology of Ohio University

In partial fulfillment

of the requirements for the degree

Doctor of Philosophy

Wei Sun

November 2006

This dissertation entitled

KINETICS OF IRON CARBONATE AND IRON SULFIDE SCALE FORMATION IN CO_2/H_2S CORROSION

by

WEI SUN

has been approved for

the Department of Chemical and Biomolecular Engineering

and the Russ College of Engineering and Technology by

Srdjan Nesic

Professor of Chemical and Biomolecular Engineering

Dennis Irwin

Dean, Russ College of Engineering and Technology

Abstract

SUN, WEI, Ph.D., November 2006, Chemical and Biomolecular Engineering

KINETICS OF IRON CARBONATE AND IRON SULFIDE SCALE FORMATION IN CO_2/H_2S CORROSION (226 pp.)

Director of Dissertation: Srdjan Nesic

Kinetics of iron carbonate and iron sulfide scale formation in CO_2/H_2S corrosion was investigated by individually studying iron carbonate formation in pure CO_2 corrosion, iron sulfide formation in N_2/H_2S corrosion, and the mixed iron carbonate/sulfide formation in CO_2/H_2S corrosion.

The first part of the project was to investigate kinetics of iron carbonate scale formation in CO_2 corrosion. A unified iron carbonate solubility expression which accounts for both temperature and ionic strength effects was proposed based on the literature data. The weight change method was developed to more accurately define kinetics of scale formation in CO_2 corrosion and demonstrated that the old data from literature are one to two orders of magnitude too high. Based on the experimental data, a reliable iron carbonate formation equation was developed to describe iron carbonate scale growth on the steel surface in CO_2 corrosion.

The second part of the project was to investigate the mechanism and kinetics of iron sulfide formation in N_2/H_2S environment. The solubility limits of hydrogen sulfide and iron sulfides were clarified based on the literature data. Using weight change method, both the corrosion rate of the steel and the retention rate of the scale were found. It was also concluded that mackinawite is the predominant iron sulfide formed on the steel

surface under the test conditions studied, most likely by a direct reaction of H_2S with the underlying steel. Based on the experimental results, a mechanistic model of uniform H_2S corrosion of mild steel was presented that was able to predict corrosion rate with time.

Finally, kinetics experiments conducted in CO_2/H_2S solution proved that the makeup of the surface scale not only depends on the water chemistry and the respective solubility of iron carbonate and iron sulfide, but also on the competitiveness of the two scale formation mechanisms. Based on the experimental data it was found that mackinawite was the predominant scale formed on the steel surface which protected the steel from corroding in CO_2/H_2S corrosion. The mechanistic model for H_2S corrosion was extended to predict the CO_2/H_2S corrosion process by considering the effect of the presence of CO_2.

Approved:

Srdjan Nesic

Professor of Chemical and Biomolecular Engineering

Dedication

To

Qiwen Sun and Xiucui Sun (my parents)

and

Mingtao Wang (my husband)

Acknowledgements

I would like to express my sincere appreciation to my advisor Dr. Srdjan Nesic, who has never given up correcting the mistakes I made, has encouraged me to broaden my viewpoint, and taught me the important things in life. His patience and dedication to directing us students on the way to success, and his goal of providing a reliable research working environment encouraged me to keep going. Under his supervision, I grew professionally and he helped me prepare for the new challenges in my career. Having him as my PhD supervisor and my lifetime advisor is one of the luckiest things in my life. I wish that these words make at least a humble effort to convey my deep gratitude and earnest appreciation.

Great thanks go to my industry mentors, Dr. Yuhua Sun and Dr. Shihuai Wang, who were always very confident in me and gave me full support and direction both in my academic work and daily life.

I would like to acknowledge Mr. Bruce Brown, Mr. Al Schubert, Mr. John Goettge, and Mr. Danny Cain for their assistance in the technical work; and the former fellow coworkers, Dr. Kunlin John Lee for his support in coursework and research, and invaluable advice in general as well as Mr. Kunal Chokshi and Mr. Omkar Nafday for working closely with me in the first two years of my PhD. Mr. Jorge Alberch deserves a special mention, for jointly conducting a series of electrochemical experiments with me. Also, Dr. Jiyong Cai, Ms. Ying Xiao, and Mr. Marc Singer for providing a relaxed and friendly work environment.

I would also like to thank the faculty members, Dr. Valerie Young, Dr. Daniel Gulino, Dr. David Young, Dr. Kendree Sampson, Dr. Gerardine Botte, Dr. Tingyue Gu,

Dr. Michael Prudich, Dr. Howard Dewald, and Dr. Liwei Chen for providing me with invaluable advice; all the fellow students, visiting scholars, and Mrs. Edie Chalfant for creating such a wonderful working environment at the Institute; and my friends Ms. Rong Hu for her true friendship and Ms. Jane Penwell for her tremendous help with improving my English and understanding the American culture.

Great thanks also go to Dr. Richard Woollam, Dr. Sandra Hernandez, and Dr. Jose Vera at BP America, Houston, Dr. Oliver Moghissi and Ms. Conchita Mendez at CC Technologies, Dublin, and Dr. Sankara Papavinasam and other staff at CANMET Materials Technology Laboratory, Ottawa, for giving me great supervision and full support while I was doing internships in their affiliations. Special thanks again to Dr. Woollam for co-supervising me to finish the thermodynamics work in this project.

I am very grateful to my parents Qiwen Sun and Xiucui Sun, who have taught me to be optimistic, enjoy the beautiful things in life and see the best in people. I would like to express my deep indebtedness to my husband Mingtao Wang for his true love and support for over ten years since I left my parents home for studying. With his love surrounding me, I kept smiling.

Last but not least, I would like to acknowledge all the sponsoring companies for providing the financial support and technical directions; CANMET MTL, Natural Resources Canada, Ottawa, for providing the equipment and support for part of this project; Ohio University for awarding me the Donald Clippinger Fellowship and NACE International for granting me the NACE Foundation Student Academic Scholarship.

Table of Contents

List of Tables

Page

List of Figures

Page

Chapter 1: Introduction

The internal carbon dioxide corrosion of mild steel in the presence of hydrogen sulfide (CO_2/H_2S corrosion) represents a significant problem for both the oil and gas industries[1-5]. Although high cost corrosion resistance alloys (CRAs) were developed to be able to resist the CO_2/H_2S corrosion, mild steel is still the most cost effective material used in CO_2/H_2S corrosion[4]. The problems of CO_2/H_2S corrosion of mild steel were firstly recognized in the 1940's and have been investigated for over 60 years[5]. However, until now the research work in the literature is still confusing and sometime contradictory[5]. Therefore, it is very important to improve the prediction and control of the CO_2/H_2S corrosion of mild steel.

In CO_2/H_2S corrosion of mild steel, both iron carbonate and iron sulfide scale can form on the steel surface. Studies have demonstrated that surface scale formation is one of the important factors governing the corrosion rate[6-12]. The surface scale can slow down the corrosion process by presenting a diffusion barrier for the species involved in the corrosion process and by covering up a part of the steel surface and preventing the underlying steel from further dissolution. As more iron carbonate or iron sulfide form, the scale grows in density as well as thickness. The scale growth depends primarily on the kinetics of scale formation. Hence it is very important to study the kinetics of iron carbonate and iron sulfide scale formation in order to further predict and control the CO_2/H_2S corrosion of mild steel. The scale formation in CO_2/H_2S corrosion may not only depend on the water chemistry and the respective solubility of iron carbonate and iron sulfides, but also on the competitiveness of the two scale formation mechanisms. Therefore, it is necessary to

investigate this project by individually studying iron carbonate formation in pure CO_2 corrosion, iron sulfide formation in N_2/H_2S corrosion, and the mixed iron carbonate/sulfide formation in CO_2/H_2S corrosion.

Others have investigated iron carbonate scale formation in pure CO_2 corrosion[13-21]. It has been commonly accepted that solid iron carbonate scale precipitates on the steel surface, when the concentrations of Fe^{2+} and CO_3^{2-} ions in the CO_2 water solution exceed the solubility limit. Therefore, first of all, this research project investigated the thermodynamics of iron carbonate in CO_2 water solution based on the literature. In the literature, two different expressions were used to describe the kinetics of iron carbonate precipitation in pure CO_2 corrosion (proposed respectively by Johnson and Tomson[20] in 1991 and van Hunnik[21] et al. in 1996). In either case the rate of precipitation is a function of iron carbonate supersaturation, the solubility limit, temperature and surface area-to-volume ratio. In the present work, the weight change method was developed as a reliable method to conduct kinetics experiments, which were used to verify the two existing kinetics expressions.

In contrast to pure CO_2 corrosion where a single corrosion product – iron carbonate forms, many types of iron sulfides may form in H_2S environment, such as amorphous ferrous sulfide, mackinawite, cubic ferrous sulfide, smythite, greigite, pyrrhotite, troilite, and pyrite, among which mackinawite is considered to form first on the steel surface by a direct surface reaction[12, 22 - 26]. Similarly, as in the investigation of iron carbonate formation, it was necessary to study the thermodynamics of hydrogen sulfide and iron sulfides in order to obtain their solubility expressions and further to understand the mechanism and kinetics of iron sulfide formation. In the literature, two

different expressions were employed to identify the kinetics of iron sulfide precipitation in sodium sulfide solutions (proposed respectively by Rickard[27] in 1995 and Harmandas and Koutsoukos[28] in 1996). The expressions which apply to mackinawite are described as a function of Fe^{2+} concentration and sulfide species' concentration. However, the actual mechanism of iron sulfide formation in H_2S environment is still unclear and it is difficult to determine whether the iron sulfide is formed by direct solid state reaction or precipitation or both. Furthermore, no expressions were previously developed to quantify the kinetics of iron sulfide scale formation on the mild steel surface in H_2S environment. Therefore, the mechanism of H_2S corrosion as well as iron sulfide formation was investigated and a model of the overall corrosion process is proposed in this work.

Although a great deal of research effort has been directed toward CO_2/H_2S corrosion, as discussed in Smith and Joosten's review paper[5], the complex chemistry and mechanism of iron sulfides formation as well as the competitiveness of iron carbonate and iron sulfide formation make it very difficult to understand the CO_2/H_2S corrosion process and subsequently to improve the accuracy of the predictions of corrosion rate. Presently, there are no expressions in the literature to quantify the kinetics of mixed iron carbonate/sulfide scale formation in CO_2/H_2S solutions. Hence kinetics experiments in CO_2/H_2S corrosion were conducted and based on the kinetic experimental data as well as the kinetic models for iron carbonate formation in CO_2 corrosion and iron sulfide formation in H_2S environment, a mechanistic model for predicting the mixed iron carbonate/sulfide scale formation in CO_2/H_2S corrosion is proposed.

From the brief description presented above, it is clear that for an improved understanding of the properties of surface scales formed in CO_2/H_2S environments as

well as the impact on the corrosion rate, a better understanding of both thermodynamics and kinetics of iron carbonate and iron sulfide formation is needed. The present research work has not only improved the understanding of both iron carbonate and iron sulfide scale formation, but has also provided a mechanistic model to predict the corrosion rate of mild steel in CO_2/H_2S corrosion for the oil and gas industry.

It should be noted that parts of the work described below have been published in the internal confidential reports to Ohio University Advisory Board meetings over the period 2003 – 2006 [29-41]. In addition, excerpts from the work were or will be published at NACE (National Association of Corrosion Engineers) International conferences, 16th ICC (International Corrosion Congress), AIChE (American Institute of Chemical Engineers), and the ECS (Electrochemical Society) [19, 42- 48].

Chapter 2: Thermodynamic study of iron (II) carbonate at elevated temperatures in sodium chloride solution

2.1 Introduction

In CO_2 corrosion, when the concentrations of Fe^{2+} and CO_3^{2-} ions in aqueous solution exceed the solubility limit K_{sp} (or the solubility product constant), solid iron carbonate precipitates or deposits on the steel surface.

$$Fe^{2+}_{(aq)} + CO_3^{2-}{}_{(aq)} \rightarrow FeCO_{3(s)} \quad (1)$$

It is important to have a reliable estimate of the solubility limit in order to predict the deposition of iron carbonate on the steel surface. The thermodynamics of iron carbonate ($FeCO_3$), siderite, has been studied in various research fields, such as geology, oceanography, sedimentology, water treatment, and corrosion[49-58]. A number of research studies[49, 50, 53-68] have been dedicated to the investigation of iron carbonate solubility limit at different conditions. However, none of them developed an expression for the iron carbonate solubility limit that covers the wide range of conditions required in the corrosion area. Therefore, this chapter is aimed at developing a more general expression for iron carbonate solubility limit based on the literature data which would include the effect of both temperature and ionic strength.

2.2 Literature review

The rather large body of work on iron carbonate solubility limit previously reported is here divided in three groups:

1. solubility limit at room temperature and very low ionic strength,

2. temperature dependence, and
3. ionic strength dependence.

The solubility limit K_{sp} (in mol^2 / L^2) which is a function of both temperature and ionic strength can be obtained from the experimental results using the following expressions[67]:

$$K_{sp} = [Fe^{2+}][CO_3^{2-}] = f(T, I) \quad (2)$$

where $[Fe^{2+}]$ and $[CO_3^{2-}]$ are the concentrations of Fe^{2+} and CO_3^{2-} in the aqueous solution when iron carbonate reaches the solubility limit in mol / L.

The ionic strength is defined as[69]:

$$I = \frac{1}{2}\sum_i c_i z_i^2 = \frac{1}{2}\left(c_1 z_1^2 + c_2 z_2^2 + ...\right) \quad (3)$$

where c_i is the concentration of different species in the aqueous solutions in mol / L, and z_i is the species charge.

2.2.1 Solubility limit at room temperature and I=0

The iron carbonate solubility limit (in mol^2 / L^2) at room temperature and the assumed ionic strength I=0 is reported ranging from 3.72×10^{-11} to 9.33×10^{-12}, as shown in Figure 1. The results, provided by different researchers[49,53-61], were obtained by various experimental techniques, including precipitation of iron carbonate from supersaturated solutions, resuspension of wet crystals and resuspension of dry crystals. Theoretically the iron carbonate solubility limit should not be affected by the experimental method. However, Jensen *et al.*[53] reported that the iron carbonate solubility limit was 3.72×10^{-11} when using wet crystals and 9.33×10^{-12} for dried crystals. When a

broader comparison is made, it has been found that the other sources of uncertainty may lead to the experimental error. For example, at T 25°C and I=0, Smith[54] found that iron carbonate solubility limit is 1.29×10^{-11} and Ptacek and Reardon[55] reported the solubility limit of 1.17×10^{-11}, which is different from 3.72×10^{-11} reported by Jensen *et a.*, and all used the same method of wet crystal re-suspension.

After careful analysis of the techniques, it has been suggested that when using the wet crystal technique (such as in Jensen and coworkers' experiments[53]) the measurement of Fe^{2+} concentration may lead to an overestimate of the solubility limit. Therefore, the two extreme values reported for the solubility limit: 3.72×10^{-11} and 3.55×10^{-11} (the first two sets of data in Figure 1), were excluded when calculating the average solubility limit of iron carbonate at room temperature and I=0. Including all other reported values as shown in Figure 1, an average solubility limit of iron carbonate at T 25°C and I=0 is calculated to be 1.28×10^{-11}.

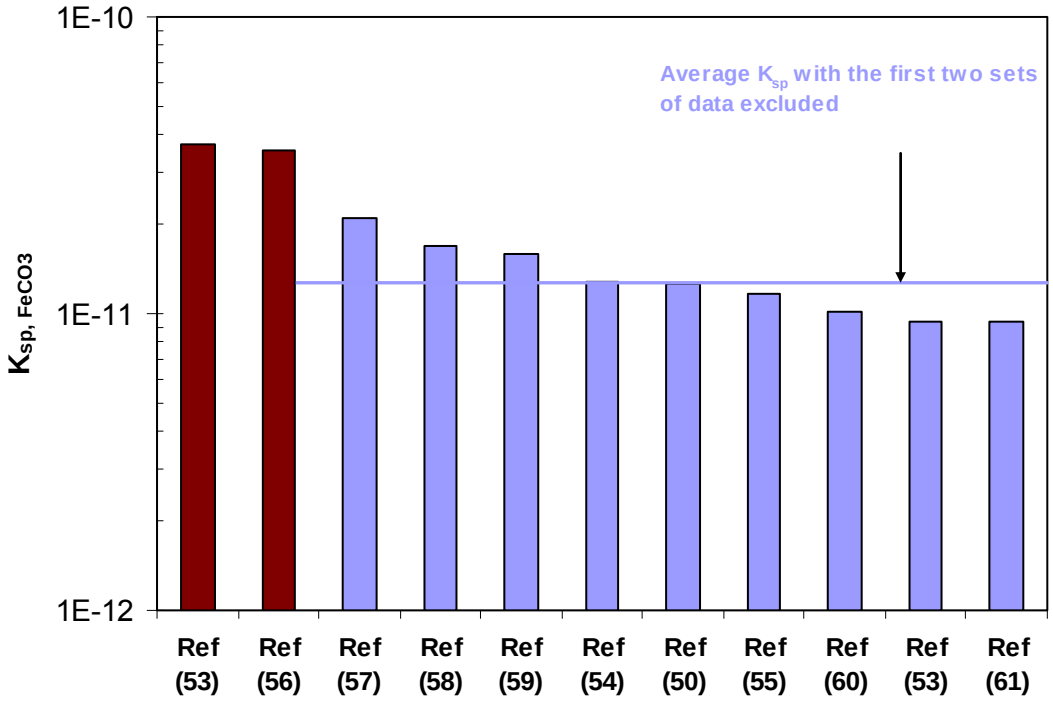

Figure 1. The published data for iron carbonate solubility limit (shown as bars) at room temperature (25°C) and ionic strength of I=0 and the average value (shown as line) which excludes the first two sets.

2.2.2 Temperature dependence

Several researchers investigated the effect of temperature on iron carbonate solubility limit by conducting experiments or using theoretical thermodynamic models. Braun[67] performed experiments to determine the effect of temperature (in the range 30°C to 80°C) on iron carbonate solubility limit and proposed equation (4).

$$log\ K_{sp} = -10.2 - 0.0314T_c \qquad (4)$$

Here temperature T_c is in °C. Using this equation to extrapolate iron carbonate solubility limit at room temperature (25°C and I=0) gives 1.04×10^{-11} which is close to the average value identified above.

Greenberg and Tomson[58] conducted a series of experiments to determine the iron carbonate solubility limit from 25°C to 94°C. The temperature dependence of the solubility constants was fitted to the equation (5) as suggested by Nordstrom *et al.* [49]:

$$log\ K_{sp} = a + bT_k + c/T_k + d\ log(T_k) \tag{5}$$

using the rigorous nonlinear least squares regression, results in equation (6):

$$log\ K_{sp} = -59.2385 - 0.041377\ T_k - \frac{2.1963}{T_k} + 24.5724\ log(T_k) \tag{6}$$

where T_k is in Kelvin.

Besides the temperature dependent experimental data provided by Braun[67], and Greenberg and Tomson[58], several researchers investigated the iron carbonate solubility limit dependence on temperature by using thermodynamic models. Helgeson[63] calculated the iron carbonate solubility limit in the temperature range from 50°C to 300°C using the van't Hoff equation:

$$\frac{d\ ln\ K_{sp}}{dT_k} = \frac{\Delta H}{RT_k{}^2} \tag{7}$$

In the equation, K_{sp} at room temperature and I=0 was 2.04×10^{-11}. They integrated equation (7) to obtain:

$$\begin{aligned} log\ K_{sp} = log\ K_{298.15} &- \frac{\Delta H^0}{2.303R}\left(\frac{1}{T_k} - \frac{1}{298.15}\right) \\ &- \frac{1}{2.303RT_k}\int_{298.15}^{T_k} \Delta C dT_k + \frac{1}{2.303RT_k}\int_{298.15}^{T_k} \Delta C d\ ln\ T_k \end{aligned} \tag{8}$$

where T_k is the temperature in Kelvin

R is the gas constant, which is equal to 8.3145 J/mol/K

ΔH^0 is the standard enthalpy of reaction in J/mol

ΔC is the standard heat capacity of reaction in J/mol/K

In the equation, average heat capacities were employed to estimate the value of ΔC because the required heat capacity functions are not available. Their predicted results (for the temperature range 50°C to 300°C) were later cited by IUPAC[64] . Based on this work IFE[65] had developed a simplified equation:

$$log\ K_{sp} = -10.13 - 0.0182T_c \tag{9}$$

However using equation (9), the predicted iron carbonate solubility limit at room temperature is 2.60×10^{-11} which is somewhat higher than the value used by Helgeson[63] and much higher than the empirical data.

Marion *et al.* [66] also determined an iron carbonate solubility limit expression based on van't Hoff equation (5). They assumed that ΔH was a constant ΔH^0 and used the value for $MgCO_3^o$ because ΔH^0 for $FeCO_3^o$ is unknown [66]. This equation (8) is simplified to read:

$$ln\ K_{sp} = ln\ K_{298.15} + \frac{\Delta H^0}{R}\left(\frac{1}{298.15} - \frac{1}{T_k}\right) \tag{10}$$

Equation (10) can be further simplified:

$$log\ K_{sp} = -14.66 + \frac{1365.17}{T_k} \tag{11}$$

Due to the fact that Marion *et al.* [66] assumed a constant ΔH^0, serious errors in calculated K_{sp} values occur at the elevated temperatures, as described by Helgeson[63]. At room

temperature, iron carbonate solubility limit obtained by using this expression is 8.32×10^{-11}, which is much higher than all values reported above.

Preis and Gamsjager[62] used a similar thermodynamic model to Equation (8) to predict the iron carbonate solubility limit, which is related to the standard enthalpy of solution $\Delta H^0(298.15)$ in J/mol and the standard entropy of solution $\Delta S^0(298.15)$ in J/mol/K by:

$$log\ K_{sp} = \frac{\Delta S^0(298.15)}{2.303R} - \frac{\Delta H^0(298.15)}{2.303R}\frac{1}{T_k} - \frac{1}{2.303RT_k}\int_{298.15}^{T_k}\Delta C dT_k + \frac{1}{2.303RT_k}\int_{298.15}^{T_k}\Delta C d\ ln T_k \quad (12)$$

However, using their equation in this form turned out to be cumbersome and was not included in the comparisons presented below.

A comparison of the iron carbonate solubility limit experimental data and values calculated by the various expressions discussed above at different temperatures is shown in Figure 2. It should be noted here that Braun[67] and Greenberg and Tomson empirical data[58] are not in agreement. The reason may be that Braun[67] used an artificial buffer solution in order to control the pH, which might have introduced errors. Hence, Greenberg and Tomson data[58] are considered as being more reliable and were used as a reference for the comparisons below.

When comparing the equations provided by Greenberg and Tomson[58] (Equation 6), Helgeson[63] (Equation 8), IFE[65] (Equation 9) and Marion[66] (Equation 12) it can be seen (Figure 2) that the Greenberg and Tomson[58] expression (Equation 6) fits their own data well, and therefore was selected as the basis for the unified model proposed below.

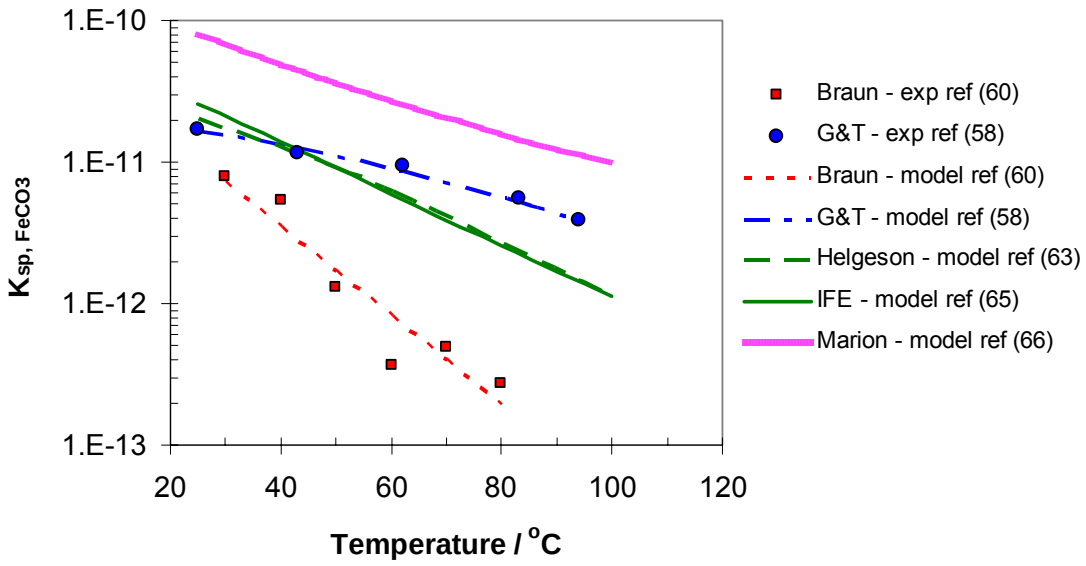

Figure 2. The experimental and calculated solubility limit data of iron carbonate vs. temperature at I=0.

2.2.3 Ionic strength dependence

There are very few data available for the effect of ionic strength. Silva *et al.*[50] experimentally investigated the iron carbonate solubility limit as a function of ionic strength in the range I=0.1 to 5.5 and proposed the following equation for room temperature (25°C):

$$\log K_{sp} = -10.9 + 2.518\, I^{0.5} - 0.657\, I \qquad (13)$$

This equation is similar to the unpublished expression provided by the Norsok Standard[68].

$$\log K_{sp} = -10.13 - 0.0182\, T_c + 2.44\, I^{0.5} - 0.72\, I \qquad (14)$$

When using Silva *et al.*[50] to extrapolate the solubility limit to ionic strength of 0 one obtains 1.26×10^{-11}, which is in good agreement with the average experimental value reported above.

2.3 Discussion and verification

2.3.1 Unified equation

From the literature review, it is found that the Greenberg and Tomson equation[58] is the best choice for describing iron carbonate solubility limit as a function of temperature. It should be noted here that Greenberg and Tomson's experiments[58] used a de-ionized water solution and assumed that ionic strength is 0. However, it can be calculated that the ionic strength was actually 0.002 because of the other ions present in the solution, such as H^+, HCO_3^-, CO_3^{2-}, and OH^-, Fe^{2+}. When this is accounted for, a slightly revised equation is obtained:

$$log\, K_{sp} = -59.3498 - 0.041377\, T_k - \frac{2.1963}{T_k} + 24.5724\, log\left(T_k\right) \qquad (15)$$

which is valid for I=0.

When the effect of ionic strength is added by combining the revised equation (15) with the Silva *et al.*[50] equation (13), the final unified equation is obtained which now includes both temperature and ionic strength:

$$\begin{aligned} log\, K_{sp} = {} & -59.3498 - 0.041377\, T_k - \frac{2.1963}{T_k} + 24.5724\, log\left(T_k\right) \\ & + 2.518\, I^{0.5} - 0.657\, I \end{aligned} \qquad (16)$$

2.3.2 Verification

The unified equation (16) was compared with empirical data at different temperatures (Figure 3) and ionic strength (Figure 4). The predicted values using the new equation correlate well with the experimental results provided by Greenberg and Tomson[58] and Silva[50]. The new equation was also employed in a water chemistry model to predict the saturation Fe^{2+} concentration in a CO_2 solution as reported by Dugstad[14]. It was found that the calculated values at different temperatures are in good agreement with the experimental data provided by Dugstad[14] (Figure 5).

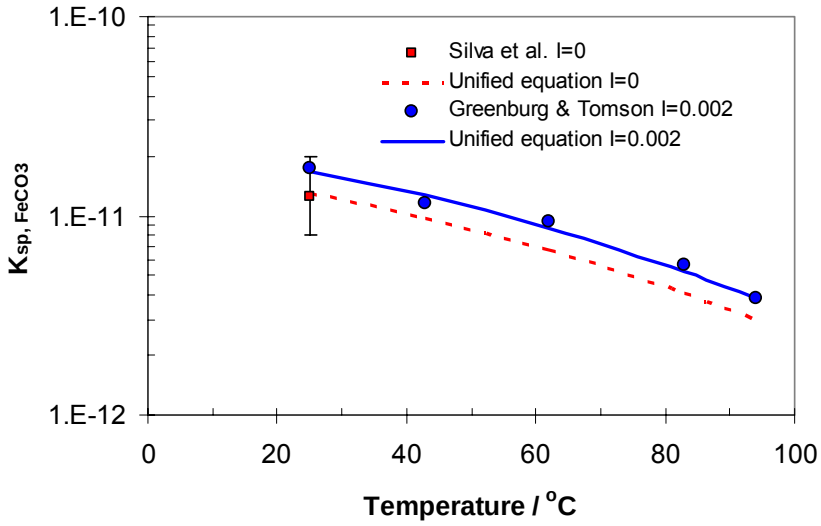

Figure 3. The experimental and calculated solubility limit of iron carbonate at different temperatures and ionic strength of 0 mol/L and 0.002 mol/L.

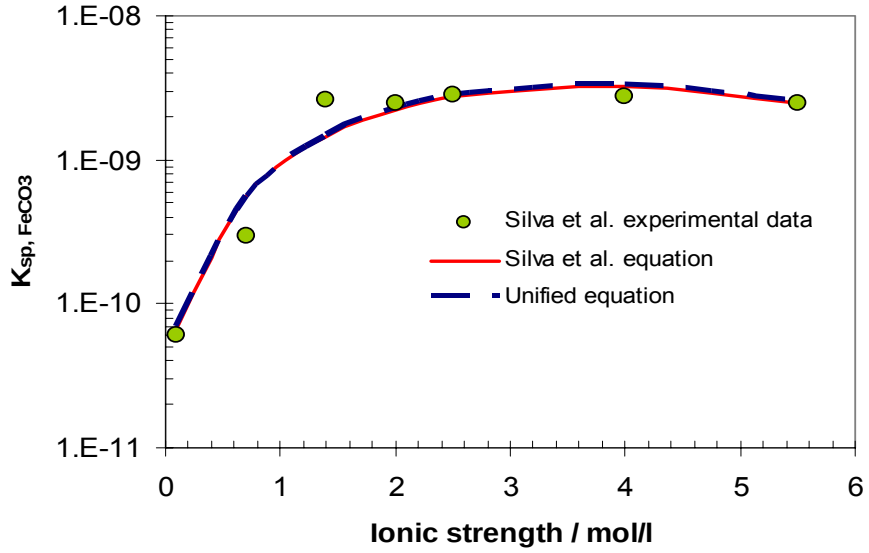

Figure 4. The experimental and calculated solubility limit of iron carbonate vs. ionic strength at room temperature.

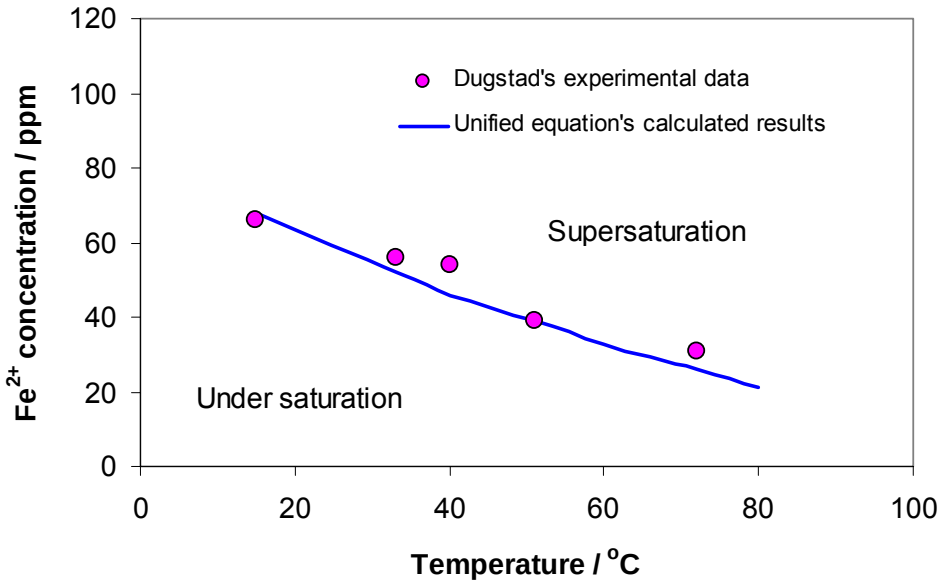

Figure 5. A comparison of the experimental saturated Fe^{2+} concentration provided by Dugstad [14] and the calculated saturated Fe^{2+} concentration by using the unified equation at different temperatures.

2.4 Summary

A unified iron carbonate solubility limit expression (16) which accounts for both temperature and ionic strength effects is developed based on the literature data. The predictions made with this unified equation agree well with the published experimental data.

Chapter 3: Kinetics of iron (II) carbonate scale formation in pure CO_2 corrosion

3.1 Introduction

In CO_2/H_2S corrosion, both iron carbonate and iron sulfide scale may form on the surface of mild steel, which is a frequent concern in the oil and gas production and transportation industries[4, 6-12]. In order to study both iron carbonate and iron sulfide scale formation in CO_2/H_2S corrosion, it is important to describe the model of iron carbonate scale formation in pure CO_2 corrosion.

In CO_2 environments, when the concentrations of Fe^{2+} and CO_3^{2-} ions exceed the solubility limit (K_{sp}) in aqueous solution, solid iron carbonate precipitates on the steel surface[13-21]. The overall reaction in the case of CO_2 corrosion can be described as follows:

$$Fe_{(s)} + CO_{2(g)} + H_2O_{(l)} \rightarrow FeCO_{3(s)} \downarrow + H_{2(g)} \uparrow \qquad (17)$$

Iron carbonate scale formation on the steel surface is generally acknowledged to be one of the most important factors governing the rate of corrosion in CO_2 environments. The iron carbonate scale can slow down the corrosion process by presenting a diffusion barrier for the species involved in the corrosion process and by covering up a portion of the steel surface and preventing the underlying steel from further dissolution.

3.2 Literature review

Iron carbonate scale that forms on mild steel in CO_2 environments is a frequent concern in the oil and gas production and transportation industries[13, 70, 71]. The scale growth depends primarily on the kinetics of scale formation. Semi-empirical growth rate

expressions have been frequently used to represent the precipitation process, particularly for engineering applications[72]. Johnson and Tomson[20] applied a semi-empirical equation (18), to develop an iron carbonate precipitation rate *PR* equation:

$$PR = k_r \frac{S}{V} \sigma^r \tag{18}$$

where k_r is kinetic constant, *S/V* is surface area-to-volume ratio, σ is the driving force, r is the reaction order. The driving force for crystallization is usually described in terms of supersaturation *SS*. Considering there was no consensus concerning which was the best driving force, Johnson and Tomson[20] fitted several equations (19) to (21) with their experimental data using a temperature ramp method in order to obtain an iron carbonate precipitation rate equation. [72, 73, 74]

$$\sigma = \left(\left(c_{Fe^{2+}} c_{CO_3^{2-}} \right)^{0.5} - K_{sp}{}^{0.5} \right) \tag{19}$$

$$\sigma = \left(\frac{\left(c_{Fe^{2+}} c_{CO_3^{2-}} \right)^{0.5} - K_{sp}{}^{0.5}}{K_{sp}{}^{0.5}} \right) = \left((SS)^{0.5} - 1 \right) \tag{20}$$

$$\sigma = ln\left(\frac{c_{Fe^{2+}} c_{CO_3^{2-}}}{K_{sp}} \right) = ln(SS) \tag{21}$$

Supersaturation *SS* is defined the ratio of species concentrations and the solubility limit K_{sp}:

$$SS = \frac{c_{Fe^{2+}} c_{CO_3^{2-}}}{K_{sp}} \tag{22}$$

Johnson and Tomson[20] found that Equation (19) fits well the experimental data, and hence developed an iron carbonate precipitation rate equation.

$$PR = k_r \frac{S}{V} K_{sp} \left\{ (SS)^{0.5} - 1 \right\}^2 \quad (23)$$

The equation (23) given by Johnson and Tomson[20] was fitted with the experimental results at the very low levels of supersaturation. According to van Hunnik *et al.* [21] it overestimated the precipitation rate, particularly at large supersaturations. The latter group proposed a nominally more accurate expression - Equation (24).

$$PR = k_r \frac{S}{V} K_{sp} \left(SS - 1 \right) \left(1 - SS^{-1} \right) \quad (24)$$

In both cases, the rate of precipitation *PR* (mol/m^{3}s) is a function of iron carbonate supersaturation (*SS*), the solubility limit (K_{sp}), temperature (via the kinetic constant k_r which obeys Arrhenius law), and surface area-to-volume ratio *S/V*.

It should be stressed here that the kinetics of scale formation in pure CO_2 corrosion by both Johnson and Tomson[20] and van Hunnik *et al.*[21] were studied using the traditional indirect technique – ferrous ion concentration measurement, which is based on measuring the decrease of ferrous ion concentration in the bulk of the solution (referred to as the "Fe^{2+} method" in the text below). It was implicitly assumed that the entire amount of ferrous ion "lost" in the solution ends up as deposited iron carbonate scale on the steel surface. Both of the authors assumed that the deposition rate of iron carbonate on the steel surface is equal to the precipitation rate of iron carbonate in the bulk of the solution. However, it is noted that iron carbonate not only deposits on the steel surface, but also precipitates elsewhere in the glass cell. Therefore, the assumption may lead to an overestimation of the deposition rate of iron carbonate on the steel surface, which is the main parameter affecting the corrosion rate of the steel. In the following, "scale retention

rate" will be employed as a new term to distinguish it from the "scale deposition rate" on the steel surface or the "scale precipitation" rate used in the literature.

3.3 Objectives

Based on the discussion above, the objectives of the present research on kinetics of iron carbonate scale formation in pure CO_2 corrosion are set as follows:

1. Develop a novel direct more reliable technique – weight change method – to investigate the scale retention rate of iron carbonate on the steel surface.
2. Test the expressions (23) and (24) from the literature using independently generated kinetics data.
3. If needed, develop a new equation to predict the iron carbonate scale retention rate on the steel surface in pure CO_2 corrosion.

3.4 Experimental setup

The present measurements were conducted in a glass cell as shown in Figure 6. The experiments were performed in the static solution with 1 bar total pressure and the temperature varying from 60ºC to 90ºC. Initially the glass cell was filled with 2 liters of de-ionized water and 1% wt. NaCl, which was heated and purged with CO_2 gas. After the solution was deoxygenated, the pH was increased to the desired pH of 6.6 by adding a deoxygenated sodium bicarbonate solution. Subsequently, the required amounts of Fe^{2+} were added in the form of a deoxygenated ferrous chloride salt ($FeCl_2.4H_2O$) solution. In various experiments supersaturation of iron carbonate in the solution was varied from 10 to 300 in order to investigate how supersaturation influenced the iron carbonate scale

retention rate on the steel surface. Then the specimens of X65 carbon steel or SS316 stainless steel were inserted into the solution as the substrates for growing the iron carbonate scale. Prior to immersion, the specimen surfaces were polished with 240, 400 and 600 grit SiC paper, rinsed with alcohol and degreased with acetone using an ultrasonic cleaner. The chemical composition of the X65 carbon steel used for the experiments is analyzed by Laboratory Testing Inc. Hatfield, PA and shown in Table 1.

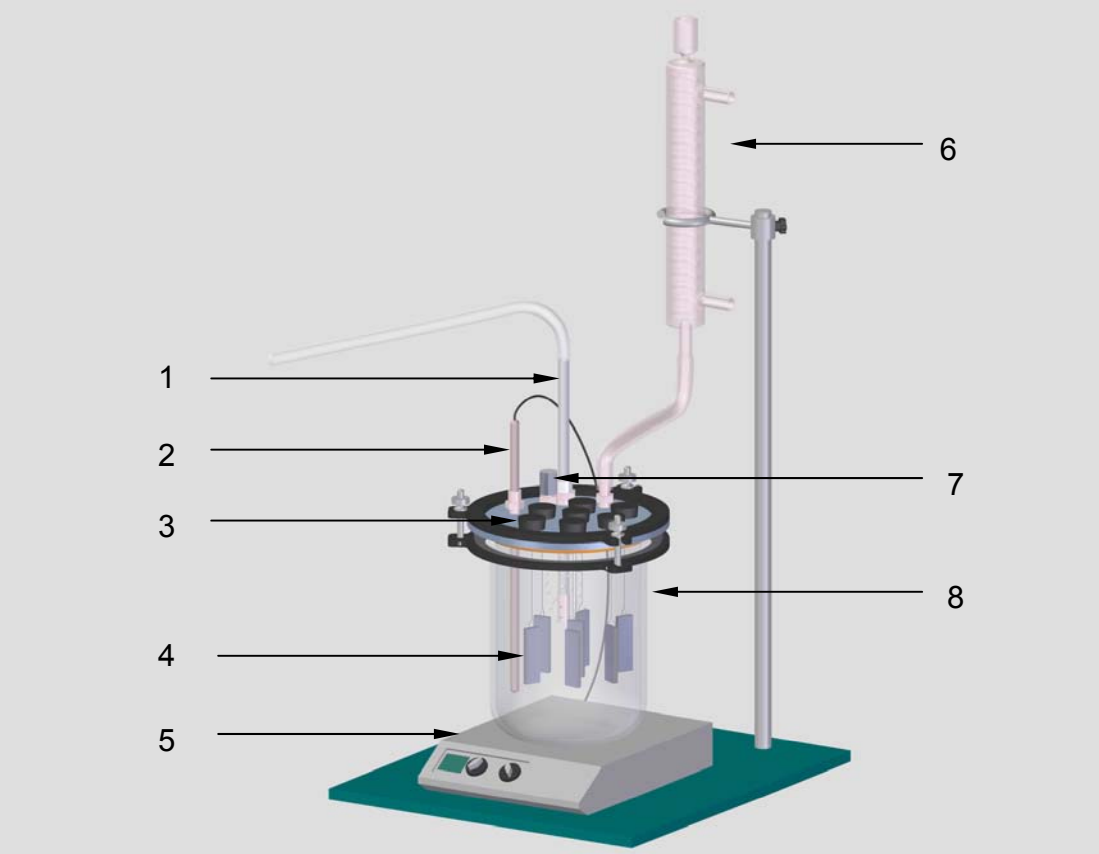

Figure 6. Schematic of the experimental test cell: 1. bubbler; 2. temperature probe; 3. rubber cork with nylon cord; 4. steel substrate; 5. hot plate; 6. condenser; 7. Cole-Parmer AgCl pH probe; 8. glass cell.

Table 1. Chemical composition of X65 (wt.%) (Fe is the balance)

C	Mn	Si	P	S	Cr	Cu	Ni	Mo	Al
0.050	1.32	0.31	0.013	0.002	0.042	0.019	0.039	0.031	0.032

Both the scale retention rate of iron carbonate and the corrosion rate of the steel were measured using a newly developed weight change method (Appendix). The indirect ferrous ion concentration measurements were also used to obtain the iron carbonate scale retention rate. Time-averaged scale retention rate of iron carbonate was obtained by subtracting the weight of the coupons which had iron carbonate scale and those after the scale was removed using Clarke's solution. Clarke's solution was prepared using 20 g antimony trioxide and 50 g stannous chloride in 1 litre hydrochloric acid at room temperature for up to 25 minutes[75]. The scale on the specimen was removed with rubber. Time-averaged corrosion rate was calculated by subtracting the weight of the coupons prior to running the experiments and after removing the iron carbonate scale. A spectrophotometer was used to measure ferrous ion concentration in the solution. The specimens with iron carbonate scale were analyzed by Scanning Electron Microscopy (SEM).

3.5 Results and discussions

3.5.1 Verification experiments

Three sets of experiments were conducted in order to verify the iron carbonate scale retention rate expressions, using X65 carbon steel substrates with different surface areas at pH 6.6, temperature of 80^{o}C, and initial Fe^{2+} 50 ppm (which then drifted down as precipitation occurred). The first set of experiments was conducted using one specimen with the surface area of 5.4 cm^2. The second set of experiments was conducted using thirty specimens each having a surface area of 2 cm^2 (total of 60 cm^2). During these experiments, six specimens were taken out of the solution every two and a half hours. In

the third set of experiments twelve specimens, each having a surface area of 21 cm^2 (total of 252 cm^2), were inserted in the solution and three specimens were taken out every two and a half hours.

As mentioned in the Introduction of Chapter 2, both Johnson and Tomson[20] and van Hunnik *et al.*[21] determined experimentally the scale retention rate of iron carbonate by an indirect technique - Fe^{2+} method (Appendix). In the present experiments the same was done, ferrous ion concentrations were measured at different times. The results show that the change of ferrous ion concentration in the solution with time was similar irrespective of the very different surface areas of the substrates (Figure 7), *i.e.*, using this method very similar scale retention rates were obtained for all surface area-to-volume ratios tested. However, according to Johnson and Tomson[20] and van Hunnik et al. [21], i.e., expressions (23) and (24), this should not happen, rather the scale retention rate on the steel surface should be directly proportional to the surface area-to-volume ratio (*S/V*). Therefore, either expressions (23) and (24) or the experimental technique had problems.

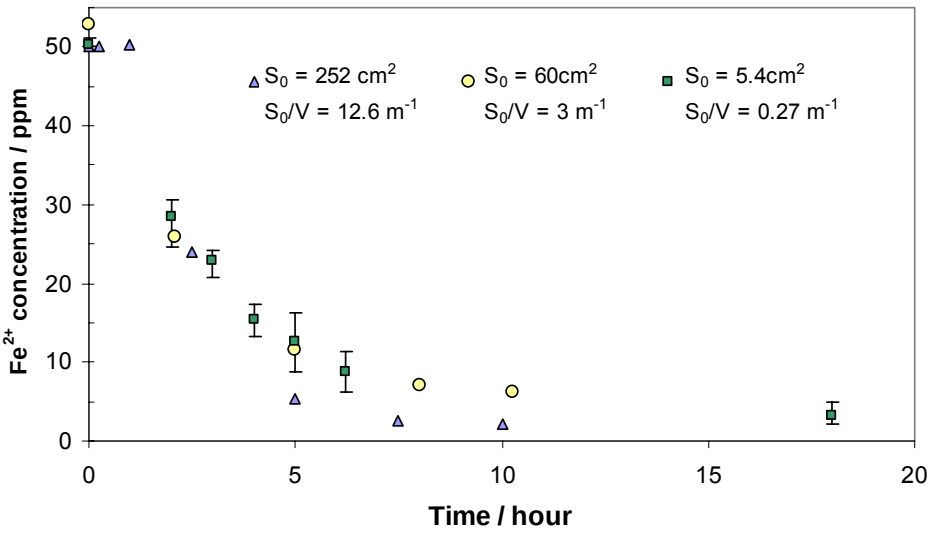

Figure 7. Ferrous ion concentration vs. reaction time for different surface areas of X65 steel substrates in pure CO_2 corrosion at pH 6.6, T=80^oC static conditions.

When the scale retention rates calculated by the Fe^{2+} method were compared to the scale retention rates obtained by the more direct weight change method it became clear where the problem lies. The results shown in Figure 8 illustrate that the scale retention rate does indeed depend on the *S/V* ratio, as expected, and that the Fe^{2+} method can be in gross error. When using substrates with a large surface area of 252 cm^2 (large *S/V*), similar scale retention rate, are obtained by using both the weight change method and the Fe^{2+} methods. However, with the decrease of the surface area of the substrate, the scale retention rate measured by the weight change method decreases while the one measured by the Fe^{2+} method does not, as previously noted. A simple mass balance for Fe^{2+} has shown that in the experiments with the small substrates (small *S/V*) most of the precipitated iron carbonate does not end up on the steel surface and therefore the key assumption implicit for this method fails. For large *S/V*, most of the iron carbonate deposits on the steel substrate and the assumption holds hence the Fe^{2+} method appears to be valid. On the other hand, the weight change method, while being more tedious, offers a more realistic estimate of the scale retention rate under all conditions. Results obtained for various *S/V* ratios all fall within the expected error margins as shown by the error bars in Figure 8. From the same figure it should be noted that the discrepancy between the two methods is smaller for smaller supersaturations.

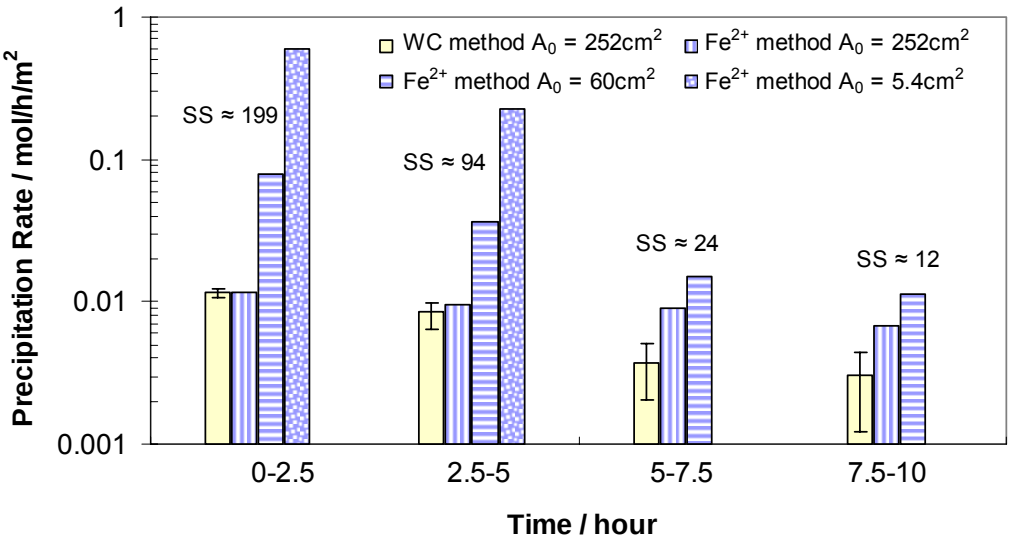

Figure 8. The comparison of differential scale retention rate of iron carbonate on X65 carbon steel in different techniques (weight change method and Fe^{2+} concentration measurement) and for different surface areas of substrates (initially S_0 = 252 cm^2, 60 cm^2, and 5.4 cm^2, which mean S_0/V = 12.6 m^{-1}, 3 m^{-1}, and 0.27 m^{-1}) in pure CO_2 corrosion under the conditions of initial Fe^{2+} concentration 50 ppm (which then drifted down), pH 6.6, T=80°C.

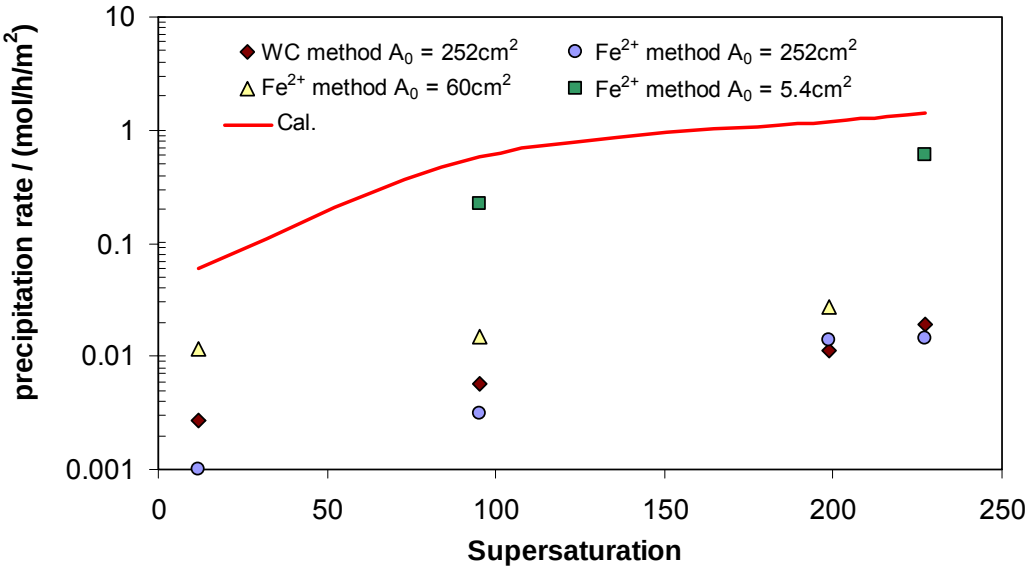

Figure 9. Experimental and calculated (using kinetics expression given by **v**an Hunnik et al. [21]) scale retention rates of iron carbonate under supersaturations of 12 to 250 at a temperature of 80°C.

It was impossible to reproduce directly the original experiments of Johnson and Tomson[20] and van Hunnik *et al.* [21] since no sufficient detail is reported in the original publications. However predictions made by the expressions (23) and (24), which were derived from their original data, were compared to the present measurements of the scale retention rate and, not surprisingly, large discrepancies were found. For example, Figure 9 shows that the more accurate experimental data obtained by weight change method are up to two orders of magnitude lower when compared to the calculated results using the more recent van Hunnik et al. [21] expression (24). However, the agreement "improves" when one compares the same predictions with the scale retention rate data obtained by the Fe^{2+} method for small *S/V* ratios, which we now know are erroneous. Therefore it is concluded that both expressions (23) and (24) overestimate the actual scale retention rate by a large margin because the experimental data used to derive them were based on the Fe^{2+} method, in which the assumption of Fe^{2+} lost in the bulk of the solution becoming $FeCO_3$ scale on the steel surface is unreliable.

3.5.2 Kinetics experiments

3.5.2.1 Free drift experiments

Kinetics experiments were conducted in static solution using X65 carbon steel as the substrate. In the first series of experiments, initial Fe^{2+} of 50 ppm (decreased as reaction proceeded), pH of 6.6 and a range of temperatures was used which varied from 60^oC to 90^oC. Figure 10 shows the change of ferrous ion concentration in the solution at different temperatures. The ferrous ion concentration in the solution at 60^oC increased initially because of the corrosion of carbon steel which overpowered the precipitation

process, and then decreased gradually with temperature as the corrosion rate decreased. When the temperature increased to 70°C, 80°C and 90°C, the ferrous ion concentration decreased steadily. Based on the rate of change of ferrous ion concentration it can be seen that the scale retention rate increased with the increase of temperature.

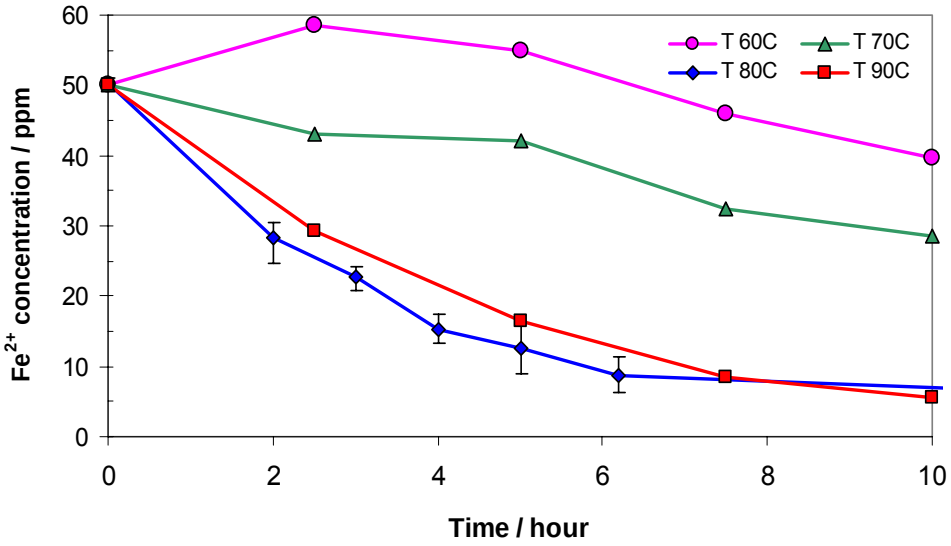

Figure 10. Fe^{2+} concentration vs. the reaction time in pure CO_2 corrosion under the conditions of initial Fe^{2+} concentration 50 ppm (which then drifted down), pH 6.6, T=60°C, 70°C, 80°C, 90°C.

Both the scale retention rate and the corrosion rate obtained by the weight change method as a function of time and supersaturation of iron carbonate at the temperature of 60°C are shown in Figure 11. Both the scale retention rate and the corrosion rate were described in the same molar unit of mol/h/m^2, in order to understand and compare how much iron carbonate scale formed ($FeCO_3$ in mol) and iron lost (Fe in mol) on the steel surface (with a surface area of 1 m^2) in an hour. The error bars represent the maximum and minimum measured scale retention rates. The scale retention rate at the temperature of 60°C increased with the increase of reaction time during the first five hours and then

became stable between 5 hours and 7.5 hours. From 7.5 hours to 10 hours the scale retention rate decreased because of the decrease of supersaturation in the bulk of the solution. Comparing the scale retention rate with the corrosion rate in the same units (mol/h/m^2), it is found that the scale retention rate is slightly higher than the corrosion rate in the first 5 hours. After 5 hours, the scale retention rate is slightly lower than the corrosion rate. The source of Fe^{2+} forming iron carbonate scale includes both Fe^{2+} released from the steel surface and Fe^{2+} provided by the bulk of the solution. Hence the corrosion rate has a significant effect on the scale retention rate of iron carbonate scale. The corrosion rate of carbon steel under the test conditions is below 1 mm/yr, as illustrated in Figure 11. A similar trend in the experimental results was obtained in the experiments at the temperature of 70°C (Figure 12). The scale retention rate increased with the increase of reaction time and then decreased after 7.5 hours.

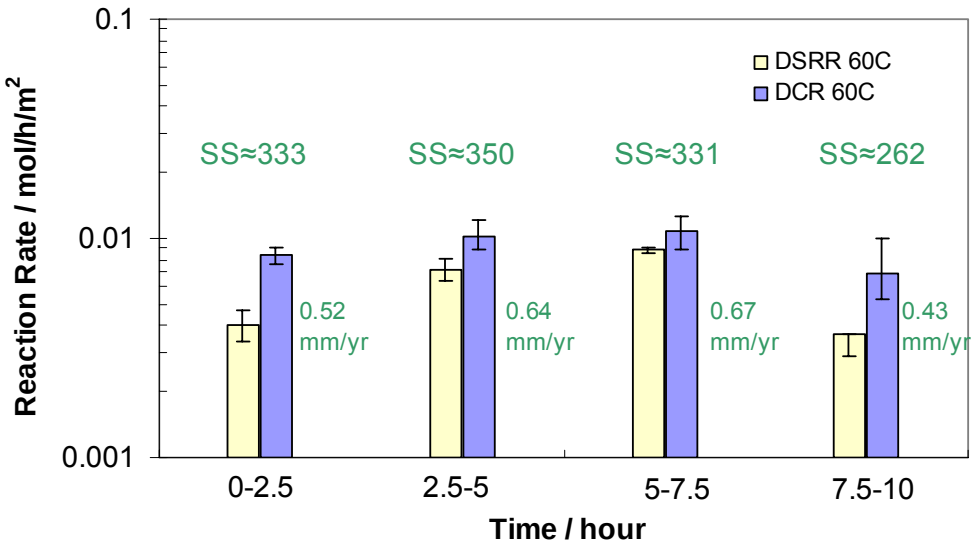

Figure 11. The comparison of differential scale retention rate of iron carbonate scale (DSRR) and differential corrosion rate of X65 carbon steel (DCR) in pure CO_2 corrosion under the conditions of initial Fe^{2+} concentration 50 ppm (which then drifted down), pH 6.6, T=60°C.

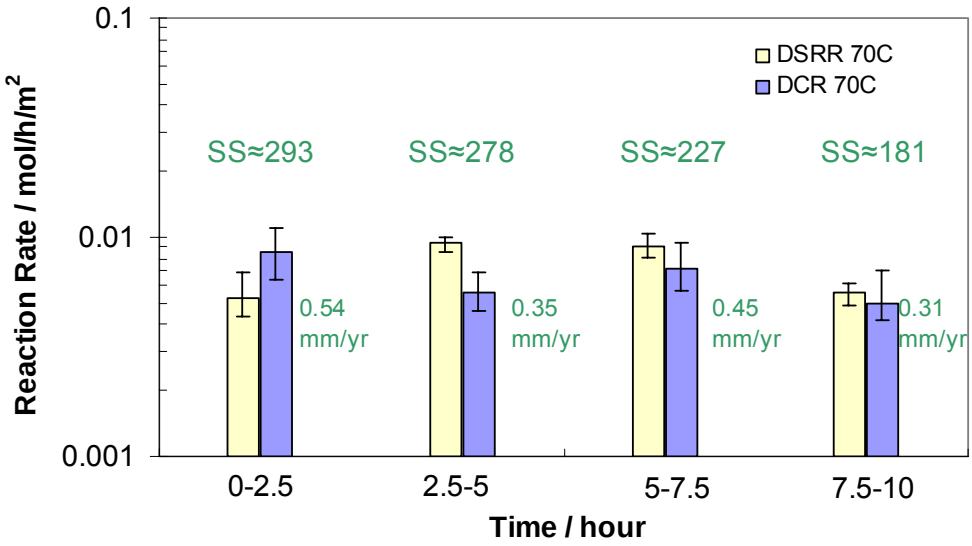

Figure 12. The comparison of differential scale retention rate of iron carbonate scale (DSRR) and differential corrosion rate of X65 carbon steel (DCR) in pure CO_2 corrosion under the conditions of initial Fe^{2+} concentration 50 ppm (which then drifted down), pH 6.6, T=70°C.

At 80°C, the scale retention rate decreased steadily with time because of the decrease of the supersaturation in the bulk of the solution (Figure 13). Since iron carbonate scale formed faster at higher temperature and was more protective, the corrosion rate decreased more with the increase of temperature. Comparing the scale retention rate with the corrosion rate in the same molar units, the scale retention rate is higher than the corrosion rate at any time in the experiments, which proves that the bulk Fe^{2+} is a more significant source of ferrous ions forming iron carbonate scale at 80°C than at the lower temperatures. Similar experimental results were obtained at 90°C (Figure 14).

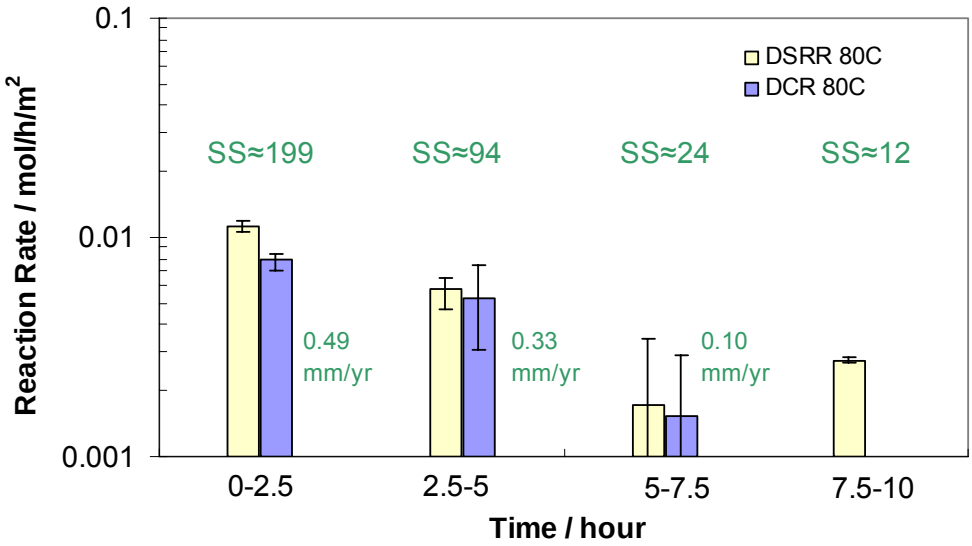

Figure 13. The comparison of differential scale retention rate of iron carbonate scale (DSRR) and differential corrosion rate of X65 carbon steel (DCR) in pure CO_2 corrosion under the conditions of initial Fe^{2+} concentration 50 ppm (which then drifted down), pH 6.6, T=80°C.

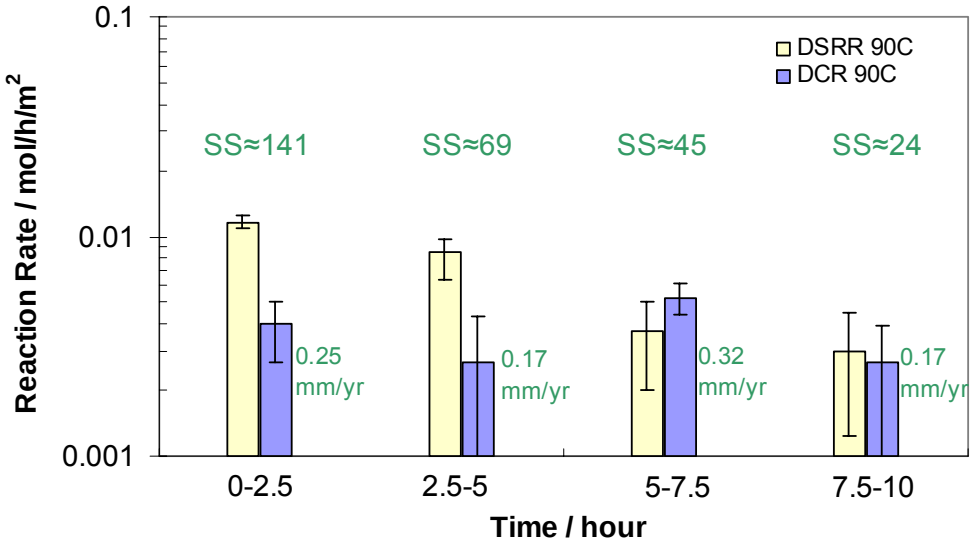

Figure 14. The comparison of differential scale retention rate of iron carbonate scale (DSRR) and differential corrosion rate of X65 carbon steel (DCR) in pure CO_2 corrosion under the conditions of initial Fe^{2+} concentration 50 ppm (which then drifted down), pH 6.6, T=90°C.

The morphology and cross section of iron carbonate scale at different temperatures (70^{o}C and 80^{o}C) as a function of time are shown in Figure 15 and Figure 16. Clearly the iron carbonate scale became denser and therefore more protective over time. By comparing the appearance of iron carbonate scale for various temperatures, it was found that the surface coverage by iron carbonate scale increased with the increase of temperature.

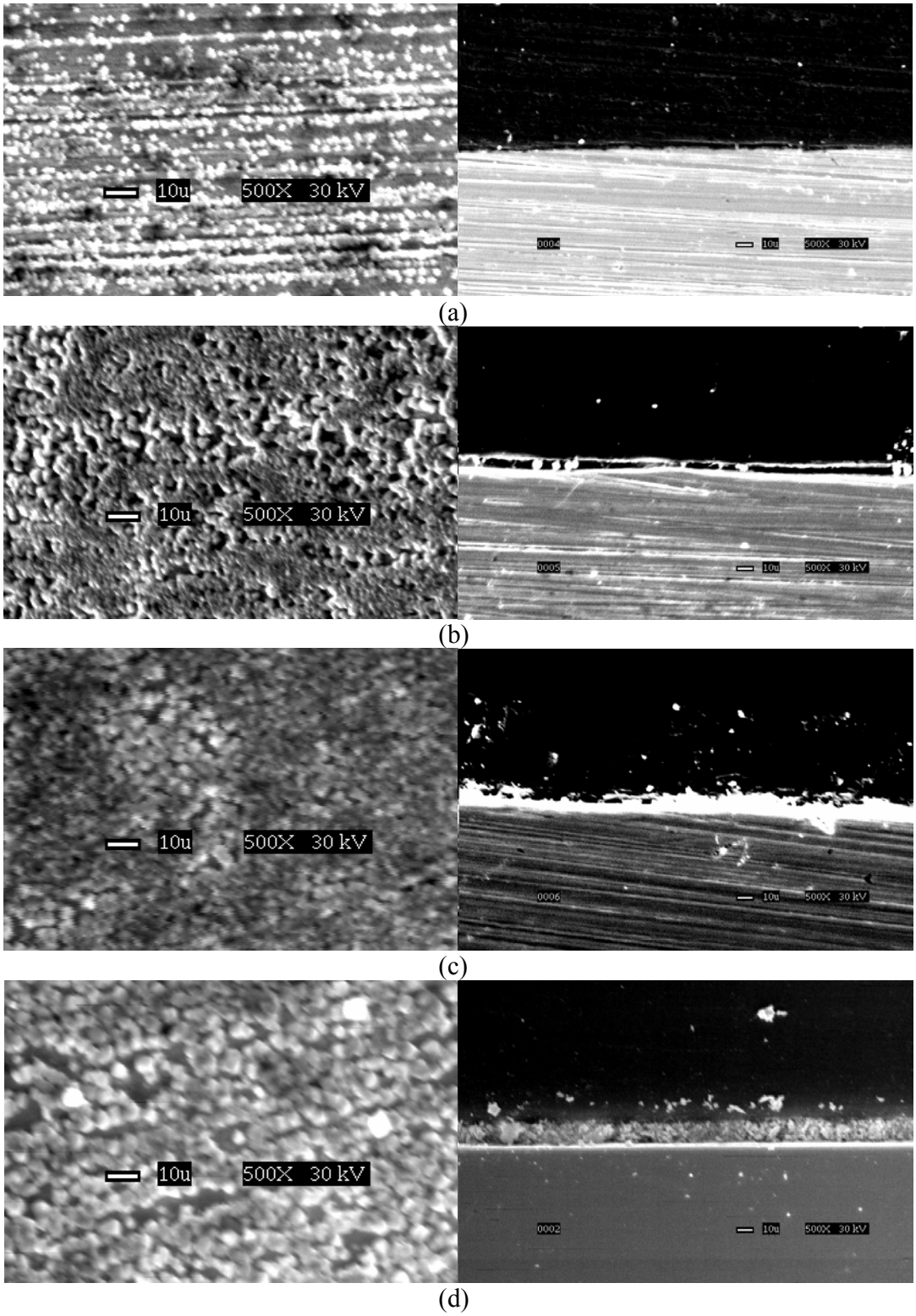

Figure 15. The top view (left) and cross section (right) of iron carbonate after a) 2.5, b) 5, c) 7.5, d) 10 hours (pH 6.6, T=70^{o}C, initial Fe^{2+} = 50 ppm (which then drifted down))

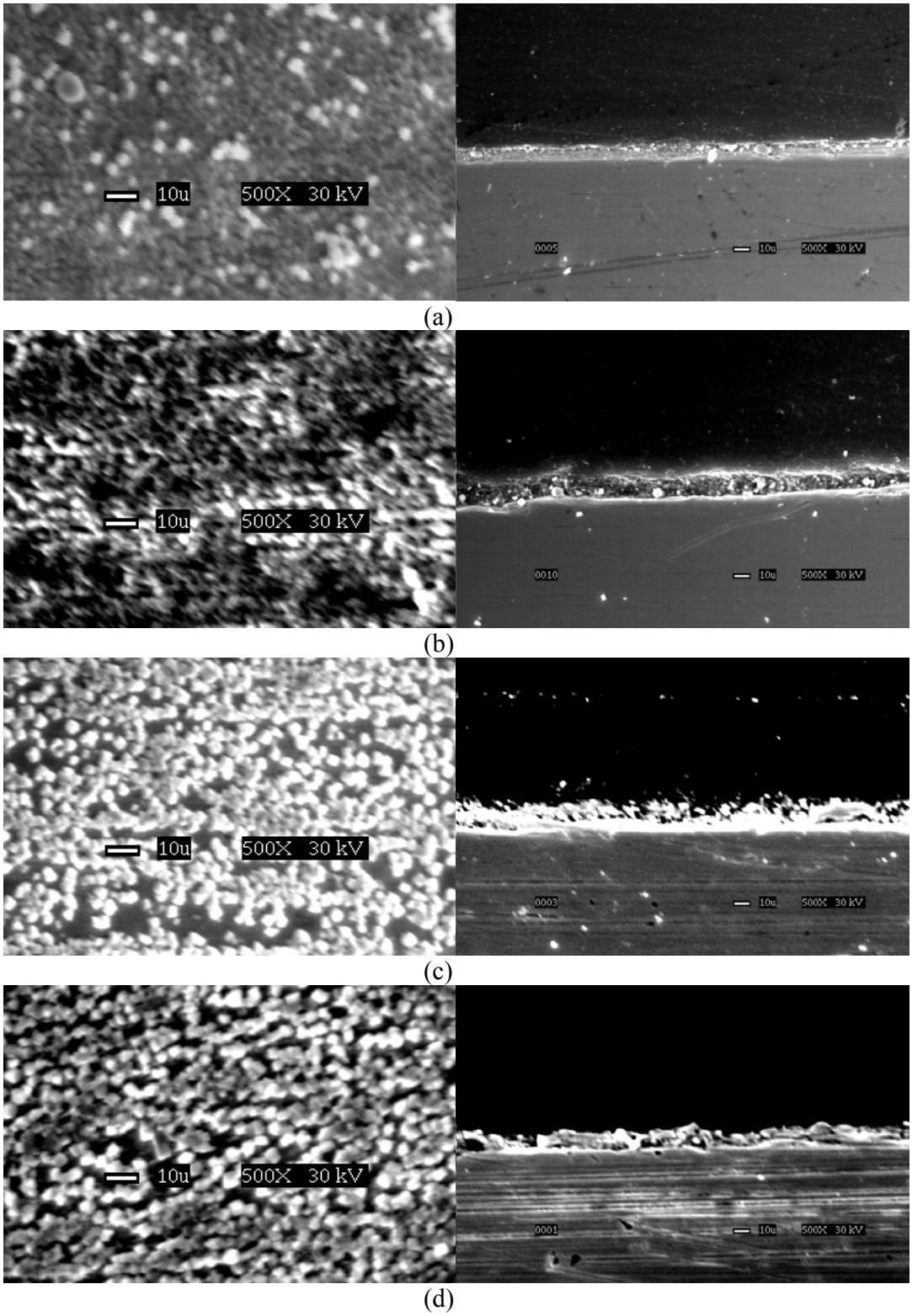

Figure 16. The top view (left) and cross section (right) of iron carbonate after a) 2.5, b) 5, c) 7.5, d) 10 hours (pH 6.6, T=80^{o}C, initial Fe^{2+} = 50 ppm (which then drifted down))

3.5.2.2 Experiments at a controlled constant supersaturation of iron carbonate

A series of more complicated experiments was conducted with X65 carbon steel at a controlled constant supersaturation in static solution with Fe^{2+} concentrations of 50 ppm and 10 ppm, pH 6.6, and temperatures of 60°C, 70°C, and 80°C. The controlled constant supersaturation was achieved by continuously dosing a deoxygenated ferrous chloride solution to the glass cell to compensate for the Fe^{2+} ions lost by precipitation. Figure 17 illustrates that both the scale retention rate and the corrosion rate of carbon steel for Fe^{2+} 50 ppm at 80°C was stable over time while the supersaturation was kept approximately 200. The corrosion rate was below 0.2 mm/yr. Figure 18 shows both the scale retention rate and the corrosion rate (T 80°C) *versus* time at Fe^{2+} 10 ppm and supersaturation of 100. The results show that the scale retention rate in the first 12 hours is slightly lower than the scale retention rate in the second 12 hours. The final corrosion rate decreased to very low values, which proved that protective iron carbonate scale formed on the steel surface after 24 hours. A comparison of the scale retention rate at various temperatures of 60°C, 70°C, and 80°C and constant supersaturation is showed in Figure 19. With the increase of temperature, the scale retention rate of iron carbonate scale increased. Overall, this series of experiments was consistent with the previous series where supersaturation changed in the course of the experiment, and has proven that by controlling the key parameters stable and reproducible results for the kinetics of iron carbonate scale formation can be obtained.

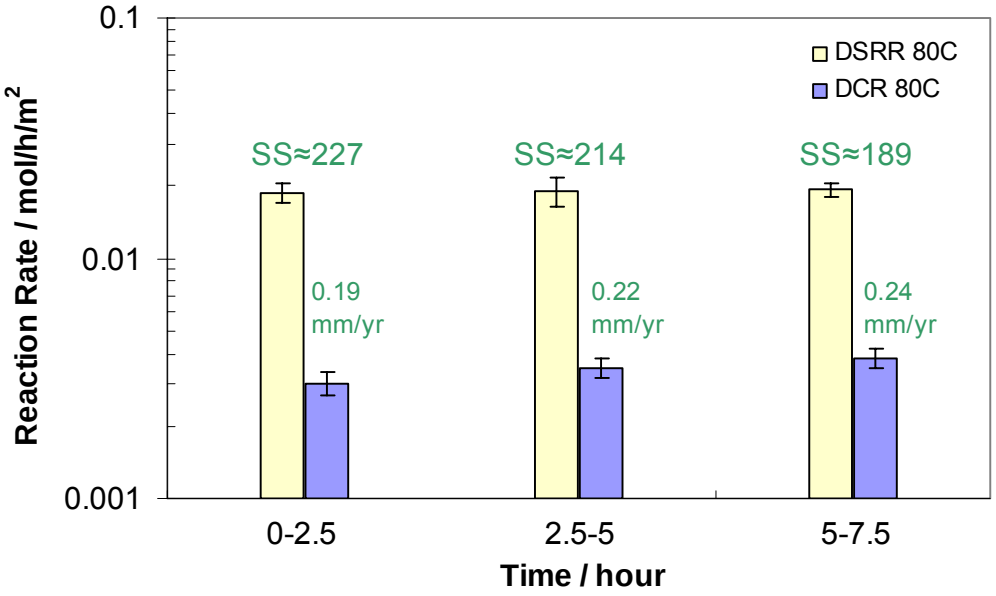

Figure 17. The comparison of differential scale retention rate of iron carbonate scale (DSRR) and differential corrosion rate of X65 carbon steel (DCR) in pure CO_2 corrosion for constant Fe^{2+} concentration 50 ppm, pH 6.6, T=80°C.

.

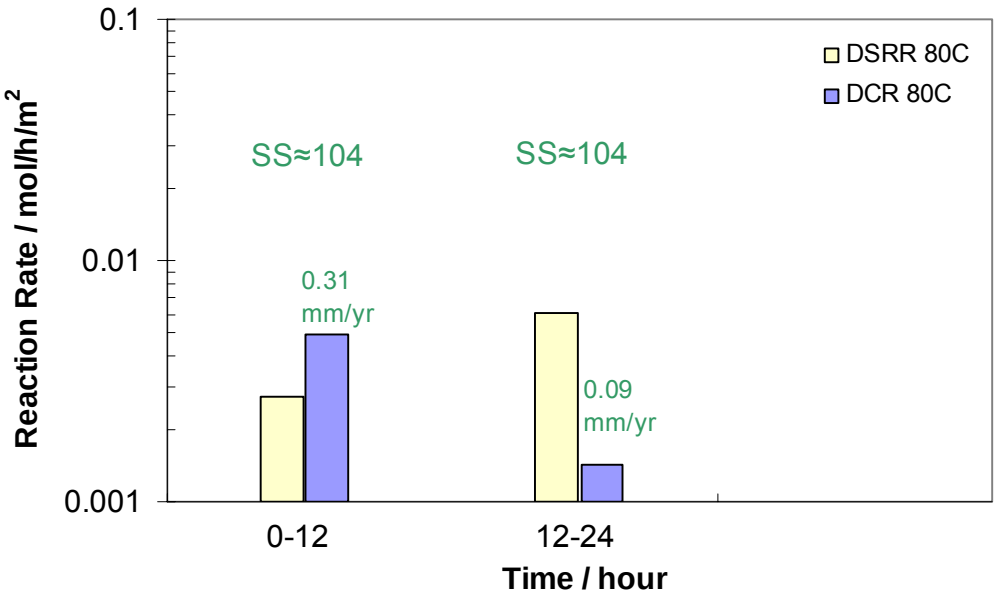

Figure 18. The comparison of differential scale retention rate of iron carbonate scale (DSRR) and differential corrosion rate of X65 carbon steel (DCR) in pure CO_2 corrosion for constant Fe^{2+} concentration 10 ppm, pH 6.6, T=80°C.

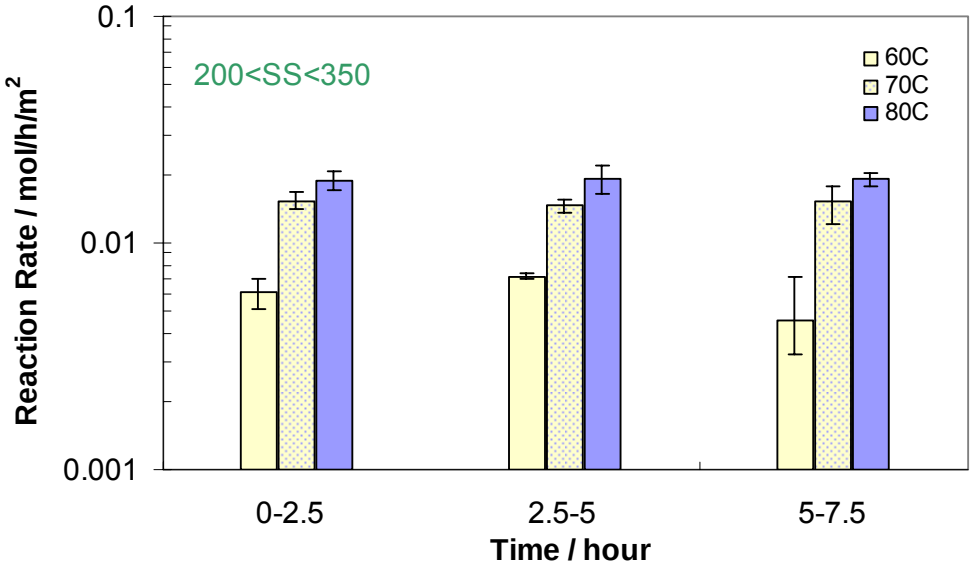

Figure 19. The comparison of differential scale retention rate of iron carbonate scale in pure CO_2 corrosion for constant Fe^{2+} concentration 50 ppm, pH 6.6, T 60°C, 70°C, and 80°C.

3.5.2.3 Experiments using stainless steel as the substrate

Based on the experimental results above, it was found that the scale retention rate of iron carbonate scale is strongly affected by the corrosion rate of the steel at low supersaturation. At high supersaturation, the corrosion rate has little effect on the scale retention rate of iron carbonate. Therefore, several experiments were conducted at different supersaturations using stainless steel as the substrate considering that stainless steel is almost inert in CO_2 environment.

The morphology of the specimen (Figure 20) shows that there was almost no growth of iron carbonate scale on the stainless steel under similar conditions e.g. at a supersaturation of 60. Iron carbonate scale formed on carbon steel because corrosion leads to a much higher supersaturation at the steel surface than in the bulk solution. When the supersaturation increased to 300, more iron carbonate crystals formed on carbon steel

than on stainless steel, as shown in Figure 21. In that case the scale formed on the stainless steel was approximately 50% of that compared to corroding carbon steel. These phenomena have also proved that the source of ferrous ions forming iron carbonate scale includes ferrous ions both released from the steel surface and those provided by the bulk of the solution. The scale retention rate of iron carbonate is directly related to corrosion and the conditions at the steel surface.

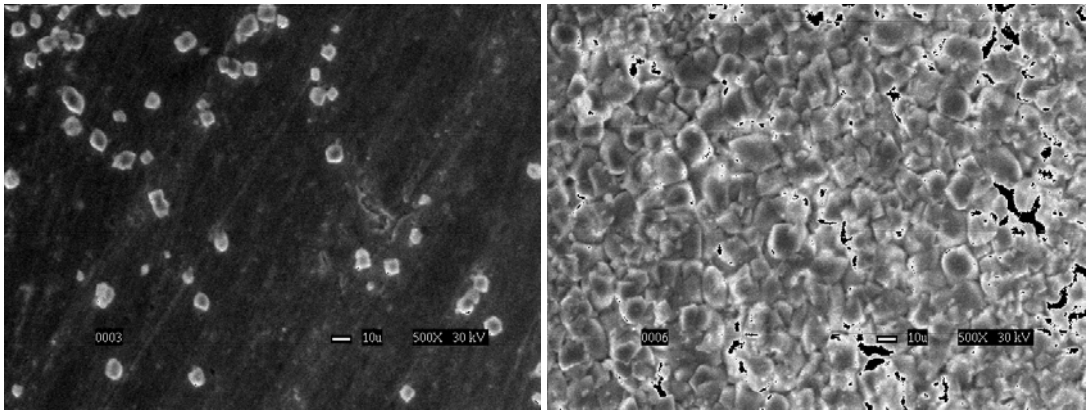

(a) (b)

Figure 20. Comparison of top views for specimens of different substrates, a) stainless steel, b) carbon steel at pH 6.6, Fe^{2+}=10 ppm, SS=60, T=80°C, static conditions.

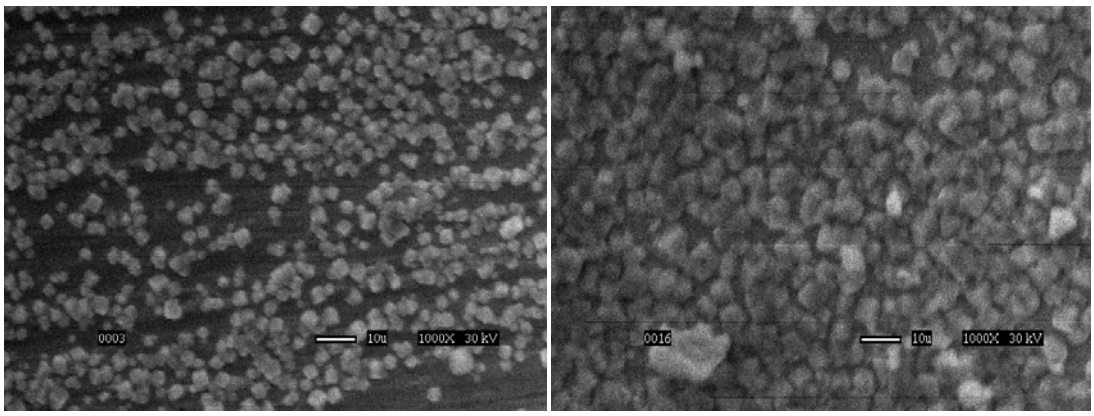

(a) (b)

Figure 21. Comparison of the top views for specimens of different substrates, a) stainless steel, b) carbon steel at pH 6.6, Fe^{2+}=50 ppm, SS=300, T=80°C, static conditions.

3.5.2.3 Scaling tendency and porosity of the scale

Both scaling tendency and porosity are employed to further understand the iron carbonate scale formation in pure CO_2 corrosion. The scaling tendency is described as follows[21]:

$$ST = \frac{SRR}{CR} \tag{25}$$

where *SRR* is the scale retention rate of iron carbonate, *CR* is the corrosion rate of the steel. The scaling tendency was calculated by using the same molar units (mol/h/m^2) for scale retention rate and the corrosion rate and is shown in Figure 22 for various experiments. The scaling tendency at the temperature of 60^{o}C and 70^{o}C varies from 0.5 to 1.5. With the temperature increasing to 80^{o}C and 90^{o}C, the scaling tendency increases above 1.5, suggesting more rapid scaling and more effective protectiveness at higher temperature. It has also been proved that at higher temperature Fe^{2+} forming iron carbonate scale comes from both Fe^{2+} in the bulk of the solution and Fe^{2+} released from the steel surface, and at lower temperature Fe^{2+} forming iron carbonate scale mainly comes from Fe^{2+} released from the steel surface.

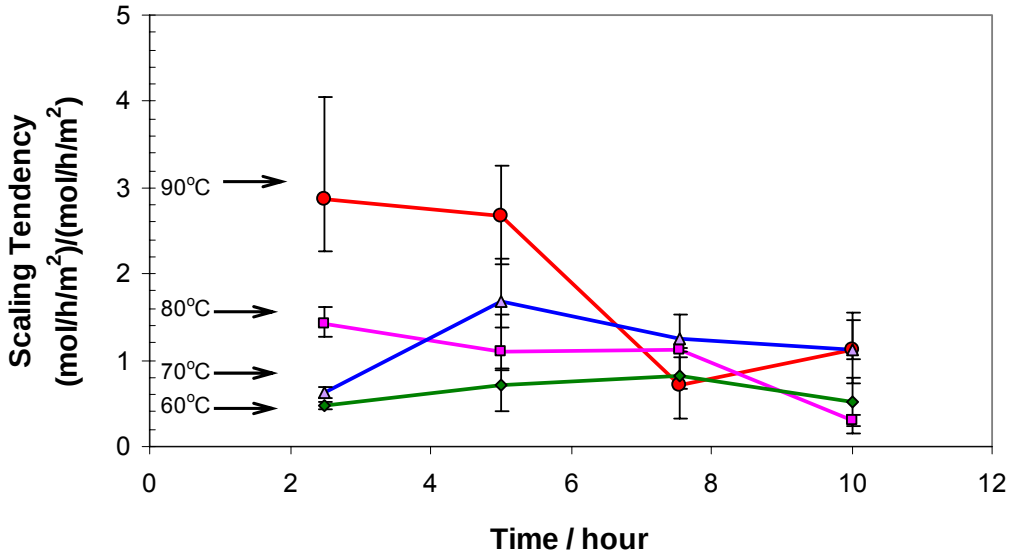

Figure 22. The comparison of scaling tendency in pure CO_2 corrosion under the conditions of initial Fe^{2+} concentration 50 ppm (which then drifted down), pH 6.6, T=60°C, 70°C, 80°C, and 90°C.

The porosity of the iron carbonate scale (ε) is calculated using the following equation (26) [18],

$$\varepsilon = \frac{V_{void}}{V_{total}} = \frac{\left(V_{total} - V_{FeCO_{3(s)}}\right)}{V_{total}} = 1 - \frac{V_{FeCO_{3(s)}}}{V_{total}} = 1 - \frac{\delta_{FeCO_{3(s)}}}{\delta_{SEM}} = 1 - \frac{\frac{m_{FeCO_{3(s)}}}{\rho_{FeCO_{3(s)}} S}}{\delta_{SEM}} \qquad (26)$$

Where δ is the thickness of the scale in m, $m_{FeCO_{3(s)}}$ is the mass of iron carbonate in kg, $\rho_{FeCO_{3(s)}}$ = 3,900 kg/m^3 is the density of iron carbonate, and S is the surface area in m^2. Both the thickness obtained by SEM and the porosity of the scale calculated by equation (26) at different temperatures and reaction time are shown in Table 2. The results show that the porosity slightly decreases with the increase of the reaction time. It has also been found that although the iron carbonate scale is protective under the test conditions, the porosity of iron carbonate is above 50%.

Table 2. The thickness (by SEM) and porosity of scale at different temperatures and reaction times under the conditions of initial Fe^{2+} concentration 50 ppm (then drifted down) and pH 6.6.

T (^{o}C)	Reaction time (hrs)	Supersaturation	Thickness of scale (μm)	Porosity
60	2.5	333	1	0.71
	5	350	2	0.59
70	2.5	293	2	0.81
	5	278	4	0.73
	7.5	227	8	0.78
	10	181	10	0.78
80	2.5	199	4	0.79
	5	94	6	0.79
	7.5	24	8	0.84
	10	12	8	0.82
90	2.5	141	4	0.79
	5	69	6	0.76

3.5.3 Iron carbonate scale retention rate equation

Semi-empirical precipitation rate expressions have been used to develop iron carbonate scale retention rate equations by Johnson and Tomson[20] and van Hunnik *et al.* [21]. As mentioned above, both of them determined experimentally the scale retention rate of iron carbonate by an indirect technique which is based on measuring the decrease of ferrous ion concentration in the bulk solution. It was implicitly assumed that the entire amount of ferrous ion "lost" by the solution ends up as deposited iron carbonate scale on the steel surface. It has been proven here that the indirect dissolved ferrous ion concentration method led to an error in calculating how much iron carbonate deposits on the steel surface because iron carbonate at high supersaturaion not only deposits on the steel surface, but also precipitates elsewhere in the solution. Hence a reliable semi-empirical scale retention rate expression was developed for corrosion engineering applications using the experimental data obtained by the direct weight change method.

The experimental data shown in the present paper were employed to fit several empirical scale retention rate expressions[76], including the equations used by Johnson and Tomson[20] - Equation (19) to Equation (21). It was found that the following equation fits the experimental data better than the other models. Therefore, Equation (27) was used as the iron carbonate scale retention rate equation.

$$SRR = k_r \frac{S}{V} K_{sp} \left(SS - 1\right) \tag{27}$$

where SRR is the scale retention rate in mol/(m^{3}s)

k_r is the kinetics constants, which is a function of temperature in kg^2/(mol m^2 s)

S/V is surface area-to-volume ratio in m^{-1}

SS is iron carbonate supersaturation

K_{sp} is iron carbonate solubility limit in (mol/L)^2 or (mol/kg)^2, assuming the density of the water solution (ρ) of 1000 kg/m^3 (or 1 kg/L).

Scale retention rate of iron carbonate SRR could also be expressed in mol/(m^{2}s), which is a more accurate expression to describe how much iron carbonate scale is retained on the steel surface. It is illustrated that SRR in mol/m^{2}h is not a function of surface area-to-volume ratio S/V - equation (28).

$$SRR = k_r \ K_{sp} \left(SS - 1\right) \tag{28}$$

in which iron carbonate solubility limit K_{sp} is a function of temperature (T) in Kelvin and ionic strength (I) in mol/L, which was developed and discussed in Chapter 2, as follows:

$$\log\left[K_{sp}\right] = -59.3498 - 0.041377\ T - \frac{2.1963}{T} + 24.5724\ \log\left(T\right) + 2.518\ I^{0.5} - 0.657\ I \tag{16}$$

The kinetic constant k_r was derived from the experimental scale retention rates via the scale retention rate equation and the Arrhenius's law with temperature. The results were fitted according to Arrhenius equation Equation (29), as shown in Figure 23:

$$k_r = e^{A-\frac{B}{RT}} \tag{29}$$

with constants of A = 28.22 and B = 64851.4 J/mol. The results are compared with the kinetics constants and scale retention expressions provided by Johnson and Tomson[20], and van Hunnik, *et al.*[21] using different scale retention rate measurements, as shown in Table 3. It is observed that there is a significant difference between the literature and the present result. The scale retention rate *versus* supersaturations at T=80^{o}C using different scale retention rate equations as well as the experimental results obtained by the weight change method is shown in Figure 24. As expected, with the increase of supersaturation, the scale retention rates predicted by various equations increase. However, the calculated scale retention rates using Johnson and Tomson[20] and van Hunnik *et al.*[21] over-predicted the magnitude of the scale retention rate by a large margin (factor 10-100). More experimental data at different temperatures and supersaturations were compared with the calculated results. It has been found that the scale retention rate predicted by the present equation is in good agreement with the experimental results (Figure 25).

Table 3. Scale retention rate constants A and B provided by different authors

Authors	Equations	Constants
Johnson and Tomson [20]	$SRR\left(\frac{mol}{m^3 \cdot s}\right) = e^{A-\frac{B}{RT}} \frac{S}{V} K_{sp} \left\{(SS)^{0.5} - 1\right\}^2$	A 56.3 B 127.3
van Hunnik et al. [21]	$SRR\left(\frac{mol}{m^3 \cdot s}\right) = e^{A-\frac{B}{RT}} \frac{S}{V} K_{sp} (SS-1)\left(1 - SS^{-1}\right)$	A 52.4 B 119.8
The present work	$SRR\left(\frac{mol}{m^3 \cdot s}\right) = e^{A-\frac{B}{RT}} \frac{S}{V} K_{sp} (SS-1)$ or $SRR\left(\frac{mol}{m^2 \cdot s}\right) = e^{A-\frac{B}{RT}} K_{sp} (SS-1)$	A 28.2 B 64.85

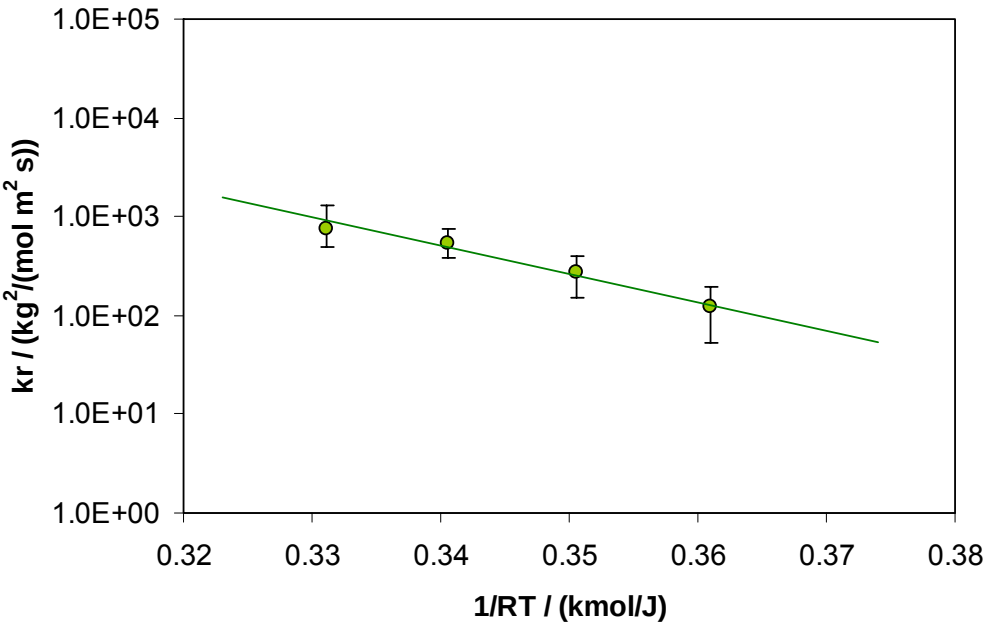

Figure 23. Fitted scale retention rate constant vs. inverse of temperature. The error bars represent the maximum and minimum kinetics constants.

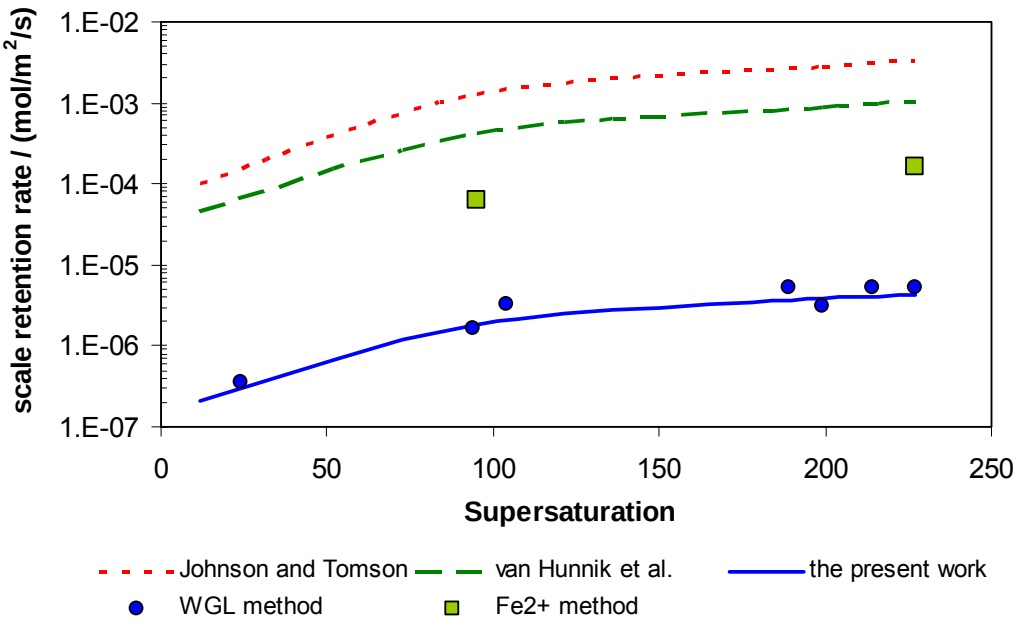

Figure 24. The comparison of the experimental scale retention rate by weight change method and the calculated scale retention rate using kinetics expressions given by Johnson and Tomson[20], van Hunnik *et al.*[21], and the present expression, under supersaturations of 24 to 250 and T=80°C.

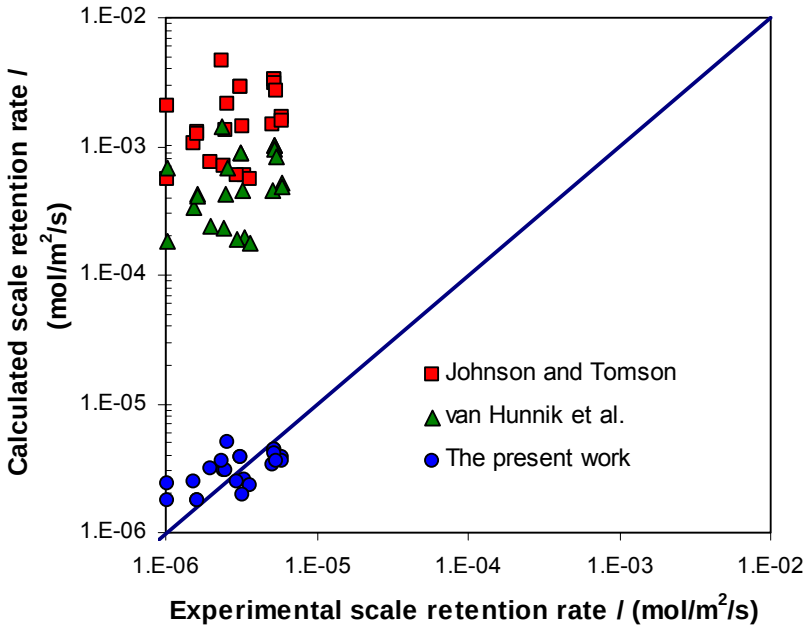

Figure 25. The comparison of the experimental scale retention rate and the calculated scale retention rate using different kinetics expressions.

3.6 Summary

The results presented in this section demonstrate that

1. The calculated results obtained by the previous kinetics expressions using the traditional dissolved ferrous ion concentration method overestimate the scale retention rate of iron carbonate on the steel surface by a large margin.
2. The source of ferrous ions forming iron carbonate scale includes ferrous ions both released from the steel surface and those provided by the bulk of the solution.
3. The scale retention rate of iron carbonate is directly related to corrosion and the conditions at the steel surface. At low supersaturation, the scale retention rate of iron carbonate scale is strongly affected by the corrosion rate of the steel. At high supersaturation, the corrosion rate has little effect on the scale retention rate of iron carbonate.
4. A reliable scale retention rate expression for engineering application is developed in this study to predict iron carbonate scale growth. As expected the scale retention rate expression is a function of supersaturation and temperature.

Chapter 4: Thermodynamic study of hydrogen sulfide and iron sulfide at elevated temperatures

4.1 Introduction

In Chapter 2 and Chapter 3, the thermodynamics of iron carbonate as well as the kinetics of scale growth has been investigated in pure CO_2 corrosion. Comparing to iron carbonate scale formed in pure CO_2 corrosion, many types of iron sulfides may form as the corrosion products in H_2S corrosion, such as amorphous ferrous sulphide (FeS), mackinawite ($Fe_{1+x}S$), cubic ferrous sulfide (FeS), smythite ($Fe_{3+x}S_4$), greigite (Fe_3S_4), pyrrhotite ($Fe_{1-x}S$), troilite (FeS), and pyrite (FeS_2), which have different crystal structures, oxidation states, and stoichiometries of Fe and S [22-26]. In order to understand the protectiveness of iron sulfide scale formation in H_2S environment, and to further study the kinetics and mechanism of scale formation, it is important to have a reliable understanding of the thermodynamics of hydrogen sulfide and iron sulfide systems.

The equilibrium constants of hydrogen sulfide and iron sulfide systems have been investigated in various research fields, such as geology, oceanography, sedimentology, water treatment, and corrosion.[22, 77-81] However, there is a significant difference between the existing dissociation constants of hydrogen sulfide and the solubility limits of iron sulfides. Therefore, the objective of this chapter was to evaluate the literature values of the solubility limits for hydrogen sulfide and iron sulfides as well as to determine the reliable solubility limits for studying the kinetics of scale formation.

4.2 Literature review

The work on the thermodynamics of hydrogen sulfide and iron sulfide systems previously reported in the literature can be divided into two groups:

1. The solubility constant (K_{H_2S}) and dissociation constants (K_1 and K_2) of hydrogen sulfide;
2. The solubility limits of iron sulfides (mackinawite $Fe_{1+x}S$, amorphous iron sulfide FeS, pyrrhotite $Fe_{1-x}S$, greigite Fe_3S_4, and pyrite FeS_2).

4.2.1 Hydrogen sulfide

When hydrogen sulfide dissolves in the water solution, the vapor-liquid equilibrium of hydrogen sulfide is described as:

$$H_2S_{(g)} \overset{K_{H_2S}}{\Leftrightarrow} H_2S_{(aq)} \tag{30}$$

Then we have the dissociation of hydrogen sulfide and dissociation of HS^- ion:

$$H_2S_{(aq)} \overset{K_1}{\Leftrightarrow} H^+_{(aq)} + HS^-_{(aq)} \tag{31}$$

$$HS^-_{(aq)} \overset{K_2}{\Leftrightarrow} H^+_{(aq)} + S^{2-}_{(aq)} \tag{32}$$

A number of researchers have investigated the thermodynamics of the hydrogen sulfide system by conducting experiments or using theoretical thermodynamic models, in order to calculate the concentrations of sulfide species. The hydrogen sulfide equilibrium constant equations of K_{H_2S} provided by various researchers are shown in Table 4. Weiss[81] proposed an equation to predict the hydrogen sulfide solubility constant K_{H_2S}, which fits the extensive measurements conducted by Douabul and Riley[82]. Several

authors later proposed more equations to predict K_{H_2S}, in which K_{H_2S} is a function of temperature.

Table 4. Equilibrium constants of K_{H_2S} in hydrogen sulfide systems

Constants	Equations	References
K_{H_2S}	$K_{H_2S} = e^{-41.0563+66.4005\left(\frac{100}{T_K}\right)+15.1060\ln\left(\frac{T_K}{100}\right)}$	Weiss[81], 1970
	$K_{H_2S} = 10^{-\frac{3898.56}{T_K}-12.4914\,ln\,T_K+0.00831109\,T_K+82.7622}$	Roberts[83], 1985
	$K_{H_2S} = \frac{10}{e^{-3.3747+0.072437\,T_K-1.10765\times10^{-4}T_K^2-\frac{1549.159}{T_K}+0.144237\,ln\,T_K}}$	Carroll & Mather [84], 1989
	$K_{H_2S} = 10^{-\left(634.27+0.2709T_K-0.11132*10^{-3}T_K^2-\frac{16719}{T_K}-261.9\,log\,T_K\right)}$	Suleimenov & Krupp [85], 1994
	$K_{H_2S} = 10^{-0.71742672-0.012145427\,T_C+5.6659982\times10^{-5}T_C^2-8.1902716\times10^{-8}T_C^3}$	Nordsveen et al [16]. (based on IUPAC[64]), 2003

A quantity of values of the first dissociation constant K_1 at room temperature are proposed by different authors and shown in Table 5, with an average of K_1 = 9.632×10^{-8}, the maximum error of 1.333×10^{-8}, and the minimum error of 3.878×10^{-8}. Several equations were developed to calculate the first dissociation constant at different temperatures, as shown in Table 6, among which the equation proposed by Suleimenov and Seward [86] is widely employed by the other researchers to calculate the sulfide species in the hydrogen sulfide system.

Table 5. Values of the first dissociation constant K_1 of H_2S in water at 25°C.

K_1	References	K_1	References
1.000×10^{-8}	Flaschka, et al. [87], 1980	1.000×10^{-7}	Goates et al. [100], 1952
5.754×10^{-8}	Day and Underwood [88], 1991		Pecsok, et al. [101], 1968
8.511×10^{-8}	Tumanova et al. [89], 1957		Kolthoff [102], 1969
8.711×10^{8}	Loy and Himmelblau [90], 1961		Ellis and Giggenbach [103], 1971
8.913×10^{8}	Ringborn [91], 1953		Skoog and West [104], 1982
	Kubli [92], 1946	1.023×10^{-7}	Kubli [92], 1946
	Su, et al. [93], 1997		Konopik and Leberl [105], 1949
9.124×10^{8}	Bruner and Zawadzki [94], 1909		Pohl [106], 1962
	Thiel and Gessner [95], 1914		Blackbarn [107], 1969
	Swift and Butler [96], 1972	1.047×10^{-7}	Khodakovskii et al. [108], 1965
	Weast [97], 1991		Berner [22], 1967
9.551×10^{8}	Ellis and Golding [98], 1959		Goldhaber and Kaplan [109], 1975
	Harris [99], 1995	1.071×10^{-7}	Wright and Maass [110], 1932
			Kapustinskii [111], 1940
		1.096×10^{-7}	Latimer [112], 1952
Average:	9.632×10^{-8}		
E_{max}	1.333×10^{-8}	E_{min}	3.878×10^{-8}

Table 6. The first dissociation constant K_1 of hydrogen sulfide at different temperatures

Constants	Equations	References
K_1	$K_1 = 10^{\frac{32216.8}{T_K}+97.7734\ln T_K-0.097611T_K-\frac{2.17087\times10^6}{T_K^2}-586.682}$	Barbero, et al. [113], 1982
	$K_1 = 10^{-\left(32.55+\frac{1519.44}{T_K}-15.672\log T_K-0.02722T_K\right)}$	Millero [114], 1986
	$K_1 = 10^{-\left(15.345-0.045676T_K+5.9666\times10^{-5}T_K^2\right)}$	Kharaka, et al.[115], 1989
	$K_1 = 10^{782.43945+0.361261T_K-1.6722\times10^{-4}T_K^2-\frac{20565.7315}{T_K}-142.741722\ln T_K}$	Suleimenvo & Seward [86], 1997

The values of the second dissociation constant K_2 at room temperature are shown in Table 7. It is noted that there are seven orders of magnitude disagreement, varying widely from 1.148×10^{-12} to 1.000×10^{-19}. Table 8 shows the equations which are used to calculate the second dissociation constant K_2.

Table 7. Value of the second dissociation constant K_2 at room temperature (20°C ~ 30°C)

K_2	**References**	K_2	**References**
1.000×10^{-19}	Myers [116], 1967	1.202×10^{-14}	Flaschka, et al. [87], 1980
6.310×10^{-18}	Yagil [117], 1967	1.259×10^{-14}	Harris [99], 1995
1.000×10^{-17}	Ellis and Giggenbach [103], 1971	1.413×10^{-14}	Muhammad and Sundarahm [122], 1961
1.000×10^{-16}	Licht, et al. [118], 1990	1.660×10^{-14}	Maronny [123], 1959
1.000×10^{-15}	Skoog and West [104], 1982	7.943×10^{-14}	Konopik and Leberl [105], 1949
1.202×10^{-15}	Knox [119], 1906	1.202×10^{-13}	Kolthoff, et al. [102], 1969
	Swift and Butler [96], 1972	1.288×10^{-13}	Blackbarn [107], 1969
	Day and Underwook [88], 1991	3.631×10^{-13}	Kubli [92], 1946
7.079×10^{-15}	Widmer and Schwarzenbach [120], 1964	1.000×10^{-12}	Su, et al. [93], 1997
1.000×10^{-14}	Ellis and Golding [98], 1959	1.148×10^{-12}	Weast [97], 1991
	Ellis and Milestone [121], 1967		
	Pecsok, et al. [101], 1968		
Average:	1.335×10^{-13}		
E_{max}	1.015×10^{-12}	E_{min}	1.335×10^{-13}

Table 8. The second dissociation constant K_2 of H_2S at different temperatures.

Constants	**Equations**	**References**
K_2	$K_2 = 10^{\frac{31286}{T_K}+94.9734 ln T_K - 0.097611 T_K - \frac{2.17087\times10^6}{T_K^2} - 607.722}$	Derived from Giggenbach [124], 1971
	$K_2 = 10^{-\left(23.93 - 0.030446 T_K + 2.4831\times10^{-5} T_K^2\right)}$	Kharaka, et al. [115], 1989
	$K_2 = 10^{(0.1333 T_C - 43.4)}$	Derived from Migdisov, et al. [125], 2002

4.2.2 Iron sulfides

In H_2S corrosion, many types of iron sulfides[23, 24] may form as the corrosion products such as amorphous iron sulfide, mackinawite, cubic iron sulfide, troilite, and pyrite. Two types of expressions are currently employed to describe the iron sulfides solubility limits: "[HS^-] based expressions" and "[S^{2-}] based expressions", as shown in Table 9. [HS^-] based expression is a function of the concentrations of Fe^{2+}, HS^-, and H^+; and [S^{2-}] based expressions is a function of the concentrations of Fe^{2+} and S^{2-}. The solubility limits of different iron sulfides at room temperature using both expressions are shown in Table 10. It is noted that using two different expressions leads to a significant difference of the calculated solubility limits. Therefore, it is meaningless to compare the solubility limits using different expressions. It is believed here that [HS^-] based expressions are more accurate because of the inaccurate prediction of S^{2-} concentration.

Table 9. Two types of expressions for the solubility limits of iron sulfides.

Iron sulfide	**[HS^-] based expressions**	**[S^{2-}] based expressions**
Amorphous FeS	$\frac{[Fe^{2+}][HS^-]}{[H^+]}$	$[Fe^{2+}][S^{2-}]$
Mackinawite	$\frac{[Fe^{2+}][HS^-]}{[H^+]}$	$[Fe^{2+}][S^{2-}]$

Table 10. The solubility limits of iron sulfides at room temperature provided by different authors.

Iron sulfide	HS^- based expression	S^{2-} based expression	References
amorphous FeS		1.36×10^{-17}	Berner [22], 1967
	1.14×10^{-3}		Morse et al. [126], 1987
mackinawite		2.83×10^{-18}	Berner [22], 1967
	2.86×10^{-4}		Morse et al. [126], 1987
	1.50×10^{-4}		Benning et al. [127], 2000
pyrrhotite	1.32×10^{-19}		Berner [22], 1967

A number of researchers studied the solubility of iron sulfides at room temperature; however, few studies have been done on the solubility of iron sulfides as a function of temperature. The solubility of mackinawite at different temperatures was investigated by Benning *et al.* [127]. He proposed an equation to calculate the solubility of mackinawite as a function of temperature. In his equation (33), the solubility of mackinawite is expressed as an equilibrium constant for the reaction (34):

$$K_{FeS} = \frac{K_{eq,FeS}}{\left(K_{1,H_2S}\right)^2} \tag{33}$$

$$FeS_{(s)} + 2H^+_{(aq)} \Leftrightarrow Fe^{2+}_{(aq)} + H_2S_{(aq)} \tag{34}$$

$$FeS_{(s)} + H_2S_{(aq)} \Leftrightarrow Fe^{2+}_{(aq)} + 2HS^-_{(aq)} \tag{35}$$

where K_{FeS} is the equilibrium constant of reaction (34). $K_{eq,FeS}$ is the equilibrium constant of the reaction (35), in $(mol/L)^2$. K_{1,H_2S} is the first dissociation constant of H_2S, in mol/L.

$K_{eq,FeS}$ is expressed as:

$$K_{eq,FeS} = \frac{\left(\alpha_{HS^-}\right)^2 \alpha_{Fe^{2+}}}{\alpha_{H_2S}} \tag{36}$$

where α_{HS^-} is the activity of HS^-, in mol/L

$\alpha_{Fe^{2+}}$ is the activity of Fe^{2+}, in mol/L

α_{H_2S} is the activity of aqueous H_2S, in mol/L

and K_{1,H_2S} is expressed as

$$K_{1,H_2S} = \frac{\alpha_{HS^-}\alpha_{H^+}}{\alpha_{H_2S}} \tag{37}$$

where α_{H^+} is the activity of H^+, in mol/L

K_{1,H_2S} is suggested to be obtained using the equation for the first dissociation constant of H_2S by Suleimenov and Seward[86] (in Table 6).

Based on Benning's equation, an HS^- based expression (38) is deduced here to predict the solubility limit of mackinawite.

$$K_{sp} = 10^{\frac{2848.779}{T_k} - 6.347 + log\left(K_{1,H_2S}\right)} \tag{38}$$

The prediction of K_{sp} at room temperature using equation (38) is in good agreement with the K_{sp} provided by other researchers[126], as shown in Table 10.

The solubility limits of amorphous iron sulfide and pyrite were determined by Helgeson[63] in the temperature range from 25°C to 300°C using the van't Hoff equation (39):

$$\frac{d\ ln\ K_{sp}}{dT} = \frac{\Delta H}{RT^2} \tag{39}$$

then integrated equation (39) to obtain:

$$log\, K_{sp} = log\, K_{298.15} - \frac{\Delta H^0}{2.303R}\left(\frac{1}{T_k} - \frac{1}{298.15}\right) - \frac{1}{2.303RT_k}\int_{298.15}^{T_k}\Delta C dT_k + \frac{1}{2.303RT_k}\int_{298.15}^{T_k}\Delta C d\, ln\, T_k \quad (40)$$

where T_k is the temperature in Kelvin

R is the gas constant (8.3145 J/mol/K)

ΔH^0 is the standard enthalpy of reaction in J/mol

ΔC is the standard heat capacity of reaction in J/mol/K

The average heat capacities were employed to estimate the value of ΔC because the required heat capacity functions are not available. The prediction solubility limits of amorphous iron sulfide and pyrite provided by Helgeson[63] at different temperature are shown in Table 11.

Table 11. The solubility limits of amorphous iron sulfide and pyrite at different temperatures provided by Helgeson[63].

Iron sulfides	**Temperature / ^{o}C**			
	25	50	60	100
amorphous FeS	1.29×10^{-19}	6.76×10^{-19}	1.10×10^{-18}	7.59×10^{-18}
pyrite	7.08×10^{-37}	3.16×10^{-34}	1.82×10^{-33}	6.76×10^{-31}

4.3 Results and discussion

In the following, the equations for hydrogen sulfide solubility constant (K_{H_2S}) and dissociation constants (K_1 and K_2) and the solubility limits of iron sulfides (K_{FeS_x}) will be evaluated.

4.3.1 The solubility constant of hydrogen sulfide (K_{H_2S})

As it was mentioned above, five equations were proposed to predict the solubility constant of hydrogen sulfide, as shown in Table 4. It has been reported that Weiss[81] developed the equation to predict the hydrogen sulfide solubility constant K_{H_2S}, which fits the extensive measurements conducted by Douabul and Riley[82]. Figure 26 shows that the predictions using the other four equations are in good agreement with the results predicted by the Weiss equation, except that the results by the Carroll equation[84] are higher than the others. Therefore, it is suggested that all the equations except the Carroll equation could be used to calculate the solubility constant of hydrogen sulfide.

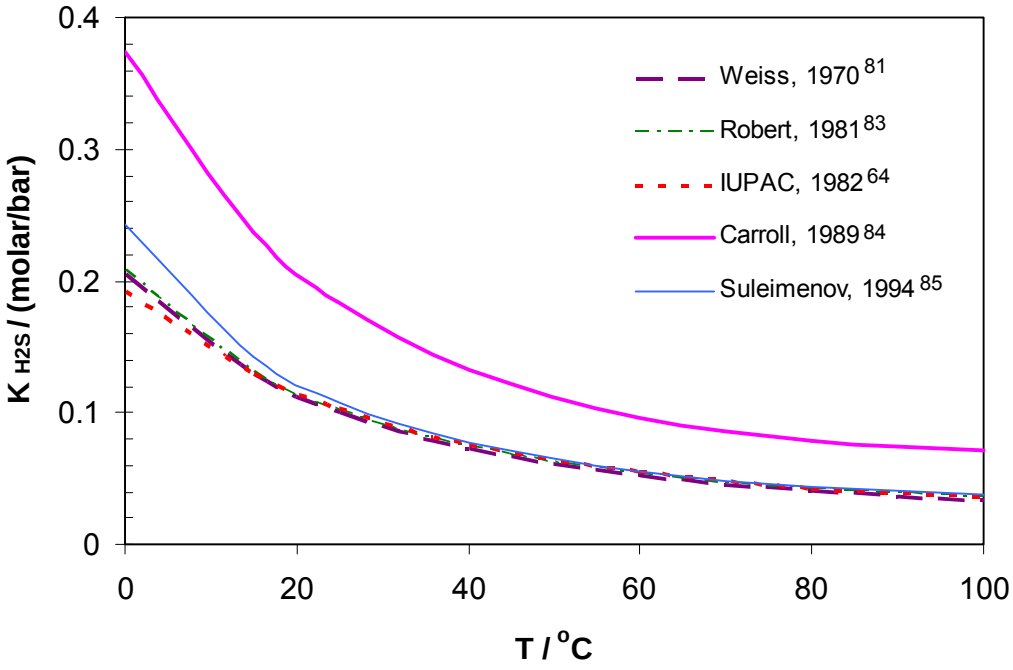

Figure 26. The comparison of hydrogen sulfide solubility K_{H_2S} predictions using different models.

4.3.2 The first dissociation constant of hydrogen sulfide (K_1)

The comparison of both the calculated and experimental first dissociation constant K_1 values at different temperatures is shown in Figure 27. It is found that all the calculated values of the first dissociation constant K_1 agree well with experimental results.

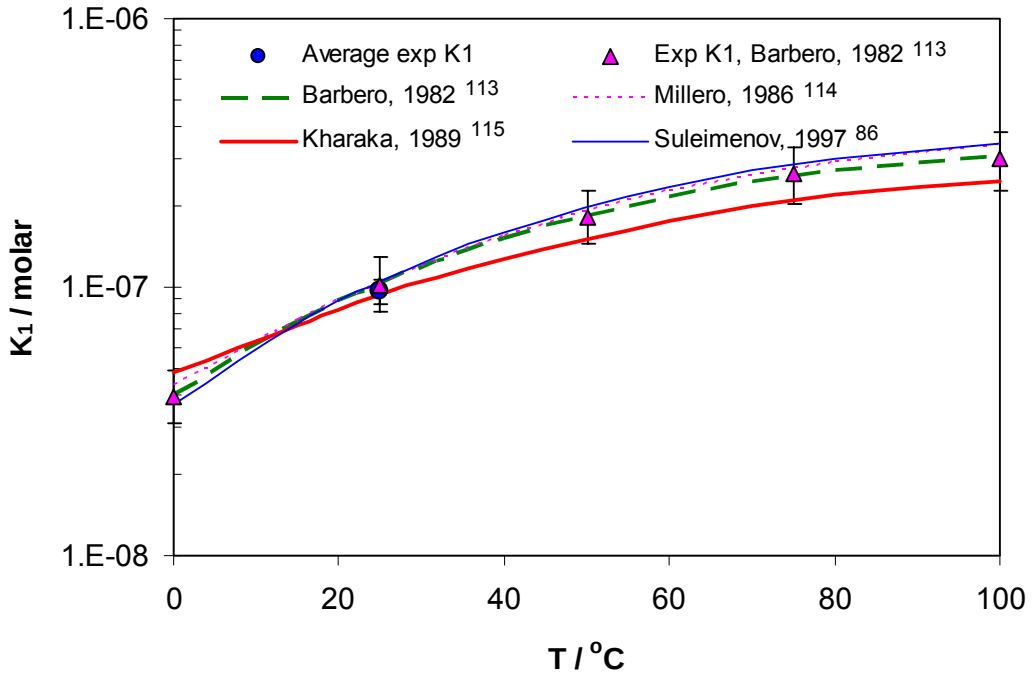

Figure 27. The comparison of experimental results and predictions of the first dissociation constants K_1 using different models.

4.3.3 The second dissociation constant of hydrogen sulfide (K_2)

The second dissociation constant K_2 at different temperatures is calculated using three different equations and shown in Figure 28. It has been found that there is no agreement for the second dissociation constant among different authors. Moreover, there is up to a seven orders of magnitude difference for the second dissociation constant at

room temperature provided by different authors. It is suggested that the researchers should avoid using the second dissociation constant to calculate the concentration of species and further to predict the solubility limit of iron sulfides.

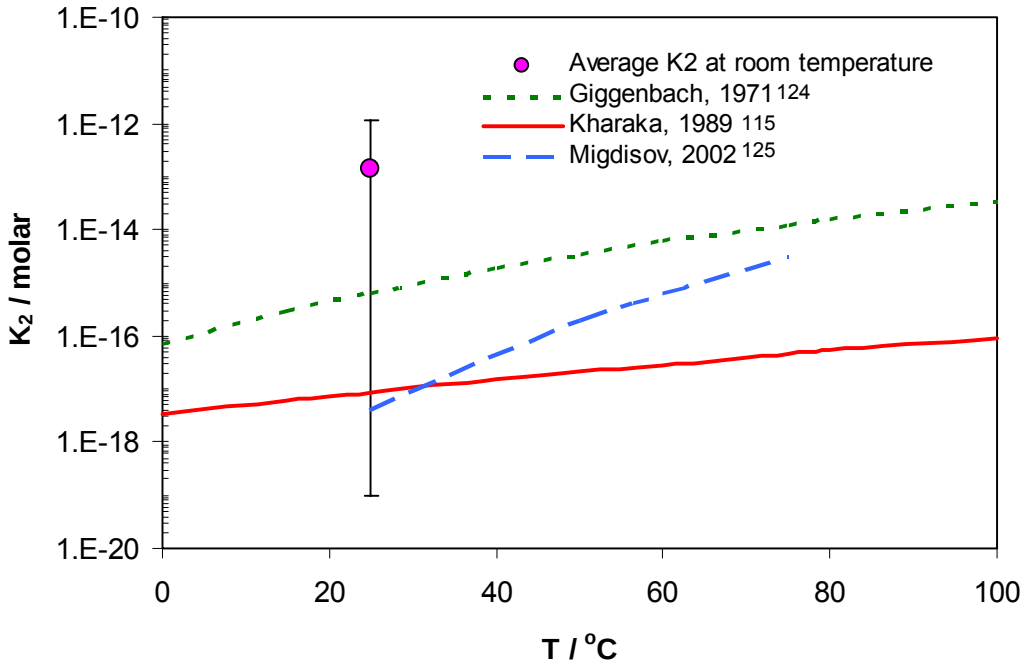

Figure 28. The comparison of predictions of the second dissociation constant K_2 using different models.

4.3.4 The solubility limit of mackinawite ($K_{sp,mck}$)

The solubility limit of mackinawite at room temperature has been investigated by several authors, as shown in Table 10. The solubility limit equation of mackinawite derived from Benning *et al.* [127] mackinawite solubility expression (38) is the only equation to predict the solubility limit of mackinawite as a function of temperature. Since it is meaningless to compare the solubility limits directly using different expressions, supersaturation is used here to investigate the accuracy of the two K_{sp} expressions.

$$SS = \frac{\frac{c_{Fe^{2+}} c_{HS^-}}{c_{H^+}}}{K_{sp,mck,HS^-}} \quad (41)$$

or $$SS = \frac{c_{Fe^{2+}} c_{S^{2-}}}{K_{sp,mck,S^{2-}}} \quad (42)$$

An example of the supersaturation of mackinawite under the conditions of T 25°C, pH 6, H_2S 1000 ppm, and Fe^{2+} 10 ppm is calculated using the three values provided by different authors (Figure 29). It is found that the results are in a reasonable agreement.

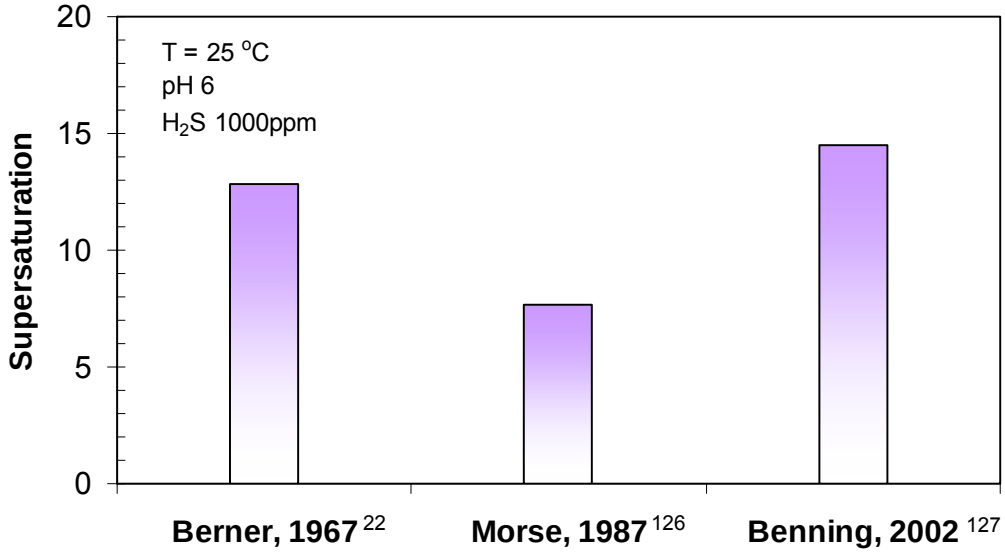

Figure 29. The supersaturation of mackinawite under the conditions of T=25°C, pH 6, H_2S 1000 ppm, and Fe^{2+} 10 ppm using three values provided by different authors.

It should be noted here that Benning *et al.* [127] selected the solubility constant and the first dissociation constant of hydrogen sulfide from Suleimenov[85, 86]. In order to be consistent, the following equations from Suleimenov[85, 86] are suggested to calculate the solubility limits of hydrogen sulfide:

$$K_{H_2S} = 10^{-\left(634.27+0.2709T_K-0.11132*10^{-3}T_K^2-\frac{16719}{T_K}-261.9\log T_K\right)} \quad (43)^{85}$$

$$K_1 = 10^{782.43945+0.361261T_K-1.6722\times10^{-4}T_K^2-\frac{20565.7315}{T_K}-142.741722\ln T_K} \quad (44)^{86}$$

4.3.5 The solubility limit of amorphous iron sulfide ($K_{sp,FeS}$)

Both the calculated solubility limits of amorphous iron sulfide at the temperature of 25°C to 100°C provided by Helgeson[63] and the experimental K_{sp} at room temperature are shown in Figure 30. The results show that there is a significant difference between the calculations and the experimental results. Use of this expression would be uncertain without further verification.

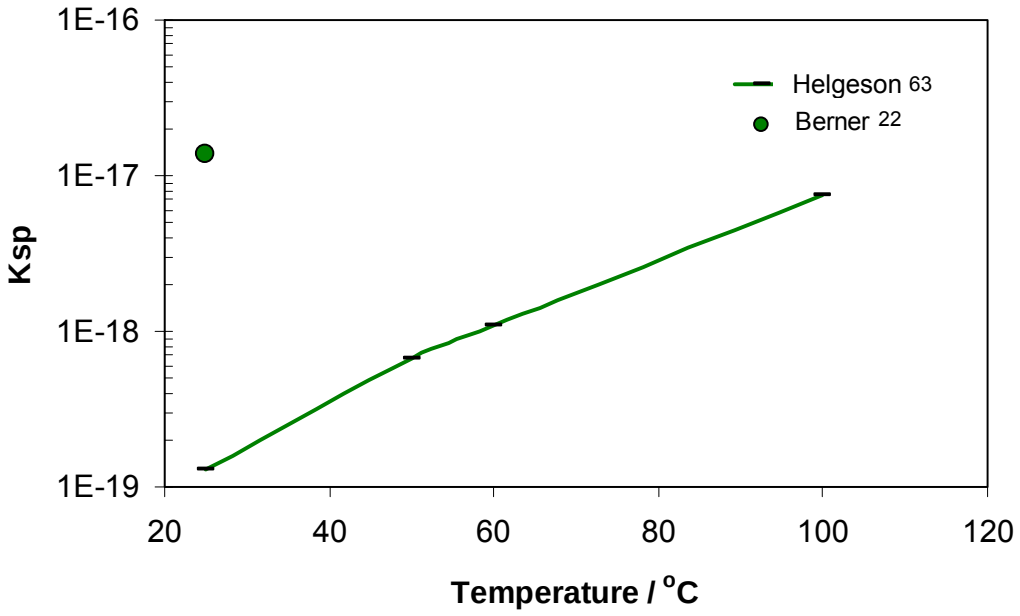

Figure 30. The comparison of K_{sp} of amorphous iron sulfide at room temperature provided by Berner[22] and the calculated K_{sp} at different temperatures by Helgeson[63].

4.3.6 The solubility limit of pyrite (K_{sp,FeS_2})

Both the calculated solubility limits of pyrite at the temperature of 25°C to 100°C and the experimental K_{sp} at room temperature are shown in Figure 31. The results show that there is a significant difference between the calculations and the experimental results and the use of this expression is questionable without further verification.

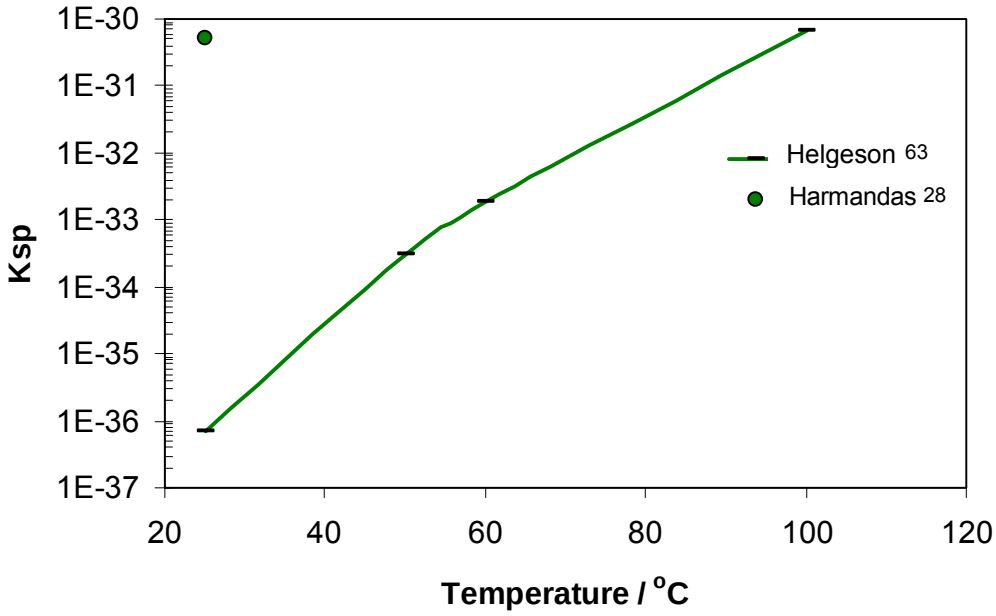

Figure 31. The comparison of K_{sp} of pyrite at room temperature provided by Harmandas[28] and the calculated K_{sp} at different temperatures by Helgeson[63].

4.4 Summary

From what was discussed above, it can been concluded that the following equations could be reliably used to study the solubility limits of hydrogen sulfide and mackinawite:

$$K_{H_2S} = 10^{-\left(634.27+0.2709T_K-0.11132*10^{-3}T_K^2-\frac{16719}{T_K}-261.9\,log\,T_K\right)} \quad (43)^{85}$$

$$K_1 = 10^{782.43945+0.361261T_K-1.6722\times10^{-4}T_K^2-\frac{20565.7315}{T_K}-142.741722\,ln\,T_K} \quad (44)^{86}$$

$$K_{sp,mck} = 10^{\frac{2848.779}{T} - 6.347 + log(K_1)} \quad (38)^{127}$$

For amorphous iron sulfide, pyrite and other forms of FeS, the published data are very inconsistent and not much can be utilized directly.

Chapter 5: The mechanism and kinetics of iron sulfide scale formation in H_2S environment

5.1 Introduction

Kinetics of iron carbonate scale formation in pure CO_2 corrosion has been investigated in Chapter 3, and a new iron carbonate scale formation model is developed to predict the kinetics of iron carbonate scale growth. In this chapter, the formation of iron sulfide scale in pure H_2S environment will be studied in order to further investigate the mixed iron carbonate and iron sulfide scale formation in CO_2/H_2S corrosion.

As mentioned before, compared to iron carbonate formation in pure CO_2 corrosion, many types of iron sulfide may form in H_2S environment. The iron sulfide scale growth depends primarily on the kinetics of the scale formation. However, the complicated mechanisms of iron sulfides formation make it difficult to quantify the kinetics of iron sulfide formation. Therefore, an understanding of the mechanism and kinetics of iron sulfide scale formation in H_2S environment is needed.

5.2 Literature review

5.2.1 The mechanism of iron sulfide scale formation in H_2S environment

A review paper of CO_2/H_2S corrosion in oilfield environments by Smith and Joosten[5] systematically describes most of the research work done in this area. It is mentioned that much of the literature is still confusing and somewhat contradictory and the mechanism of CO_2/H_2S corrosion is still unclear. The mechanism of iron sulfide scale formation in H_2S corrosion was reviewed by Lee in his recent PhD dissertation[128]. In the

following, the current understanding of the mechanisms of iron sulfide scale formation will be briefly summarized.

Meyer *et al.*[2] observed that in the saturated hydrogen sulfide solutions, a porous mackinawite layer was followed by a mackinawite scale on the steel surface, and subsequently changed to pyrrhotite and pyrite.

Shoesmith *et al.*[25, 26] systematically investigated the nature of iron sulfides formed on the steel exposed to the saturated H_2S solution at room temperature (Figure 32) and proposed that a mackinawite layer initially formed on the steel surface by a solid-state reaction and then cracked easily. When more ferrous ions were released from the steel surface, cubic ferrous sulfide and troilite precipitated on the steel surface because of high local supersaturation of iron sulfide. If oxygen was involved in the system, it may form thiospinel greigite on the steel surface. At very high concentration of H_2S, pyrrhotite, marcasite, and pyrite may form on the steel surface.

Benning *et al.* [127] conducted experiments and reported that mackinawite was stable in four months in the reduced sulfur solutions at low temperature and the formation rate of pyrite from a precursor mackinawite below 100^{o}C is insignificant in the solutions of low H_2S concentration. The conversion of mackinawite to pyrite was a multi-step reaction process involving changes in aqueous sulfur species causing solid-state transformation of mackinawite to pyrite via the intermediate greigite.

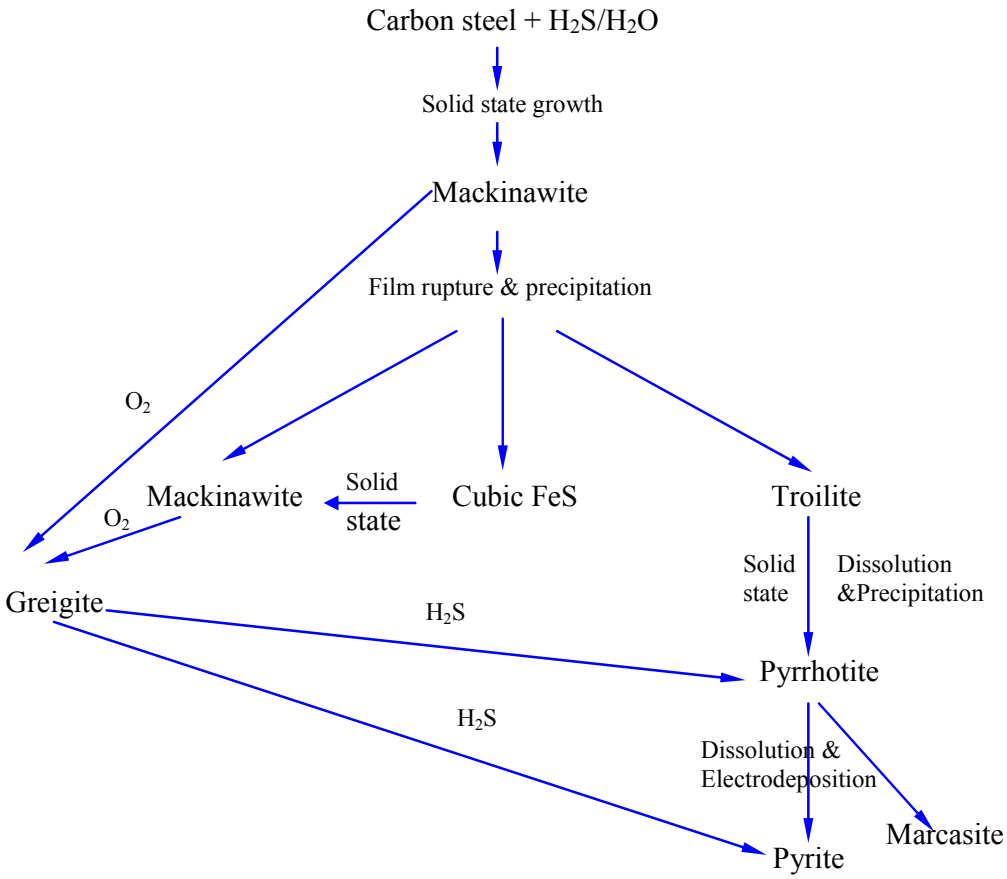

Figure 32. Corrosion sequence for carbon steel in aqueous H_2S solution[25, 26]

Anderko and coworkers [8-10] developed a Pourbaix $E - pH$ diagram for the multi-component and non-ideal aqueous iron sulfide solution to predict the stability of various iron sulfide species under different conditions. The diagram indicated that the formation of iron monosulfide followed a sequence of $Fe(HS)^+$, amorphous ferrous sulfide, mackinawite, and pyrrhotite. Iron monosulfides transform to pyrite most likely through greigite and marcasite, as illustrated in Figure 33. Their predictions were in agreement with the experimental data on iron sulfide formation in H_2S solution.

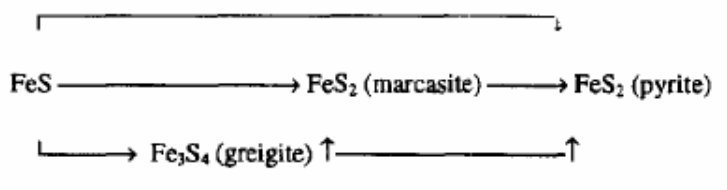

Figure 33. The reaction sequence for steel in the H_2S solution[8].

Smith *et al.*[6, 7, 12] proposed a model to predict the corrosion products at different H_2S concentrations and temperature in CO_2/H_2S solution and reported that mackinawite was the predominant species at low H_2S concentration and temperature. With the increase of H_2S concentration, mackinawite might be substituted by pyrrhotite and then pyrite. It was also suggested in their paper that the thermodynamics favored either pyrrhotite or pyrite as the corrosion products; however, the rapid kinetics of mackinawite formation made it as the initial corrosion product. Based on the literature[23, 129], the authors proposed two mechanisms of H_2S corrosion (Figure 34), the latter of which is more preferable and described as follows:

1. H_2S diffuses to the steel surface,
2. H_2S reacts with the steel to form mackinawite scale on the surface,
3. Mackinawite scale dissolves to $Fe(HS)^+$ and HS^-,
4. $Fe(HS)^+$ diffuses away from the steel surface, and
5. More H_2S diffuses to react with the exposed steel.

This corrosion process keeps producing very thin "tarnish" of mackinawite layer which continually forms and dissolves. Smith *et al.*[6,7,12] proposed this explanation for mackinawite formation and defined the boundary conditions between the mackinawite corrosion product region and the other corrosion products, as shown in Figure 35. However, in their papers the transition boundary conditions were not reported.

Path 1:

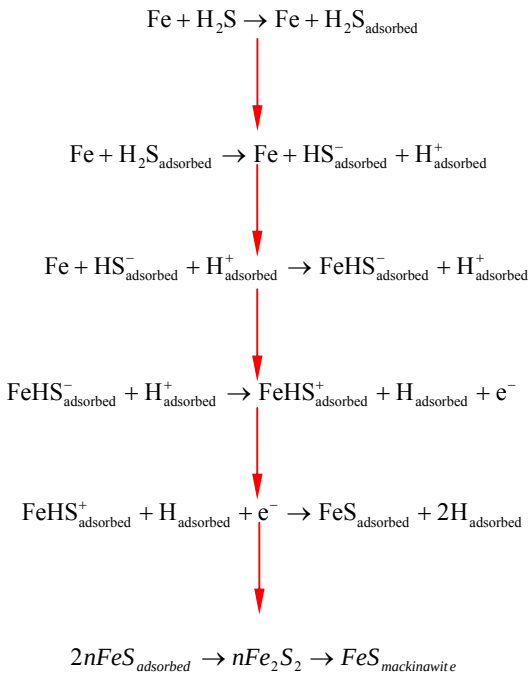

Path 2:

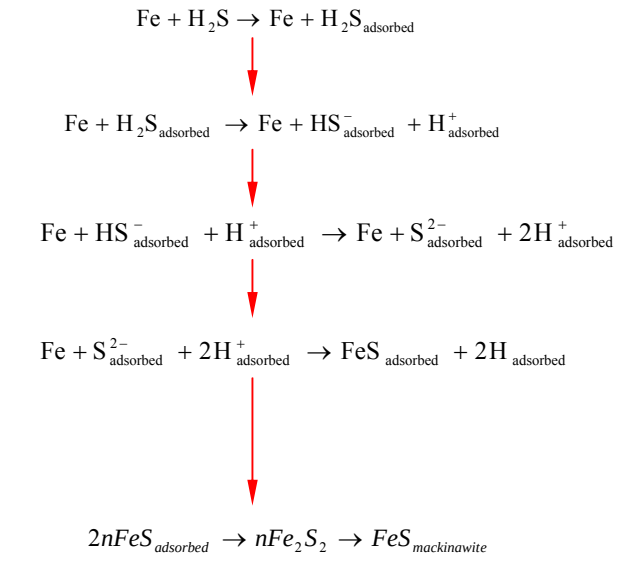

Figure 34. Two mechanisms for H_2S corrosion[7]. After the initial adsorption of H_2S on the steel surface, mackinawite can be formed from amorphous FeS either by Path 1 or Path 2.

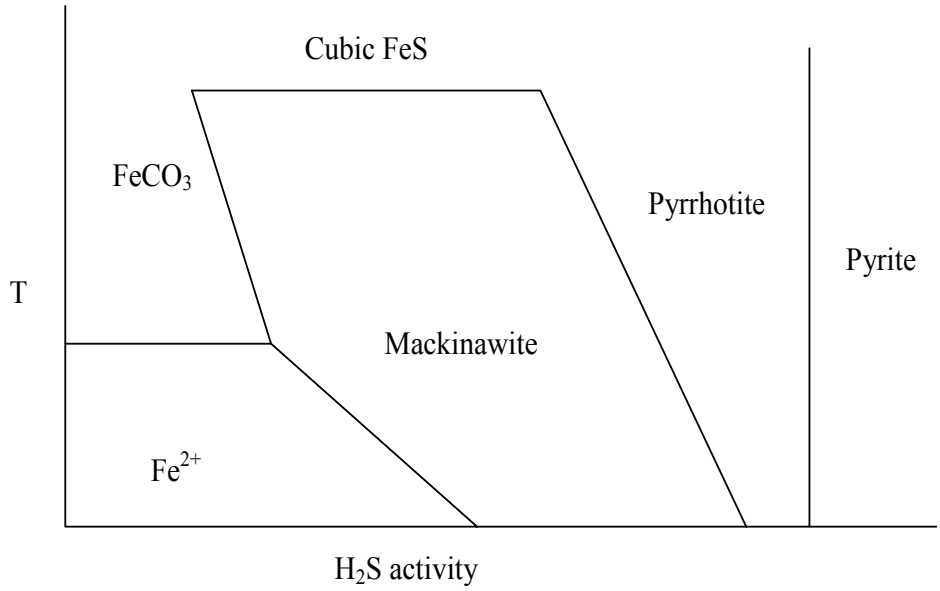

Figure 35. Corrosion product relationships in CO_2/H_2S solutions[12]

5.2.2 The kinetics of iron sulfide scale formation in H_2S environment

As mentioned several times, many types of iron sulfides may form in H_2S environments, such as amorphous ferrous sulfide, mackinawite, cubic ferrous sulfide, smythite, greigite, pyrrhotite, troilite, and pyrite. Among those iron sulfides, it has been known that mackinawite is the prevalent iron sulfide formed on the steel surface and usually forms as a precursor to other types of sulfides and therefore needs to be quantified first.

Rickard[27] investigated the kinetics of FeS precipitation and described FeS precipitation rate as a function of Fe^{2+} concentration and hydrogen sulfide concentration.

$$\frac{d[FeS]}{dt} = k a_{Fe^{2+}} \, a_{H_2S} \tag{45}$$

In the paper, Rickard did not mention whether FeS is amorphous iron sulfide or mackinawite. However, it has been mentioned in his previous paper[80] that the precipitated iron sulfide formed in the solution was amorphous iron sulfide with a broad peak equivalent to the strong basal reflection of mackinawite and it may take two years to form the well crystalline mackinawite at room temperature under the test conditions. Therefore, it has been estimated that FeS formed in the solution might be amorphous iron sulfide or very small mackinawite crystals (nano-sized).

Harmandas and Koutsoukos[28] investigated the formation of iron sulfides in aqueous solutions and proposed the expression (46) to describe the kinetics of both amorphous iron sulfide and mackinawite formation.

$$R_P = k\sigma_S^m \tag{46}$$

where k is the rate constant, σ_S is the relative solution supersaturation with respect to the solid phase forming, and m is the apparent order of the reaction.

It should be noted that both expressions provided by Rickard[27] and Harmandas and Koutsoukos[28] were obtained by using ferrous ion concentration measurements which has been proven in Chapter 3 to be unreliable to obtain the scale retention rate on the steel surface[42]. Furthermore, no kinetics experiments have been conducted for an H_2S purged corrosion system, which is more complex than the sulfide salt system (without purging H_2S gas) because electrochemical corrosion, precipitation and solid state chemical reaction may occur on the steel surface simultaneously. From the discussion above, it is clear that for an improved understanding of the nature of surface scales formed in H_2S environment as well as their protective properties, a better understanding

of the mechanism and kinetics of mackinawite scale formation in the H_2S environment is needed.

5.3 Objectives

The objectives of this chapter include:

1. Investigate the water chemistry in the H_2S solution
2. Quantify the scale retention rate of iron sulfide and the corrosion rate of carbon steel in the H_2S environment
3. Analyze the iron sulfide scale formed in the H_2S environment
4. Investigate the mechanism of iron sulfide scale formation in the H_2S environment
5. Based on the experimental data, develop a mechanistic model of hydrogen sulfide corrosion

5.4 Experimental procedure

5.4.1 Experimental setup

The schematic of the experimental setup is shown in Figure 36. The concentration of H_2S was controlled by gas mass-flow controllers and was mixed through a gas mixer to obtain a desired H_2S concentration. The gas rotameter was used to evenly distribute the mixed gas into the two glass cells. An H_2S monitor system with three alarm sensors was installed in H_2S laboratory to detect H_2S gas leaking in H_2S laboratory. The solenoid valve was used to automatically shut down the H_2S gas if the power in the H_2S laboratory

was shut down, the alarm system was on, or seal switched in the fume hood for several problems, for example, the motor of the fume hood is burned out.

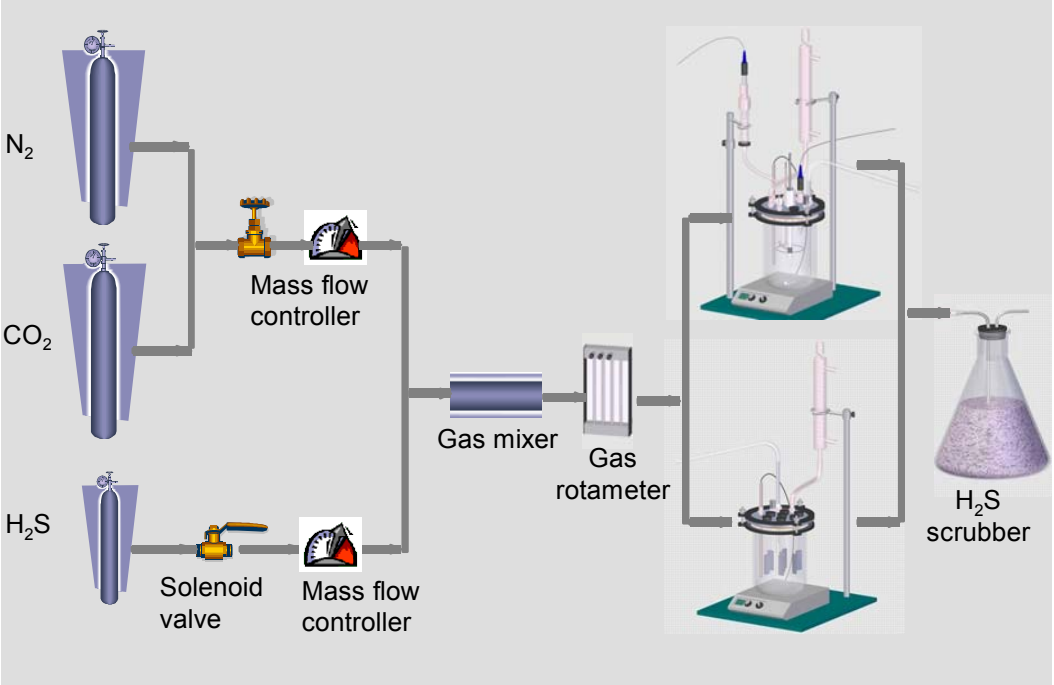

Figure 36. A schematic of the apparatus.

5.4.2 Experimental procedure

As shown in Figure 36, both the electrochemical glass cell and the weight change measurement glass cell were used to conduct the experiments simultaneously. Each glass cell was filled with 2 liters of distilled water with 1 wt% NaCl. The solution was heated to a desired temperature and purged with N_2. After the solution was deoxygenated, the pH was adjusted to the desired value by adding a deoxygenated hydrogen chloride solution and sodium hydroxide solution.

Electrochemical corrosion measurements were performed by using a Gamry PC monitoring system. Potentiodynamic sweep was used to investigate the corrosion

mechanism. Both linear polarization resistance (LPR) and weight change method (WCM) were used to measure the corrosion rate (Appendix). Cylindrical specimens with a surface area of 5.4 cm^2 were inserted in the solution long enough to reach a stable potential (10 minutes) before LPR measurement and then cathodic and anodic sweeps were taken. Identical rectangular samples with a surface area of 21 cm^2 were placed in the same environment for 24 hours to obtain results by weight change measurements.

Weight change measurement was taken in another glass cell. Six specimens were inserted into the same glass cell as the substrate for scale formation. Prior to immersion, the specimen surfaces were polished successively with 320, 400 and 600 grit SiC paper, rinsed with alcohol, and degreased using acetone. Subsequently, a given amount of H_2S was added into the system. Later, the required amounts of Fe^{2+} were added in the form of a deoxygenated ferrous chloride salt ($FeCl_2.4H_2O$) solution. Some of the experiments were repeated in order to test reproducibility. X65 carbon steel, C1018 carbon steel, and SS316 stainless steel were used as substrates to study the scale formation in H_2S environments.

Both scale retention rate and corrosion rate were measured by the weight change method. Time-averaged scale retention rate of iron sulfide scale was obtained by subtracting the weight of the coupons which had iron sulfide scale and those after the scale was removed. Time-averaged corrosion rate was calculated by subtracting the weight of the coupons prior to running the experiments and after removing the iron sulfide scale. A spectrophotometer was used to measure ferrous ion concentration in the solution (Appendix). The specimens with the iron sulfide scale on it were analyzed using several surface analysis techniques, such as Scanning Electron Microscopy (SEM/EDS),

X-ray Diffraction methodology (XRD), and Electron Probe Micro-analyzer (EPMA) (Appendix).

5.5 Results and discussions

5.5.1 Water chemistry of H_2S solution

5.5.1.1 The concentrations of species in the liquid phase

The approach to calculate the concentrations of species in the liquid phase was developed by Brown *et al.*[130] and will be simply described here. When hydrogen sulfide dissolves in the water solution, the vapor-liquid equilibrium of hydrogen sulfide is described as in Chapter 4:

$$H_2S_{(g)} \overset{K_{H_2S}}{\Leftrightarrow} H_2S_{(aq)} \tag{30}$$

Then we have the dissociation of hydrogen sulfide and dissociation of HS^- ion:

$$H_2S_{(aq)} \overset{K_1}{\Leftrightarrow} H^+_{(aq)} + HS^-_{(aq)} \tag{31}$$

$$HS^-_{(aq)} \overset{K_2}{\Leftrightarrow} H^+_{(aq)} + S^{2-}_{(aq)} \tag{32}$$

In an open system, Henry's law can be used to calculate the vapor-liquid equilibrium of hydrogen sulfide:

$$c_{H_2S} H_{H_2S} = P_{H_2S} \tag{47}$$

where c_{H_2S} is the concentration of hydrogen sulfide in the solution, H_{H_2S} is the Henry's constant, and P_{H_2S} is the partial pressure of hydrogen sulfide. When the concentration of dissolved hydrogen sulfide is calculated, the reactions in H_2S environment will be described by reactions as follows:

$$K_1 = \frac{c_{H^+} c_{HS^-}}{c_{H_2S}} \tag{48}$$

$$K_2 = \frac{c_{H^+} c_{S^{2-}}}{c_{HS^-}} \tag{49}$$

$$K_W = \frac{c_{H^+} c_{OH^-}}{c_{H_2O}} \tag{50}$$

An electroneutrality condition is required as expressed by:

$$c_{H^+} = c_{HS^-} + 2\, c_{S^{2-}} + c_{OH^-} \tag{51}$$

When there are other species such as Fe^{2+}, Na^+, and Cl^- in the solution, it is required to add the concentrations of the additional species in the electroneutrality equation.

In the closed system, the partial pressure of H_2S gas is not constant and the concentration of H_2S in gaseous phase is an unknown. However, the total amount of sulfide species in the aqueous and gas phase remains constant. Hence, the mass conservation equation is added in order to describe the closed system.

$$\Sigma[\,sulfide\ species\,] = c_{H_2S_{(g)}} + c_{H_2S_{(aq)}} + c_{HS^-_{(aq)}} + c_{S^{2-}_{(aq)}} \tag{52}$$

For these equations, the reaction constants are obtained from the literature. The Henry's constant H_{H_2S} of hydrogen sulfide is a function of the solubility constant.

$$H_{H_2S} = \frac{1}{K_{H_2S}} \tag{53}$$

The solubility of hydrogen sulfide and the first ionization constant recommended in Chapter 4, and the second ionization constant of hydrogen sulfide developed by Kharaka *et al.* [115] are used to calculate the species' concentration.

$$K_{H_2S} = 10^{-\left(634.27+0.2709T_K-0.11132*10^{-3}T_K^2-\frac{16719}{T_K}-261.9\log T_K\right)} \tag{43}^{85}$$

$$K_1 = 10^{782.43945+0.361261T_K-1.6722\times10^{-4}T_K^2-\frac{20565.7315}{T_K}-142.741722\ln T_K} \quad (44)^{86}$$

$$K_2 = 10^{-\left(23.93-0.030446T_K+2.4831\times10^{-5}T_K^2\right)} \quad (54)^{115}$$

Based on the above H_2S vapor - liquid equilibrium model described by Brown *et al.*[130], an excel spreadsheet is developed to calculate the concentrations of all the species, such as $c_{H_2S_{(g)}}$, $c_{H_2S_{(aq)}}$, $c_{HS^-_{(aq)}}$, and $c_{S^{2-}_{(aq)}}$ at different concentrations of H_2S in the gas inlet, as shown in Table 12. Figure 37 show that temperature has a small effect on the sulfuric species concentration when the gas inlet concentration is kept constant. With the increase of temperature, both aqueous H_2S concentration and HS^- concentration decrease; however, S^{2-} concentration slightly increase. It is also noted that S^{2-} concentration is negligible compared to the aqueous H_2S concentration and HS^- concentration.

Table 12. The concentrations of sulfide species at different concentrations of H_2S in the gas inlet in H_2S solution at pH 5 and P_{tot} 1 bar.

Temperature / °C	**H_2S concentration in the gas inlet / %**	$c_{H_2S_{(g)}}$ **ppm**	$c_{H_2S_{(g)}}$ **pa**	$c_{H_2S_{(aq)}}$ **mol/l**	$c_{HS^-_{(aq)}}$ **mol/l**	$c_{S^{2-}_{(aq)}}$ **mol/l**
25	0.01	76	9.8	9.4E-6	9.89E-8	8.62E-20
	0.1	763	98	9.4E-5	9.89E-7	8.62E-19
	1	7644	981	9.4E-4	9.89E-6	8.62E-18
	10	78015	9808	9.4E-3	9.89E-5	8.62E-17
60	0.1	702	81	4E-5	9.51E-7	2.72E-18
	1	7038	813	4E-4	9.51E-6	2.72E-17
	10	71714	8132	4E-3	9.51E-5	2.72E-16
80	0.0075	43	4	1.58E-6	4.76E-8	2.53E-19
	0.015	85	8	3.16E-6	9.52E-8	5.06E-19
	0.024	136	13	5.06E-6	1.52E-7	8.09E-19
	0.04	227	22	8.44E-6	2.54E-7	1.35E-18
	0.1	569	54	2.11E-5	6.35E-7	3.37E-18
	1	5695	539	2.11E-4	6.35E-6	3.37E-17
	10	57821	5392	2.11E-3	6.35E-5	3.37E-16

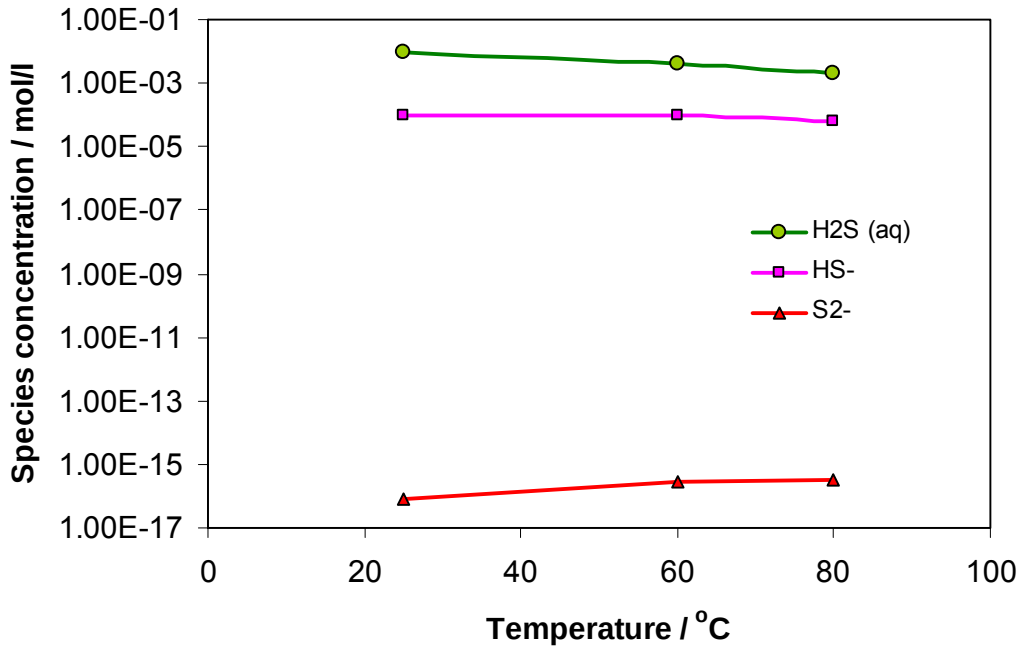

Figure 37. The effect of temperature on the concentration of sulfide species at the H_2S gas inlet concentration of 10%, P_{tot} 1 bar, and pH 5.

5.5.1.2 Supersaturation of mackinawite

Supersaturation of mackinawite is calculated in order to investigate the mechanism and kinetics of mackinawite scale formation in H_2S environment. Supersaturation of mackinawite depends on the solubility limit of mackinawite in the water solution. The solubility limit of mackinawite at different temperatures was recommended in Chapter 4 to use the equation proposed by Benning, *et al.*[127]:

$$K_{sp,mck} = 10^{\frac{2848.779}{T_k} - 6.347 + log(K_1)} \tag{38}$$

Supersaturation of mackinawite is calculated using the following equation,

$$SS = \frac{\frac{c_{Fe^{2+}} c_{HS^-}}{c_{H^+}}}{K_{sp,mack.}} \tag{55}$$

The supersaturation of mackinawite under the different test conditions was calculated and shown from Figure 38 to Figure 40. At room temperature, the supersaturation of mackinawite *versus* pH under the conditions of Fe^{2+} concentrations of 2, 10, and 50 ppm and H_2S concentrations of 0.1%, 1%, and 10% in the gas inlet is shown in Figure 38. It has been found that under the test conditions mackinawite is under-saturated when pH is below 4 and supersaturated when pH is above 6. With the increase of temperature to 60°C and 80°C, mackinawite is supersaturated when pH is above 5. Therefore, the supersaturation of mackinawite is used to determine the test matrix for the kinetics experiments in the H_2S system.

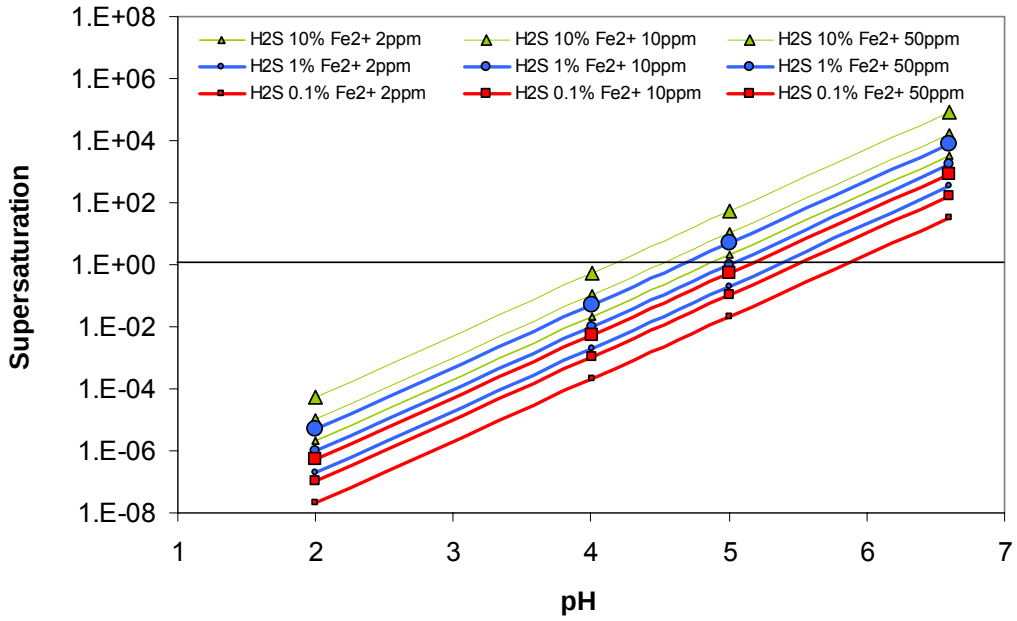

Figure 38. Supersaturation of mackinawite at T=25°C under the conditions of different pH, H_2S concentration in the gas inlet (0.1%, 1%, and 10%) and Fe^{2+} concentration (2 ppm, 10 ppm, and 50 ppm).

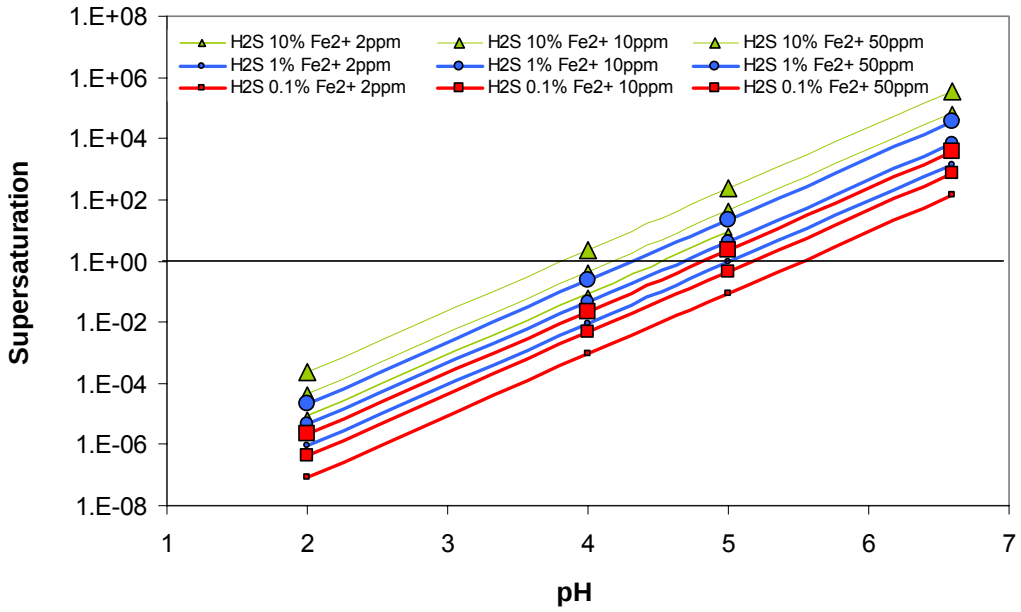

Figure 39. Supersaturation of mackinawite at T=60°C under the conditions of different pH, H_2S concentration in the gas inlet (0.1%, 1%, and 10%) and Fe^{2+} concentration (2 ppm, 10 ppm, and 50 ppm).

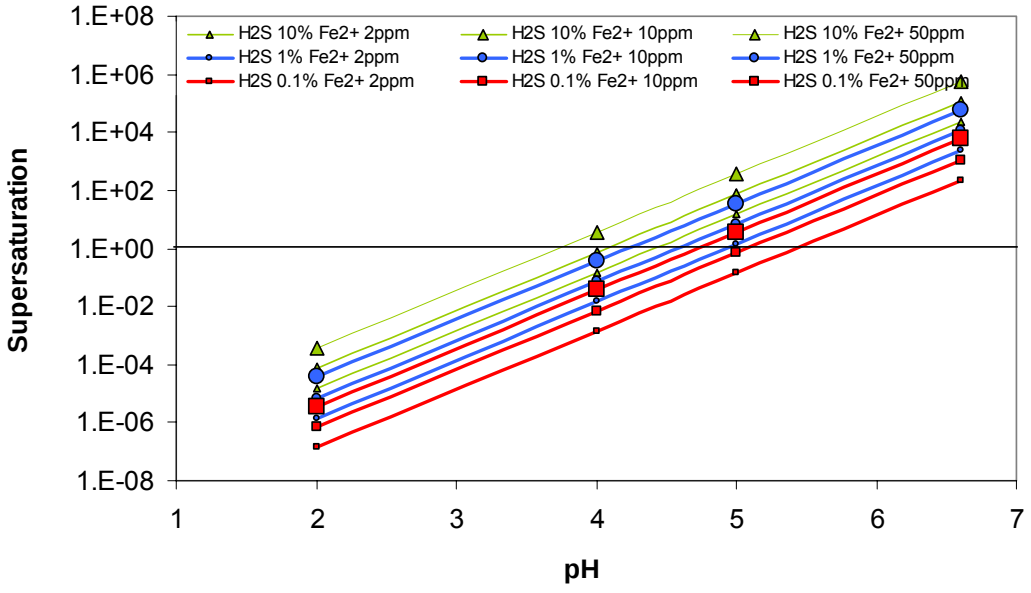

Figure 40. Supersaturation of mackinawite at T=80°C under the conditions of different pH, H_2S concentration in the gas inlet (0.1%, 1%, and 10%) and Fe^{2+} concentration (2 ppm, 10 ppm, and 50 ppm).

5.5.2 Experiments in solutions under-saturated with mackinawite

5.5.2.1 Test matrix

Experiments at mackinawite under-saturated conditions were conducted in order to understand the mechanism of H_2S corrosion without the precipitation of mackinawite. The test matrix of the experiments is shown in Table 13, which is based on the calculation of mackinawite supersaturation as mentioned above. The saturation of mackinawite under different test conditions is shown in Table 14. The chemical composition of the C1018 carbon steel used for the experiments is analyzed by Laboratory Testing Inc. Hatfield, PA and shown in Table 15.

Table 13: Test matrix of experiments

Parameter	**Description**
Material	C1018 carbon steel
Solution	De-ionized water with 1 wt% of NaCl, purged with N_2
Temperature ^oC	25
Total Pressure (bar)	1
H_2S Pressure (bar)	0.076 millibar (76 ppm)
H_2S aq	9.4×10^{-6} mol/l
pH	2, 3, 4, 5

Table 14. The degree of under-saturation of mackinawite at different Fe^{2+} concentration and pH under the conditions of room temperature and H_2S concentration of 0.01% in the gas inlet.

Fe^{2+} / ppm	**pH**	**Degree of under-saturation**
1	2	1.04E-9
1	3	1.04E-7
1	4	1.04E-5
1	5	1.04E-3

Table 15. The chemical composition of C1018 (wt.%) (Fe is the balance)

C	Mn	Si	P	S	Cr	Cu	Ni	Mo	Al
0.19	0.83	0.22	0.015	0.013	0.13	0.16	0.016	0.042	0..004

5.5.2.2 Experiments in pure N_2 and H_2S/N_2 environments

A number of experiments were conducted in both pure N_2 and H_2S/N_2 solutions under the test conditions of H_2S concentration 100 ppm, room temperature, and pH 2, 3, 4, and 5. Figure 41 to Figure 44 show the comparison of the potentiodynamic sweeps for pure N_2 and H_2S/N_2 systems at different pH. The values of the Tafel slopes were obtained to be β_a = 60 mV/decade, β_c = 120 mV/decade and the 'B' value was calculated to be 17 mV. It has been found that H_2S inhibits the anodic reaction while not the cathodic reactions in the solution of pH 2 (Figure 41). With the increase of pH to 3 and 4 (Figure 42 and Figure 43), H_2S has little effect on both the anodic reaction and the cathodic reactions. At pH 5, H_2S slightly increases the corrosion rate (Figure 44). Through analyzing the sweeps, it has been noted that the cathodic reactions are most likely controlled by the charge transfer. Comparisons of both corrosion currents and potentiodynamic sweeps diagrams in pure N_2 system at different pH are shown in Figure 45. The data illustrate that with the increase of pH, the corrosion current gradually decreases. Comparing the potentiodynamic sweeps at different pH in H_2S/N_2 environment (Figure 46), similar trend of corrosion currents in H_2S/N_2 environment is obtained as in pure N_2 system.

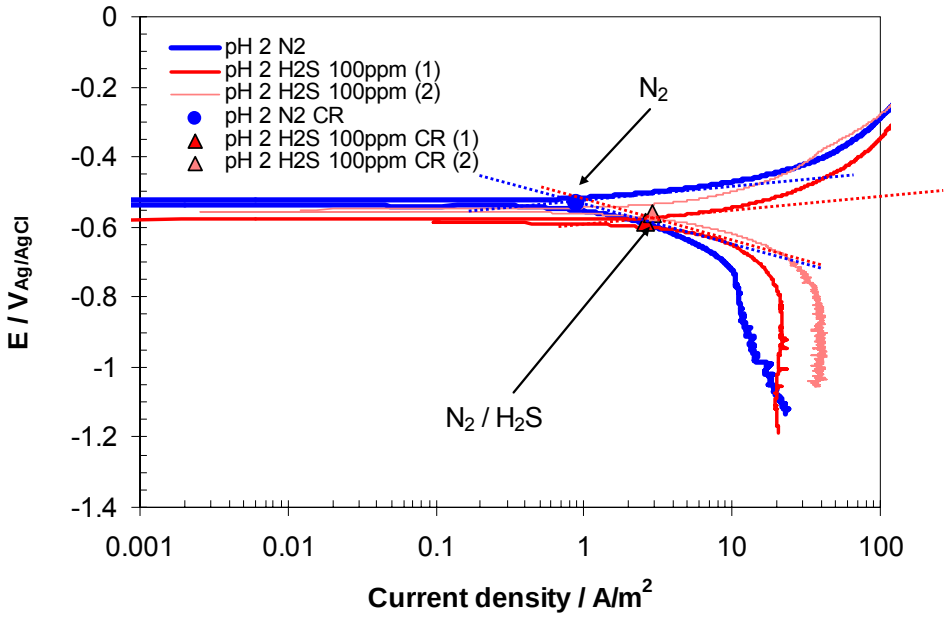

Figure 41. The comparison of potentiodynamic sweeps for both pure N_2 and N_2/H_2S (100 ppm) environments under the conditions of pH 2, T=25°C, and static solution.

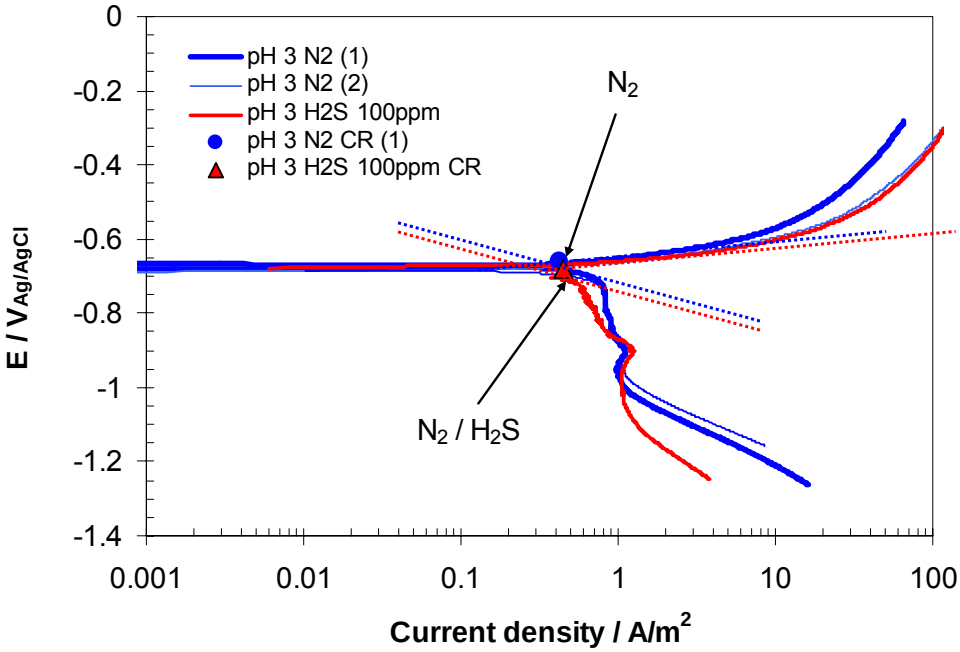

Figure 42. The comparison of potentiodynamic sweeps for both pure N_2 and N_2/H_2S (100 ppm) environments under the conditions of pH 3, T=25°C, and static solution.

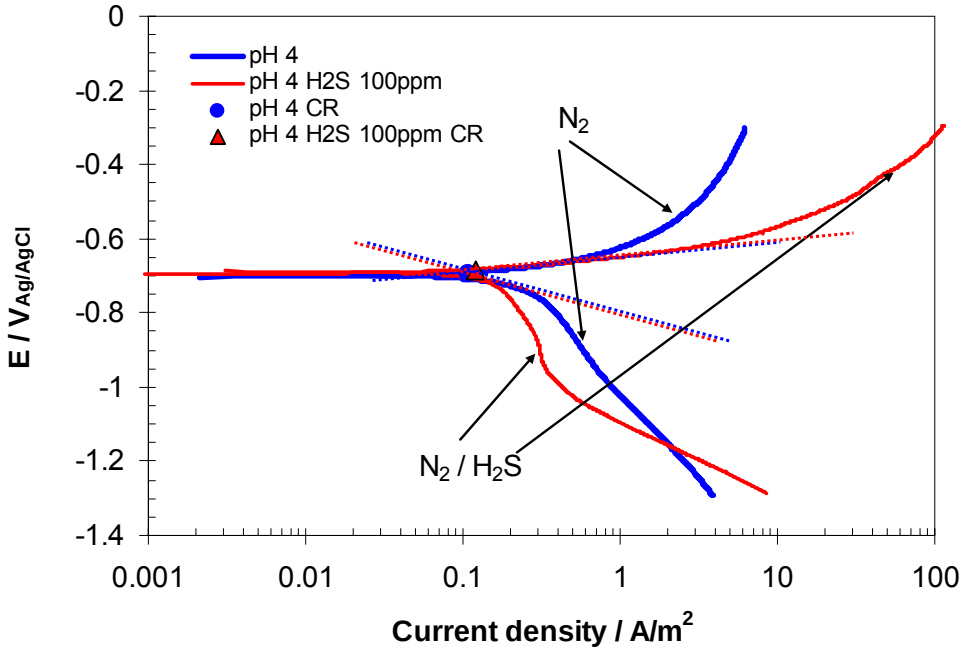

Figure 43. The comparison of potentiodynamic sweeps for both pure N_2 and N_2/H_2S (100 ppm) environments under the conditions of pH 4, T=25°C, and static solution.

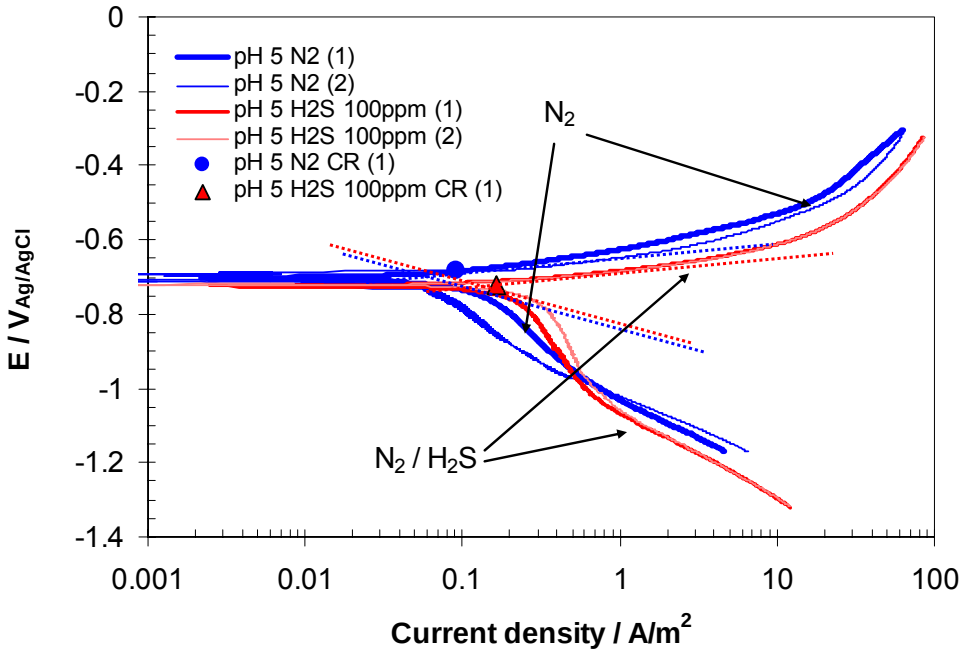

Figure 44. The comparison of potentiodynamic sweeps for both pure N_2 and N_2/H_2S (100 ppm) environments under the conditions of pH 5, T=25°C, and static solution.

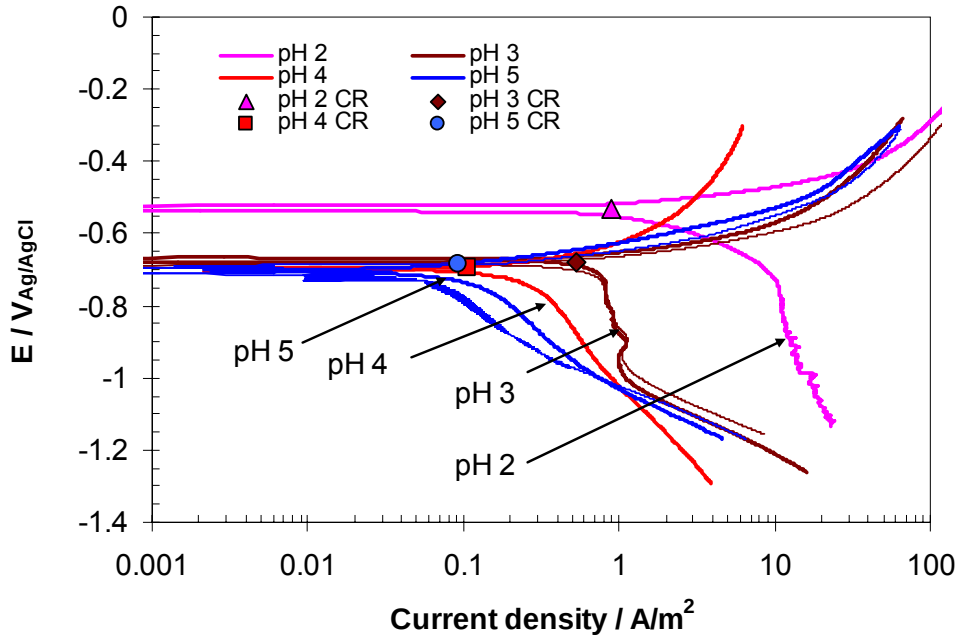

Figure 45. The comparison of potentiodynamic sweeps for pure N_2 environments under the conditions of pH from 2 to 5, T=25°C, and static solution.

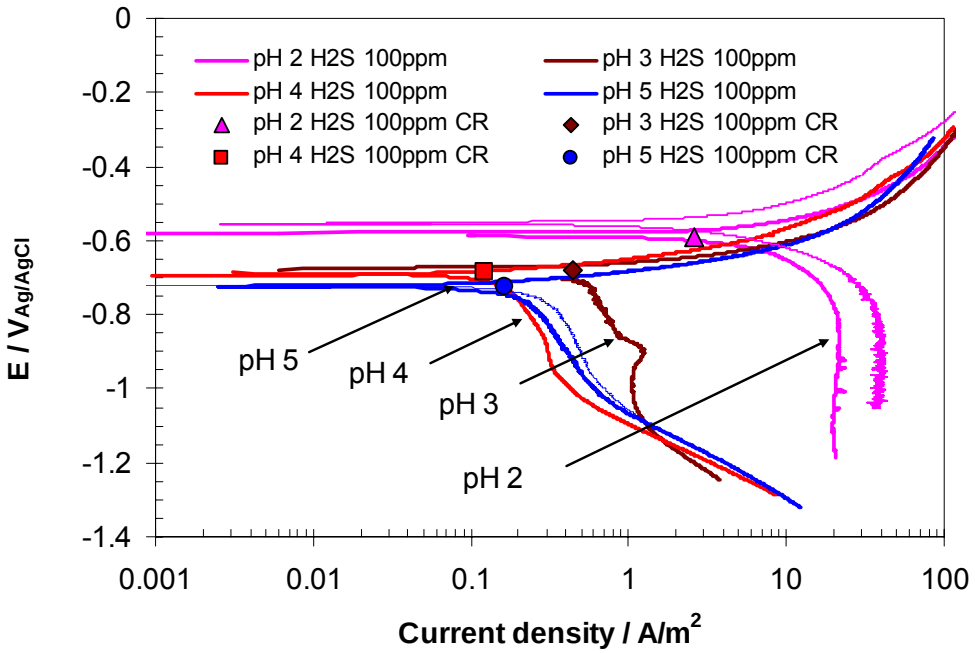

Figure 46. The comparison of potentiodynamic sweeps for N_2/H_2S (100 ppm) environments under the conditions of pH from 2 to 5, T=25°C, and static solution.

A comparison of corrosion rate at different pH in both pure N_2 and H_2S/N_2 environments is shown in Figure 47. With the increase of pH, the corrosion rate decreased as expected. At a very low pH of 2, the corrosion rate is accelerated significantly to 3 mm/yr by purging H_2S/N_2 mixture (Figure 48). However, H_2S has no significant effect on the corrosion rates at pH 3, 4, and 5. The potentiodynamic sweep data (Figure 41) illustrate that H_2S accelerates the corrosion rates at pH 2 in N_2 environment by accelerating the anodic reaction. Therefore, it is suggested that H_2S reacts with the steel to form a thin mackinawite layer and the mackinawite layer immediately dissolves because of the high acidity of the solution.

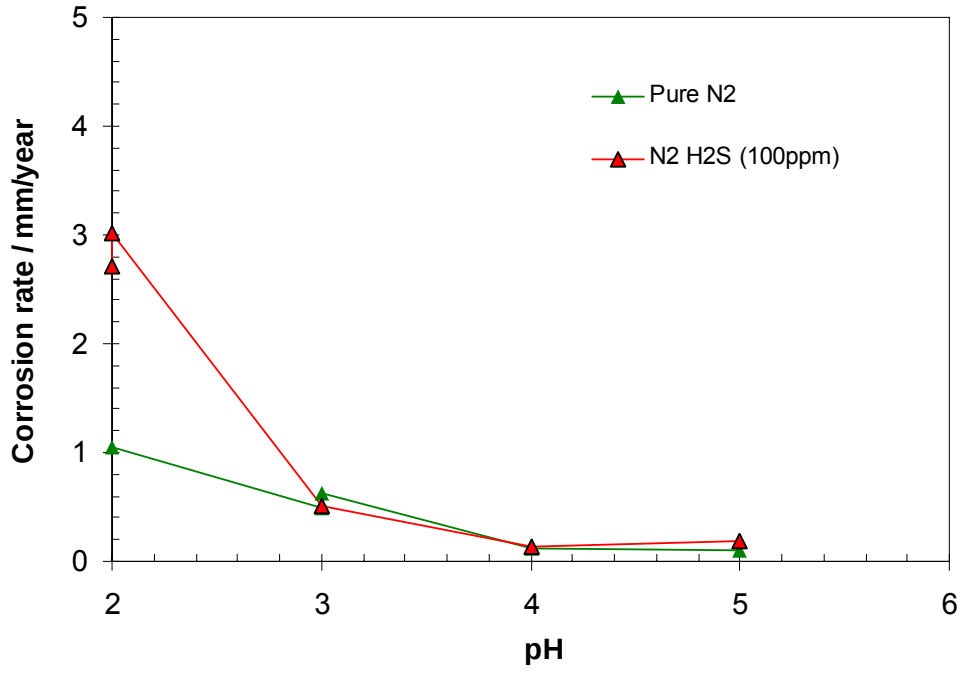

Figure 47. Corrosion rate vs. pH for both pure N_2 and N_2/H_2S (100 ppm) environments under the conditions of T=25^{o}C, and static solution.

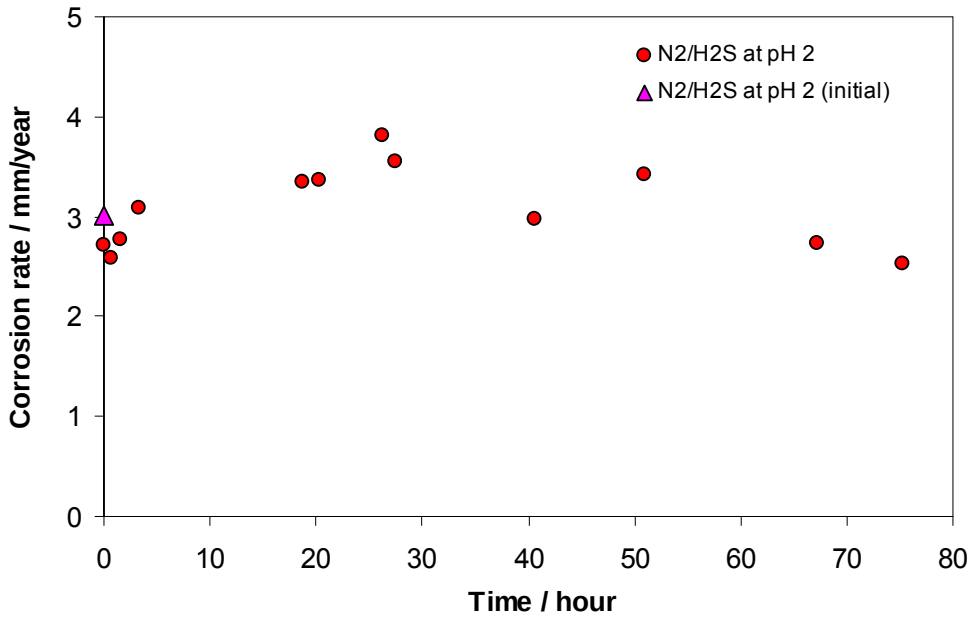

Figure 48. Corrosion rate vs. reaction time for N_2/H_2S (100 ppm) environments under the conditions of pH 2, T=25°C, and static solution.

5.5.3 Kinetics experiments in solutions supersaturated with mackinawite

5.5.3.1 Test matrix

Experiments at mackinawite supersaturated conditions were conducted in order to understand both the mechanism and kinetics of mackinawite scale formation in H_2S environment. The test matrix of the experiments is shown in Figure 16. The saturation of mackinawite under the test conditions is shown in Table 17.

Table 16: Test matrix of experiments

Parameter	**Description**
Material	X65 carbon steel
Solution	De-ionized water with 1 wt% of NaCl, purged with N_2
Temperature °C	25, 60, 80
Total Pressure (bar)	1
H_2S in the gas inlet	0.0075%, 0.015%, 0.024%, 0.04%, 0.1%, 1%, and 10%
pH	5 - 6.6

Table 17. The supersaturation of mackinawite at different test conditions

Temperature / ^{o}C	H_2S concentration in the gas inlet / %	Fe^{2+} / ppm	pH	SS
25	1	2	5	0.21
		10	5	1.04
		50	5	5.22
	10	2	5	2.09
		10	5	10.4
		50	5	52.2
60	1	2	5	0.9
		10	5	4.49
		50	5	22.5
	10	2	5	8.99
		10	5	44.9
		50	5	225
80	0.0075	50	5	0.27
		50	6.6	428
	0.015	50	5	0.54
		50	6.6	856
	0.024	50	5	0.86
		50	6.6	1370
	0.04	2	5	0.06
	0.1	2	5	0.14
		10	5	0.72
		50	5	3.6
	1	2	5	1.44
		10	5	7.2
		50	5	36
	10	2	5	14.4
		10	5	72
		50	5	360

5.5.3.2 Kinetics experiments at the temperatures of 25^{o}C, 60^{o}C, and 80^{o}C

Kinetics experiments were conducted in the static solution using X65 carbon steel as the substrate under a certain test conditions. The first series of experiments were conducted at the temperature of 25^{o}C, initial Fe^{2+} 0 ppm, 10 ppm, and 50 ppm, and H_2S 1% and 10%. Figure 49 shows both the scale retention rate of iron sulfide and the

corrosion rate of the steel as a function of H_2S concentration in the first hour. Both the scale retention rate and corrosion rate were described in the same unit of mol/h/m^2, in order to compare how much iron sulfide scale retained (FeS in mol) and iron lost (Fe in mol) on the steel surface (with a surface area of 1 m^2) in an hour. It was found that the corrosion rate of carbon steel is higher than the retention rate of iron sulfide under the test conditions. The scale retention rate in the first hour remained constant at different Fe^{2+} concentration and H_2S concentration. The corrosion rate expressed in mm/year is shown in Figure 50 and it is found that the corrosion rate is approximately 1.3 to 1.8 mm/year at different H_2S and Fe^{2+} concentration. When the reaction time increased to 20 hours, the scale retention rate decreased at the H_2S concentration of 10%, as illustrated in Figure 51. It is estimated that the higher corrosion rate at H_2S concentration of 10% results in a lower scale retention rate. However, no significant effect of Fe^{2+} concentration on either the scale retention rate or the corrosion rate was found. Figure 52 shows the corrosion rate in twenty four hours decreased to 0.2 to 0.4 mm/year, illustrating that the scale formed on the steel surface can partially protect the steel from corroding.

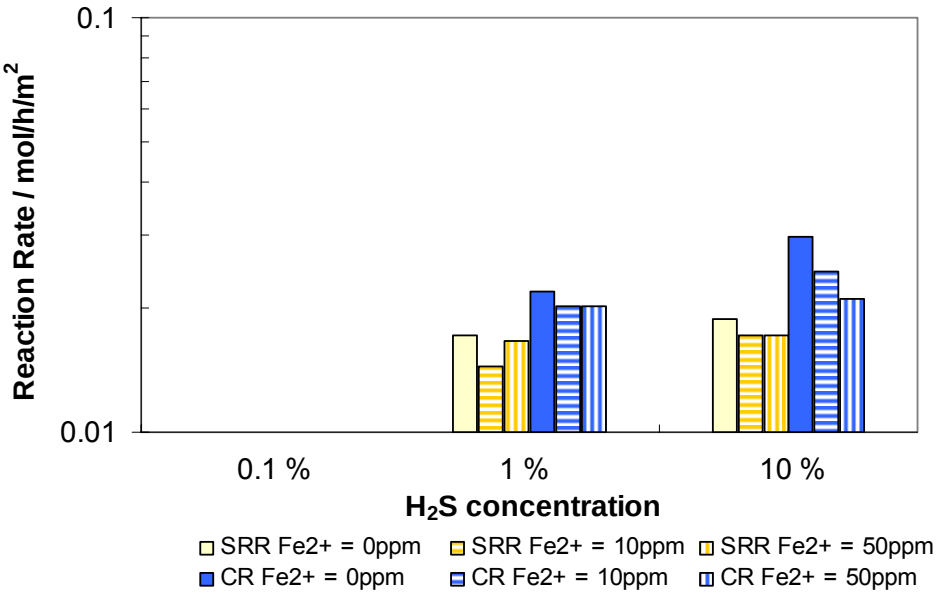

Figure 49. Both the retention rate of iron sulfide formed on X65 carbon steel surface and the corrosion rate of X65 carbon steel in the same molar unit at different H_2S concentration and initial Fe^{2+} concentration in the solution with H_2S/N_2 under the conditions of T=25°C, the total reaction time is 1 hour.

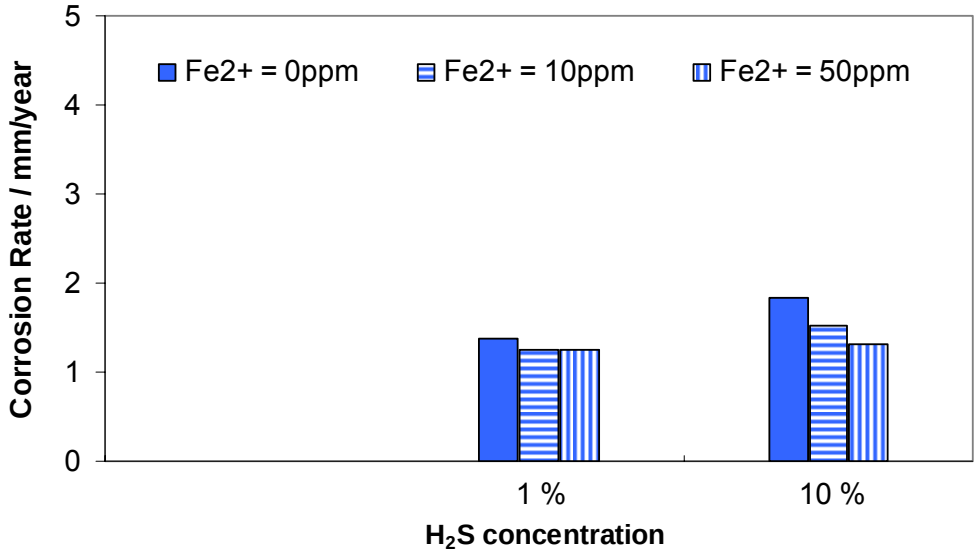

Figure 50. The corrosion rate of X65 carbon steel in mm/year at different H_2S concentration and initial Fe^{2+} concentration in the solution with H_2S/N_2 under the conditions of T=25°C, the total reaction time is 1 hour.

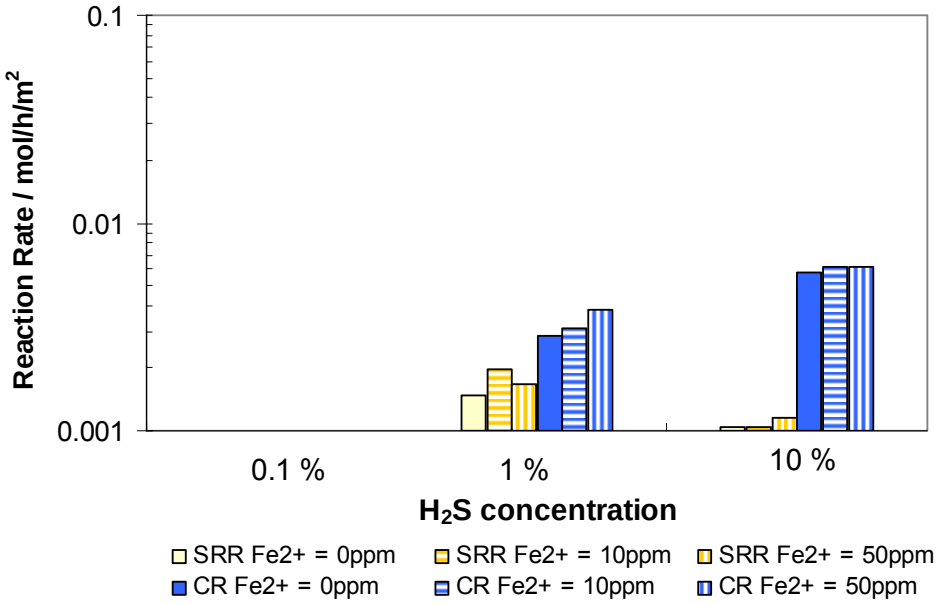

Figure 51. Both the retention rate of iron sulfide formed on X65 carbon steel surface and the corrosion rate of X65 carbon steel in the same molar unit at different H_2S concentration and initial Fe^{2+} concentration in the solution with H_2S/N_2 at T=25°C, the total reaction time is 24 hours.

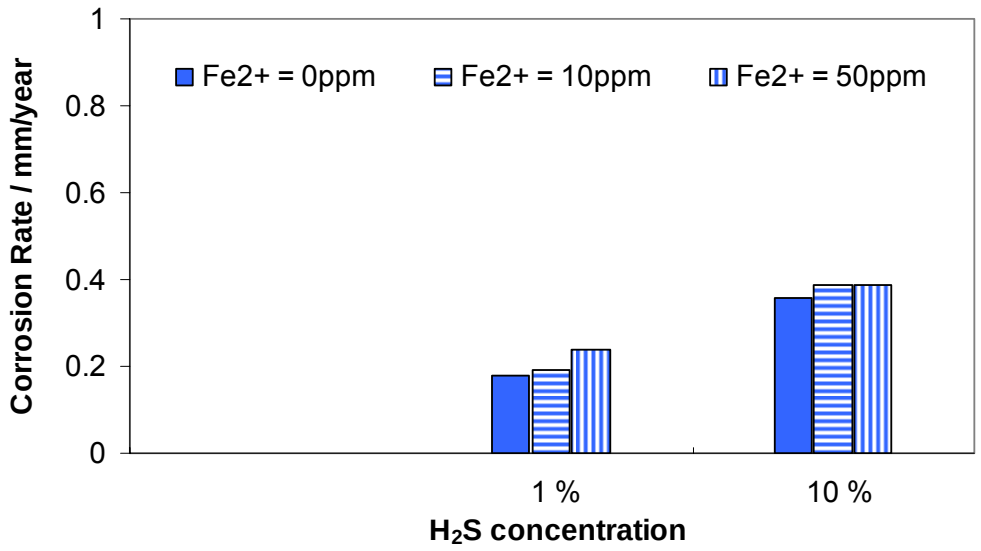

Figure 52. The corrosion rate of X65 carbon steel in mm/year at different H_2S concentration and initial Fe^{2+} concentration in the solution with H_2S/N_2 at T=25°C, the total reaction time is 24 hours.

The morphology of iron sulfide scale formed on the X65 carbon steel surface is shown from Figure 53 to Figure 58, and it has been proved that the iron sulfide scale formed in the first hour covered the steel surface well; however, the scale formed in 24 hours at room temperature under all the test conditions appears to be more fragmented.

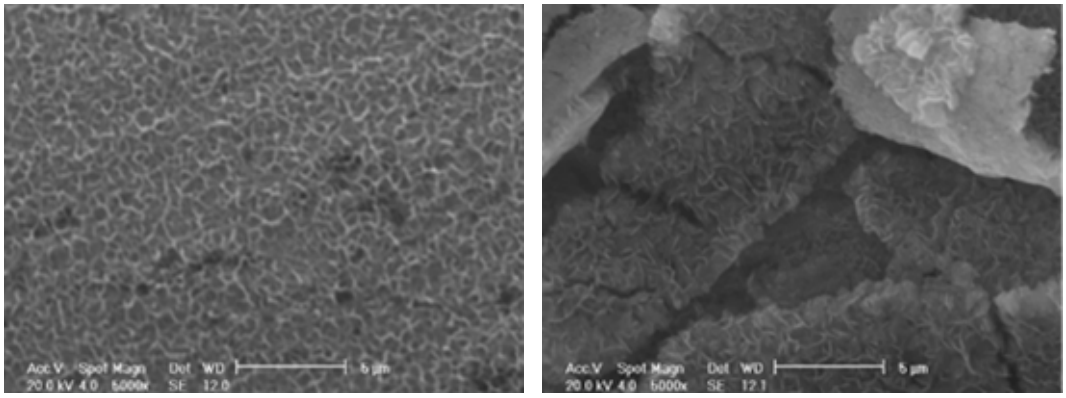

(A) (B)

Figure 53. The morphology (5000x) of iron sulfide formed on the X65 carbon steel surface under the conditions of 1% H_2S (H_2S/N_2 gas), T=25°C, pH 5.1~6.0, Fe^{2+} = 0 ppm, the total reaction time is (A) 1 hour, (B) 19 hours.

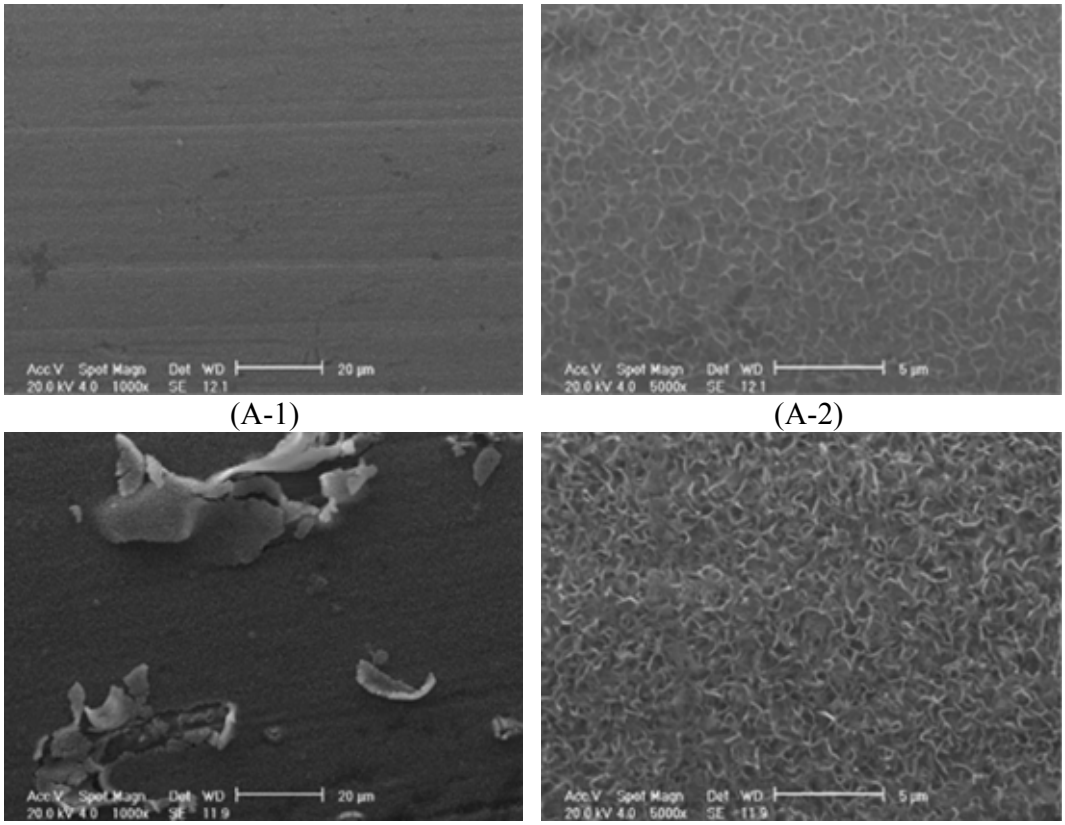

Figure 54. The morphology (at 1000x and 5000x) of iron sulfide formed on the X65 carbon steel surface under the conditions of 1% H_2S (H_2S/N_2 gas), T=25^oC, pH 5.2~5.6, Fe^{2+} = 10 ppm, the total reaction time is (A) 1 hour, (B) 19 hours.

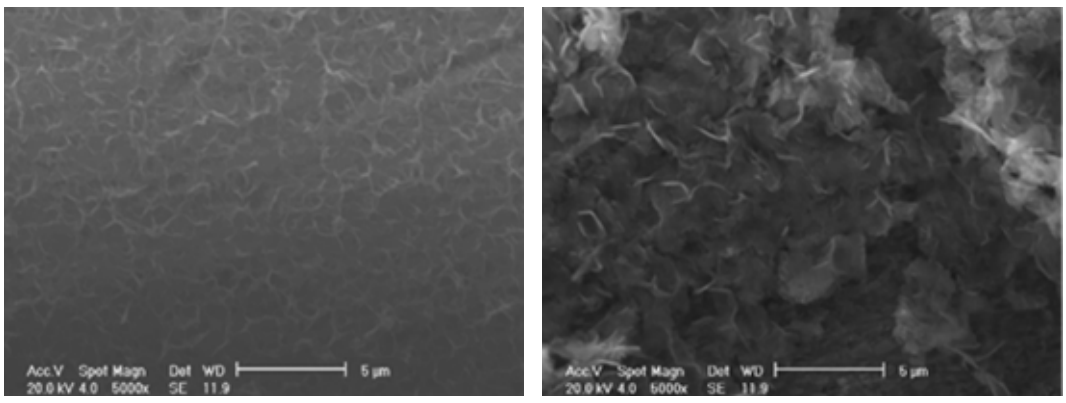

Figure 55. The morphology (5000x) of iron sulfide formed on the X65 carbon steel surface under the conditions of 1% H_2S (H_2S/N_2 gas), T=25^oC, pH 5.2~5.4, Fe^{2+} = 50 ppm, the total reaction time is (A) 1 hour, (B) 19 hours.

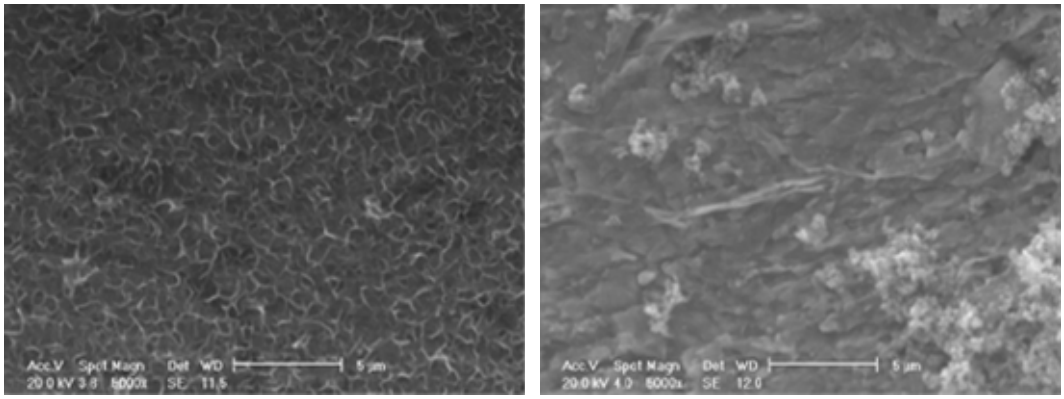

(A) (B)

Figure 56. The morphology (5000x) of iron sulfide formed on the X65 carbon steel surface under the conditions of 10% H_2S (H_2S/N_2 gas), T=25°C, pH 5, Fe^{2+} = 0 ppm, the total reaction time is (A) 1 hour, (B) 21 hours.

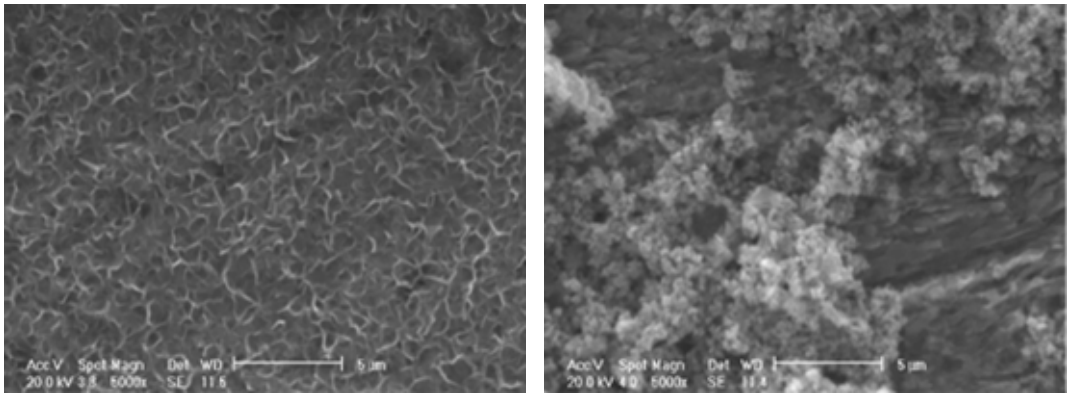

(A) (B)

Figure 57. The morphology (5000x) of iron sulfide formed on the X65 carbon steel surface under the conditions of 10% H_2S (H_2S/N_2 gas), T=25°C, pH 5, Fe^{2+} = 10 ppm, the total reaction time is (A) 1 hour, (B) 21 hours.

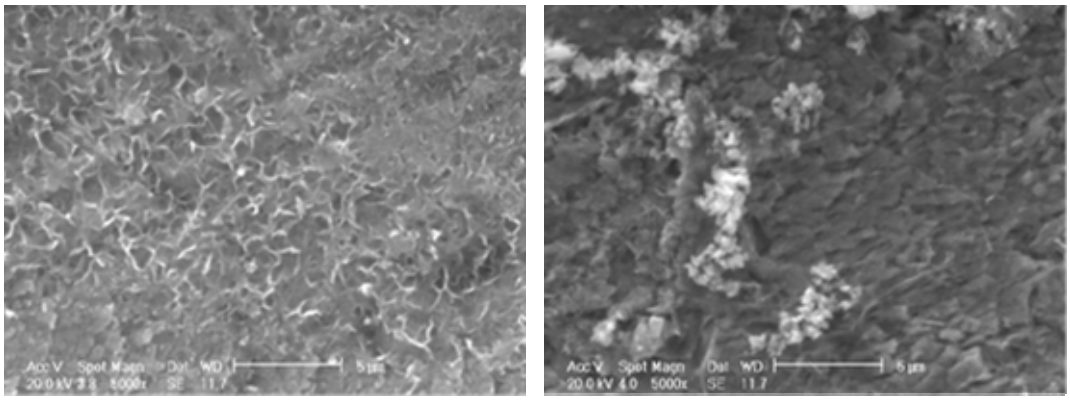

(A) (B)

Figure 58. The morphology (5000x) of iron sulfide formed on the X65 carbon steel surface under the conditions of 10% H_2S (H_2S/N_2 gas), T=25°C, pH 5, Fe^{2+} = 50 ppm, the total reaction time is (A) 1 hour, (B) 21 hours.

Another set of experiments was performed at the temperature of 60^{o}C under the conditions of Fe^{2+} concentration of 0 ppm, 10 ppm, and 50 ppm, and H_2S concentrations of 1% and 10%. Both the retention rate of iron sulfide scale and the corrosion rate of X65 carbon steel in the first hour increases with the increase of H_2S concentration and keeps constant at different Fe^{2+} concentrations, as shown in Figure 59. Figure 60 shows the corrosion rate is approximately 2 to 3 mm/year at different H_2S and Fe^{2+} concentration. Figure 61 shows that the retention rate of iron sulfide scale and the corrosion rate of X65 in 20 hours are much lower than the reaction rate obtained in one hour (Figure 59). Figure 62 shows the corrosion rate drifted down to 0.3 to 0.8 mm/year in twenty hours. It is proved that the scale formed on the steel surface can partially protect the steel from corroding and also the scale retention rate is affected by the corrosion rate of the steel.

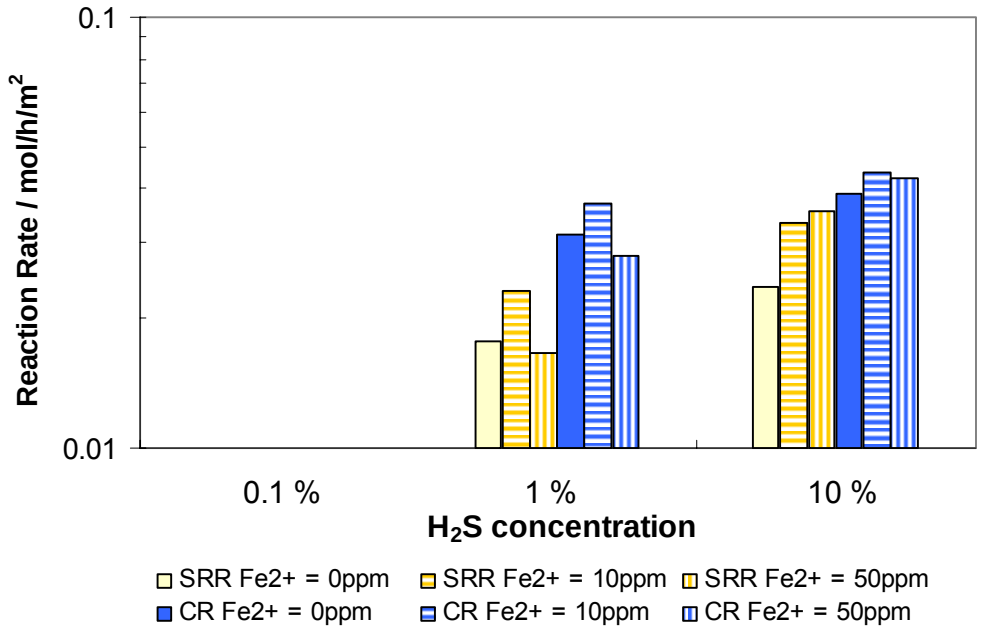

Figure 59. Both the retention rate of iron sulfide formed on X65 carbon steel surface and the corrosion rate of X65 carbon steel in the same molar unit at different H_2S concentration and initial Fe^{2+} concentration in the solution with H_2S/N_2 at T=60°C, the total reaction time is 1 hour.

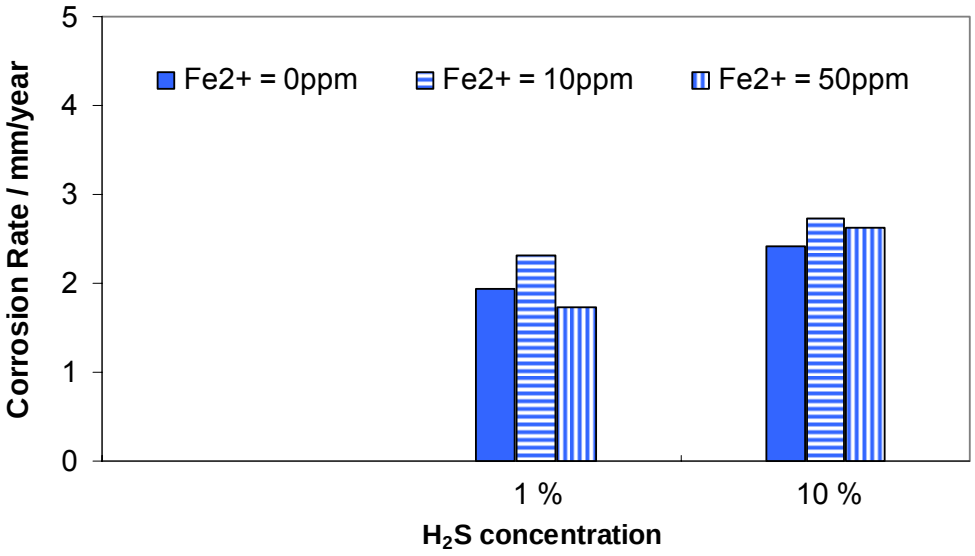

Figure 60. The corrosion rate of X65 carbon steel in mm/year at different H_2S concentration and initial Fe^{2+} concentration in the solution with H_2S/N_2 at T=60°C, the total reaction time is 1 hour.

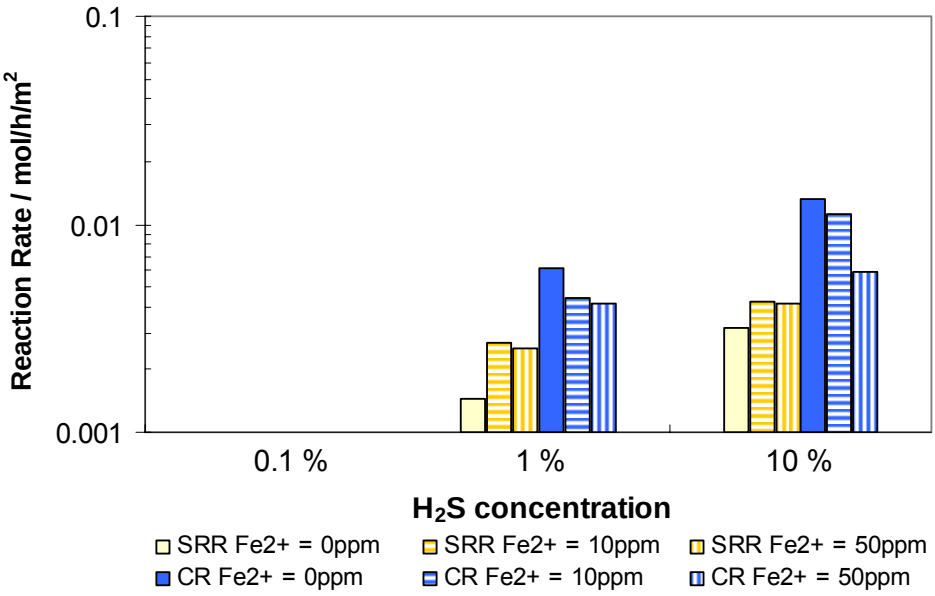

Figure 61. Both the retention rate of iron sulfide formed on X65 carbon steel surface and the corrosion rate of X65 carbon steel in the same molar unit at different H_2S concentration and initial Fe^{2+} concentration in the solution with H_2S/N_2 at T=60°C, the total reaction time is 24 hours.

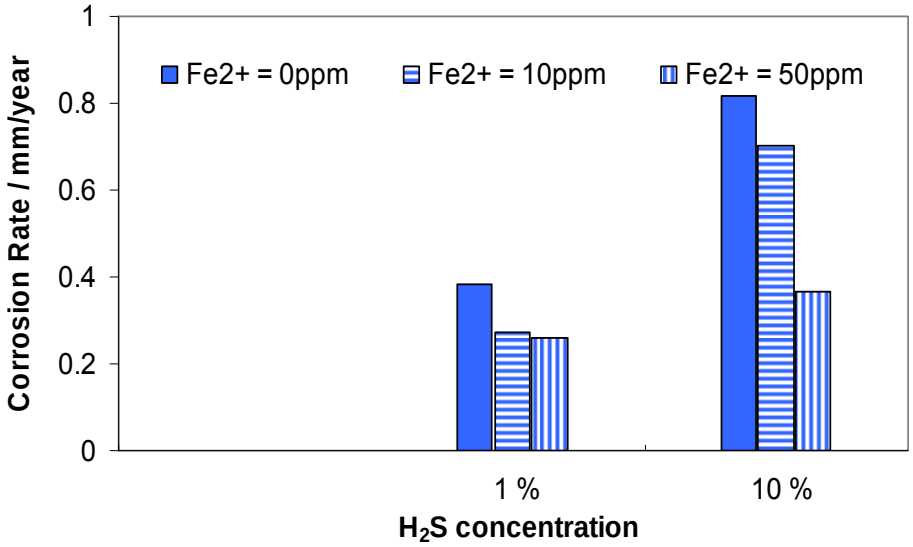

Figure 62. The corrosion rate of X65 carbon steel in mm/year at different H_2S concentration and initial Fe^{2+} concentration in the solution with H_2S/N_2 at T=60°C, the total reaction time is 24 hours.

The morphologies of iron sulfide scale formed on the X65 carbon steel surface at temperature of 60°C under the different test conditions are shown from Figure 63 to Figure 68. At H_2S concentration of 1%, the iron sulfide scale evenly covered the steel surface in the first hour and with more amorphous film on the top in twenty four hours, as shown in Figure 63, Figure 64, and Figure 65. With the increase of H_2S concentration to 10%, the iron sulfide scale formed on the steel surface with some parts fragmented in both the first hour and twenty four hours (Figure 66 to Figure 68). Compared the morphologies of iron sulfide at different Fe^{2+} concentration, it is found that Fe^{2+} has little effect on the scale formation.

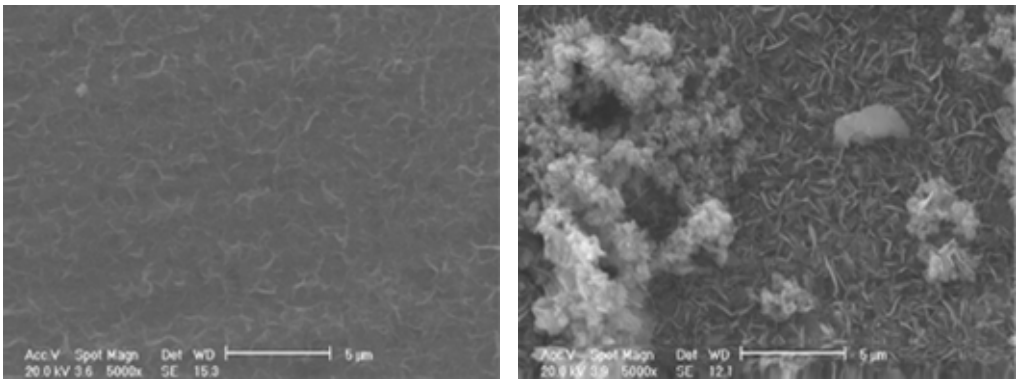

(A) (B)

Figure 63. The morphology (5000x) of iron sulfide formed on the X65 carbon steel surface under the conditions of 1% H_2S (H_2S/N_2 gas), T=60°C, pH 5, Fe^{2+} = 0 ppm, the total reaction time is (A) 1 hour, (B) 22 hours.

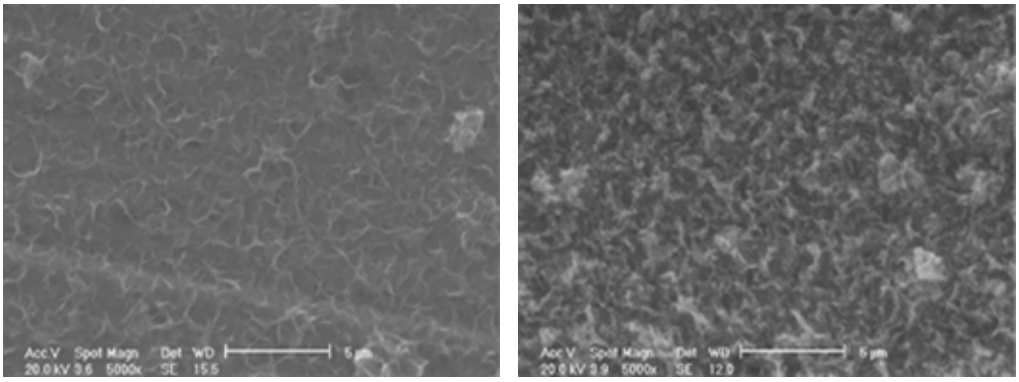

(A) (A)

Figure 64. The morphology (5000x) of iron sulfide formed on the X65 carbon steel surface under the conditions of 1% H_2S (H_2S/N_2 gas), T=60°C, pH 5, Fe^{2+} = 10 ppm, the total reaction time is (A) 1 hour, (B) 22 hours.

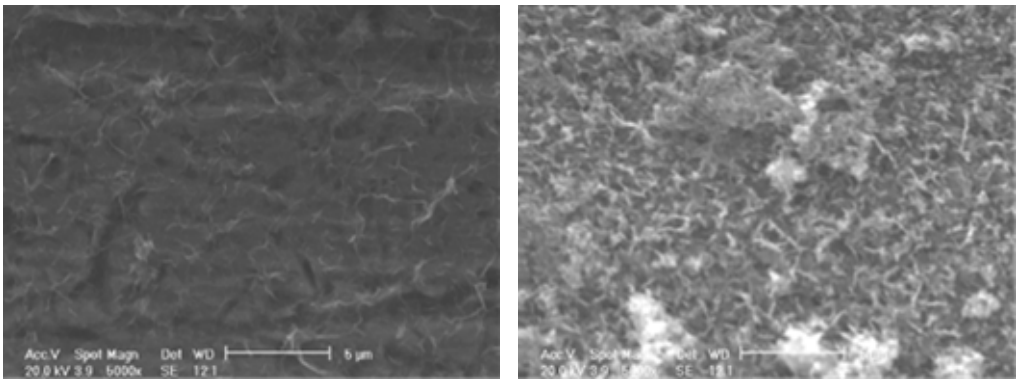

(A) (B)

Figure 65. The morphology (5000x) of iron sulfide films formed on the X65 carbon steel surface under the conditions of 1% H_2S (H_2S/N_2 gas), T=60°C, pH 5, Fe^{2+} = 50 ppm, the total reaction time is (A) 1 hour, (B) 22 hours.

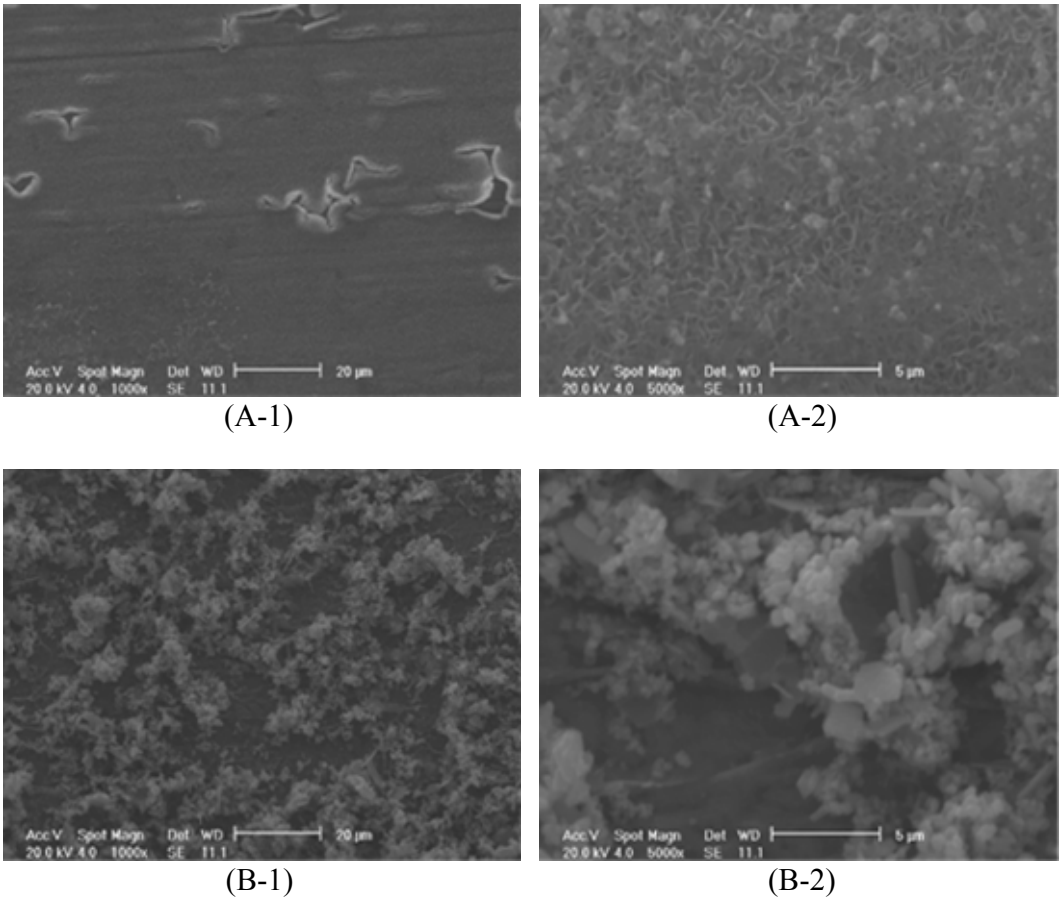

Figure 66. The morphology (at 1000x and 5000x) of iron sulfide formed on the X65 carbon steel surface under the conditions of 10% H_2S (H_2S/N_2 gas), T=60°C, pH 4.8~5.1, Fe^{2+} = 0 ppm, the total reaction time is (A) 1 hour, (B) 19 hours.

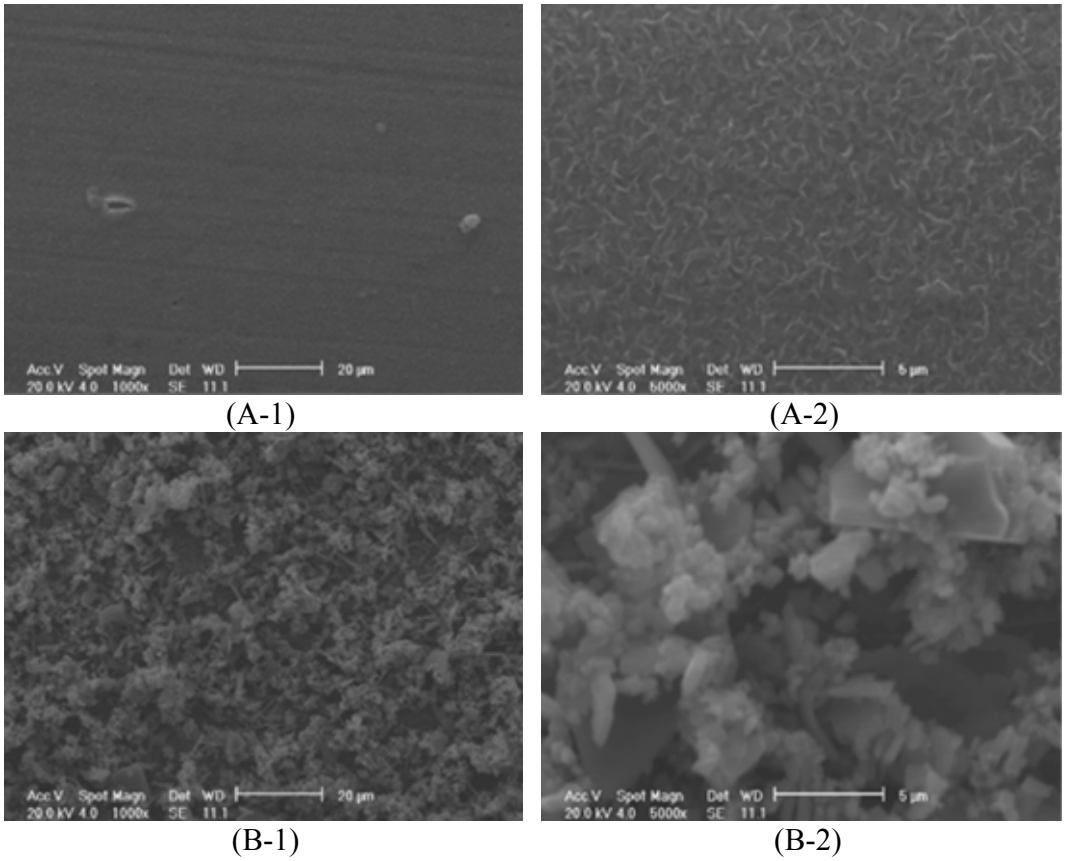

Figure 67. The morphology (at 1000x and 5000x) of iron sulfide formed on the X65 carbon steel surface under the conditions of 10% H_2S (H_2S/N_2 gas), T=60^oC, pH 4.8~5.1, Fe^{2+} = 10 ppm, the total reaction time is (A) 1 hour, (B) 19 hours.

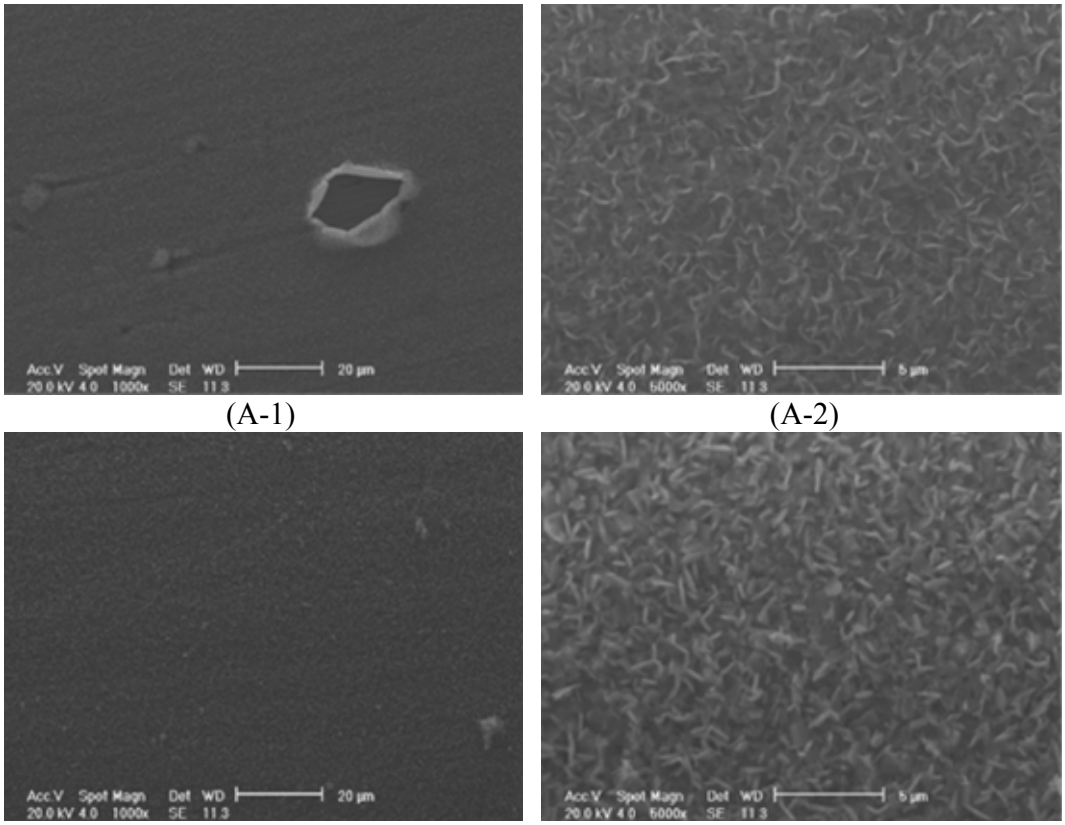

Figure 68. The morphology (at 1000x and 5000x) of iron sulfide films formed on the X65 carbon steel surface under the conditions of 10% H_2S (H_2S/N_2 gas), T=60^oC, pH 4.8~5.1, Fe^{2+} = 50 ppm, the total reaction time is (A) 1 hour, (B) 19 hours.

Electron probe micro-analyzer (EPMA) was employed to analyze the specimen which is covered with iron sulfide scale under the conditions of T 60^oC, H_2S 10%, Fe^{2+} 50 ppm, and the reaction time of 19 hours. Based on CASINO electron beam-Fe-S specimen interaction simulation, electron beam accelerated by 20 kV would have an interaction volume penetrating about 2-3 μm into the scale. The EPMA result (65.36 wt.% of Fe and 32.795 wt.% of S, which can be normalized to 53.366 at.% of Fe and 46.635 at.% of S) shows that the scale composition is consistent with mackinawite. The slightly Fe enrichment is related to the contribution of substrate Fe in the measurement.

The third set of experiments was conducted at the temperature of 80^{o}C. Figure 69 shows the retention rate of iron sulfide and the corrosion rate of X65 in the first hour under the conditions of initial Fe^{2+} concentration of 0 ppm, 10 ppm and 50 ppm, and H_2S concentration of 0.1%, 1% and 10%. As shown in Figure 69, both the retention rate of iron sulfide scale and the corrosion rate of X65 increased with the increase of H_2S concentration and did not alter much with the increase of Fe^{2+} concentration. Figure 70 shows that the corrosion rate is about 1.5 to 3 mm/year. With the total reaction time increasing to 24 hours, similar trends at different H_2S concentrations and Fe^{2+} concentrations in 24 hours were obtained as the experimental data in one hour. Both the scale retention rate and corrosion rate decreased, as illustrated in Figure 71. The corrosion rate drifted down below 0.6 mm/year, as shown in Figure 72. The error bars in the figures represent the maximum and minimum measured the scale retention rates and the corrosion rates.

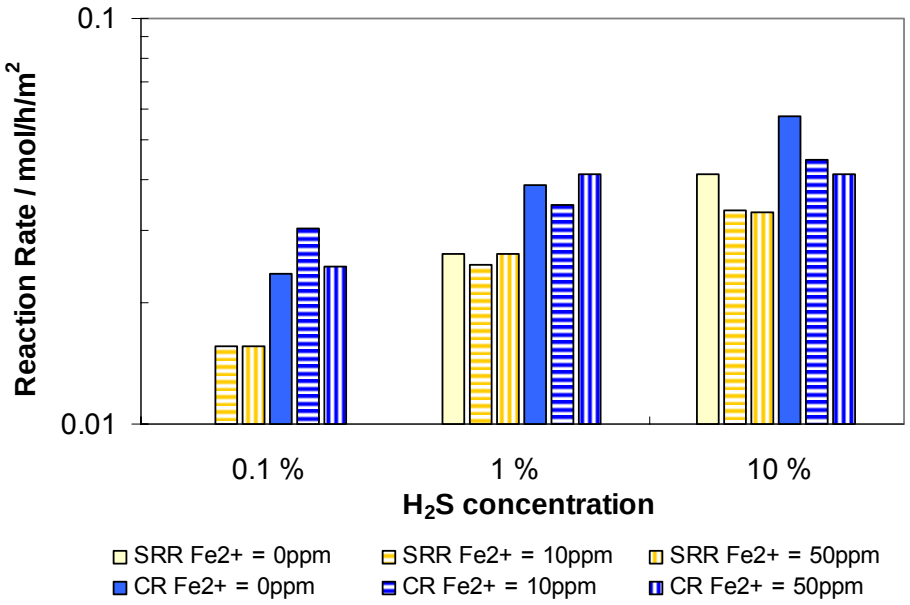

Figure 69. Both the retention rate of iron sulfide formed on X65 carbon steel surface and the corrosion rate of X65 carbon steel in the same molar unit at different H_2S concentration and initial Fe^{2+} concentration in the solution with H_2S/N_2 at T=80°C, the total reaction time is 1 hour.

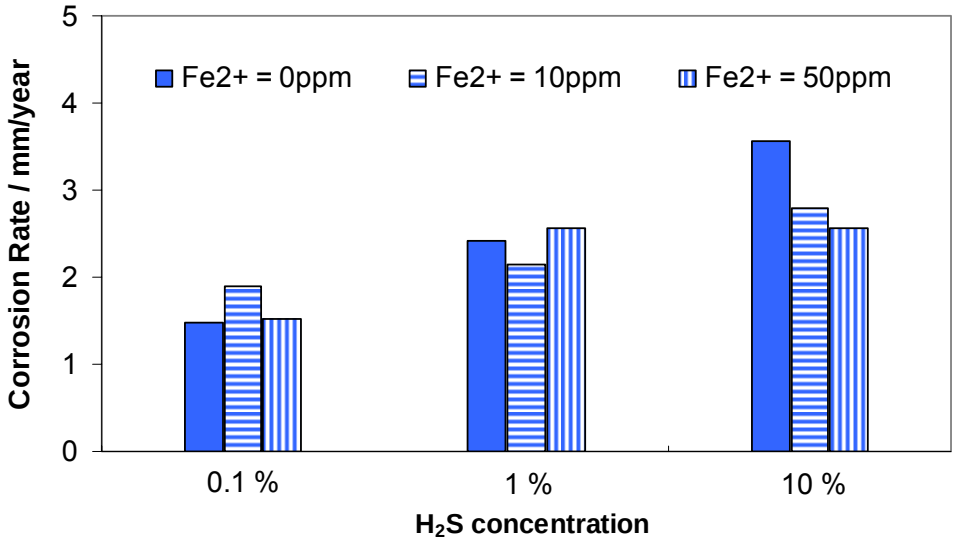

Figure 70. The corrosion rate of X65 carbon steel in mm/year at different H_2S concentration and initial Fe^{2+} concentration in the solution with H_2S/N_2 at T=80°C, the total reaction time is 1 hour.

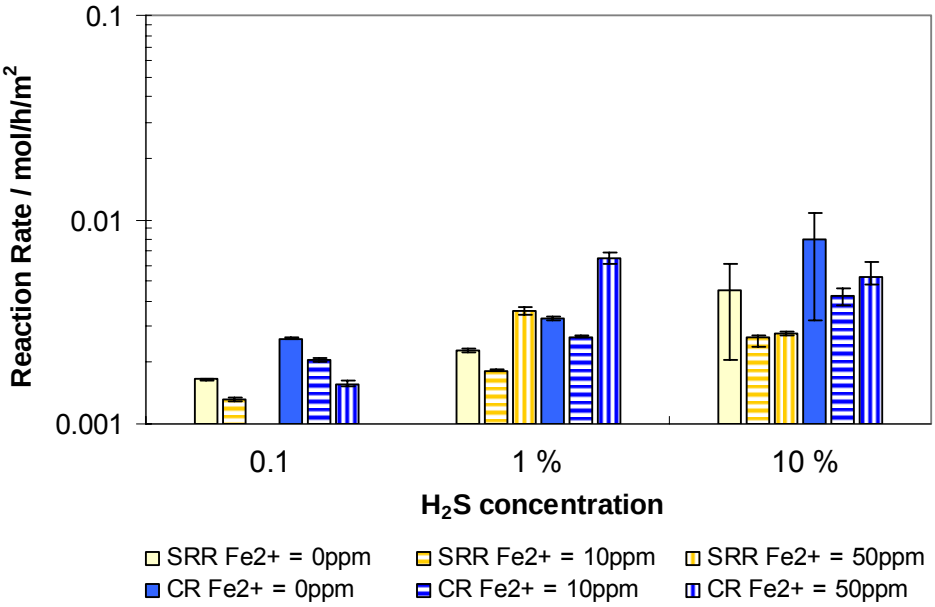

Figure 71. Both the retention rate of iron sulfide formed on X65 carbon steel surface and the corrosion rate of X65 carbon steel in the same molar unit at different H_2S concentration and initial Fe^{2+} concentration in the solution with H_2S/N_2 at T=80°C, the total reaction time is 24 hours.

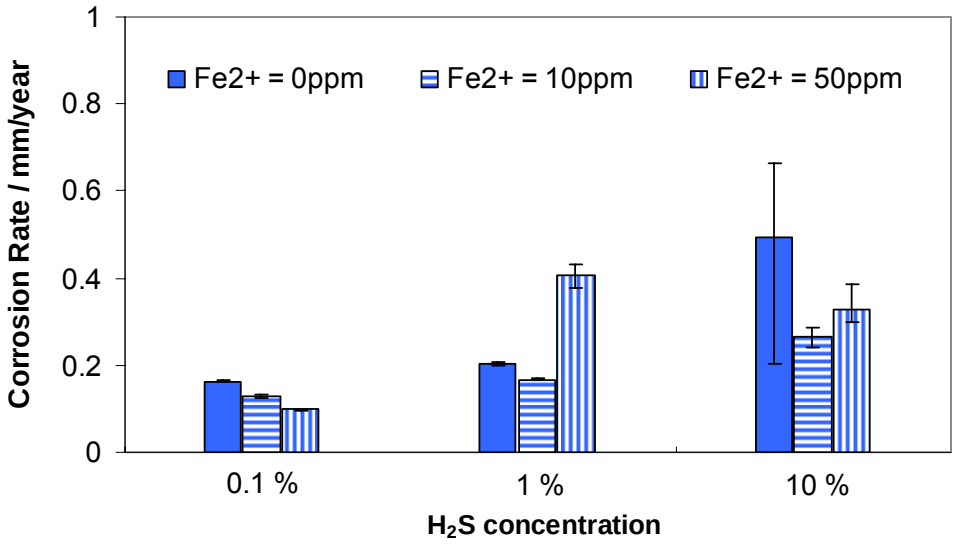

Figure 72. The corrosion rate of X65 carbon steel in mm/year at different H_2S concentration and initial Fe^{2+} concentration in the solution with H_2S/N_2 at T=80°C, the total reaction time is 24 hours.

Figure 73 to Figure 78 show the morphology of iron sulfide scale formed on the X65 carbon steel surface at different Fe^{2+} concentrations of 0 ppm and 50 ppm, H_2S concentrations of 0.1%, 1%, and 10%, and reaction time of 1 hour and twenty four hours. It is found that there is little iron sulfide scale formed on the steel surface at H_2S concentration of 0.1% in the first hour, illustrated in Figure 73 (A) and Figure 74 (A). With the increase of the reaction time to approximately 24 hours, the steel surface is evenly covered by the iron sulfide scale. Comparing the morphology of iron sulfide scale shown in Figure 73 and Figure 74, Fe^{2+} concentration does not affect the iron sulfide formation at the temperature of 80^oC and H_2S concentration of 0.1%. While increasing H_2S concentration to 1%, the iron sulfide scale forms in the first one hour and evenly covers the steel surface, and then the scale becomes more protective in 23 hours, as shown in Figure 75 and Figure 76. No effect of Fe^{2+} concentration is identified at H_2S concentration of 1%. With the increase of H_2S concentration to 10%, even more iron sulfide scale forms on the steel surface in the first hour (Figure 77 and Figure 78). The cross sections of the scale formed under different test conditions are shown in Figure 79 in one hour and Figure 80 and Figure 81 in twenty four hours. The thickness of the scale is approximately 10 to 15 μm. The figures show that there is a delaminated scale.

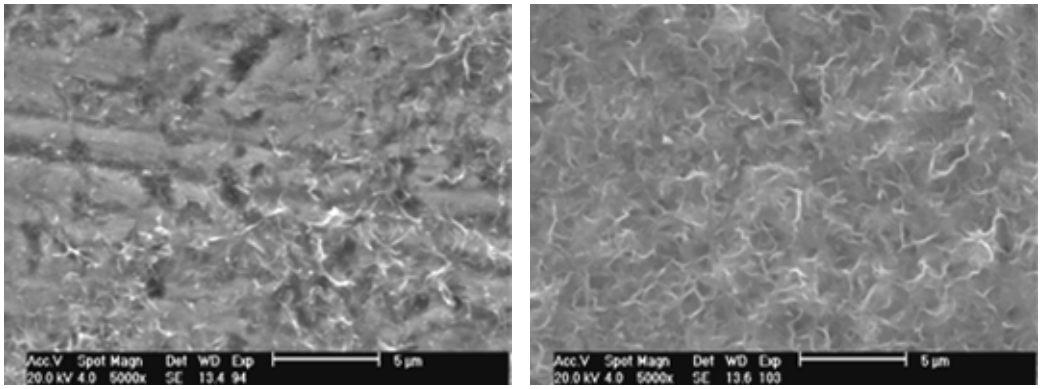

(A) (B)

Figure 73. The morphology (5000x) of iron sulfide scale formed on the X65 carbon steel surface under the conditions of 0.1% H_2S (H_2S/N_2 gas), T=80°C, pH 5.5, Fe^{2+} = 0 ppm, the total reaction time is (A) 1 hour, (B) 25.5 hours.

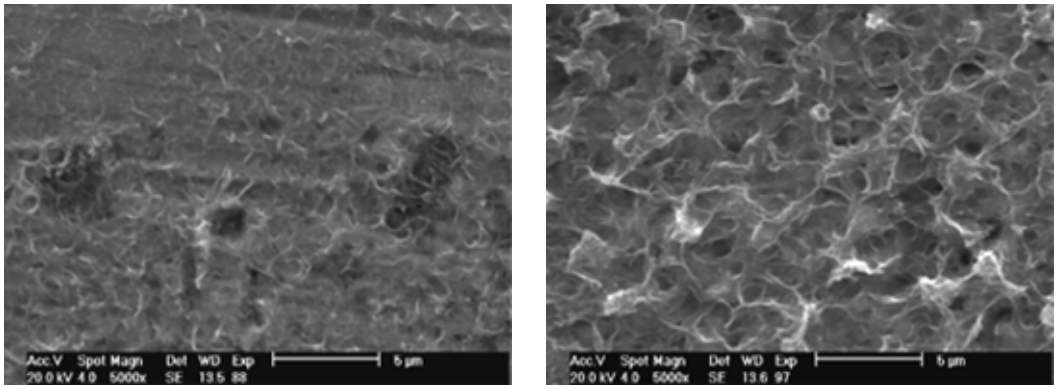

(A) (B)

Figure 74. The morphology (at 1000x and 5000x) of iron sulfide scale formed on the X65 carbon steel surface under the conditions of 0.1% H_2S (H_2S/N_2 gas), T=80°C, pH 5.5, Fe^{2+} = 50 ppm, the total reaction time is (A) 1 hour, (B) 25.5 hours.

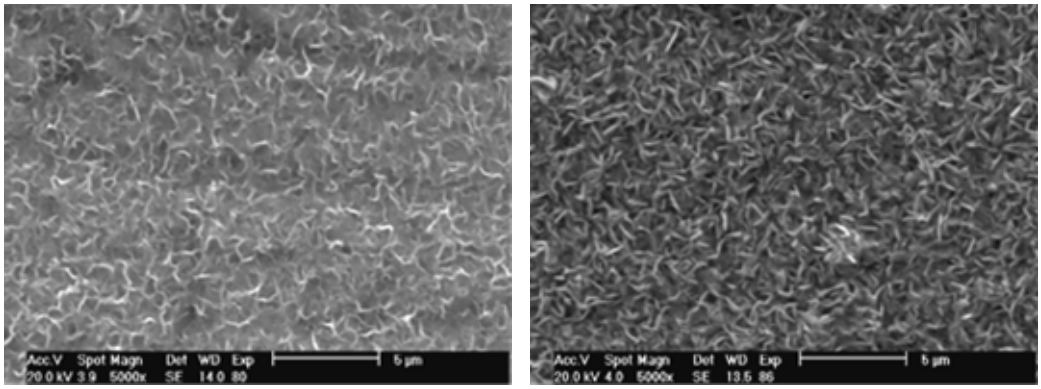

(A) (B)

Figure 75. The morphology (5000x) of iron sulfide scale formed on the X65 carbon steel surface under the conditions of 1% H_2S (H_2S/N_2 gas), T=80°C, pH 5.5, Fe^{2+} = 0 ppm, the total reaction time is (A) 1 hour, (B) 23 hours.

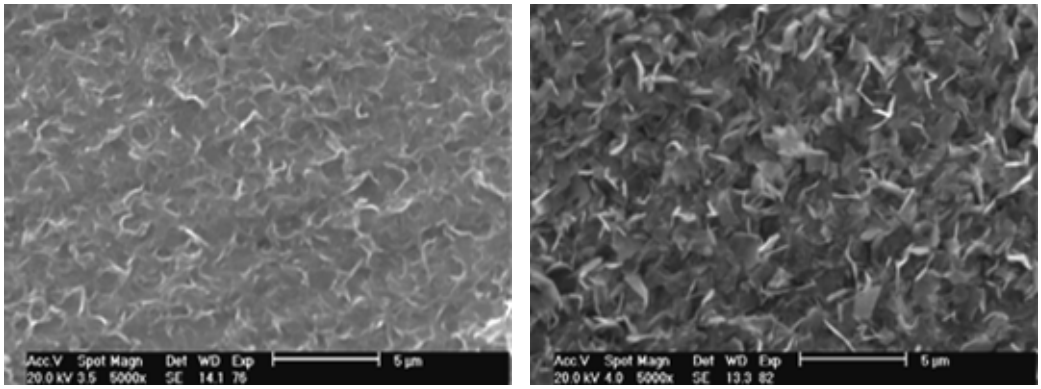

(A) (B)

Figure 76. The morphology (5000x) of iron sulfide scale formed on the X65 carbon steel surface under the conditions of 1% H_2S (H_2S/N_2 gas), T=80°C, pH 5.5, Fe^{2+} = 50 ppm, the total reaction time is (A) 1 hour, (B) 23 hours.

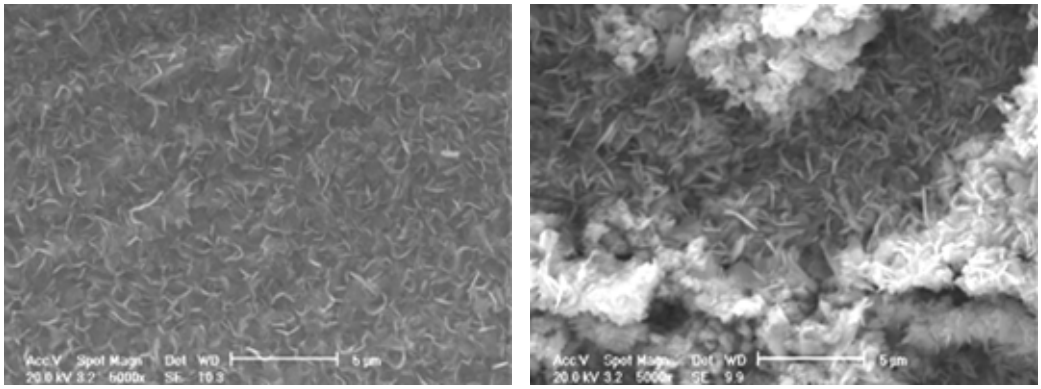

(A) (B)

Figure 77. The morphology (5000x) of iron sulfide scale formed on the X65 carbon steel surface under the conditions of 10% H_2S (H_2S/N_2 gas), T=80°C, pH 5.2, Fe^{2+} = 0 ppm, the total reaction time is (A) 1 hour, (B) 24 hours.

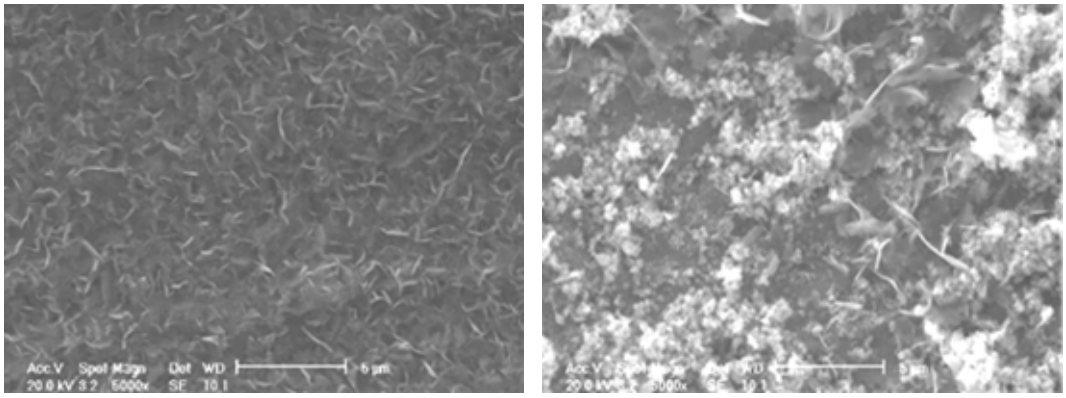

(A) (B)

Figure 78. The morphology (5000x) of iron sulfide scale formed on the X65 carbon steel surface under the conditions of 10% H_2S (H_2S/N_2 gas), T=80°C, pH 5.2, Fe^{2+} = 50 ppm, the total reaction time is (A) 1 hour, (B) 24 hours.

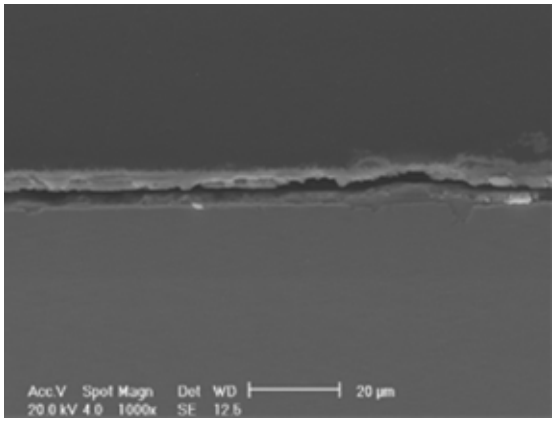

Figure 79. Cross section of the films formed on the X65 carbon steel surface (at 1000x) under the conditions of 10% H_2S (H_2S/CO_2 gas), T=80°C, pH 5, Fe^{2+}=0 ppm, the total reaction time is 1 hour.

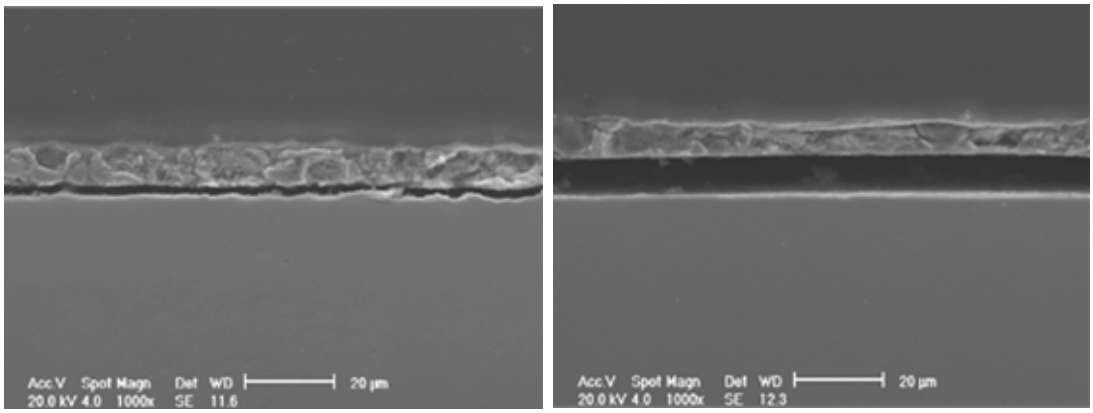

(A) (B)

Figure 80. Cross section of the scale formed on the X65 carbon steel surface (at 1000x) under the conditions of 0.1% H_2S (H_2S/N_2 gas), T=80°C, pH 5, (A) Fe^{2+}=0 ppm, (B) Fe^{2+}=50ppm, the total reaction time is 24 hours.

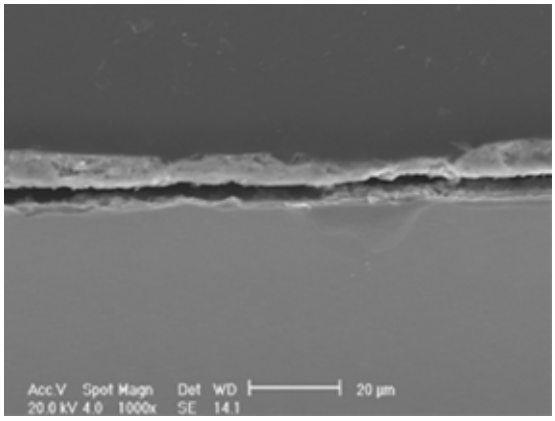

Figure 81. Cross section of the scale formed on the X65 carbon steel surface (at 1000x) under the conditions of 1% H_2S (H_2S/N_2 gas), T=80°C, pH 5, Fe^{2+}=0 ppm, the total reaction time is 24 hours.

The XRD results of iron sulfide scale are shown from Figure 82 to Figure 87. Mackinawite is the only product formed on the X65 carbon steel surface under the test conditions. The XPS results (Figure 88) of iron sulfide scale formed on the steel surface under the conditions of T 80°C, pH 5, Fe^{2+} 0 ppm, H_2S 10%, and the reaction time 23 hours show that FeS is the predominant product formed on the steel surface, which are in good agreement with the XRD results. Small amount of S element is detected by XPS because iron sulfide scale on the surface of the specimen gets oxidized while in air.

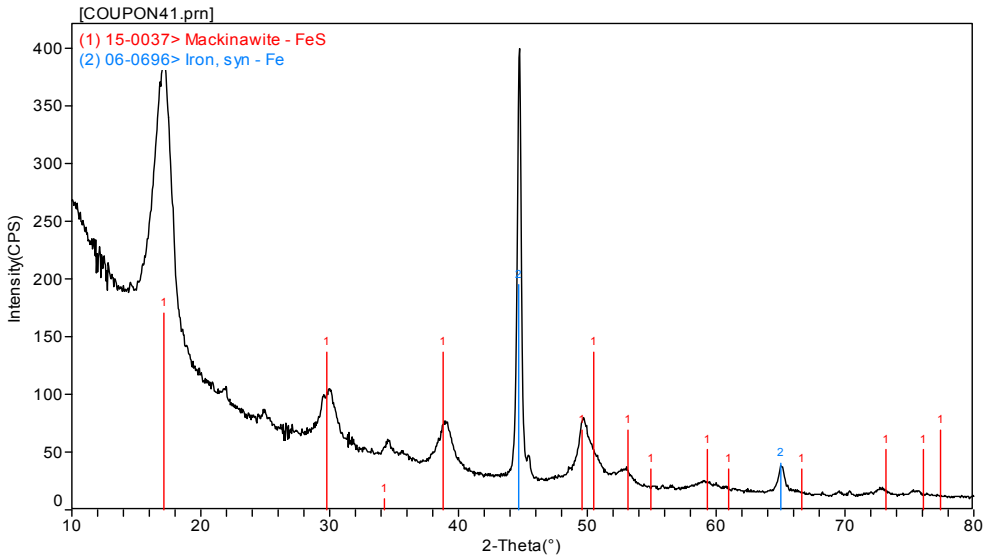

Figure 82. XRD results of iron sulfide films formed on the X65 carbon steel surface under the conditions of 1% H_2S (H_2S/N_2 gas), T=80°C, pH 5.5, Fe^{2+} = 0 ppm, the total reaction time is 1 hour.

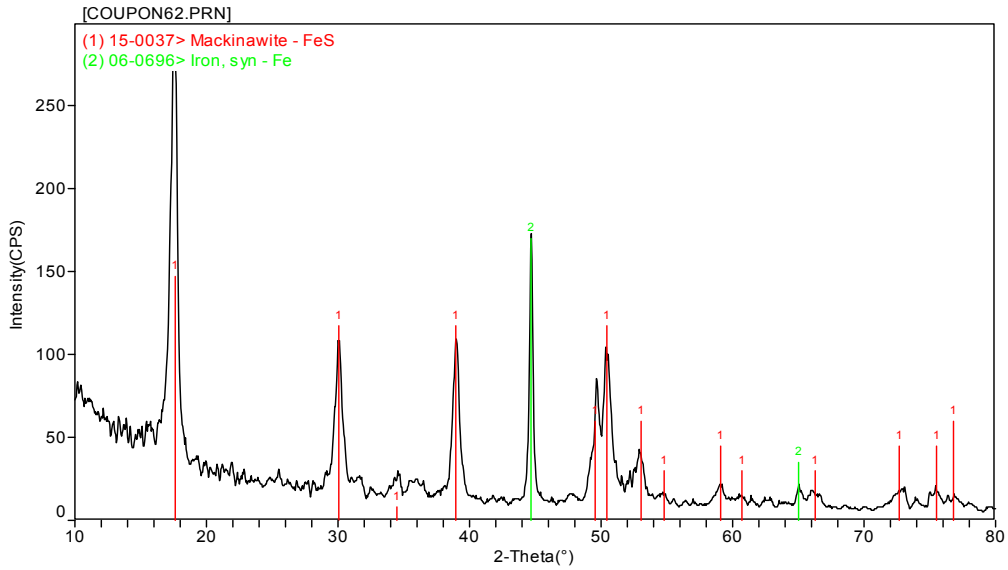

Figure 83. XRD results of iron sulfide films formed on the X65 carbon steel surface under the conditions of 10% H_2S (H_2S/N_2 gas), T=80°C, pH 5.2, Fe^{2+} = 0 ppm, the total reaction time is 1 hour.

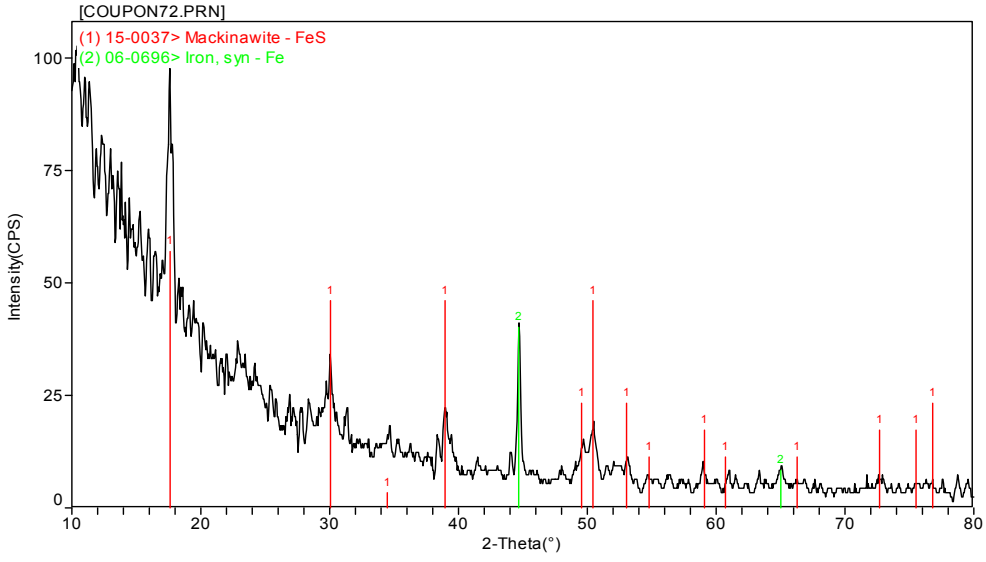

Figure 84. XRD results of iron sulfide films formed on the X65 carbon steel surface under the conditions of 10% H_2S (H_2S/N_2 gas), T=80°C, pH 5.2, Fe^{2+} = 50 ppm, the total reaction time is 1 hour.

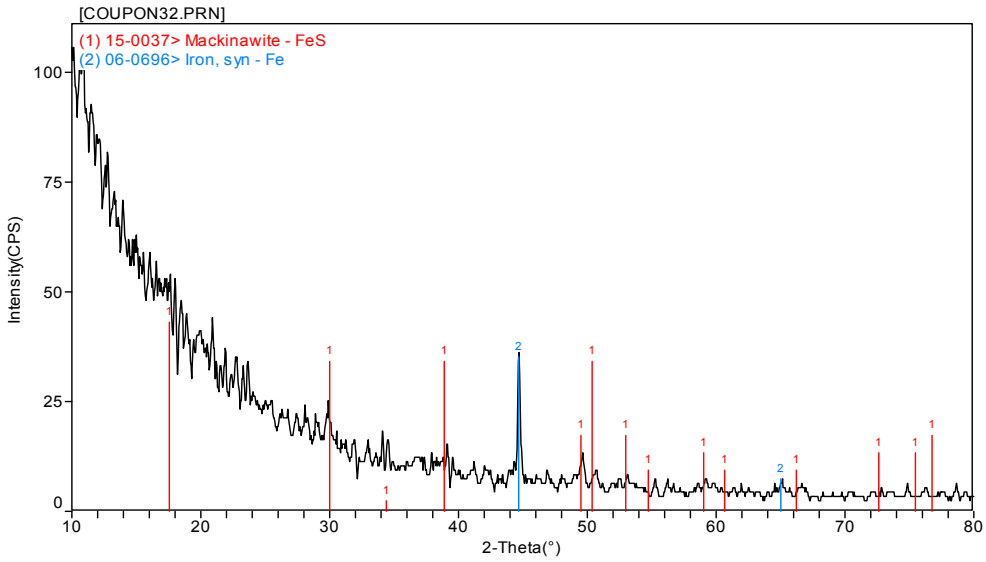

Figure 85. XRD results of iron sulfide films formed on the X65 carbon steel surface under the conditions of 0.1% H_2S (H_2S/N_2 gas), T=80°C, pH 5.5, Fe^{2+} = 10 ppm, the total reaction time is 25.5 hours.

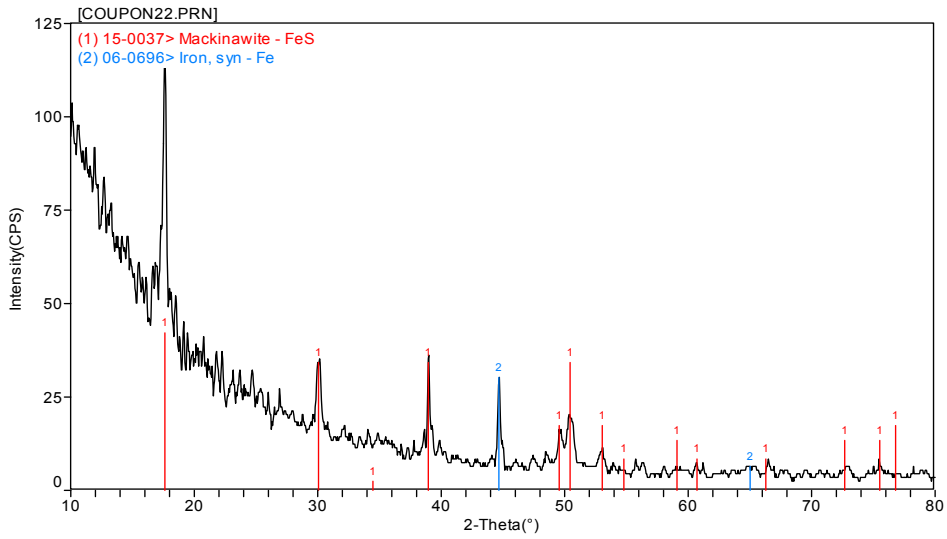

Figure 86. XRD results of iron sulfide scale formed on the X65 carbon steel surface under the conditions of 1% H_2S (H_2S/N_2 gas), T=80°C, pH 5.5, Fe^{2+} = 10 ppm, the total reaction time is 23 hours.

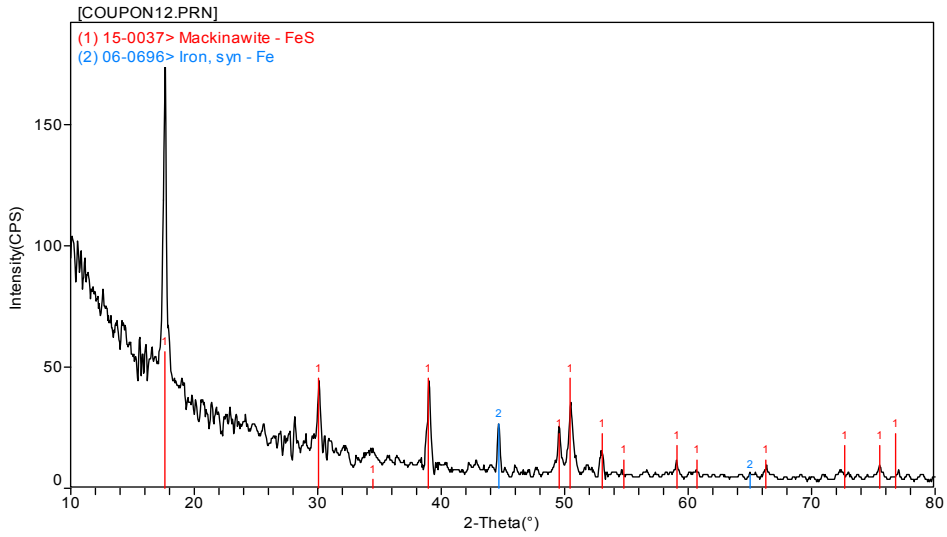

Figure 87. XRD results of iron sulfide scale formed on the X65 carbon steel surface under the conditions of 10% H_2S (H_2S/N_2 gas), T=80°C, pH 5.2, Fe^{2+} = 10 ppm, the total reaction time is 24 hours.

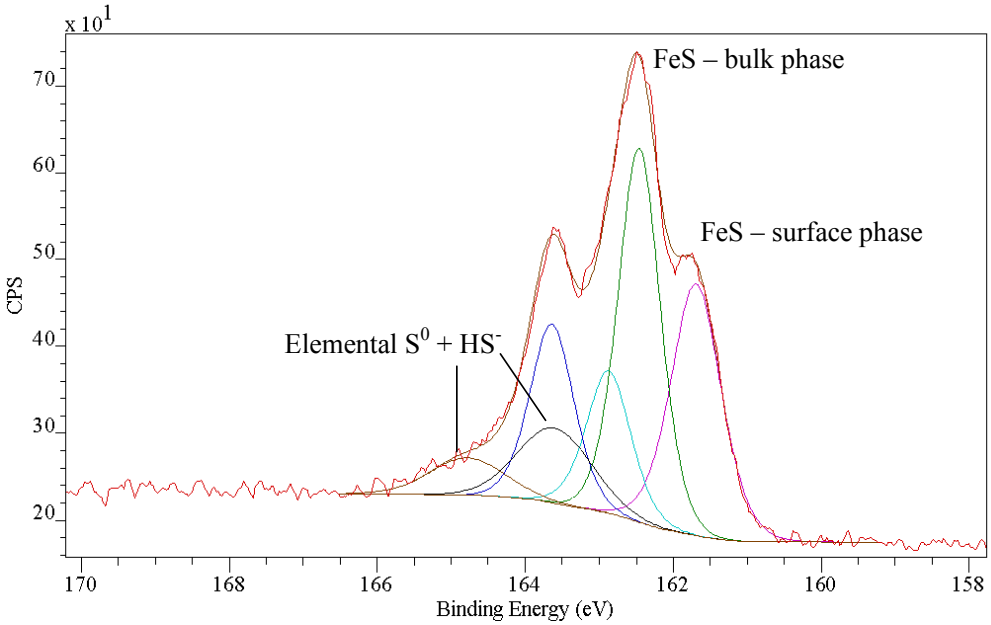

Figure 88. XPS multiplex S2p spectrum recorded at the surface of specimen under the conditions of T=80°C, pH 5, Fe^{2+} 0 ppm, H_2S 10%, and reaction time 23 hours.

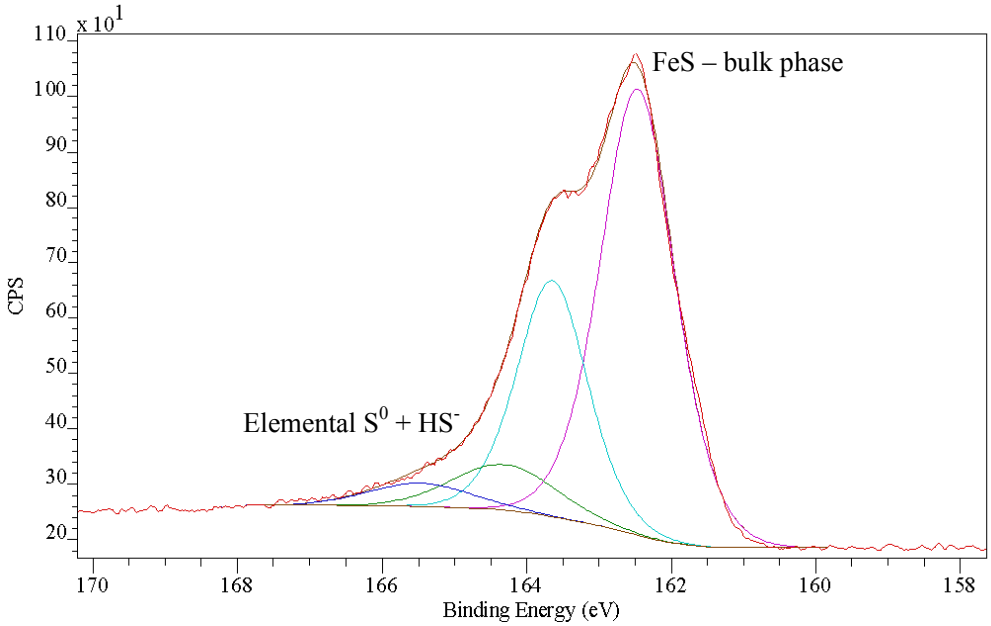

Figure 89. XPS multiplex S2p spectrum recorded following 100Å ion etch for the specimen under the conditions of T=80°C, pH 5, Fe^{2+} 0 ppm, H_2S 10%, and reaction time 23 hours.

From the above discussion, it has been found that the corrosion of steel has a significant effect on the iron sulfide scale retention rate. Therefore, a number of experiments were conducted using much more corrosion-resistant stainless steel as the substrate under the similar test conditions as using mild X65 carbon steel. The corrosion rate of stainless steel is below 0.04 mm/year under all the test conditions. The results show that there is almost no iron sulfide scale formed on the stainless steel surface. An example of the morphology of the stainless steel specimens proves that there is little iron sulfide scale formed on the stainless steel surface (Figure 90).

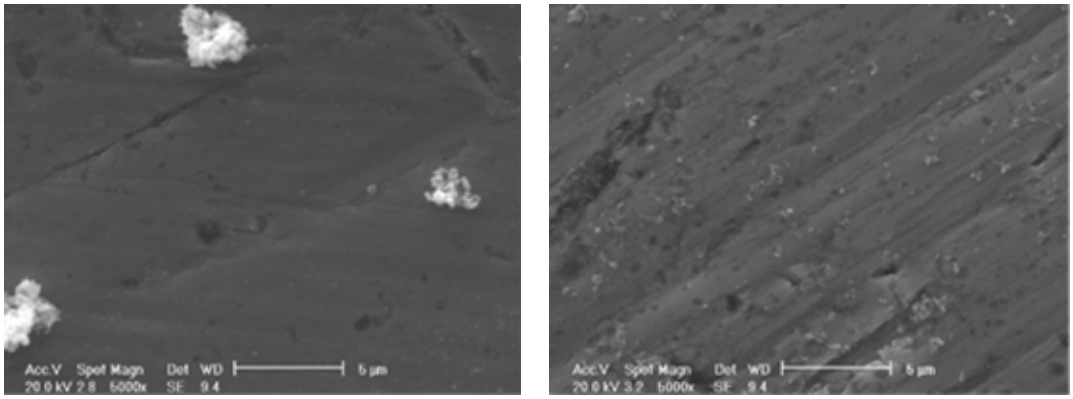

(A) (B)

Figure 90. The morphology (5000x) of the stainless steel specimen under the conditions of 10% H_2S (H_2S/N_2 gas), T=80^oC, pH 5, (A) Fe^{2+} = 0 ppm, (B) Fe^{2+} = 50 ppm, and the total reaction time 24 hours.

It has been found that there is no significant effect of Fe^{2+} concentration on both the corrosion rate and the scale retention rate. Therefore, it is concluded that Fe^{2+} concentration has little effect on both the corrosion rate and the scale retention rate under the test conditions. In addition, compared to X65 carbon steel, there is little scale formed on the stainless steel surface. Therefore, it is suggested that mackinawite scale is formed on the steel surface, most likely by solid state reaction.

5.6 Modeling

5.6.1 Summary of experimental results

It was observed above that in pure H_2S corrosion of mild steel there was no significant effect of dissolved Fe^{2+} concentration on neither the corrosion rate nor the iron sulfide scale retention rate. This was in sharp contrast with pure CO_2 corrosion where the iron carbonate scale formation rate is a strong function of Fe^{2+} concentration, i.e., it depends heavily on iron carbonate supersaturation, which is a major driving force for iron carbonate scale formation by precipitation. Actually it was long known that iron sulfide

films form even in solutions which are well undersaturated,[25] i.e., at pH much lower than pH 5.0 - 5.5 which was used in this study. In addition, the structure and morphology of the iron sulfide scale formed in H_2S corrosion (which was identified primarily as mackinawite) is very different from the iron carbonate scale formed in CO_2 corrosion. It is also observed that filmed crystalline iron sulfide films, with cracks and delaminations, often with the imprint of the underlying metal surface clearly visible even after long exposures. Therefore it is hypothesized here that iron sulfide films observed in the experiments form primarily by a direct heterogeneous chemical reaction between H_2S and iron at the steel surface (often referred to as a "solid state reaction").* This hypothesis does not exclude the possibility of iron sulfide films forming by precipitation in supersaturated solutions over long periods of time, however in the relatively short duration experiments the main mechanism of iron sulfide formation is the direct chemical reaction between H_2S and the steel surface. Even more importantly it is thought that the thin and tight iron sulfide films formed in this way are one of the most important controlling factors in H_2S corrosion.

5.6.1.1 Effect of H_2S concentration

A number of experiments were conducted to investigate the effect of H_2S gas concentration on the mackinawite scale formation in the solutions with H_2S/N_2 at the temperature of 80^oC. Figure 91 shows the comparison of corrosion rate and scale retention rates expressed in the same molar units *versus* H_2S gas concentration after a 1 hour exposure. The value for the scaling tendency which is the ratio of the two rates is

* This hypothesis is not entirely new, it has been mentioned a number of times in various publications on H_2S corrosion of steel. [12, 25]

also shown. The comparison indicates that both the corrosion rate and scale retention rate increase with the increase of H_2S gas concentration, however, the corrosion rate is always higher than the scale retention rate. The scaling tendency under the test conditions indicates that between 40% and 72% of the iron consumed by corrosion ended up as iron sulfide on the steel surface, with the balance lost to the solution. The scaling tendency is calculated using the following equation:

$$ST = \frac{Scale\ Retention\ Rate\left(mol/s/m^2\right)}{Corrosion\ Rate\left(mol/s/m^2\right)} \tag{56}$$

As a very small increase in dissolved Fe^{2+} was measured in the solution it was concluded that electrochemical iron dissolution is not the cause of the observed $ST<1$, rather some of the iron sulfide that formed on the steel by the solid state reaction has spalled off in a spontaneous process probably due to intrinsic growth stresses (since no flow was present in these experiments that would impose extrinsic hydrodynamic stresses). In Figure 92 the same kind of data is presented for a 24 hour exposure where a broader range of H_2S gas concentrations was used: 75 ppm – 10%. The same conclusions apply as for the 1 hour exposure with the exception that the magnitude of both the corrosion rate and scale retention rate is almost an order of magnitude lower. Interestingly, the scaling tendency remains in approximately the same range 33 - 70% suggesting that between one and two thirds of the iron sulfide that is formed by the corrosion process is lost to the solution by spalling.

The reduction in reaction rate with time is accentuated by the direct comparison of the 1-hour and 24-hour corrosion rates (Figure 93) and scale retention rates (Figure 94) at different H_2S gas concentration. Clearly the iron sulfide scale that is retained on the surface over time becomes gradually more protective.

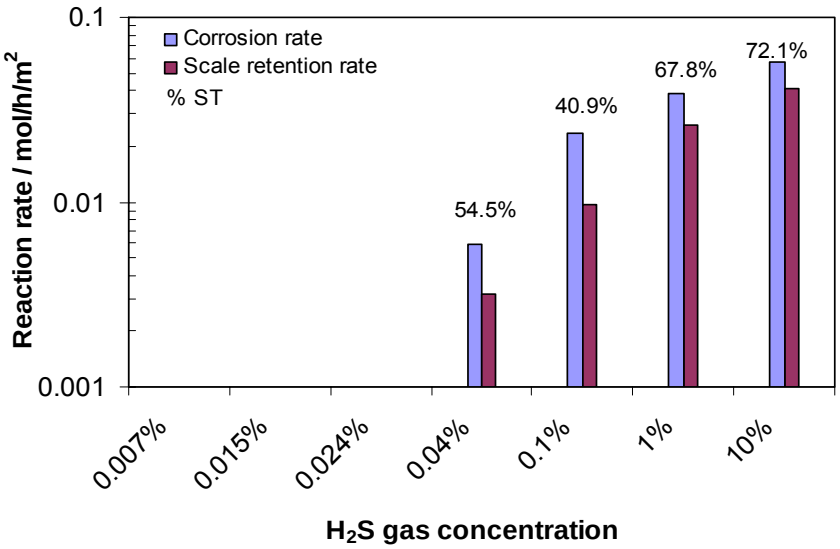

Figure 91. The comparison of corrosion rate (CR) and scale retention rate (SRR) in the same molar units as a function of H_2S gas concentration; ST=SRR/CR stands for Scaling Tendency; total pressure p=1 bar, T=80°C, initial Fe^{2+} aqueous concentration: 0 ppm, pH 5.0-5.5, reaction time 1 hr.

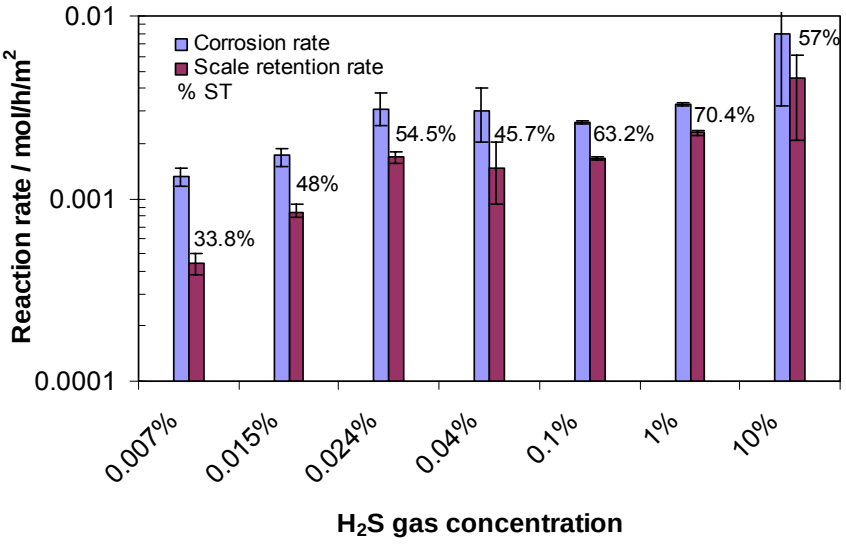

Figure 92. The comparison of corrosion rate (CR) and scale retention rate (SRR) in the same molar units as a function of H_2S gas concentration; ST=SRR/CR stands for Scaling Tendency; total pressure p=1 bar, T=80°C, initial Fe^{2+} aqueous concentration: 0 ppm, pH 5.0-5.5, reaction time: 24 hr.

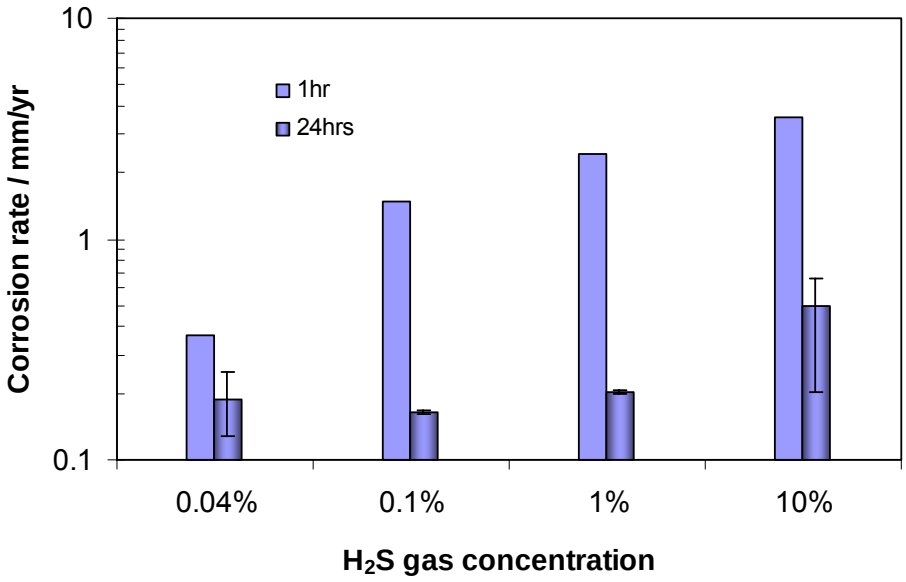

Figure 93. The corrosion rate vs. H_2S gas concentration after 1 hr and 24 hr exposure at total pressure p=1 bar, T=80°C, initial Fe^{2+} aqueous concentration: 0 ppm, pH 5.0-5.5.

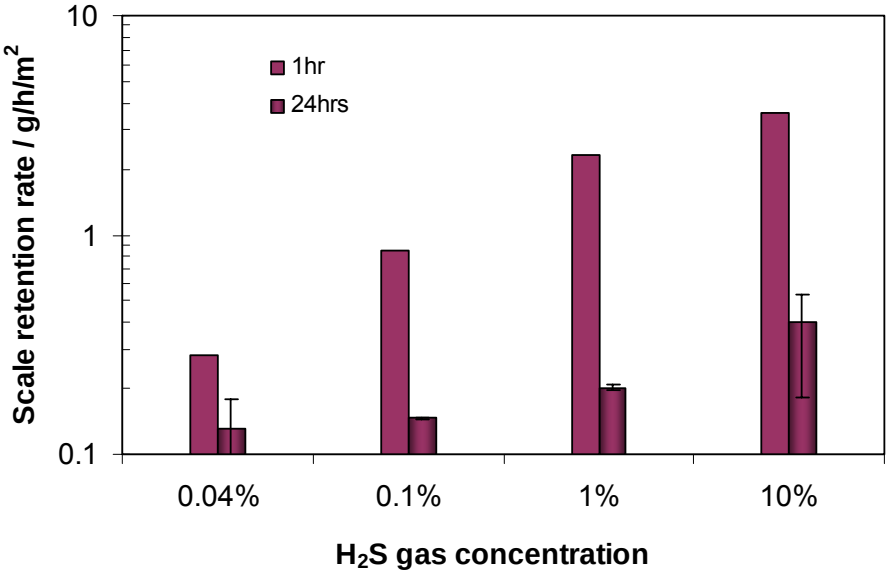

Figure 94. The scale retention rate vs. H_2S gas concentration after 1 hr and 24 hr exposure at total pressure p=1 bar, T=80°C, initial Fe^{2+} aqueous concentration: 0 ppm, pH 5.0-5.5.

5.6.1.2 Effect of temperature

The effect of temperature on both the corrosion rate and the scale retention rate is shown in Figure 95 for a 1 hour exposure and in Figure 96 for a 24 hour exposure at 1% H_2S gas concentration. Very weak temperature dependence is observed even for the shorter term exposure which all but disappears for the longer exposure times. The same is obtained in experiments at H_2S gas concentrations of 10%, as shown in Figure 97 and Figure 98. This seems to suggest that the corrosion rate is predominantly controlled by the presence of the iron sulfide scale, with the effect increasing over time.

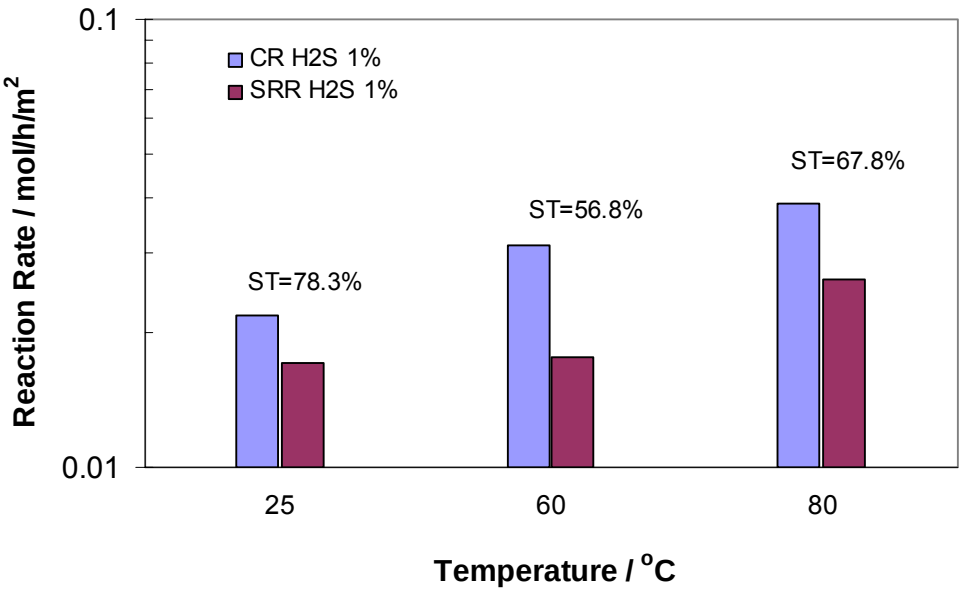

Figure 95. The corrosion rate (CR) and scale retention rate (SRR) vs. temperature, ST=SRR/CR stands for Scaling Tendency; conditions: total pressure p=1 bar, H_2S gas concentration is 1%, initial Fe^{2+} aqueous concentration: 0 ppm, pH 5.0 - 5.5, reaction time: 1 hr.

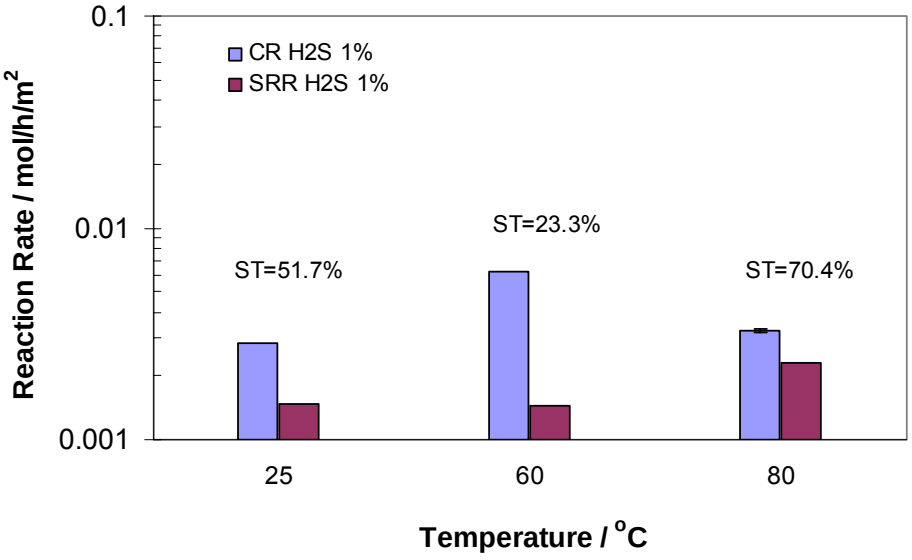

Figure 96. The corrosion rate (CR) and scale retention rate (SRR) vs. temperature, ST=SRR/CR stands for Scaling Tendency; conditions: total pressure p=1 bar, H_2S gas concentration: 1%, initial Fe^{2+} aqueous concentration: 0 ppm, pH 5.0 - 5.5, reaction time: 24 hr.

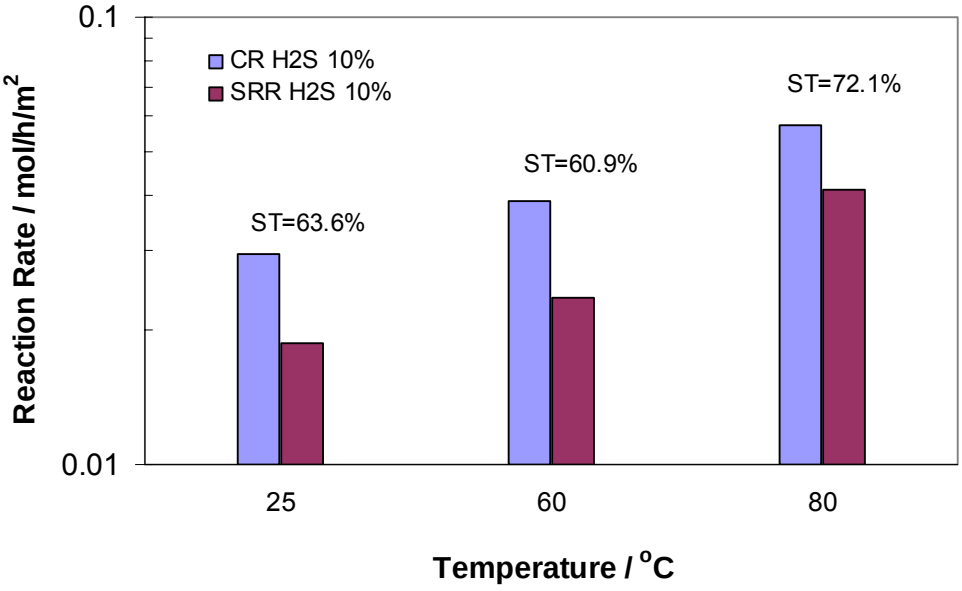

Figure 97. The corrosion rate (CR) and scale retention rate (SRR) vs. temperature, ST=SRR/CR stands for Scaling Tendency; conditions: total pressure p=1 bar, H_2S gas concentration: 10%, initial Fe^{2+} aqueous concentration: 0 ppm, pH 5.0 - 5.5, and reaction time 1 hr.

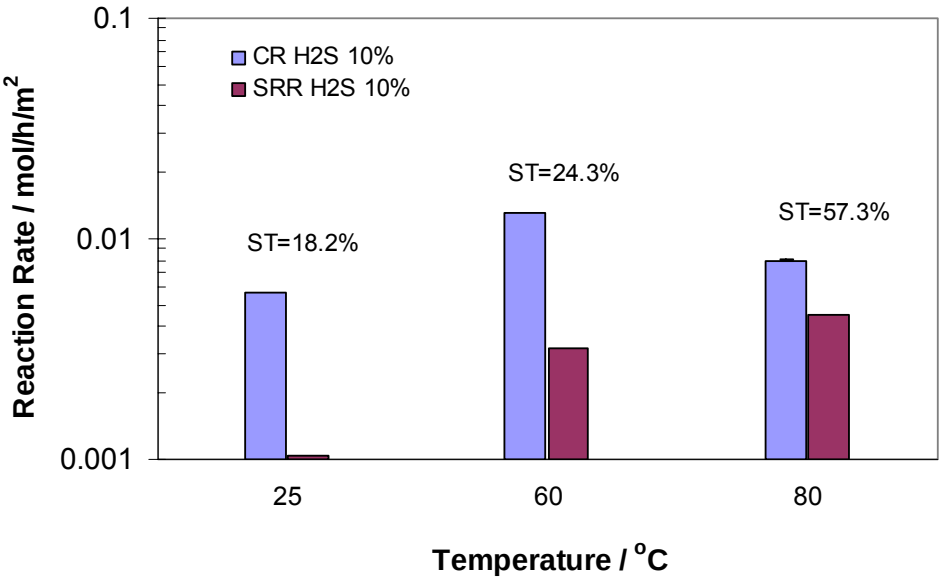

Figure 98. The corrosion rate (CR) and scale retention rate (SRR) vs. temperature, ST=SRR/CR stands for Scaling Tendency; conditions: total pressure p=1 bar, H_2S gas concentration: 10%, initial Fe^{2+} aqueous concentration: 0ppm, pH 5.0 - 5.5, and reaction time: 24 hr.

5.6.1.3 Effect of flow rate

The effect of flow rate has been investigated by varying the rotation rate of the cylindrical working electrode (with a diameter of 1.2 cm and an area of 5.4 cm^2) up to 8000 rpm which corresponds to a peripheral velocity of approximately 4 m/s and a wall-shear stress of 57 Pa, in experiments done with 400 ppm of H_2S in the gas phase. The corrosion rate as a function of reaction time at different velocities is shown in Figure 99. The corrosion rate clearly increases with velocity and the effect is much more pronounced for shorter exposure times. For longer exposures in flowing conditions, the corrosion rates decrease significantly just as they did in experiments conducted under stagnant conditions, due to a buildup of a protective iron sulfide scale. However, as shown in Figure 100, the scaling tendency, which is approximately 50% in static

conditions, decreases to below 20% under flowing conditions. This suggests that a much larger fraction of the iron sulfide scale formed in the corrosion process is lost to the solution due to the hydrodynamic stresses induced by the flow. Iron sulfide film dissolution could be excluded due to a slight supersaturation of the solution with respect to mackinawite.

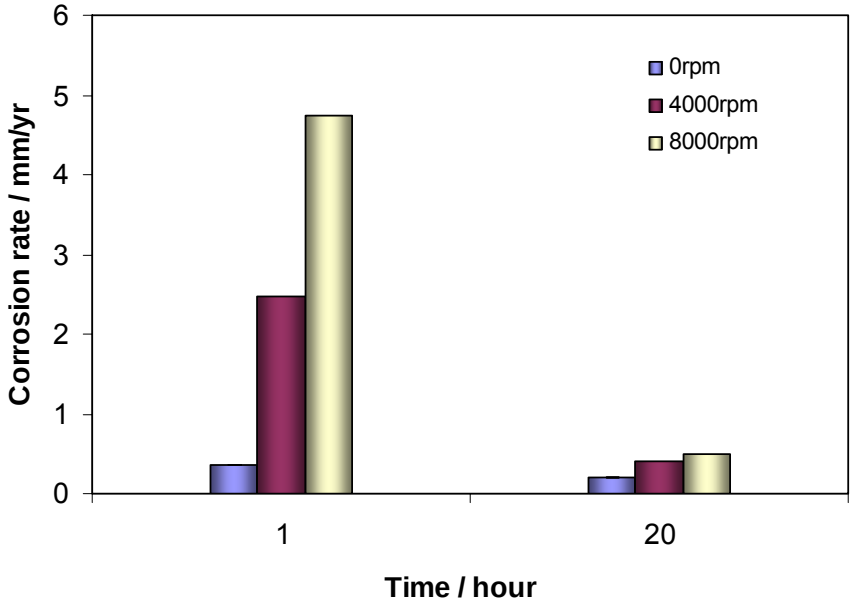

Figure 99. The corrosion rate vs. time for different rotational speeds; conditions: total pressure p=1 bar, T=25^{o}C**,** H_2S gas concentration: 0.04%, initial Fe^{2+} aqueous concentration: 0 ppm, pH 5.0-5.5.

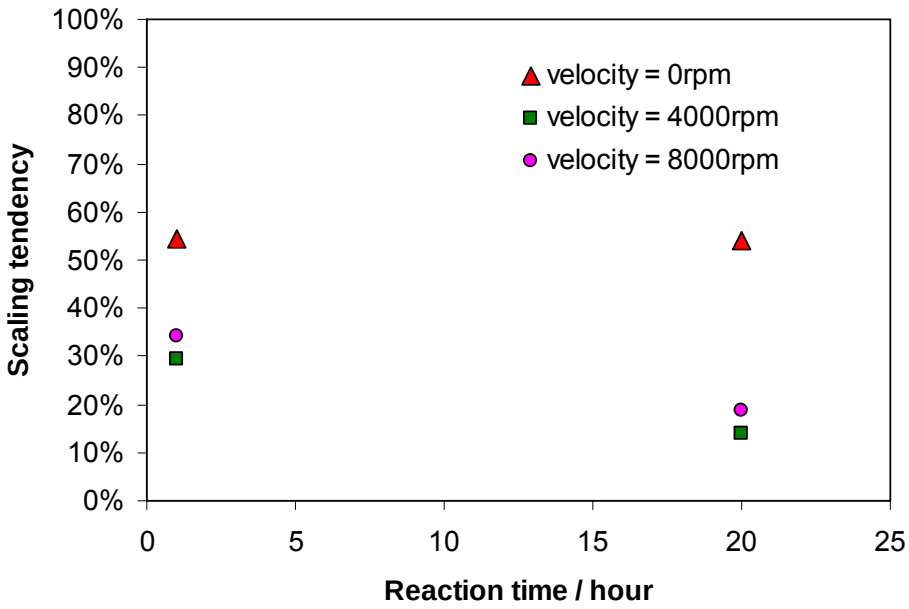

Figure 100. The comparison of scaling tendency vs. reaction time under the conditions of total pressure p=1 bar, T=25°C, H_2S gas concentration 0.04%, initial Fe^{2+} aqueous concentration 0 ppm, and velocity 0, 4000, and 8000 rpm.

The morphology of the scale formed on the steel surface at different velocities is shown in Figure 101. At velocity 100 rpm, there are porous iron sulfide layer formed on the steel surface; while at velocity 8000 rpm, most of the porous iron sulfide layer was removed from the steel surface.

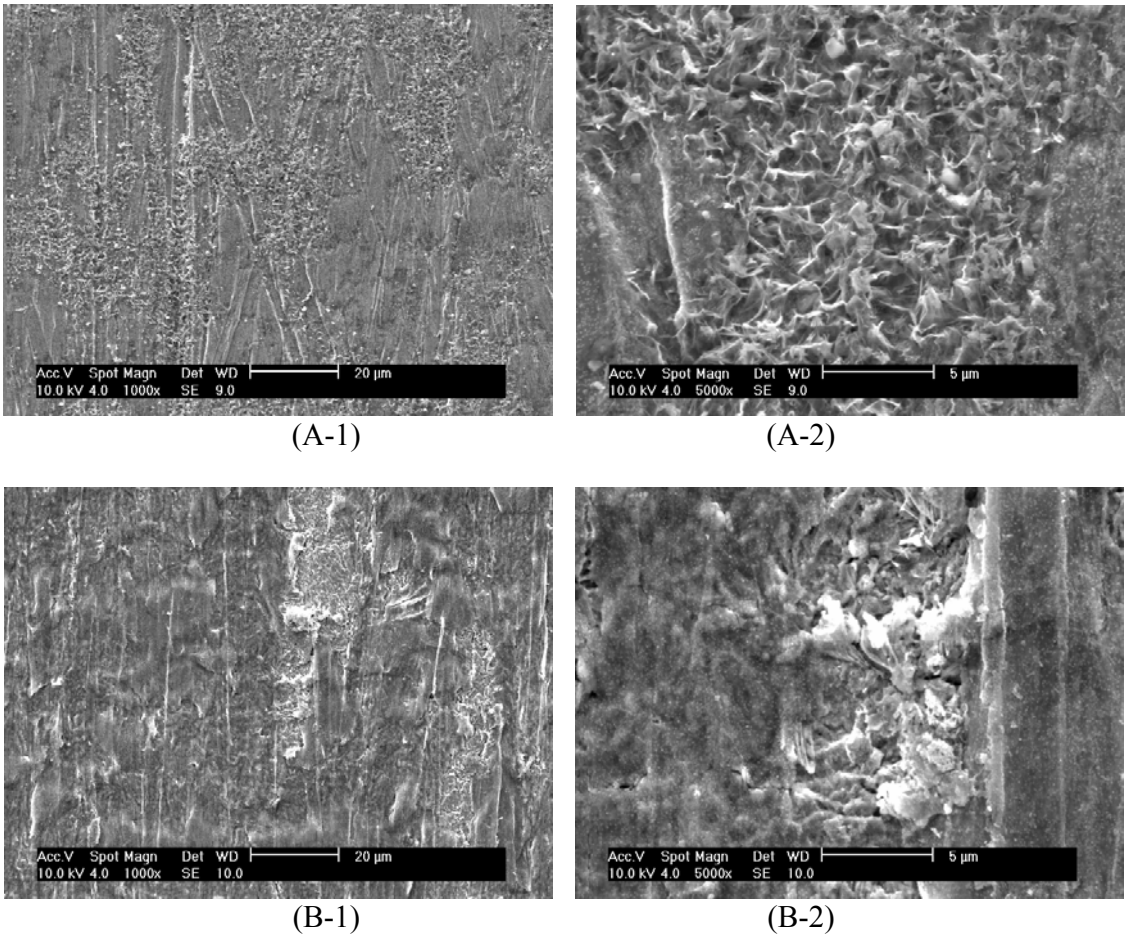

Figure 101. The morphology (1000x and 5000x) of the scale on the X65 steel surface under the conditions of 0.04% H_2S (H_2S/N_2 gas), T=80^oC, pH 5, the total reaction time 20 hours, (A) velocity = 100 rpm, (B) velocity = 8000 rpm.

5.6.2 Modeling of H_2S corrosion

5.6.2.1 Physico-chemical model

There seems to be a consensus that mackinawite scale forms on the steel surface as a product of H_2S corrosion[6, 12, 23-26]. In this study mackinawite was also found to be the dominant iron sulfide species, as previously described. Clearly, other types of iron sulfide film were observed in the past on steel surfaces attacked by H_2S, particularly in long exposures; however it is still unclear what effect this variation may have on the corrosion rate.

Based on an analogy with iron carbonate formation in CO_2 solutions and due to its rather low solubility, mackinawite was also thought to form by a precipitation mechanism[43]. While this is clearly a theoretical possibility, as argued above, mackinawite formation via a direct heterogeneous chemical reaction with iron on the steel surface seems to be the more relevant mechanism. Many pieces of evidence seem to support this conclusion:

1. very high reactivity of H_2S with iron, mackinawite scale has been shown to form extremely fast (order of seconds) [25, 26, 132], which is much faster than what one would expect from typical kinetics of a precipitation process[25];
2. formation of mackinawite scale in highly undersaturated solutions (pH 2 - 3) where it is thermodynamically unstable (soluble[*]) [25];
3. no effect of solution supersaturation level on the rate of mackinawite formation [43]; structure of mackinawite scale often containing cracks and delaminations, with steel surface imprint visible even after rather long exposures [43] (also Figure 102);
4. amount of mackinawite scale always being smaller than the amount of iron lost to corrosion of mild steel (expressed in molar units, see for example Figure 91 - Figure 98) and a lack of substantial mackinawite scale formation

[*] A case can be made that reasoning about solubility of iron sulfide based on conditions *in the bulk* is invalid as at a steel surface, due to corrosion of iron, there always exists a somewhat higher pH and a possibility to exceed the solubility limit, even in acidic solutions. In an extreme this would apply to any pH (however low) as well as to other precipitating salts such as iron carbonate. In reality, iron carbonate films are *never* observed at pH significantly below the solubility limit (based on bulk conditions) while iron sulfide films *are*. This fact undermines the theoretically plausible argument about the exclusive importance of surface conditions. In addition, basing arguments on a surface pH, which is virtually immeasurable, is not very practical and is incompatible with the bulk of the chemical and electrochemical literature.

on stainless steel and other corrosion resistant alloys (Figure 103), both suggesting that the iron "source" in mackinawite is the metal itself, rather than the bulk solution;

5. very similar structure and morphology of the mackinawite scale seen in high temperature sulfidation of mild steel exposed to gaseous and hydrocarbon environments[133, 134, 135].

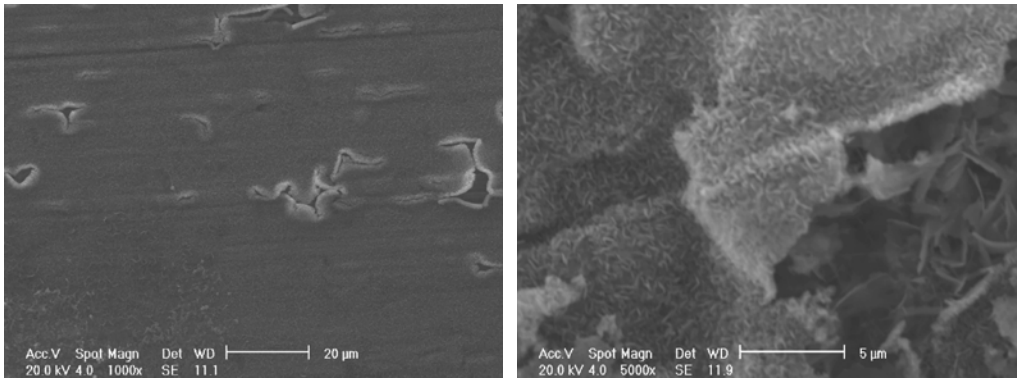

(A) (B)

Figure 102. The film morphology showing polishing marks on the X65 mild steel (A) 1000x and (B) 5000x, under the conditions of total pressure p=1 bar, initial Fe^{2+} aqueous concentration 0 ppm, H_2S gas concentration 10%, T=60°C, reaction time 1 hour, pH 5.0 - 5.5, and velocity 0 rpm.

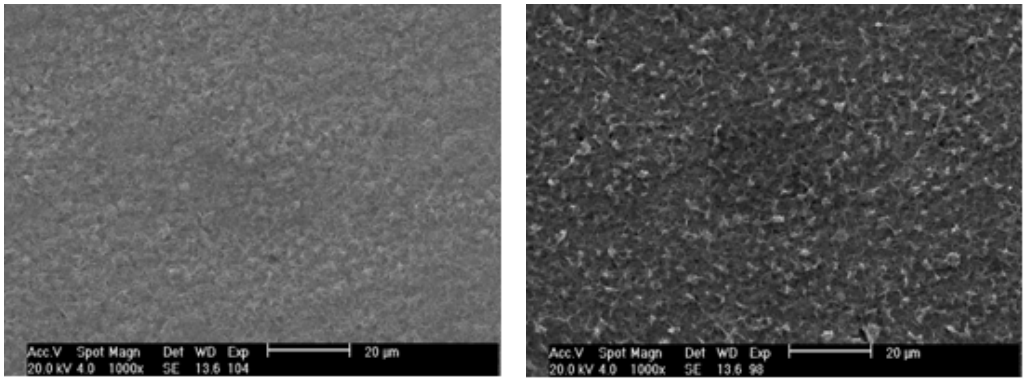

(A-1) (A-2)

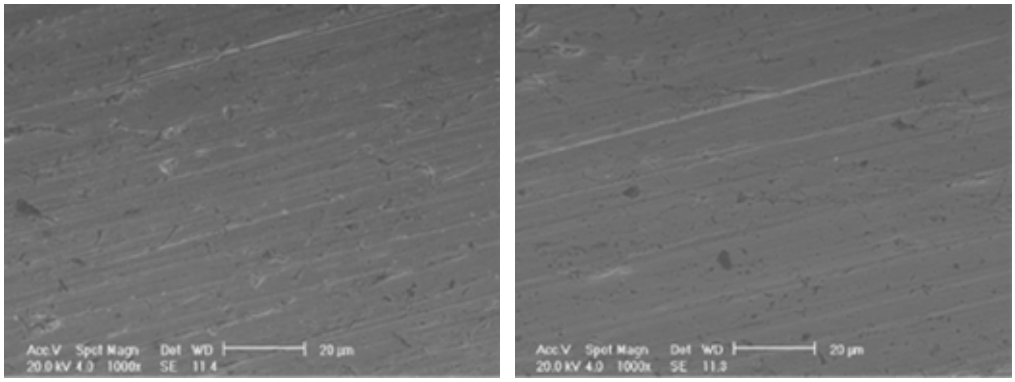

(B-1) (B-2)

Figure 103. The film morphology on the different steel surface (A-1) X65 mild steel Fe^{2+} 0 ppm, (A-2) X65 mild steel Fe^{2+} 50 ppm, (B-1) 316 stainless steel Fe^{2+} 0 ppm, (B-2) 316 stainless steel Fe^{2+} 50 ppm, under the conditions of total pressure p=1 bar, H_2S gas concentration 0.1%, T 80°C, reaction time 24 hours, pH 5.0 - 5.5, and velocity 0 rpm.

If this is accepted as sufficient evidence, it can be concluded that the corrosion of mild steel in H_2S aqueous environments proceeds by a very fast direct heterogeneous chemical reaction at the steel surface to form a solid adherent mackinawite scale. The overall reaction scheme can be written as:

$$Fe_{(s)} + H_2S_{(aq)} \Rightarrow FeS_{(s)} + H_{2(g)} \quad (57)$$

As both the initial and final state of Fe is solid, this reaction is often referred to as the "solid state corrosion reaction". The formed mackinawite scale may dissolve depending on the solution saturation level. For the typical pH range seen in oilfield brines (pH 4 – 7)

the solution is almost always supersaturated with respect to iron sulfide and the mackinawite scale does not dissolve, actually in long exposures it may grow slowly by precipitation from the bulk[136]. If the pH is decreased below pH 4 the dissolution rate will increase to a point where in the range pH 2 – pH 3 no mackinawite can be detected on the steel surface.[25]

Even if aqueous H_2S is a weak acid just like carbonic acid, the corrosion mechanism proposed above differs in sequence from what is believed to happen to steel exposed to pure CO_2 solutions in the same pH range (pH 4 – 7). In CO_2 corrosion of steel, iron first dissolves to form aqueous Fe^{2+} which then may or may not precipitate at the metal surface to form iron carbonate (e.g. below pH 5 iron carbonate typically does not form and above pH 6 it is almost always there). In H_2S solutions, mild steel corrosion proceeds to first form a mackinawite scale which then may or may not dissolve.

This first layer (tarnish) of mackinawite that forms very fast is extremely thin (<< 1 μm) and is invisible to the naked eye and even by a typical SEM [132]. However it is rather protective and for example reduces a CO_2 driven corrosion rate typically by an order of magnitude[132].

With increased exposure times, at high H_2S concentrations and temperature, the thin mackinawite film grows rapidly. It is still unclear whether this growth is supported by H_2S penetration through the crystalline layer (by solid state diffusion) or is it by ionic conduction of S^{2-} , HS^- , Fe^{2+}, etc. through the semiconductive mackinawite matrix. Outward diffusion of ferrous species is consistent with an electrochemical iron dissolution mechanism and a mackinawite continued growth at the outer film/solution interface. The inward diffusion of sulfide species is consistent with the here proposed

direct chemical reaction mechanism (57) and leads to mackinawite formation at the inner film interface with the steel. In both cases the mechanical integrity of the growing layer is weakened. Outward migration of Fe^{2+} leaves "voids" at the metal/mackinawite interface, i.e., it "undermines" the film what manifests itself as poor "adhesion" of the film to the steel. Inward diffusion of the sulfide species leads to internal stresses in the film as described below.

In the latter scenario, the solid state corrosion reaction (57) keeps generating mackinawite at the inner interface of the mackinawite film with the steel. This leads to epitaxial stresses arising from the different crystal lattice constants of the source iron and the iron sulfide that formed in its place[133]. What is more important, the solid FeS is calculated to be 2.56 times more voluminous than the iron it replaced, at the mackinawite/steel interface. This, so called Pilling-Bedworth ratio (PBR)[133], leads to an increase of internal compressive stresses in the mackinawite scale. When the mechanical limit of the mackinawite is exceeded micro-cracking of the film occurs, thereby relieving the stresses and the process starts all over again. These micro-cracks, which most likely occur at mackinawite grain boundaries, serve as preferred pathways for more rapid penetration of sulfide species which fuel the solid state reaction (57) to go further and faster[137]. It is expected that in some instances, at stress concentration points, large cracks in the film may appear as shown in Figure 102. The sulfide species penetrate even more easily at these locations to feed the corrosion reaction (57), which make even more sulfide film at those locations and cause even more internal stressing and film failure. It is not difficult to see how this feed-forward scenario could lead locally to an exponential growth of the reaction rate and localized corrosion. This scenario also offers an

explanation for an apparently odd occurrence in H_2S corrosion: experimental observations indicate that pits are usually full of iron sulfide and even have a "cap" of sulfide which is thicker than elsewhere on the steel surface, as shown in Figure 104 provided by Brown[138]. This appearance is very different from localized attack in CO_2 corrosion where pits are bare with the surrounding steel covered with a protective film. Finally, in this scenario the hydrogen gas evolved by the corrosion reaction (57) builds up at the steel/film interface as it diffuses out through the mackinawite film with difficulty. This may lead to the retardation of the atomic hydrogen recombination reaction and hydrogen penetration into the steel. Indeed, the hydrogen built-up at the steel/film interface may even "bubble out" and cause further damage to the mackinawite film. The last few points are purely hypothetical and were discussed here only because they are consistent with proposed mechanism of H_2S corrosion of steel and the resulting iron sulfide film growth. As there is no direct evidence for them in the short term experiments presented here, these hypotheses needs to be directly confirmed in the future.

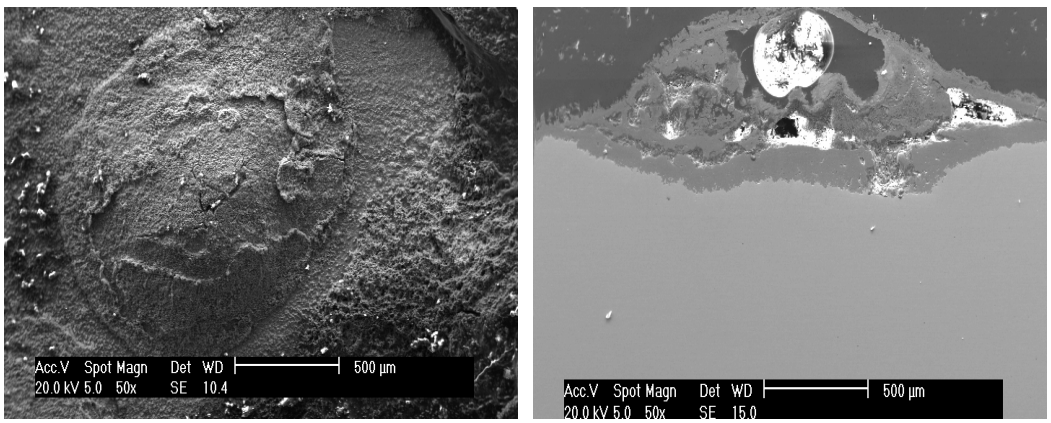

(A) (B)

Figure 104. The morphology (A) and cross section (B) of the localize attack on the X65 mild steel surface in CO_2/H_2S environment under the conditions of P_{tot} 8 bar, P_{H2S} 8 mbar, P_{CO2} 7.5 bar, T=60°C, and the total reaction time is 10 days[138].

As the mackinawite film goes through the growth / micro-cracking cycle it thickens. As larger crack appear, whole layers of the film may partially delaminate from the steel surface starting another cycle of rapid film growth underneath, as shown from Figure 79 to Figure 81. Over longer exposures, this cyclic growth / delamination process leads to a layered outer sulfide scale which is very porous. As this outer scale grows it will spontaneously spall a process assisted by flow. Notwithstanding, if the bulk solution is undersaturated (typically at 3<pH<4) the outer porous mackinawite scale will dissolve away as fast as it forms, what may happen even to tight inner mackinawite film at pH<3.[25]

In summary, in H_2S corrosion of mild steel two types of mackinawite layers form on the steel surface:

1. a very thin (<<1 μm) and tight inner film and
2. a much thicker (1-10 μm) layered outer scale which is loose and very porous.

The outer scale may be intermixed with any iron sulfide or iron carbonate that may have precipitated out given the right water chemistry and long exposure time, what would change its properties and appearance. Both the inner mackinawite film and the outer scale act as barriers for the diffusion of the sulfide species[*] fueling the solid state corrosion reaction (57). This is in addition to the diffusion through the aqueous mass transfer boundary layer.

5.6.2.1 Mathematical model

---

[*] The outward diffusion by the Fe^{2+} may be neglected as it is inconsistent with the proposed solid state corrosion reaction (57) and would lead to a formation of a very different looking and behaving sulfide film which is more akin to iron carbonate.

Based on the experimental results and the description of the H_2S corrosion process presented above a mathematical model can be constructed. The key assumptions are:

1. the corrosion process happens via a direct heterogeneous solid state reaction (57) at the steel surface;
2. there is always a very thin (<<1 μm) but dense film of mackinawite at the steel surface which acts as a solid state diffusion barrier for the sulfide species involved in the corrosion reaction;
3. this films continuously goes through a cyclic process of growth, cracking and delamination, what generates the outer mackinawite scale;
4. this outer scale grows in thickness (typically >1 μm) over time and also presents a diffusion barrier;
5. the outer scale is layered, very porous and rather loosely attached, over time it peels and spalls, a process aggravated by the flow.
6. Due to the presence of the thick mackinawite film and possibly the outer scale it is assumed that the corrosion rate of steel in H_2S solutions is always under mass transfer control.

One can write the flux of sulfide species due to:

1. convective diffusion through the mass transfer boundary layer

$$Flux_{H_2S} = k_{m,H_2S}\left(c_{b,H_2S} - c_{o,H_2S}\right) \tag{58}$$

2. molecular diffusion through the liquid in the porous outer scale

$$Flux_{H_2S} = \frac{D_{H_2S}\,\varepsilon\,\Psi}{\delta_{os}}\left(c_{o,H_2S} - c_{i,H_2S}\right) \tag{59}$$

3. solid state diffusion through the inner mackinawite film

$$Flux_{H_2S} = A_{H_2S} e^{-\frac{B_{H_2S}}{RT_k}} ln\left(\frac{c_{i,H_2S}}{c_{s,H_2S}}\right) \quad (60)$$

where:

$Flux_{H_2S}$ is expressed in mol/(m^{2}s),

k_{m,H_2S} is the mass transfer coefficient for H_2S in the hydrodynamic boundary layer, $k_{m,H_2S} = 1.00 \times 10^{-4}$ in nearly stagnant condition, in m/s,

c_{b,H_2S} is the bulk concentration of H_2S in the liquid phase in mol/(m^{3}s),

c_{o,H_2S} is the interfacial concentration of H_2S at the outer scale/solution interface in mol/m^3,

D_{H_2S} is the diffusion coefficient for dissolved H_2S in water, $D_{H_2S} = 2.00 \times 10^{-9}$, in m^2/s,

ε is the outer mackinawite scale porosity,

Ψ is the outer mackinawite scale tortuosity factor,

c_{i,H_2S} is the interfacial concentration of H_2S at the inner scale/film interface in mol/m^3.

δ_{os} is the thickness of the mackinawite scale $\delta_{os} = m_{os} / \left(\rho_{FeS}\ A\right)$ in m,

m_{os} is the mass of the mackinawite scale in kg,

A is the surface area of the steel in m^2,

A_{H_2S}, B_{H_2S} are the Arrhenius constants, $A_{H_2S} = 1.30 \times 10^{-4}$ mol/(m^{2}s) and $B_{H_2S} = 15500$ J/mol,

T_k is the temperature in Kelvin,

c_{s,H_2S} is the concentration of H_2S on the steel surface and is set to 1.00×10^{-7} in mol/m^3.

In a steady state the three fluxes are equal to each other and are equal to the corrosion rate CR_{H_2S}. By eliminating the unknown interfacial concentrations c_{o,H_2S} and c_{i,H_2S} from equations (58) to (60), the following equation is obtained for the corrosion rate of steel due to H_2S:

$$CR_{H_2S} = A_{H_2S} e^{-\frac{B_{H_2S}}{RT_k}} ln \frac{c_{b,H_2S} - CR_{H_2S}\left(\frac{\delta_{0.5}}{D_{H_2S}\varepsilon\Psi} + \frac{1}{k_{m,H_2S}}\right)}{c_{s,H_2S}} \quad (61)$$

This is a nonlinear equation with respect to CR_{H_2S} which does not have a explicit solution but can be solved by using a simple numerical algorithm such as Newton's gradient method or similar. These are available as ready-made routines in spreadsheet applications or in any common computer programming language. The prediction for CR_{H_2S} depends on a number of constants used in the model which can be either found in handbooks (such as D_{H_2S}), calculated from established theory (e.g. k_{m,H_2S}) or are determined from the experiments (e.g. A_{H_2S}, B_{H_2S}, c_{s,H_2S}). The unknown properties of the outer sulfide scale change with time and need to be calculated as described below.

It is assumed that the amount of scale retained on the metal surface at any point in time depends on the balance of:

1. scale formation (generated by spalling of the thin mackinawite film underneath it and by precipitation from the solution), and

2. scale damage (by hydrodynamic stresses and/or by chemical dissolution)

$$\underbrace{SRR}_{\substack{\text{scale}\\\text{retention}\\\text{rate}}} = \underbrace{SFR}_{\substack{\text{scale}\\\text{formation}\\\text{rate}}} - \underbrace{SDR}_{\substack{\text{scale}\\\text{damage}\\\text{rate}}} \tag{62}$$

where all the terms are expressed in mol/(m^{2}s). As in this study it was found that precipitation of iron sulfide did not play a significant role, neither did chemical dissolution of the scale it can be written:

$$\underbrace{SRR}_{\substack{\text{scale}\\\text{retention}\\\text{rate}}} = \underbrace{CR}_{\substack{\text{corrosion}\\\text{rate}}} - \underbrace{SDR_m}_{\substack{\text{mechanical}\\\text{scale damage}\\\text{rate}}} \tag{63}$$

Experiments have shown that even in stagnant conditions about half of the sulfide scale that formed was lost from the steel surface by spalling, i.e. $SDR_m \approx 0.5\,CR$. Furthermore, the rate of scale removal in flowing conditions increased with velocity (Figure 100) and one can write:

$$SDR_m = 0.5\left(1 + c\,v^a\right)CR \tag{64}$$

where c and a are experimentally determined constants for a rotating cylinder flow geometry. Clearly more experimentation is required to determine how and if they apply in pipe flow.

Once the scale retention rate SRR is known, the change in mass of the outer scale can be easily calculated as:

$$\Delta m_{os} = SRR\ \ M_{FeS}\ A\ \ \Delta t \tag{65}$$

where M_{FeS} is the molar mass of iron sulfide in kg/mol, Δt is the time interval in seconds. The porosity of the outer mackinawite scale was determined to be very high ($\varepsilon \approx 0.9$), however due to its layered structure the tortuosity factor was found to be very low $\Psi = 0.003$.

A time-marching procedure could now be established where:

1. the corrosion rate CR_{H_2S} in the absence of sulfide scale can be calculated by using equation (61), and assuming $\delta_{os} = 0$,
2. the amount of sulfide scale Δm_{os} formed over a time interval Δt is calculated by using equation (65),
3. the new corrosion rate CR_{H_2S} in the presence of sulfide scale can be calculated by using equation (61),
4. a new time interval Δt is set and steps 2 and 3 repeated.

A small complication arises from the fact that at very low H_2S gas concentrations (ppm range) iron sulfide still forms and controls the corrosion rate; however the corrosion process is largely driven by the reduction of protons.* In an analogy with the approach laid above, the convective diffusion flux of protons through the mass transfer boundary layer is:

$$Flux_{H^+} = k_{m,H^+}\left(c_{b,H^+} - c_{o,H^+}\right) \tag{66}$$

which in a steady state is equal to the diffusion flux through the pores of the iron sulfide scale:

$$Flux_{H^+} = \frac{D_{H^+}\,\varepsilon\,\Psi}{\delta_{oc}}\left(c_{o,H^+} - c_{i,H^+}\right) \tag{67}$$

which is equal to the solid state diffusion flux through the thin mackinawite film:

$$Flux_{H^+} = A_{H^+} e^{-\frac{B_{H^+}}{RT_k}} ln\left(\frac{c_{i,H^+}}{c_{s,H^+}}\right) \tag{68}$$

---

* Similar is true in combined CO_2/H_2S corrosion of steel which is driven by CO_2 but largely controlled by the presence of iron sulfide films. Mixed CO_2/H_2S corrosion is not considered here.

which is equal to the corrosion rate by protons CR_{H^+}. By eliminating the unknown interfacial concentrations c_{o,H^+} and c_{i,H^+} from equations (66) to (68), the following expression is obtained for the corrosion rate driven by protons and controlled by the presence of the iron sulfide scale:

$$CR_{H^+} = A_{H^+} e^{-\frac{B_{H^+}}{RT_k}} ln \frac{c_{b,H^+} - CR_{H^+}\left(\frac{\delta_{0.5}}{D_{H^+}\varepsilon\Psi} + \frac{1}{k_{m,H^+}}\right)}{c_{s,H^+}} \tag{69}$$

where

$Flux_{H^+}$ is expressed in mol/(m^{2}s),

k_{m,H^+} is the mass transfer coefficient for protons in the hydrodynamic boundary layer, $k_{m,H^+} = 3.00 \times 10^{-4}$ in nearly stagnant condition, in m/s,

c_{b,H^+} is the bulk concentration of H^+ in the liquid phase in mol/m^3,

c_{o,H^+} is the interfacial concentration of H^+ at the outer scale/solution interface in mol/m^3,

D_{H^+} is the diffusion coefficient for dissolved H^+ in water, $D_{H^+} = 2.80 \times 10^{-8}$, in m^2/s,

c_{i,H^+} is the interfacial concentration of H^+ at the inner scale/film interface in mol/m^3.

A_{H^+}, B_{H^+} are the Arrhenius constants, $A_{H^+} = 3.9 \times 10^{-4}$ mol/(m^{2}s) and $B_{H^+} = 15500$ J/mol.

c_{s,H^+} is the concentration of H^+ on the steel surface and is set to 1.00×10^{-7} in mol/m^3.

The total rate of corrosion is equal to the sum of the corrosion caused by H_2S and the corrosion caused by H^+.

$$CR = CR_{H_2S} + CR_{H^+} \tag{70}$$

5.6.3 Verification of the model

The model predictions are compared with the experimental results at different test conditions. Figure 105 shows the comparison of the corrosion rate *versus* the reaction time for a series of experiments done at 80^{o}C. One should keep in mind that the experimental results are time-averages over 1 h and 1-24 h periods while the predictions represent "instantaneous" corrosion rates. Clearly the model successfully captures the downward trend of the corrosion rate with time as well as the undesirable effect of high H_2S concentrations on the general corrosion rate. Figure 106 shows the comparison of the measured and predicted scale retention at different reaction times. The predicted scale growth is rapid in the first few hours and then gradually levels off, leading to what is often referred to as a "parabolic film growth regime". After all the cases available in this experimental study were simulated with the model, the comparison of the predicted H_2S corrosion rates and the measured values is shown in Figure 107. Overall one can claim reasonable agreement keeping in mind the scatter in the experimental results.

The model was tested by making simulations outside the range of parameters used in the experimental study described above, i.e. the model was used to extrapolate the corrosion rates to higher partial pressures of H_2S as well as much longer exposure times

(both are very complicated and expensive to achieve in a laboratory setting). In Figure 108 one can see the predictions ranging from partial pressure of H_2S as low as 0.16 Pa in the gas phase (what corresponds to 1.6 ppm at 1 bar total pressure) all the way up to 2.7 bar H_2S partial pressure. The simulations were extended to 10 years and shown on a log-scale. Clearly, the corrosion rate decreases to a very low value in all cases, while at the lowest H_2S concentration it may take less than a day at the highest it may take as long as few years. The film thickness prediction is shown in Figure 109, indicating a scale thickness which is only a few mm thick even at the highest H_2S partial pressures and in very long exposures.

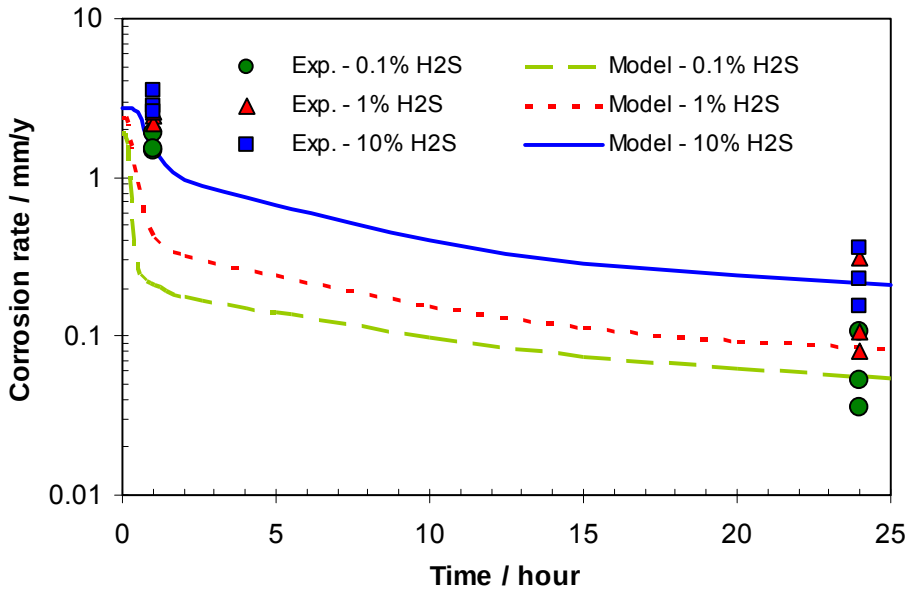

Figure 105. The experimental and prediction corrosion rate vs. time under the conditions of total pressure p=1 bar, H_2S gas concentration from 0.1% to 10%, T=80^{o}C, reaction time of 1 hour and 24 hours, pH 5.0 - 5.5, and velocity 0 rpm.

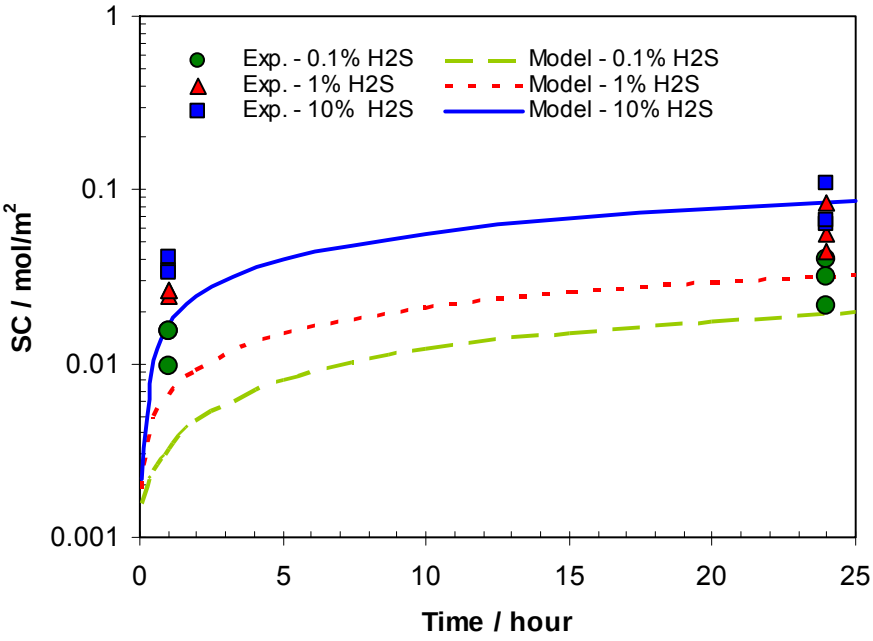

Figure 106. The experimental results and predictions of the scale retention vs. time under the conditions of total pressure p=1 bar, H_2S gas concentration from 0.1% to 10%, T=80°C, reaction time of 1 hour and 24 hours, pH 5.0 - 5.5, and velocity 0 rpm.

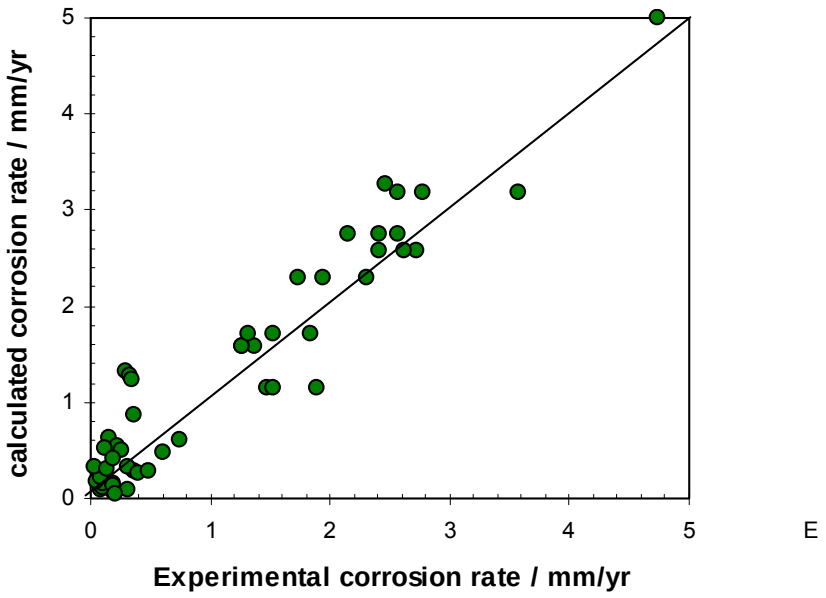

Figure 107. The comparison of the experimental corrosion rate and the calculated corrosion rate under the conditions of total pressure p=1 bar, H_2S gas concentration from 0.0075% to 10%, T 25°C, 60°C, and 80°C, reaction time of 1 hour and 24 hours, pH 5.0 - 5.5, and velocity from 0 rpm to 8000 rpm.

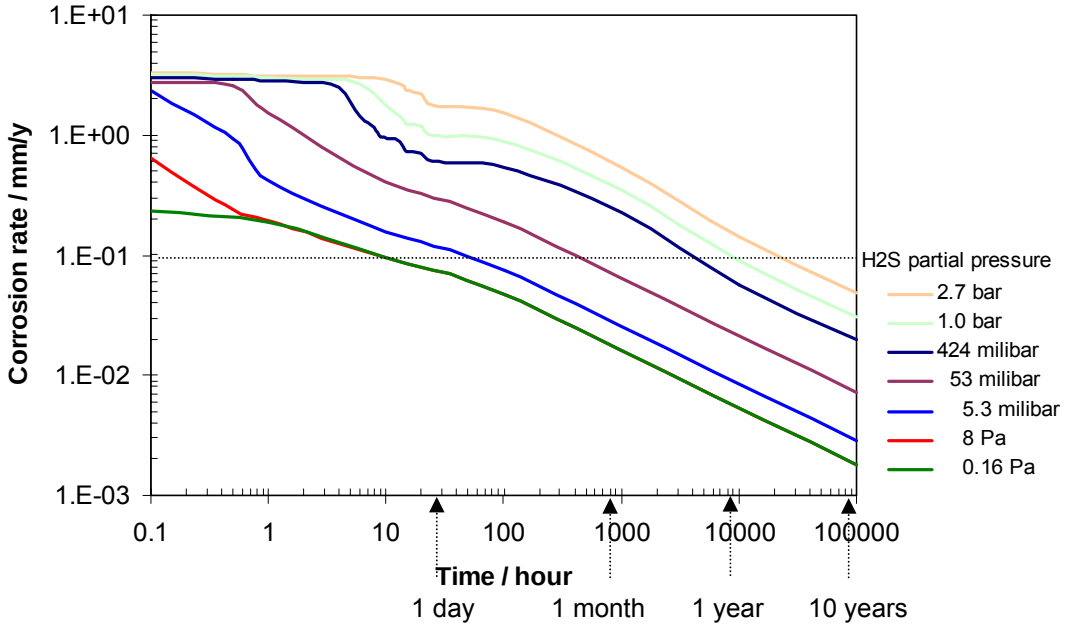

Figure 108. Simulated corrosion rate as a function of time for a range of H_2S partial pressures; conditions T=80°C, pH 5, and static.

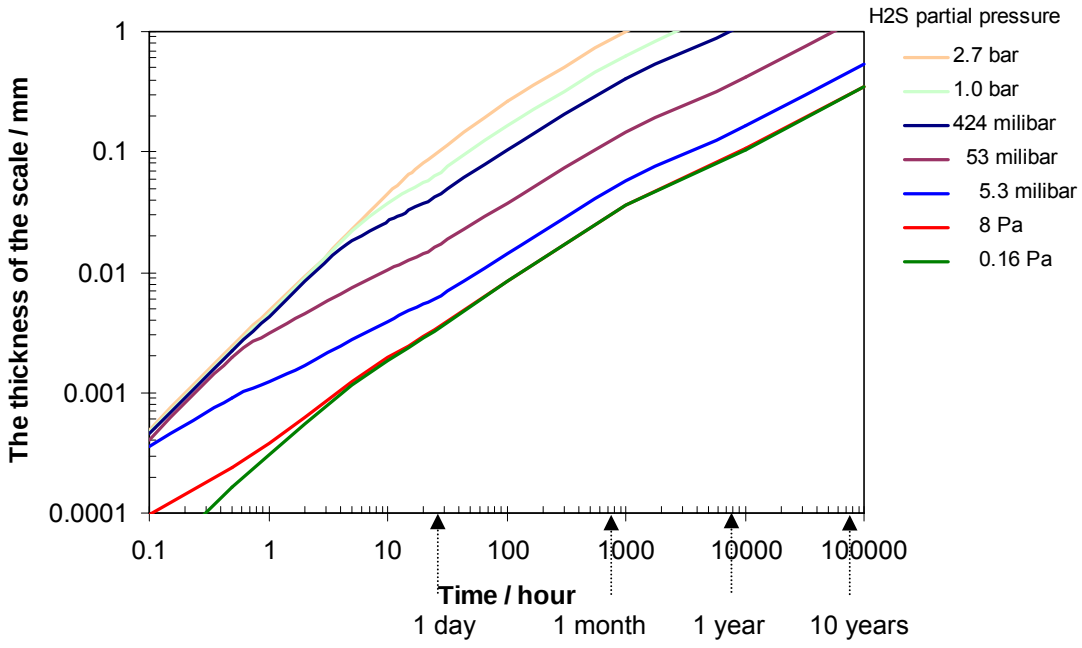

Figure 109. Simulated sulfide scale thickness as a function of time for a range of H_2S partial pressures; conditions: T=80°C, pH 5, and static.

5.7 Summary

The most important findings presented in this chapter are:

1. Mackinawite is the dominant iron sulfide formed on the steel surface, most likely by solid state reaction.
2. The corrosion rate of carbon steel in H_2S corrosion is affected by H_2S concentration, temperature, velocity, and the protectiveness of the scale. Fe^{2+} concentration has little effect on the corrosion rate of carbon steel.
3. The scale retained on the steel surface depends on both the scale formation rate and the scale damage rate. The scale formation rate includes both the corrosion rate and precipitation rate. The scale damage rate includes the damages by both mechanical removal and chemical removal.
4. A mechanistic model of H_2S corrosion is developed to accurately predict the H_2S corrosion process.

Chapter 6: The mechanism and kinetics of mixed iron carbonate/sulfide scale formation in CO_2/H_2S corrosion

6.1 Introduction

In CO_2/H_2S corrosion, both iron carbonate and iron sulfide scale can form on the steel surface. In Chapter 3, the kinetics of iron carbonate scale formation in the pure CO_2 corrosion was reported and a new iron carbonate scale precipitation expression was developed to quantify kinetics of iron carbonate scale formation. In Chapter 5, the kinetics of iron sulfide scale formation in H_2S/N_2 environments was reported and a mechanistic model of H_2S corrosion was proposed to accurately describe the H_2S corrosion process.

There are no expressions in the literature to quantify the kinetics of scale formation in CO_2/H_2S solutions. The makeup of the surface scale under these conditions will not only depend on the chemistry of the brine and the respective solubility of iron carbonate and iron sulfide, but also on the competitive kinetics of the two scale formation mechanisms. Therefore, for an improved understanding of the surface scales formed in CO_2/H_2S environments and their protective properties, a better understanding of the kinetics of scale formation in CO_2/H_2S environments is needed. This chapter is aimed at investigating the scale formation in CO_2/H_2S environments.

6.2 Objectives

The objectives of this chapter include:

1. Quantify the corrosion rate of carbon steel and the scale retention rate in CO_2/H_2S environment,

2. Analyze the scale formed in CO_2/H_2S environment,
3. Investigate the mechanism of mixed iron sulfide/carbonate scale formation in CO_2/H_2S environment,
4. Based on the experimental data, model the kinetics of scale formation in CO_2/H_2S corrosion.

6.3 Results and discussion

6.3.1 Experiments in solutions under-saturated with mackinawite

6.3.1.1 Test matrix

Experiments at mackinawite under-saturated conditions in CO_2/H_2S corrosion were conducted in order to understand the effect of mackinawite scale on the CO_2 corrosion. The test matrix of the experiments is shown in Table 18, which is similar as the test matrix for H_2S/N_2 system (Table 13). The saturation of mackinawite under the different test conditions is shown in Table 19.

Table 18: Test matrix of experiments

Parameter	**Description**
Material	C1018 carbon steel
Solution	De-ionized water with 1 wt% of NaCl, purged with CO_2
Temperature ^oC	25
Total pressure (bar)	1
H_2S pressure (bar)	0.076 millibar (76 ppm)
H_2S aq	9.4×10^{-6} mol/l
pH	2, 5

Table 19. The degree of under-saturation of mackinawite at different Fe^{2+} concentration and pH under the conditions of room temperature and H_2S concentration of 0.01% in the gas inlet.

Fe^{2+} / ppm	pH	Degree of under-saturation
1	2	1.04E-9
1	5	1.04E-3

6.3.1.2 Experiments in pure CO_2 and H_2S/CO_2 environments

Experiments were conducted in both pure CO_2 and H_2S/CO_2 environments under the test conditions of H_2S concentration 100 ppm, room temperature, and pH varying at 2 and 5. Figure 110 shows both the corrosion currents and potentiodynamic sweeps exhibit the same behavior in the H_2S/CO_2 environment as in the pure CO_2 environment at pH 2. With the increase of pH to 5 (Figure 111), the corrosion currents slightly decrease when H_2S is added into the system, illustrating that H_2S retards the corrosion rate under this test condition. The comparisons of corrosion currents and sweeps at both pH 2 and pH 5 are shown in Figure 112. It is found that with the increase of pH, both the corrosion current and the corrosion potential decrease.

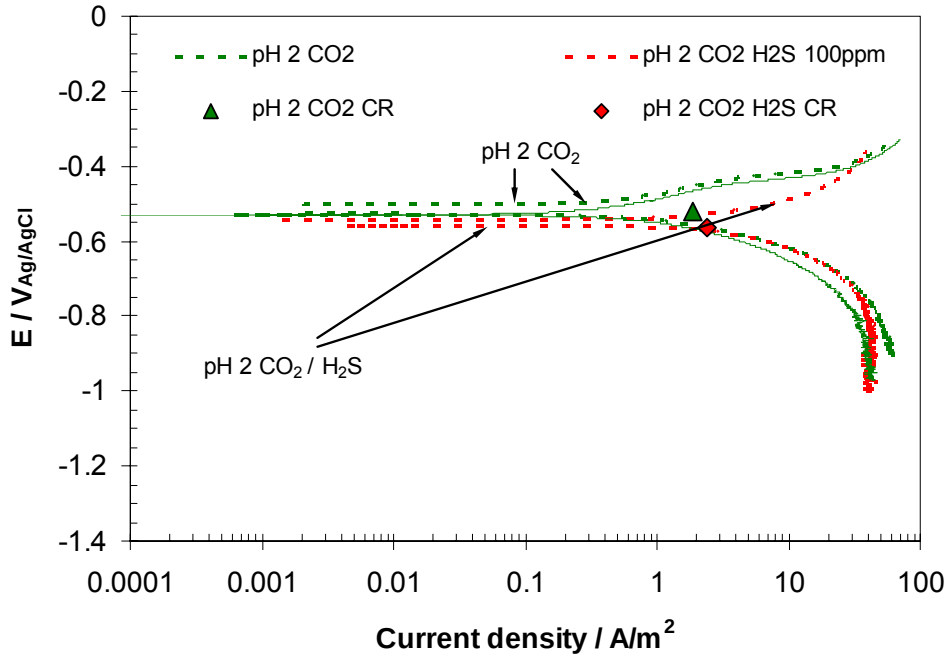

Figure 110. The comparison of potentiodynamic sweeps for pure CO_2 and CO_2/H_2S (100 ppm) environments under the conditions of pH 2, T=25°C, and static solution.

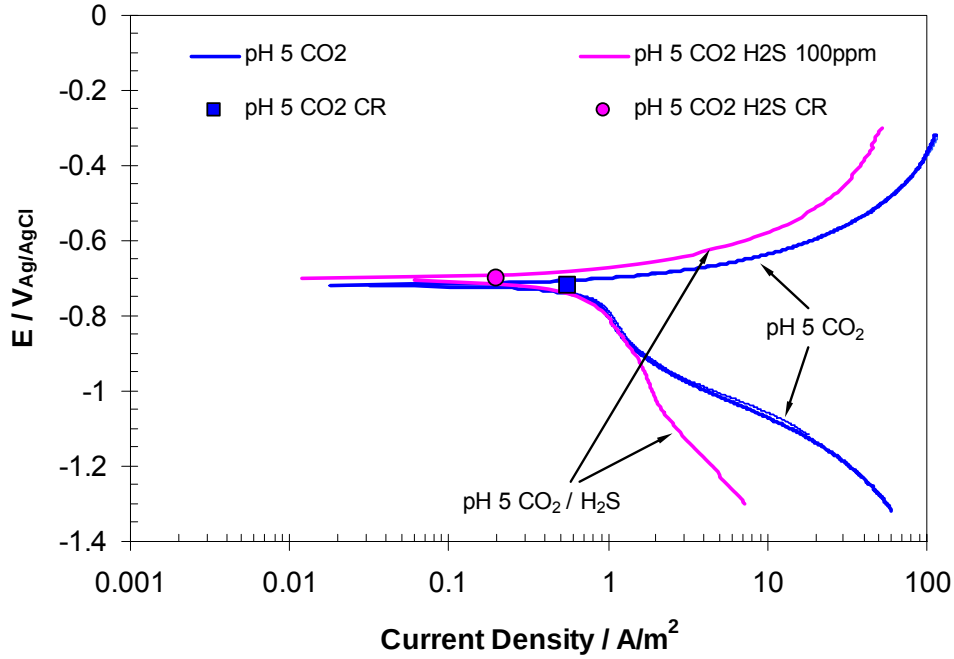

Figure 111. The comparison of potentiodynamic sweeps for pure CO_2 and CO_2/H_2S (100 ppm) environments under the conditions of pH 5, T=25°C, and static solution.

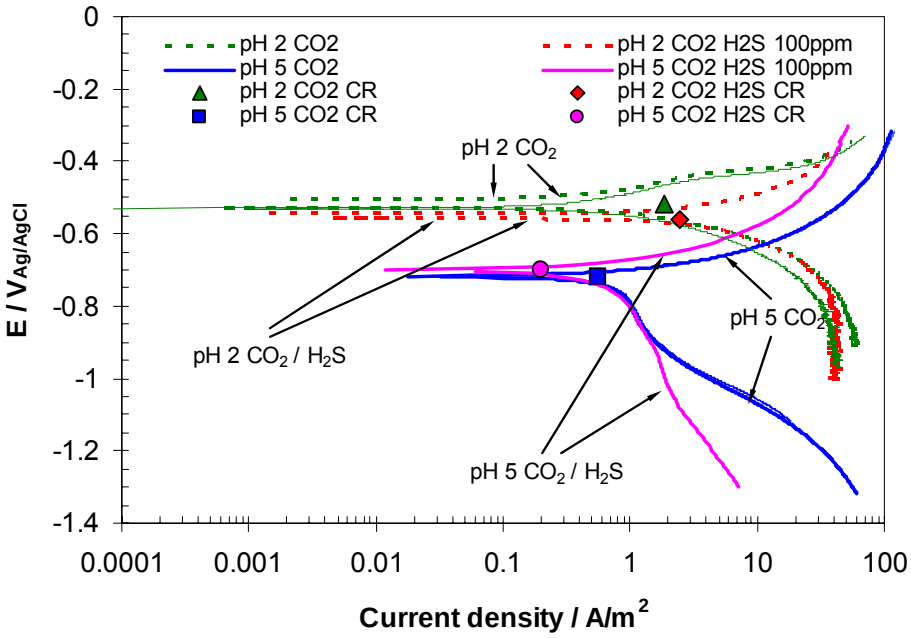

Figure 112. The comparison of potentiodynamic sweeps for pure CO_2 and CO_2/H_2S (100 ppm) environments under the conditions of pH 2 and 5, T=25°C, and static solution.

6.3.1.3 Comparisons of experiments in N_2, CO_2, N_2/H_2S, and CO_2/H_2S solutions

The comparisons of the experimental results in pure N_2, pure CO_2, N_2/H_2S, and CO_2/H_2S solutions are shown in Figure 113, Figure 114, and Figure 115. Figure 113 shows that at pH 2, the H_2S slightly accelerates the anodic reaction but not cathodic reactions in both N_2/H_2S and CO_2/H_2S solutions, resulting in a higher corrosion current. At pH 5 the corrosion currents are similar for pure N_2, N_2/H_2S, and CO_2/H_2S systems (Figure 114). However, H_2S retards anodic reactions in CO_2/H_2S solution compared with pure CO_2 solution.

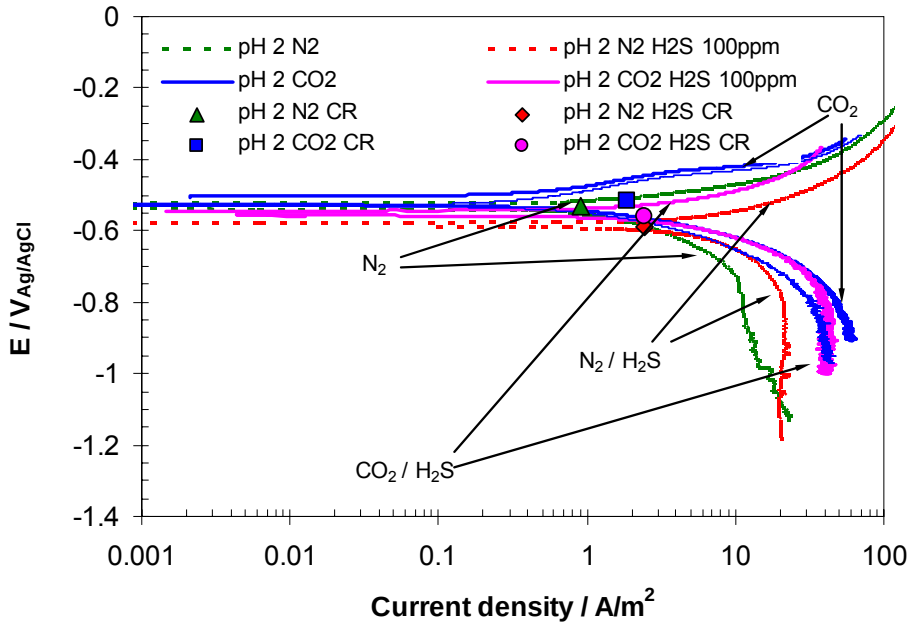

Figure 113. The comparison of potentiodynamic sweeps for pure N_2, pure CO_2, N_2/H_2S (100 ppm), and CO_2/H_2S (100 ppm) environments under the conditions of pH 2, T=25°C, and static solution.

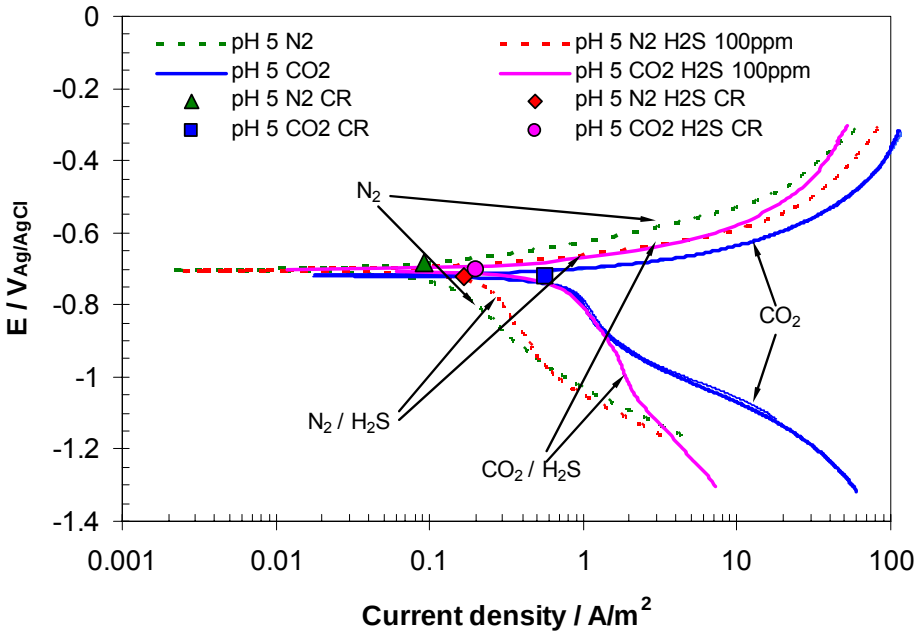

Figure 114. The comparison of potentiodynamic sweeps for pure N_2, pure CO_2, N_2/H_2S (100 ppm), and CO_2/H_2S (100 ppm) environments under the conditions of pH 2, T=25°C, and static solution.

The corrosion rate measured by both LPR and weight change method in the four systems at different pH are shown in Figure 115. The results show that H_2S accelerates the corrosion rate at pH 2 and retards the corrosion rate at pH 5, which is in good agreement with the potentiodynamic sweep results. However, there is a large difference between the corrosion rates measured by LPR and weight change method. It is speculated that a possible surface catalytic reaction of H_2S and the steel may lead to this peculiar phenomenon.

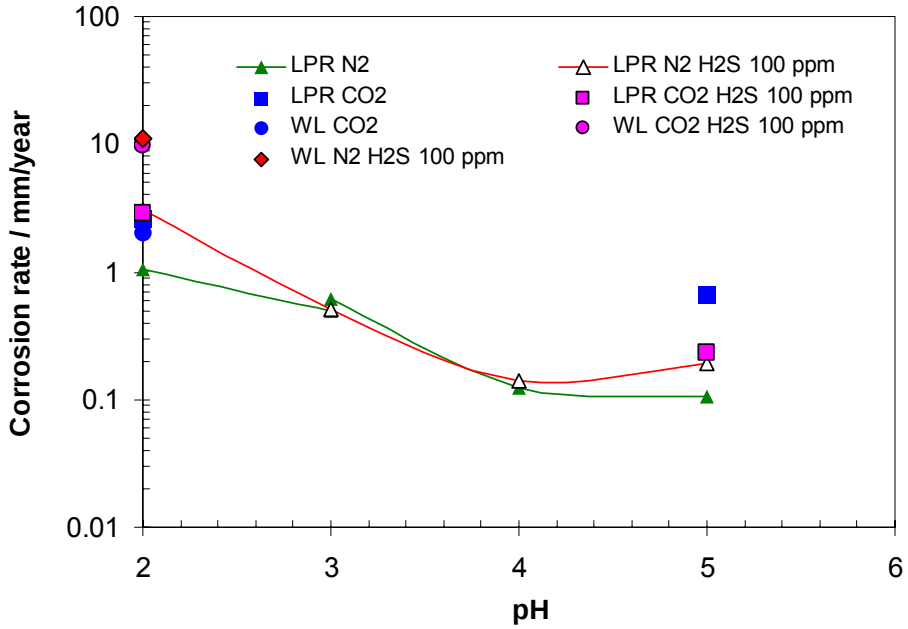

Figure 115. Corrosion rate (by both LPR and weight change method) vs. pH in pure N_2, pure CO_2, N_2/H_2S (100 ppm), and CO_2/H_2S (100 ppm) environments under the conditions of T=25°C, and static solution.

6.3.2 Kinetics experiments in solutions supersaturated with mackinawite

6.3.2.1 Test matrix

Experiments at mackinawite supersaturated conditions were conducted in order to understand the competitiveness of both iron carbonate and mackinawite scale formation mechanism in CO_2/H_2S environment. The test matrix of the experiments is shown in Table 20. The saturations of both iron carbonate and mackinawite under the test conditions are shown in Table 21.

Table 20: Test matrix of experiments

Parameter	**Description**
Material	X65 carbon steel
Solution	De-ionized water with 1 wt% of NaCl, purged with CO_2
Temperature ^oC	60 and 80
Total Pressure (bar)	1
H_2S in the gas inlet	0.1%, 1%, and 10%
pH	6.6

Table 21. The degree of saturation of both iron carbonate and mackinawite at different test conditions

Temperature / ^oC	**H_2S concentration in the gas inlet / %**	**Fe^{2+} / ppm**	SS_{FeCO_3}	SS_{FeS}
60	1	2	14.5	1566
		10	72	7832
		50	362	39163
	10	2	13	15665
		10	66	78323
		50	329	391618
80	0.1	2	12	247
		10	61	1234
		50	304	6172
	1	2	12	2468
		10	60	12336
		50	301	61680
	10	2	11	24671
		10	55	123358
		50	274	616788

6.3.2.2 Kinetics experiments in H_2S/CO_2 system at the temperatures of 60^oC and 80^oC.

Several experiments were performed in the solutions with CO_2/H_2S at the temperature of 60^oC under the conditions of Fe^{2+} concentrations of 0 ppm, 10 ppm, and 50 ppm, and H_2S concentrations of 1% and 10%. The retention rate of the scale and the corrosion rate of X65 carbon steel in the reaction time of first hour are shown in Figure 116. The scale retention rate increased with the increase of H_2S concentration and the corrosion rate almost kept constant. The corrosion rate expressed in mm/year is shown in Figure 117 and it is found that the corrosion rate is approximately 2 mm/year at different conditions. The scale retention rate of the scale and the corrosion rate of X65 carbon steel in twenty four hours are shown in Figure 118, similar to the 1-hour data, the scale retention rate increased with H_2S concentration, but the corrosion rate remained roughly constant. However, it is noticed that there is a difference in the vertical scales in Figure 118 *versus* Figure 116. Both the scale retention rate and the corrosion rate are approximately ten times lower at 24-hour than at 1-hour. This can be seen more clearly by comparing Figure 117 and Figure 119. The reduction in both the scale retention rate and the corrosion rate over time illustrates that the scale formed on the steel surface can partially protect the steel from corroding.

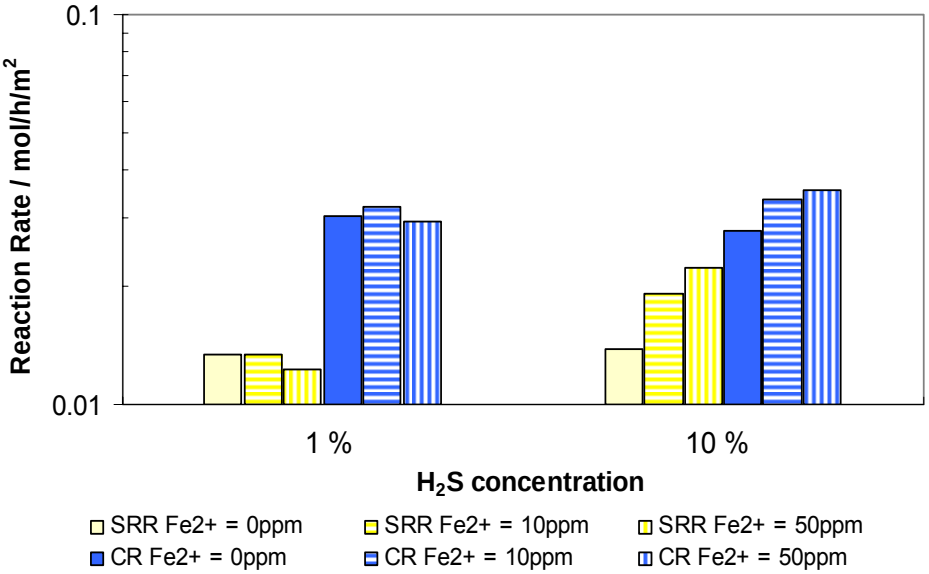

Figure 116. Both the retention rate of iron sulfide formed on X65 carbon steel surface and the corrosion rate of X65 carbon steel in the same molar unit at different H_2S concentration and initial Fe^{2+} concentration in the solution with CO_2/H_2S under the conditions of T=60°C, the total reaction time is 1 hour.

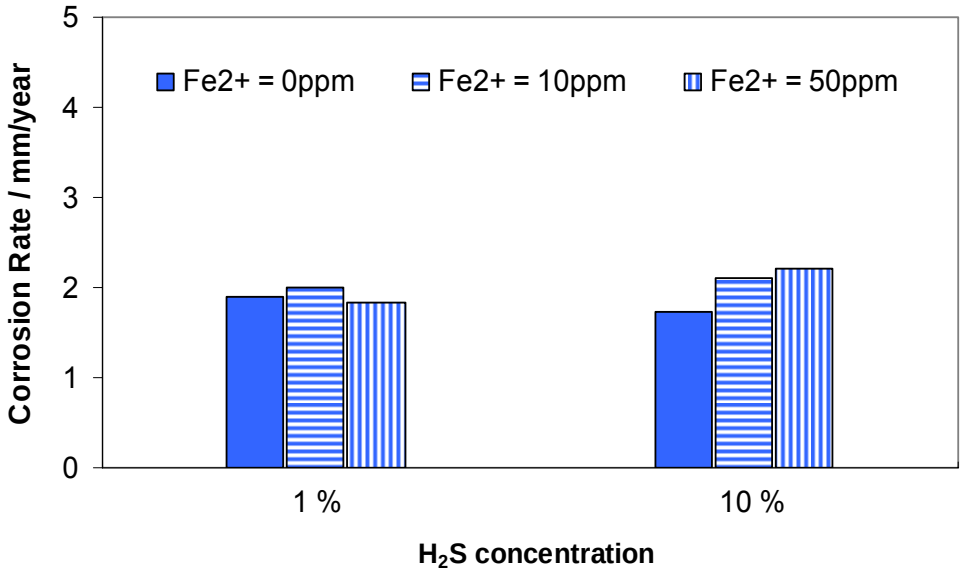

Figure 117. The corrosion rate of X65 carbon steel in mm/year at different H_2S concentration and initial Fe^{2+} concentration in the solution with CO_2/H_2S under the conditions of T=60°C, the total reaction time is 1 hour.

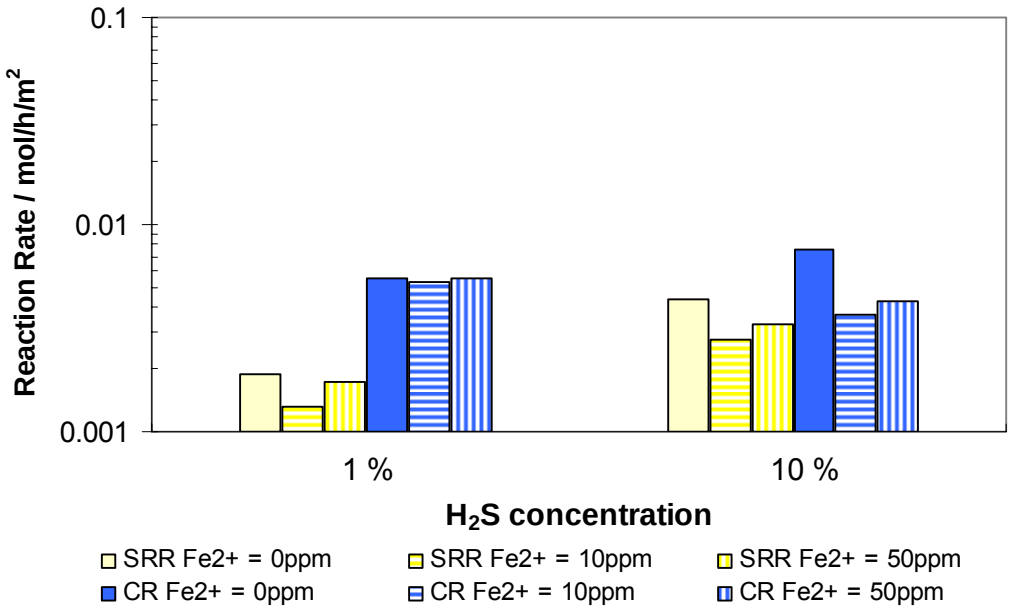

Figure 118. Both the retention rate of iron sulfide formed on X65 carbon steel surface and the corrosion rate of X65 carbon steel in the same molar unit at different H_2S concentration and initial Fe^{2+} concentration in the solution with CO_2/H_2S under the conditions of T=60°C, the total reaction time is 24 hours.

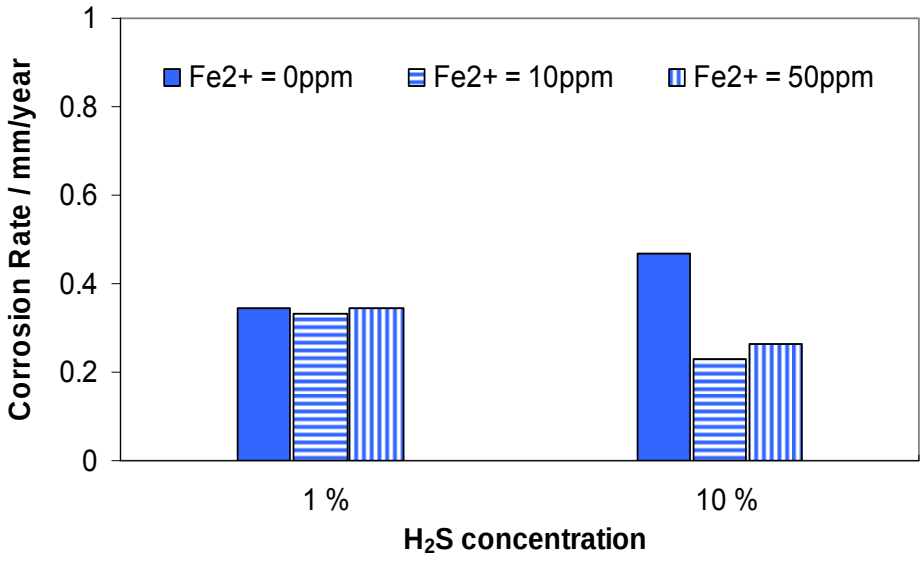

Figure 119. The corrosion rate of X65 carbon steel in mm/year at different H_2S concentration and initial Fe^{2+} concentration in the solution with CO_2/H_2S under the conditions of T=60°C, the total reaction time is 24 hours.

The morphology and EDS analysis of the scale formed on the steel surface at the 60^{o}C are shown from Figure 120 to Figure 123. At an H_2S concentration of 1%, with an increase of reaction time from one hour to twenty hours, more iron sulfide formed on the steel surface at the initial Fe^{2+} concentration of both 0 ppm (Figure 120) and 50 ppm (Figure 121). However, the morphology of the scale is not affected by the concentration of Fe^{2+}, which proves that Fe^{2+} has little effect on the scale retention rate and corrosion rate as mentioned above. When increasing the H_2S concentration from 1% to 10% (Figure 122 and Figure 123), again more iron sulfide formed on the steel surface, illustrating that H_2S has an effect on the scale retention rate and corrosion rate. All the EDS analysis results show that iron sulfide is the only corrosion product formed on the steel surface.

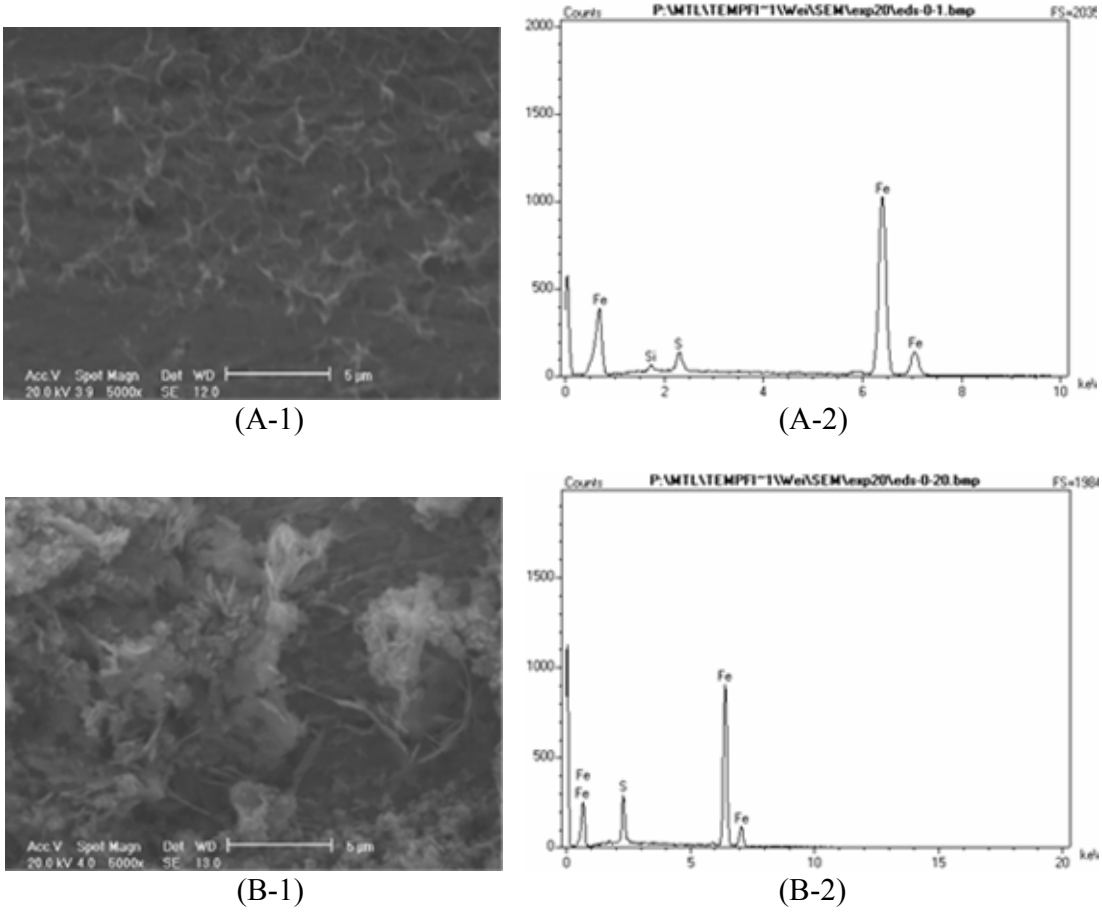

Figure 120. The morphology (at 5000x) and EDS results of iron sulfide scale formed on the X65 carbon steel surface under the conditions of 1% H_2S (H_2S/CO_2 gas), T=60°C, pH 6.4~6.6, Fe^{2+} = 0 ppm, the total reaction time is (A) 1 hour, (B) 20 hours.

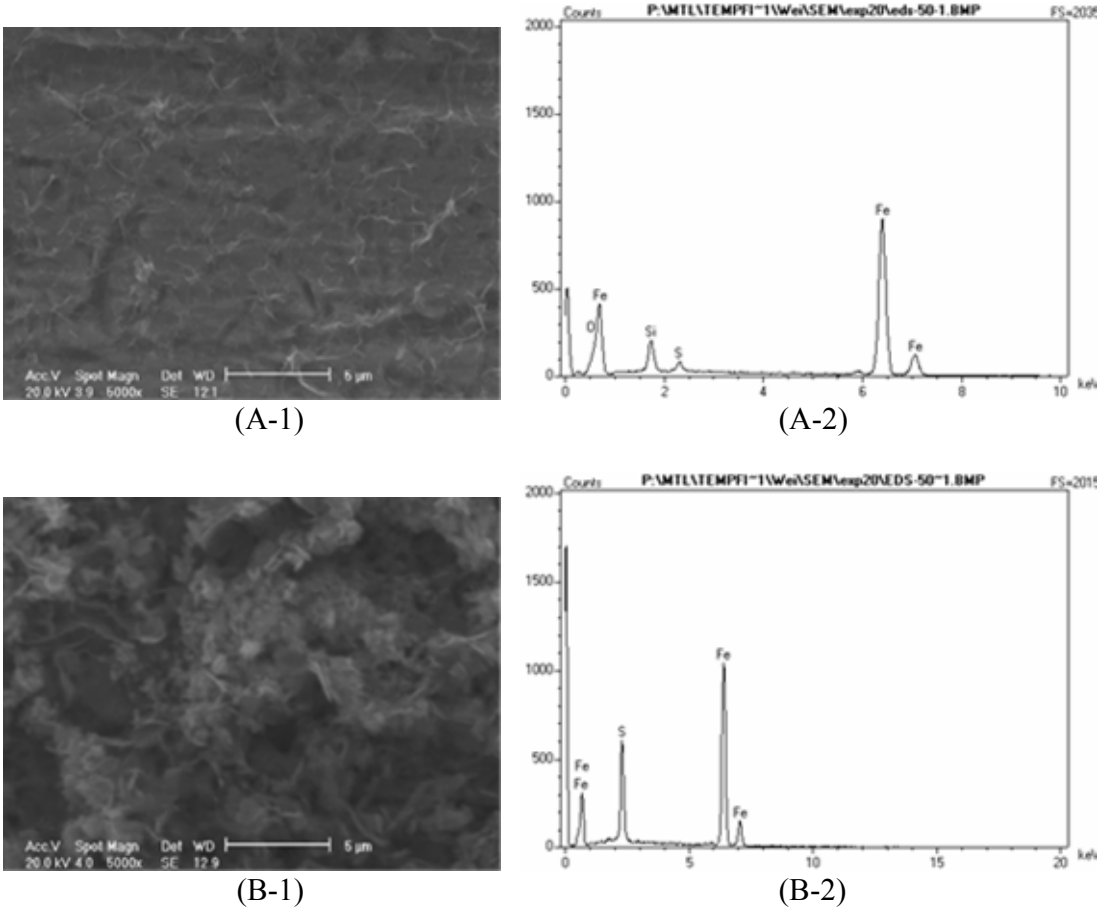

(A-1) (A-2)

(B-1) (B-2)

Figure 121. The morphology (at 5000x) and EDS results of iron sulfide scale formed on the X65 carbon steel surface under the conditions of 1% H_2S (H_2S/CO_2 gas), T=60^oC, pH 6.6, Fe^{2+} = 50 ppm, the total reaction time is (A) 1 hour, (B) 20 hours.

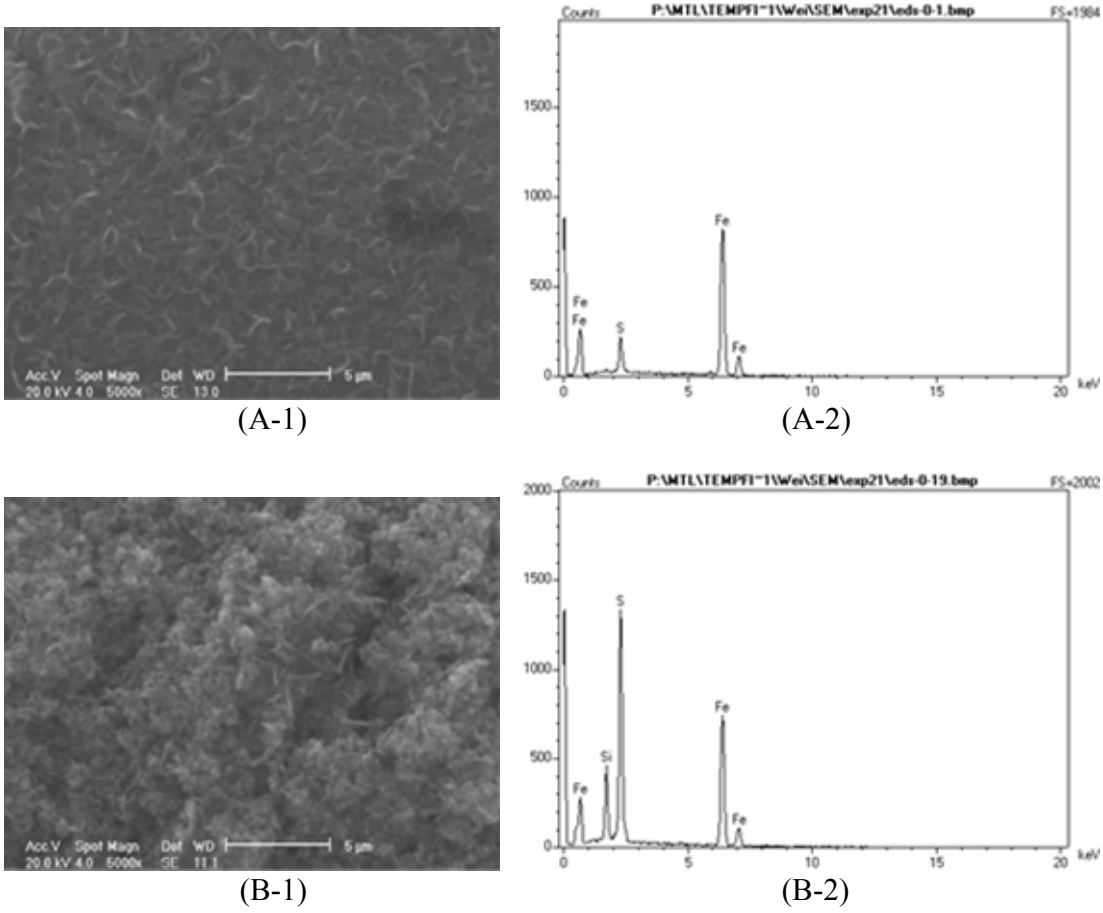

Figure 122. The morphology (at 5000x) and EDS results of iron sulfide scale formed on the X65 carbon steel surface under the conditions of 10% H_2S (H_2S/CO_2 gas), T=60^oC, pH 6.5~6.6, Fe^{2+} = 0 ppm, the total reaction time is (A) 1 hour, (B) 19 hours.

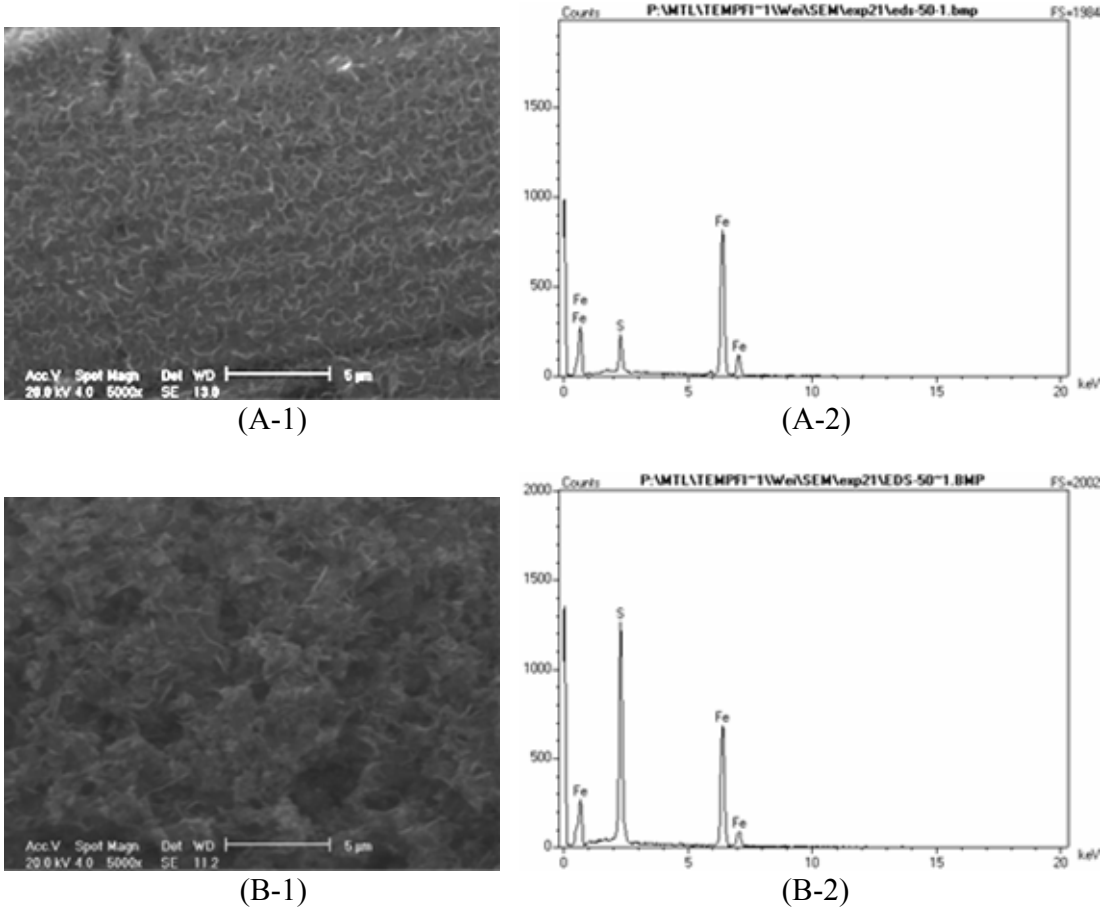

Figure 123. The morphology (at 5000x) and EDS results of iron sulfide scale formed on the X65 carbon steel surface under the conditions of 10% H_2S (H_2S/CO_2 gas), T=60^oC, pH 6.5~6.6, Fe^{2+} = 50 ppm, the total reaction time is (A) 1 hour, (B) 19 hours.

More experiments were conducted to investigate the scale formation in the solutions with H_2S/CO_2 at the temperature of 80^oC under the conditions of initial Fe^{2+} concentrations of 0ppm, 10ppm and 50ppm, H_2S concentrations of 0.1%, 1% and 10%, and the reaction times are one hour and one day. Figure 124 shows the scale retention rate and the corrosion rate of X65 carbon steel in the reaction time of one hour. Both the scale retention rate and corrosion rate increase with the increase of H_2S concentration in the first hour. The corrosion rates varied from 1.5 mm/year to 3 mm/year with the

increase of H_2S concentration from 0.1% to 10%, as shown in Figure 125. Figure 126 illustrates the scale retention rate and corrosion rate in the reaction time of 24 hours. Both scale retention rate and corrosion rate increase with H_2S concentration increasing from 0.1% to 1% and then decrease from 1% to 10%. Compared to the reaction in one hour, it is found that both scale retention rate and corrosion rate drifted down in twenty four hours. Figure 127 shows the corrosion rate in twenty four hours is about 0.2 to 0.5 mm/year. It is also noted that ferrous ion concentration has no significant effects on either scale retention rate or corrosion rate. Similar trends of scale retention rate and corrosion rate in H_2S/CO_2 system were obtained as the experiments conducted in the solutions with H_2S/N_2.

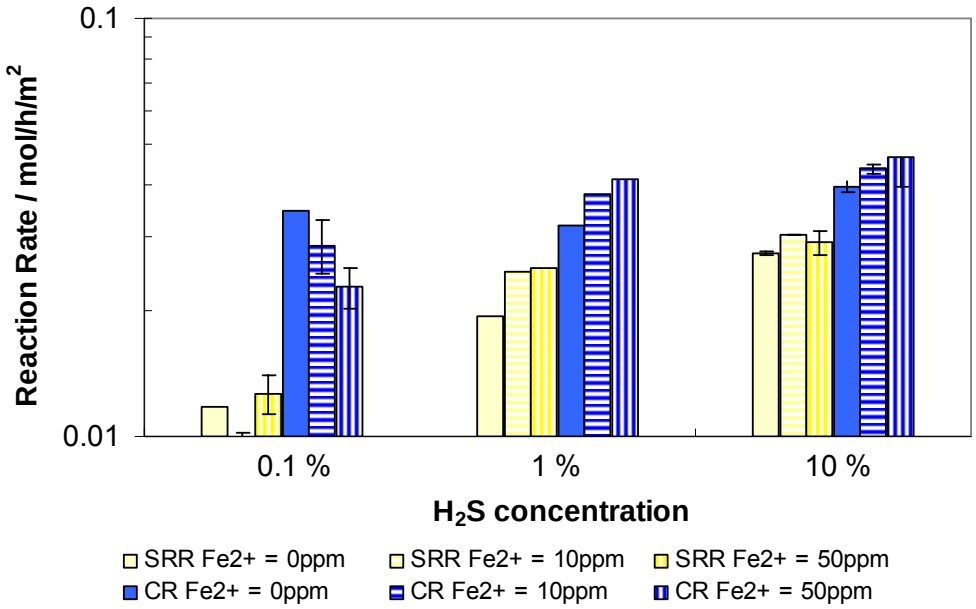

Figure 124. Both the retention rate of iron sulfide formed on X65 carbon steel surface and the corrosion rate of X65 carbon steel in the same molar unit at different H_2S concentration and initial Fe^{2+} concentration in the solution with CO_2/H_2S under the conditions of T=80°C, the total reaction time is 1 hour.

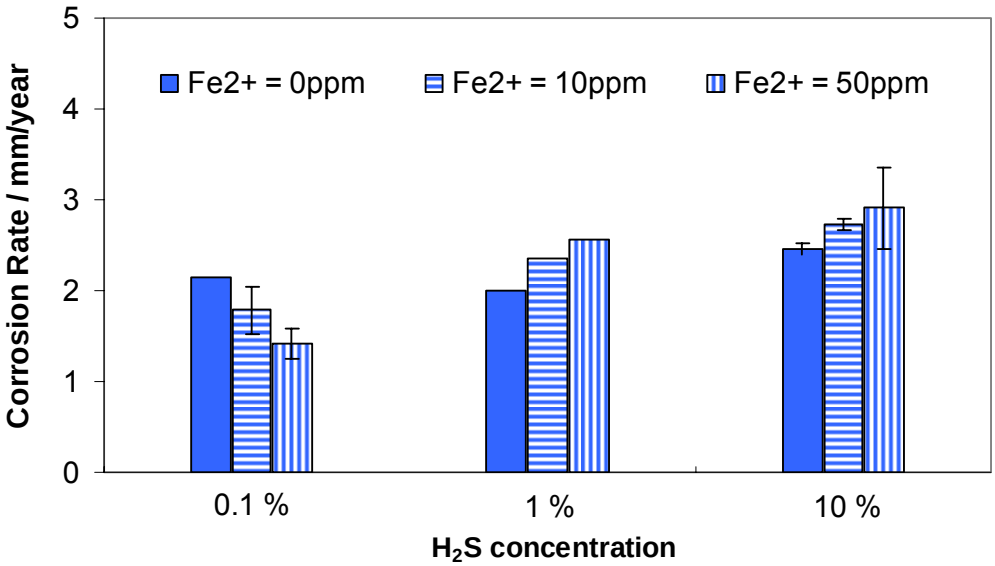

Figure 125. The corrosion rate of X65 carbon steel in mm/year at different H_2S concentration and initial Fe^{2+} concentration in the solution with CO_2/H_2S under the conditions of T=80°C, the total reaction time is 1 hour.

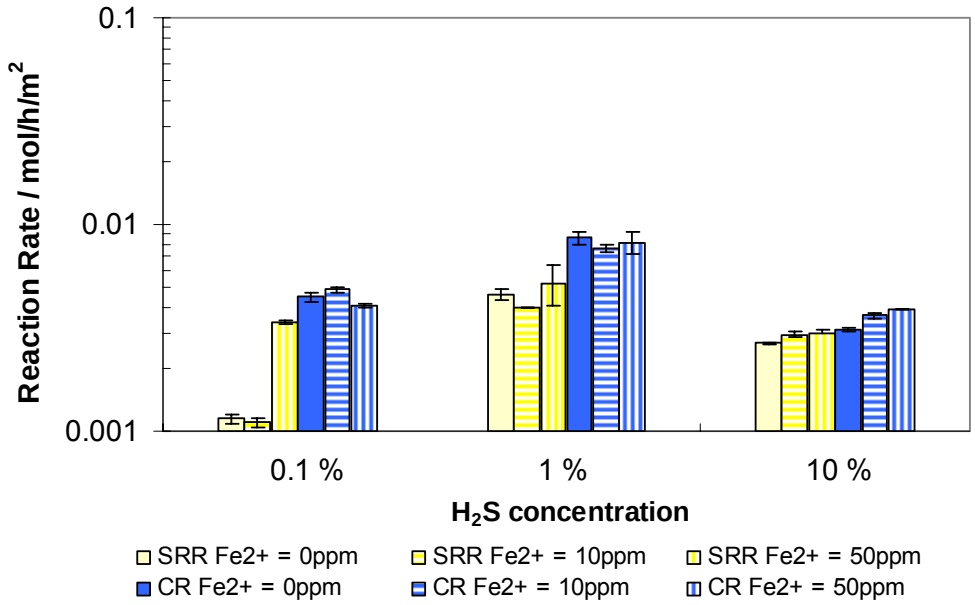

Figure 126. Both the retention rate of iron sulfide formed on X65 carbon steel surface and the corrosion rate of X65 carbon steel in the same molar unit at different H_2S concentration and initial Fe^{2+} concentration in the solution with CO_2/H_2S under the conditions of T=80°C, the total reaction time is 24 hours.

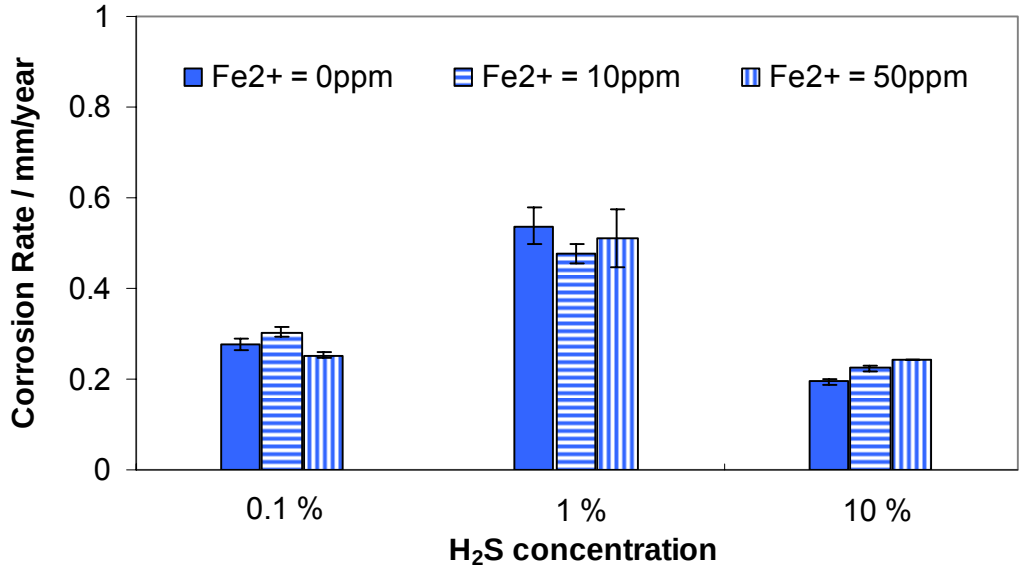

Figure 127. The corrosion rate of X65 carbon steel in mm/year at different H_2S concentration and initial Fe^{2+} concentration in the solution with CO_2/H_2S under the conditions of T=80°C, the total reaction time is 24 hours.

Figure 128 to Figure 135 show the morphology and EDS analysis results of the scale formed in the solutions with H_2S/CO_2 under the conditions of temperature 80°C, pH 6.6, initial Fe^{2+} concentrations of 0 ppm and 50 ppm, H_2S concentrations of 0.1%, 1%, and 10%, and reaction time of one hour and twenty four hours. At H_2S concentration of 0.1% and Fe^{2+} concentrations of 0 ppm (Figure 128) and 10 ppm (Figure 129), only iron sulfide scale formed on the X65 steel surface; while increasing Fe^{2+} concentration to 50 ppm (Figure 130), both iron sulfide scale and iron carbonate crystals formed on the steel surface.

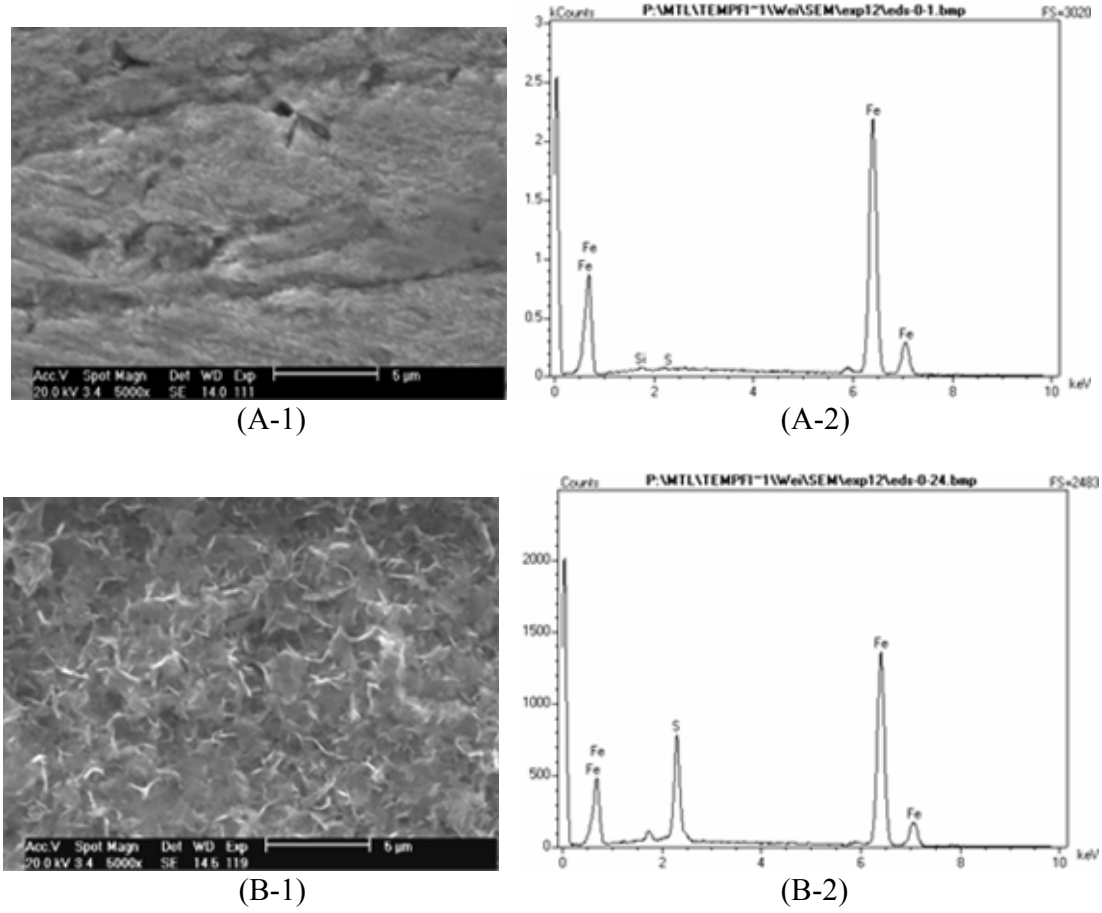

(A-1) (A-2)

(B-1) (B-2)

Figure 128. The morphology (5000x) and EDS results of scale formed on the X65 carbon steel surface under the conditions of 0.1% H_2S (H_2S/CO_2 gas), T=80°C, pH 6.5~6.6, Fe^{2+} = 0 ppm, the total reaction time is (A) 1 hour, (B) 24 hours.

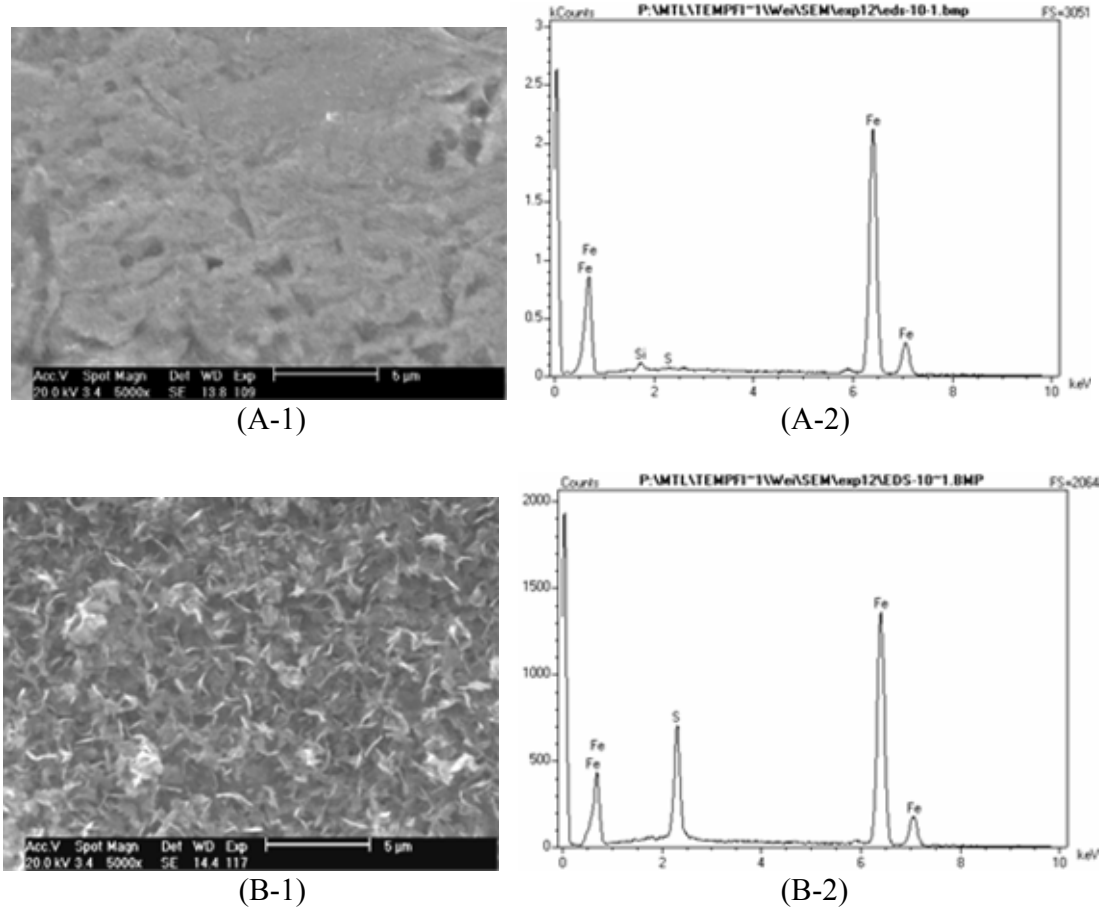

Figure 129. The morphology (5000x) and EDS results of scale formed on the X65 carbon steel surface under the conditions of 0.1% H_2S (H_2S/CO_2 gas), T=80°C, pH 6.5~6.6, Fe^{2+} = 10 ppm, the total reaction time is (A) 1 hour, (B) 24 hours.

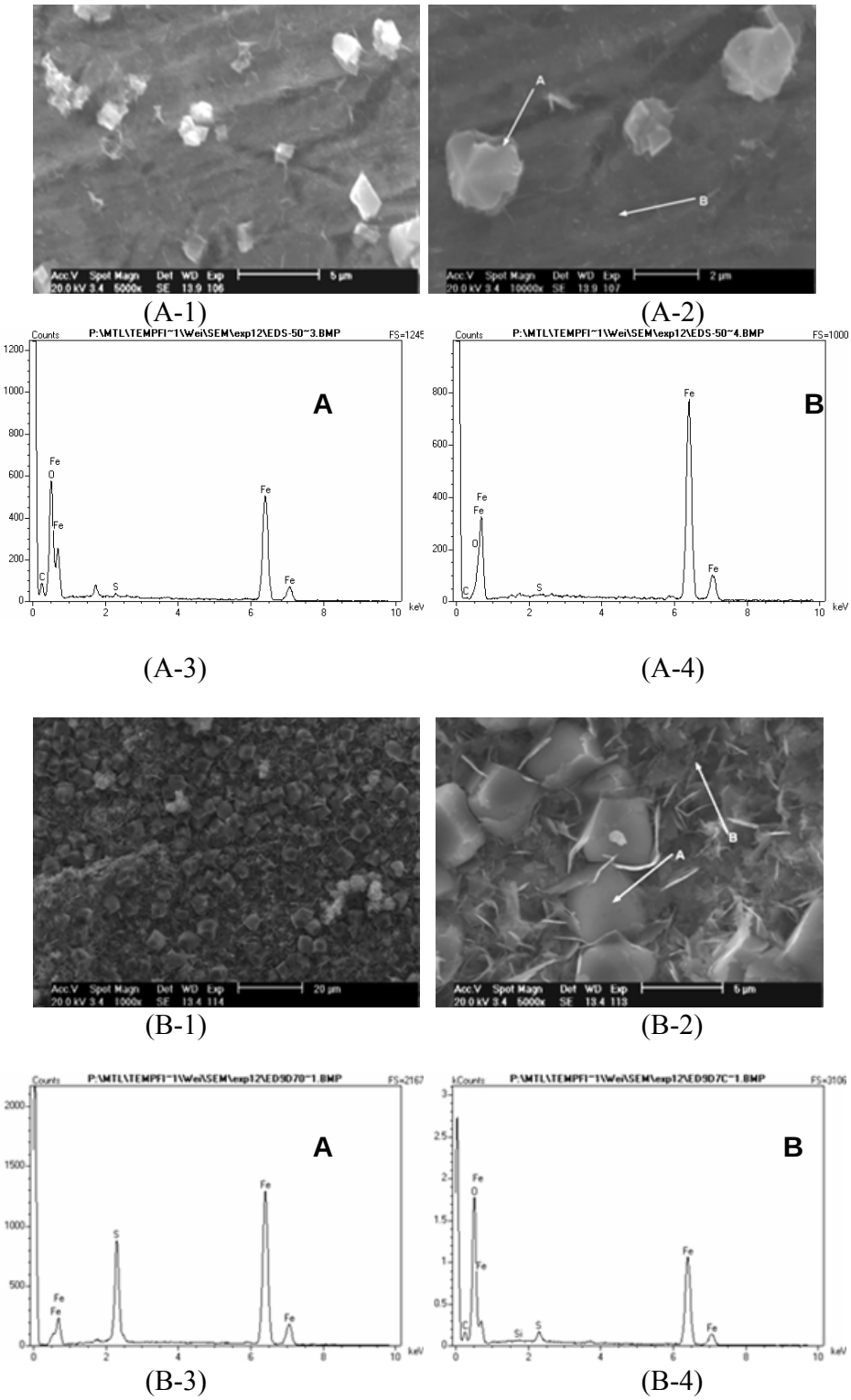

Figure 130. The morphology of scale formed on the X65 carbon steel surface under the conditions of 0.1% H_2S (H_2S/CO_2 gas), T=80°C, pH 6.5~6.6, Fe^{2+} = 50 ppm, the total reaction time is (A) 1 hour, (B) 24 hours.

With the increase of H_2S concentration to 1%, EDS results show that both iron carbonate and iron sulfide formed on the steel surface at Fe^{2+} concentrations of 0 ppm and 10 ppm (Figure 131 and Figure 132). However, the morphology of the scale shows that there was no iron carbonate crystal formed on the steel surface. It is assumed that the fast iron sulfide formation was the dominant reaction, which made it difficult for iron carbonate to form crystals. Increasing Fe^{2+} concentration to 50 ppm, both iron carbonate and iron sulfide scale formed on the steel surface in the first hour, and in twenty four hours most products were iron sulfide (Figure 133).

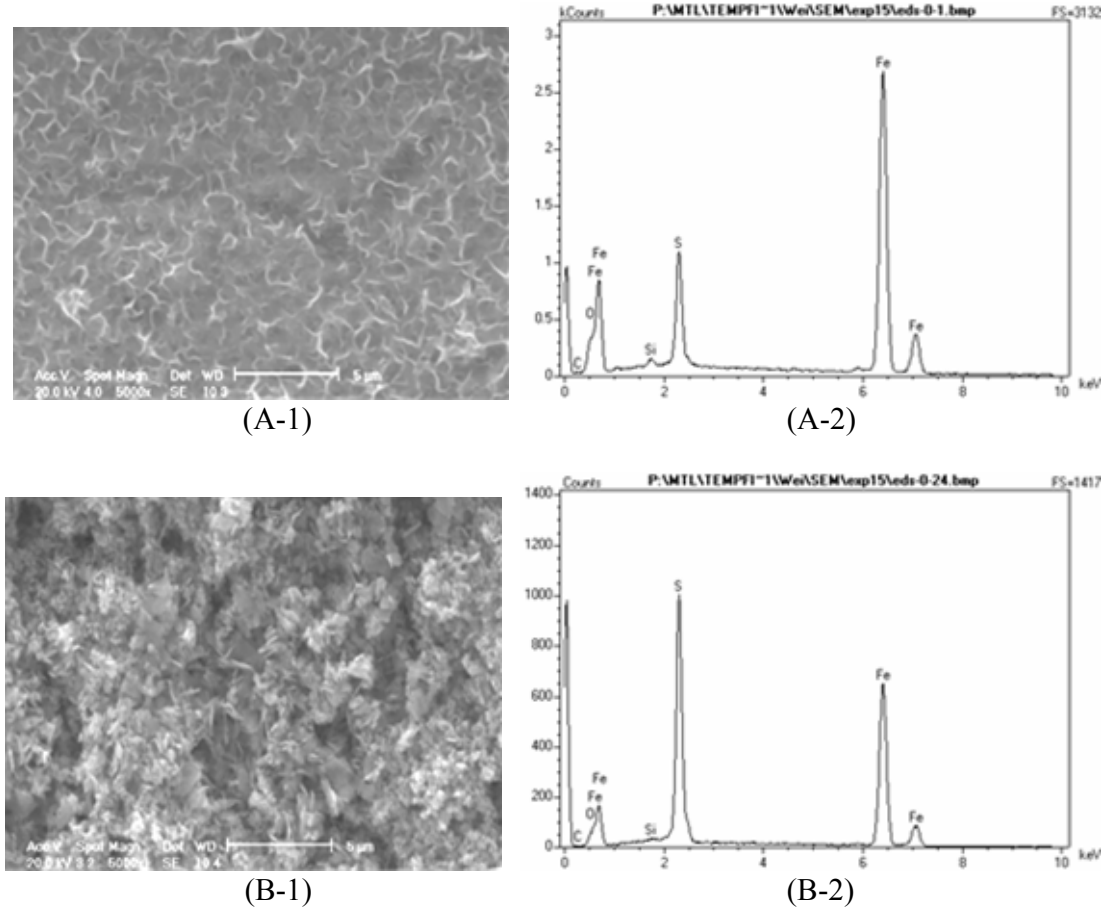

Figure 131. The morphology (5000x) and EDS results of scale formed on the X65 carbon steel surface under the conditions of 1% H_2S (H_2S/CO_2 gas), T=80°C, pH 6.5~6.6, Fe^{2+} = 0 ppm, the total reaction time is (A) 1 hour, (B) 24 hours.

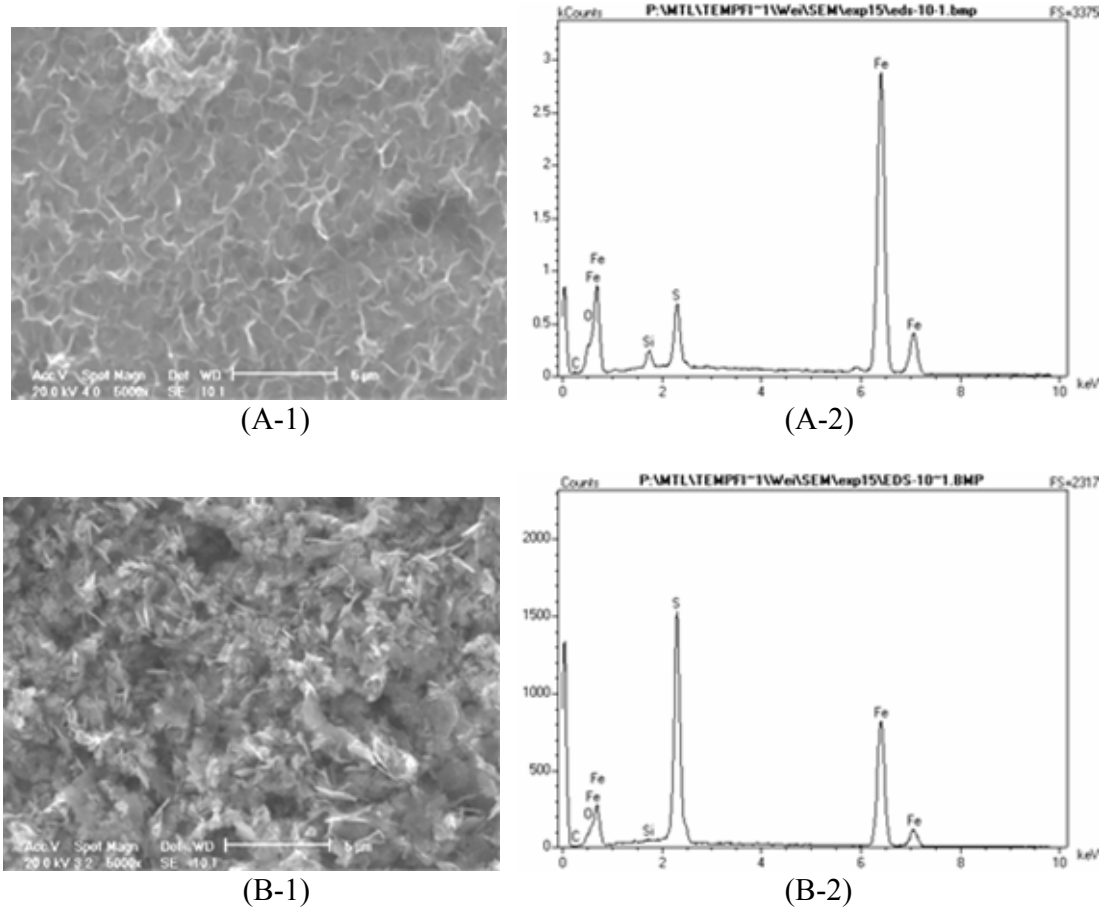

(A-1) (A-2)

(B-1) (B-2)

Figure 132. The morphology (5000x) and EDS results of scale formed on the X65 carbon steel surface under the conditions of 1% H_2S (H_2S/CO_2 gas), T=80°C, pH 6.5~6.6, Fe^{2+} = 10 ppm, the total reaction time is (A) 1 hour, (B) 24 hours.

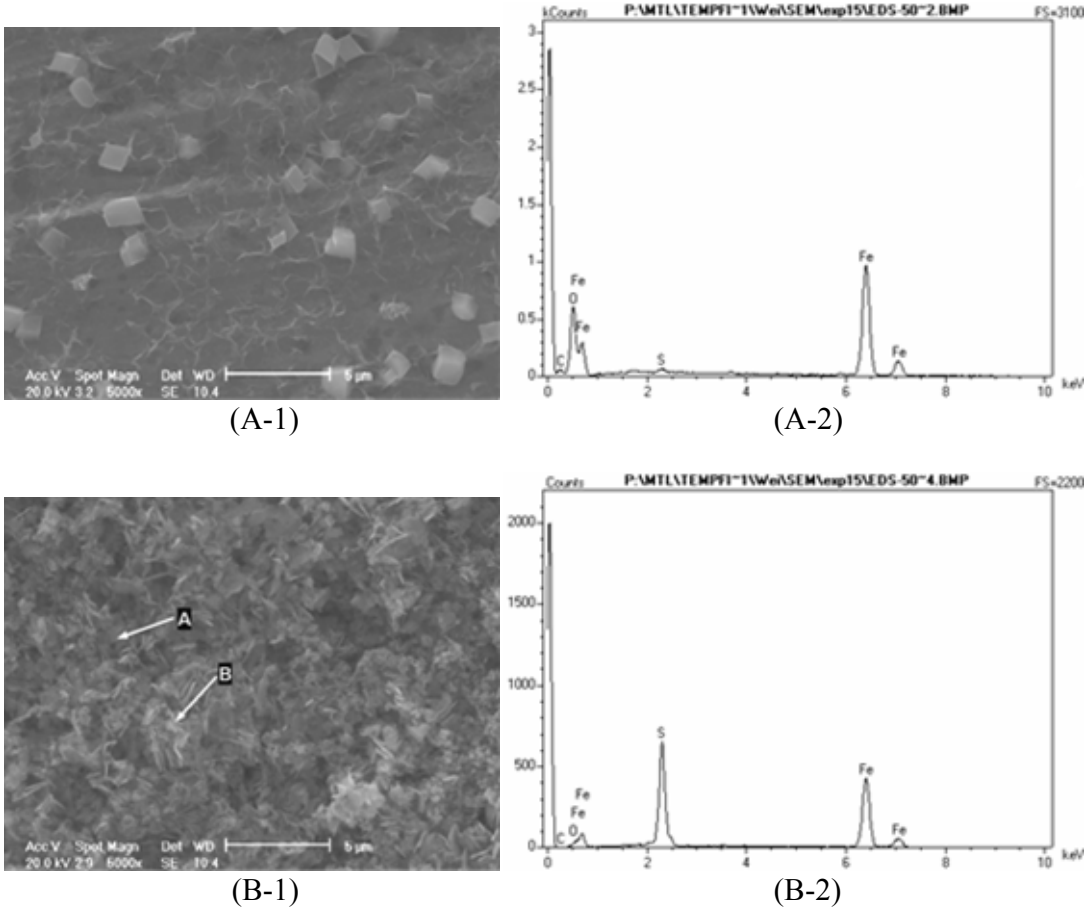

Figure 133. The morphology (5000x) and EDS results of scale formed on the X65 carbon steel surface under the conditions of 1% H_2S (H_2S/CO_2 gas), T=80°C, pH 6.5~6.6, Fe^{2+} = 50 ppm, the total reaction time is (A) 1 hour, (B) 24 hours.

When H_2S concentration increased to 10%, both the morphology and EDS results illustrate that no iron carbonate formed on the steel surface at Fe^{2+} concentrations of 0ppm and 50ppm, as shown in Figure 134 and Figure 135. Therefore, at H_2S concentration 10%, iron sulfide formation is the dominant reaction in CO_2/H_2S system.

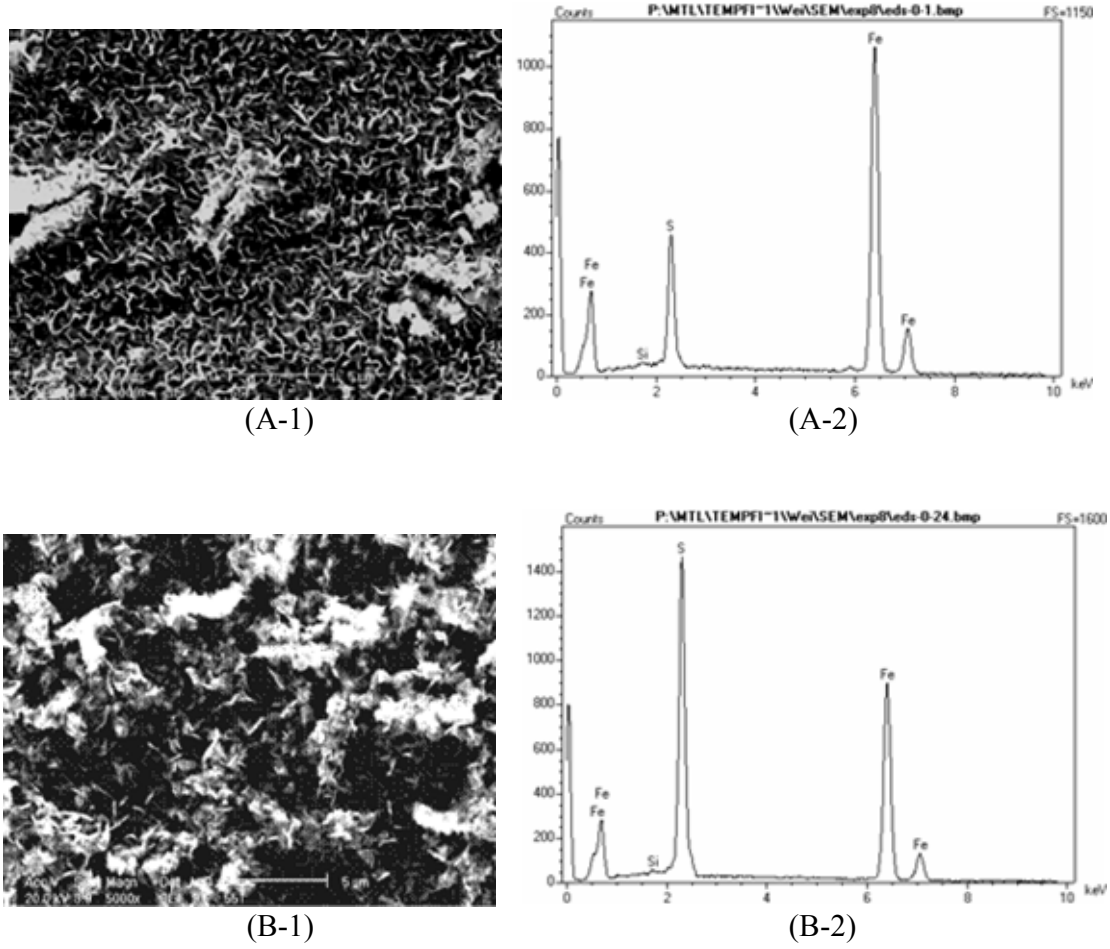

Figure 134. The morphology (5000x) and EDS results of scale formed on the X65 carbon steel surface under the conditions of 10% H_2S (H_2S/CO_2 gas), T=80°C, pH 6.5~6.6, Fe^{2+} = 0 ppm, the total reaction time is (A) 0.83 hour, (B) 24 hours.

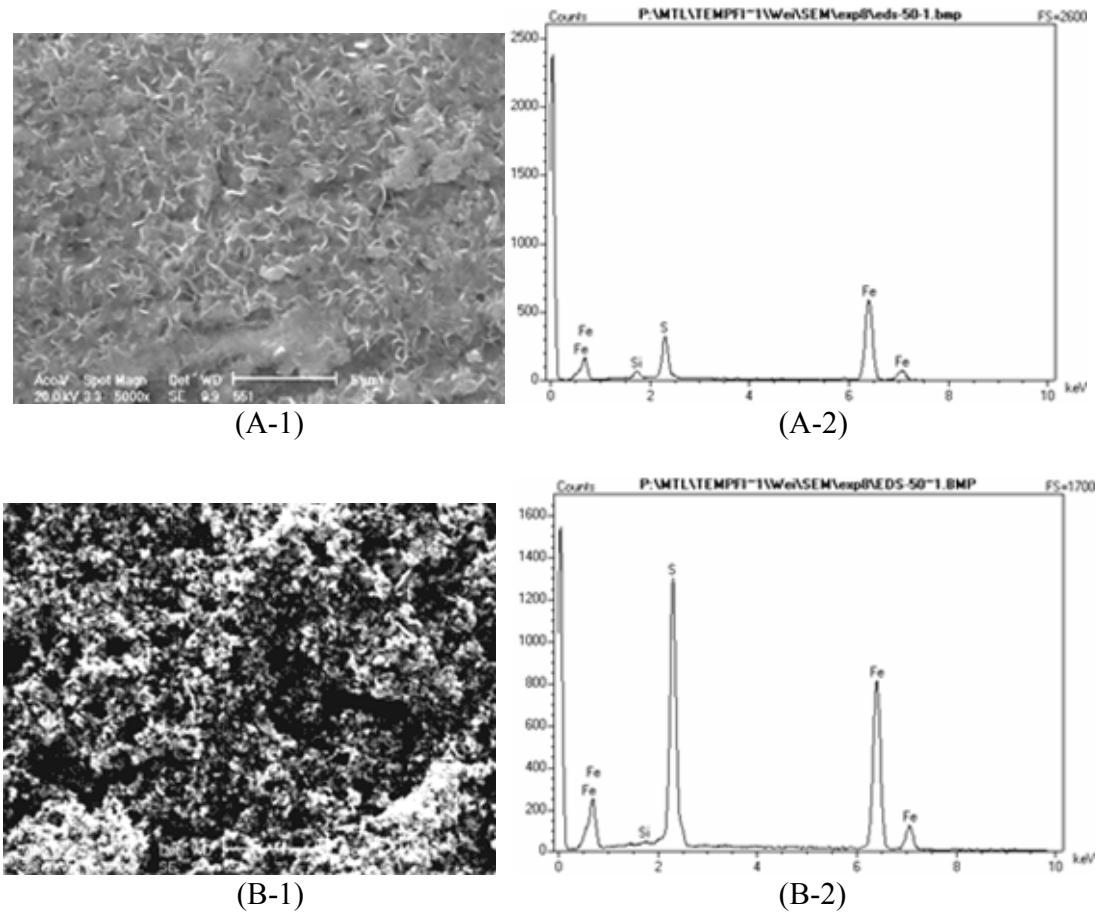

Figure 135. The morphology (5000x) and EDS results of scale formed on the X65 carbon steel surface under the conditions of 10% H_2S (H_2S/CO_2 gas), T=80°C, pH 6.5~6.6, Fe^{2+} = 50 ppm, the total reaction time is (A) 0.83 hour, (B) 24 hours.

The cross sections of the scale under the different test conditions are shown from Figure 136 to Figure 138. Figure 136 shows the cross section of the scale formed at H_2S concentration of 0.1% and Fe^{2+} concentration 0 ppm, 10 ppm, and 50 ppm. It is noted that at Fe^{2+} 0 ppm and 10 ppm, the thicknesses of the scale are similarly equal to 10 to 15 μm. At Fe^{2+} 50 ppm, the scale is much tighter and more protective due to the uniform iron carbonate scale formation.

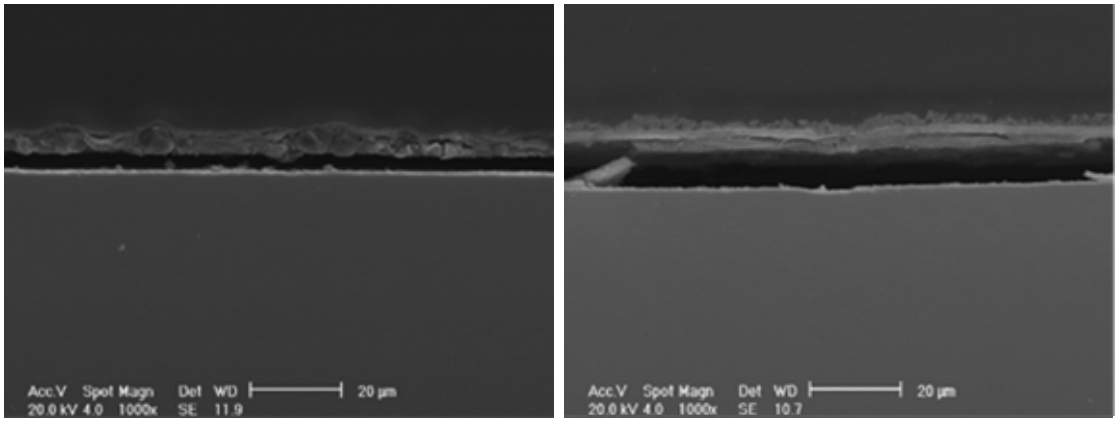

(A) (B)

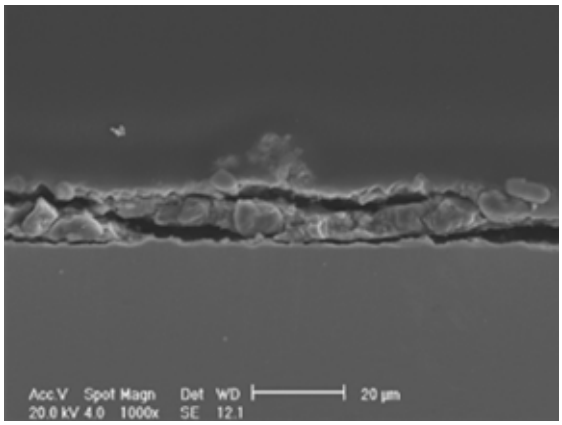

(C)

Figure 136. Cross section of the scale formed on the X65 carbon steel surface (at 1000x) under the conditions of 0.1% H_2S (H_2S/CO_2 gas), T=80°C, pH 6.5~6.6, (A) Fe^{2+}=0 ppm, (B) Fe^{2+}=10 ppm, (C) Fe^{2+}=50 ppm, the total reaction time is 24 hours.

When H_2S concentration is increased to 1% and 10%, the cross section of the scale shows that the thickness of the scale keeps approximately 10 to 15 μm (Figure 137 and Figure 138), which is similar to the thickness of the scale at H_2S 0.1%. This phenomenon illustrates that the scale retention rate and corrosion rate have no significant effect on the thickness of the scale because part of the porous iron sulfide scale formed on the steel surface was removed by the mechanical damage due to the scale internal stress.

The cross section pictures also suggest that a very thin iron sulfide layer formed by solid state reaction may exist on the steel surface.

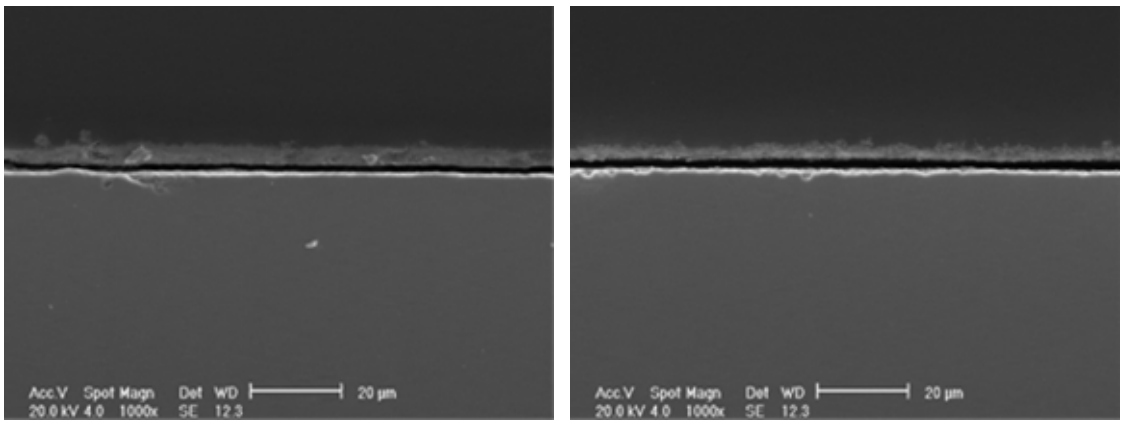

(A) (B)

Figure 137. Cross section of the scale formed on the X65 carbon steel surface (at 1000x) under the conditions of 1% H_2S (H_2S/CO_2 gas), T=80°C, pH 6.5~6.6, (A) Fe^{2+}=0 ppm, (B) Fe^{2+}=10 ppm, the total reaction time is 24 hours.

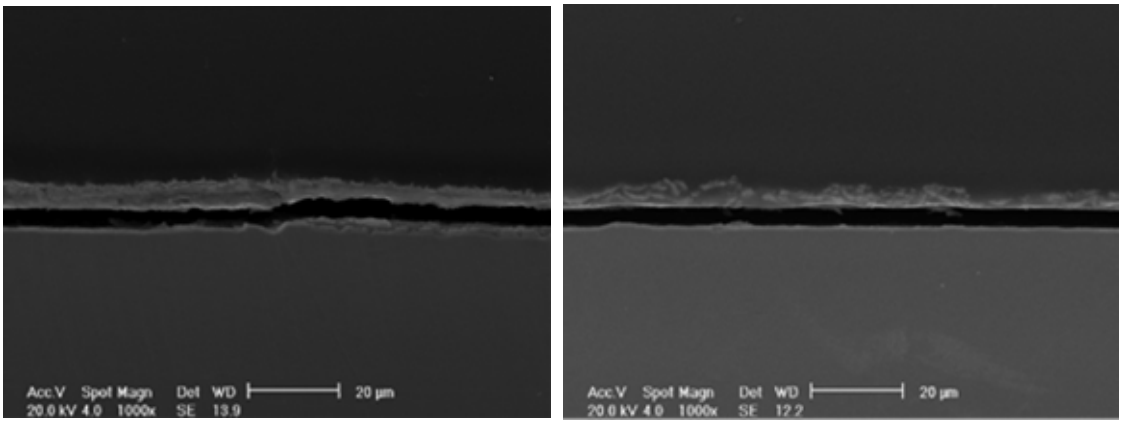

(A) (B)

Figure 138. Cross section of the scale formed on the X65 carbon steel surface (at 1000x) under the conditions of 10% H_2S (H_2S/CO_2 gas), T=80°C, pH 6.5~6.6, (A) Fe^{2+}=0 ppm, (B) Fe^{2+}=10 ppm, the total reaction time is 24 hours.

Figure 139 to Figure 141 show the XRD results of the scale formed on the X65 steel surface under the test conditions of H_2S concentrations of 0.1%, 1%, and 10%, T 80°C, pH 6.6, Fe^{2+} concentration of 50ppm, and the total reaction time is 24 hours. The XRD results show that mackinawite is the dominant iron sulfide formed on the steel surface. It is also found that both iron carbonate and mackinawite formed on the steel surface at H_2S concentration of 0.1%, and only mackinawite scale formed at H_2S concentration of 1% and 10%. The XRD results are in good agreement with the SEM/EDS results (Figure 128 to Figure 135).

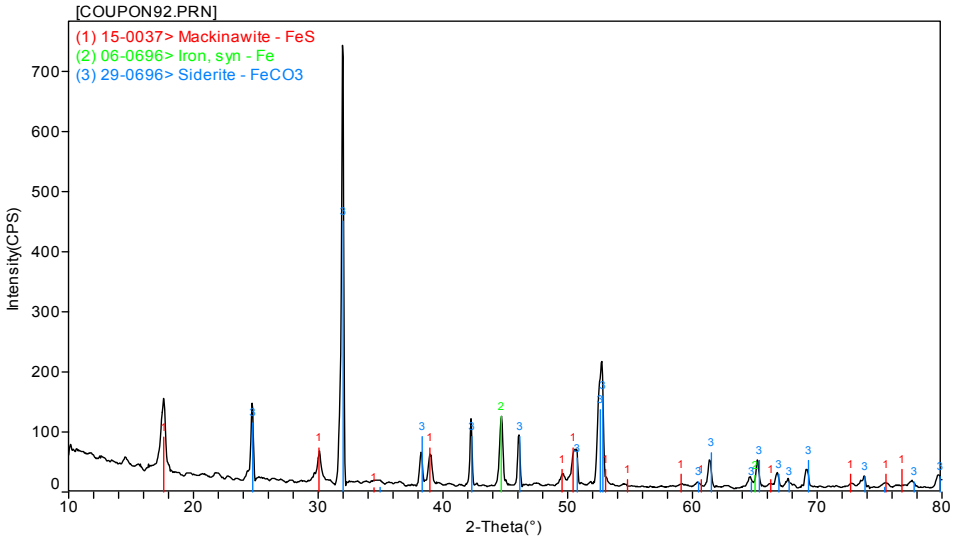

Figure 139. XRD results of the scale formed on the X65 carbon steel surface under the conditions of 0.1% H_2S (H_2S/CO_2 gas), T=80°C, pH 6.5~6.6, Fe^{2+} = 50 ppm, the total reaction time is 24 hours.

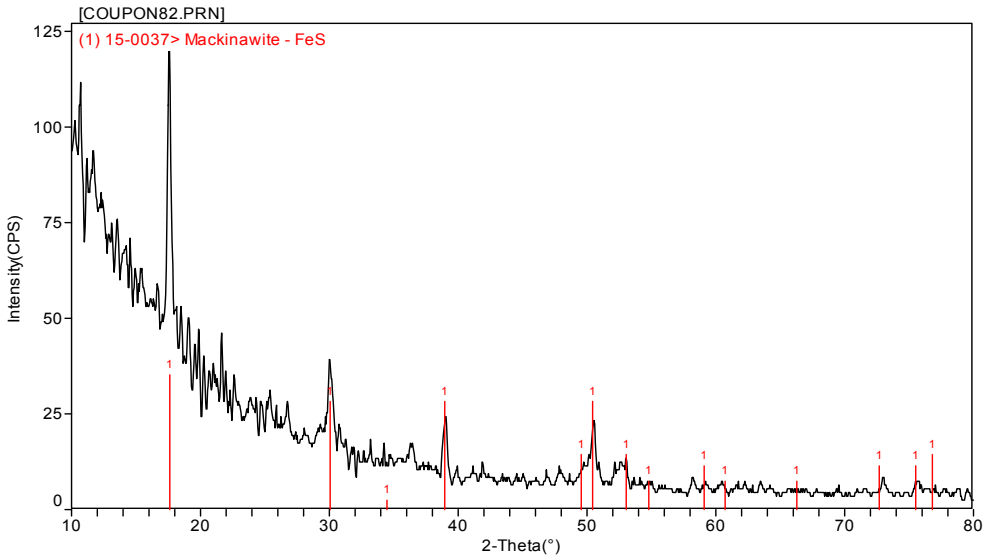

Figure 140. XRD results of the scale formed on the X65 carbon steel surface under the conditions of 1% H_2S (H_2S/CO_2 gas), T=80°C, pH 6.5~6.6, Fe^{2+} = 50 ppm, the total reaction time is 24 hours.

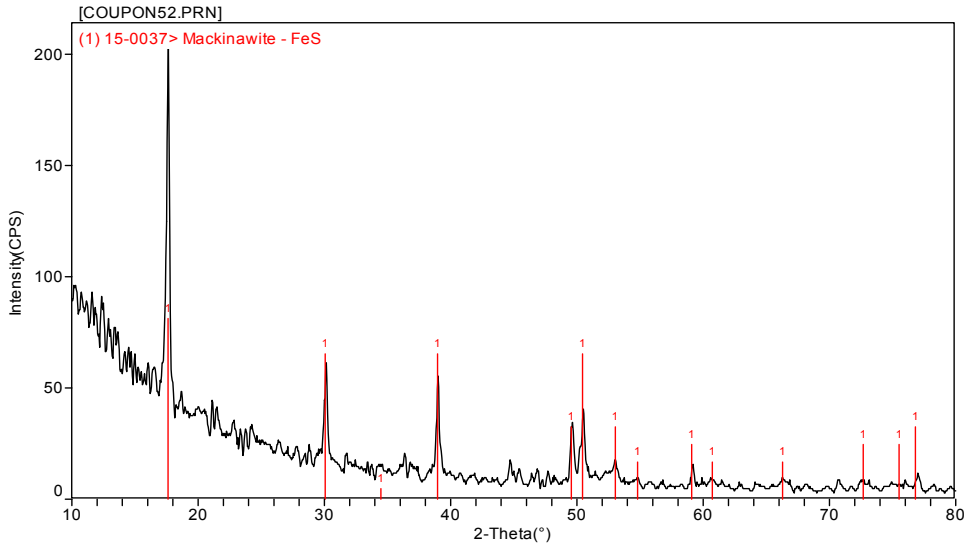

Figure 141. XRD results of the scale formed on the X65 carbon steel surface under the conditions of 10% H_2S (H_2S/CO_2 gas), T=80°C, pH 6.5~6.6, Fe^{2+} = 50 ppm, the total reaction time is 24 hours.

6.4 Modeling

6.4.1 Modeling of CO_2/H_2S corrosion

Based on the experimental results above, it is concluded that mackinawite scale formation is the dominant process in most cases of CO_2/H_2S corrosion. In a few cases, iron carbonate crystals may grow with mackinawite scale, for example the experiments with 0.1% H_2S, Fe^{2+} 50 ppm, and T 80^oC (Figure 130). However it is known in Chapter 5 that mackinawite scale forms extremely fast, hence mackinawite scale always forms as the first layer on the steel surface and iron carbonate crystals may precipitate in the outer mackinawite scale, as shown in Figure 130. Therefore, it will be here assumed that mackinawite is the dominant scale that protects the steel from corroding and the description of the H_2S corrosion process presented above for pure H_2S corrosion is also applicable for CO_2/H_2S corrosion. It is understood that the assumptions about iron carbonate scale formation having little effect on the CO_2/H_2S corrosion process is a simplification, however within the framework of the present project it does allow development of a useful predictive model.

Based on the mechanistic model of H_2S corrosion presented above, a similar model is proposed for CO_2/H_2S corrosion, as follows. The total rate of corrosion in CO_2/H_2S corrosion is equal to the sum of the corrosion caused by H_2S, the corrosion caused by H^+, and the corrosion caused by CO_2.

$$CR = CR_{H_2S} + CR_{H^+} + CR_{CO_2} \tag{71}$$

For the corrosion rates caused by H_2S and H^+ the same expressions can be used as in H_2S/N_2 environment,

$$CR_{H_2S} = A_{H_2S} e^{-\frac{B_{H_2S}}{RT}} \ln \frac{c_{b,H_2S} - CR_{H_2S}\left(\frac{\delta_{0.5}}{D_{H_2S}\varepsilon\Psi} + \frac{1}{k_{m,H_2S}}\right)}{c_{s,H_2S}} \tag{61}$$

$$CR_{H^+} = A_{H^+} e^{-\frac{B_{H^+}}{RT}} \ln \frac{c_{b,H^+} - CR_{H^+}\left(\frac{\delta_{0.5}}{D_{H^+}\varepsilon\Psi} + \frac{1}{k_{m,H^+}}\right)}{c_{s,H^+}} \tag{69}$$

In addition for the flux of CO_2, one can write:

1. convective diffusion through the mass transfer boundary layer

$$Flux_{CO_2} = k_{m,CO_2}\left(c_{b,CO_2} - c_{o,CO_2}\right) \tag{72}$$

2. molecular diffusion through the liquid in the porous outer scale

$$Flux_{CO_2} = \frac{D_{CO_2}\varepsilon\Psi}{\delta_{0.5}}\left(c_{o,CO_2} - c_{i,CO_2}\right) \tag{73}$$

3. solid state diffusion through the inner mackinawite film

$$Flux_{CO_2} = A_{CO_2} e^{-\frac{B_{CO_2}}{RT}} \ln\left(\frac{c_{i,CO_2}}{c_{s,CO_2}}\right) \tag{74}$$

which is equal to the corrosion rate in the presence of CO_2, CR_{CO_2},

where

$Flux_{CO_2}$ is expressed in mol/(m^{2}s),

k_{m,CO_2} is the mass transfer coefficient for CO_2 in the hydrodynamic boundary layer, $k_{m,CO_2} = 1.00 \times 10^{-4}$ in nearly stagnant condition, in m/s,

c_{b,CO_2} is the bulk concentration of CO_2 in the liquid phase in mol/m^3,

c_{o,CO_2} is the interfacial concentration of CO_2 at the outer scale/solution interface in mol/m^3,

D_{CO_2} is the diffusion coefficient for dissolved CO_2 in water, $D_{CO_2} = 1.96 \times 10^{-9}$, in m^2/s,

ε is the outer scale porosity,

Ψ is the outer scale tortuosity factor,

c_{i,CO_2} is the interfacial concentration of CO_2 at the inner scale/film interface in mol/m^3.

δ_{os} is the thickness of the mackinawite scale $\delta_{os} = m_{os} / (\rho_{FeS}\ A)$ in m,

m_{os} is the mass of the mackinawite scale in kg,

A is the surface area of the steel in m^2,

A_{CO_2}, B_{CO_2} are the Arrhenius constants, $A_{CO_2} = 2.6 \times 10^{-5}$ mol/(m^2s) and $B_{CO_2} = 15500$ J/mol

T is the temperature in Kelvin,

c_{s,CO_2} is the concentration of CO_2 on the steel surface in mol/m^3.

By eliminating the unknown interfacial concentrations, c_{o,CO_2} and c_{i,CO_2} from equations (72) to (74), the following expression is obtained for the corrosion rate driven by the presence of CO_2 and controlled by the presence of the iron sulfide scale:

$$CR_{CO_2} = A_{CO_2} e^{-\frac{B_{CO_2}}{RT}} \ln \frac{c_{b,CO_2} - CR_{CO_2}\left(\frac{\delta_{os}}{D_{CO_2}\varepsilon\Psi} + \frac{1}{k_{m,CO_2}}\right)}{c_{s,CO_2}} \qquad (75)$$

In H_2S corrosion model, pure mass transfer limit is assumed and the c_{s,H_2S} and c_{s,H^+} are set to be virtually zero (practically a very small value of $1.00 \times 10^{-7}\ mol/m^3$). In CO_2 corrosion, carbonic acid is the corrosive species and therefore CO_2 hydration to form

carbonic acid is a rate controlling process. Therefore, the corrosion current on the steel surface caused by CO_2 can be expressed in terms of the limiting rate of carbonic acid hydration as follows:[139]

$$CR_{CO_2} = c_{s,CO_2} \left(D_{H_2CO_3} k_{hyd}^{f} K_{hyd} \right)^{0.5} f_{H_2CO_3} \tag{76}$$

where

$D_{H_2CO_3}$ is the diffusion coefficient of carbonic acid in m^2/s,

K_{hyd} is the equilibrium constant for the CO_2 hydration reaction,

k_{hyd}^{f} is the forward reaction rate for the CO_2 hydration reaction,

$f_{H_2CO_3}$ is the flow factor, including the effect of the reaction diffusion layer on the limiting current, set to unity.

Based on equation (76), the unknown c_{s,CO_2} is expressed as follows,

$$c_{s,CO_2} = \frac{CR_{CO_2}}{\left(D_{H_2CO_3} k_{hyd}^{f} K_{hyd} \right)^{0.5} f_{H_2CO_3}} \tag{77}$$

Therefore, equation (75) can be expressed as:

$$CR_{CO_2} = A_{CO_2} e^{-\frac{B_{CO_2}}{RT}} \ln \frac{c_{b,CO_2} - CR_{CO_2} \left(\frac{\delta_{os}}{D_{CO_2} \varepsilon \Psi} + \frac{1}{k_{m,CO_2}} \right)}{\frac{CR_{CO_2}}{\left(D_{H_2CO_3} k_{hyd}^{f} K_{hyd} \right)^{0.5} f_{H_2CO_3}}} \tag{78}$$

By solving the above equation, the corrosion rates caused by the presence of CO_2 can be obtained. The total corrosion rate in CO_2/H_2S corrosion will be:

$$CR = CR_{H_2S} + CR_{H^+} + CR_{CO_2} \tag{71}$$

6.4.2 Verification of the model

The model predictions are compared with the experimental results at different test conditions of CO_2/H_2S corrosion. Figure 142 shows the comparison of the corrosion rate vs. the reaction time for a series of experiments done at 80^oC. The model can successfully capture the downward trend of the corrosion rate with time. Figure 143 shows the comparison of the measured and predicted scale retention at different reaction times. The predicted scale growth is similar as the scale formed in H_2S environment, rapid in the first few hours and then gradually leveling off because the model considers the negligible effect of iron carbonate precipitation. After all the cases available in this experimental study were simulated with the model, the comparison of the predicted corrosion rates and the measured values are in reasonable agreement, as shown in Figure 144. The scatter observed can be ascribed to the experimental error, the negligible effect of Fe^{2+} concentration, as well as to the assumption about the lack of influence of iron carbonate precipitation on the scale structure, as described above.

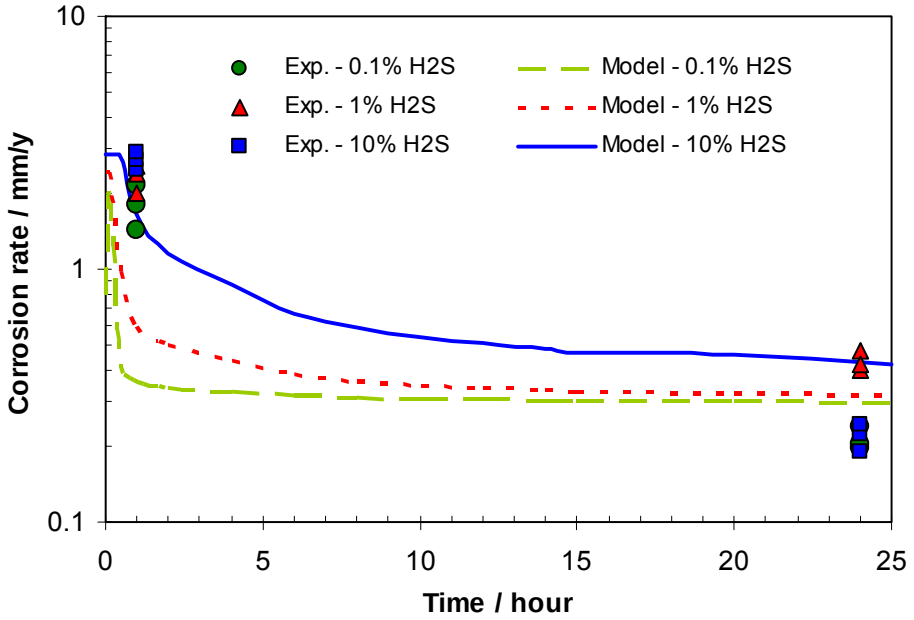

Figure 142. The experimental and prediction corrosion rate vs. time in CO_2/H_2S solutions under the conditions of total pressure p=1 bar, H_2S gas concentration from 0.1% to 10%, T=80°C, reaction time of 1 hour and 24 hours, pH 5.0-5.5, and static solution.

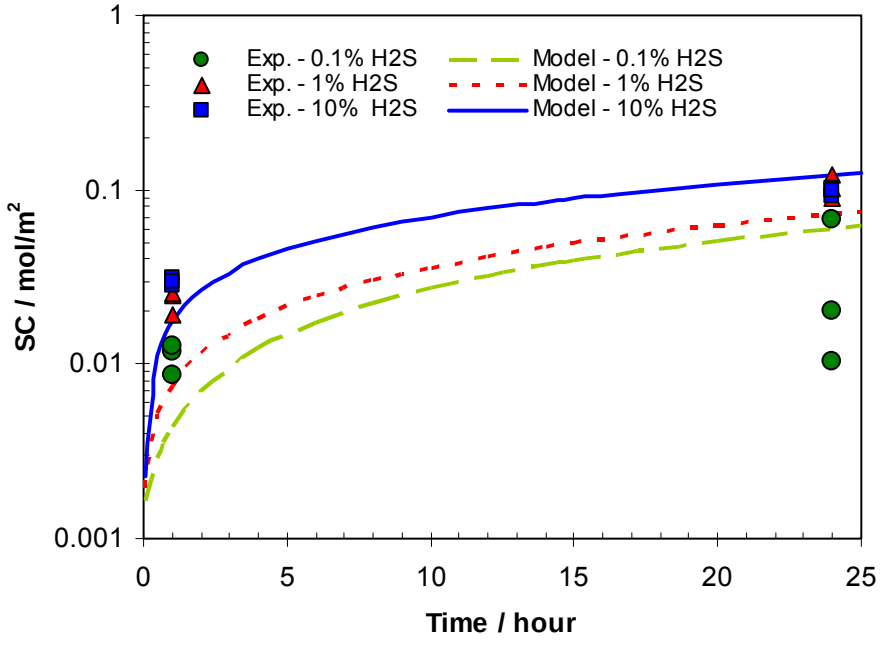

Figure 143. The experimental results and predictions of the scale retention vs. time in CO_2/H_2S solutions under the conditions of total pressure p=1 bar, H_2S gas concentration from 0.1% to 10%, T=80°C, reaction time of 1 hour and 24 hours, pH 5.0-5.5, and static solution.

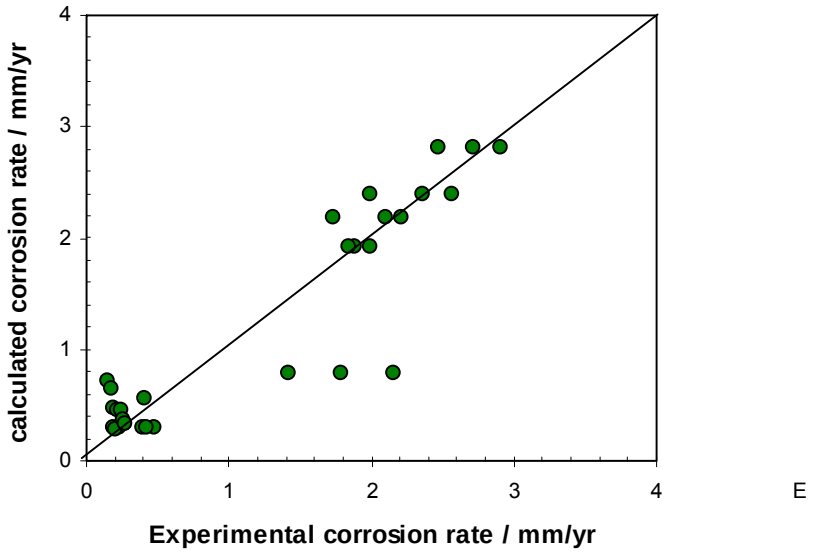

Figure 144. The comparison of the experimental corrosion rate and the calculated corrosion rate in CO_2/H_2S solutions under the conditions of total pressure p=1 bar, H_2S gas concentration from 0.01% to 10%, T 25°C, 60°C, and 80°C, reaction time of 1 hour and 24 hours, pH 5.0-5.5, and static conditions.

6.5 Summary

The primary findings described in this chapter are:

1. Kinetics experiments in CO_2/H_2S solution prove that the makeup of the surface scale not only depends on the water chemistry and the respective solubility of iron carbonate and iron sulfides, but also on the competitiveness of the two scale formation mechanisms. Only at very high supersaturation of iron carbonate are both iron carbonate and mackinawite scale are found on the steel surface, with iron carbonate in the outer portion of the mackinawite scale.
2. It is concluded from the experimental results that mackinawite is the dominant scale formed on the steel surface, which protects the steel from corroding in CO_2/H_2S corrosion.

3. The mechanistic model for pure H_2S corrosion is extended to predict the CO_2/H_2S corrosion process by considering the effect of the presence of CO_2.

Chapter 7: Conclusions

1. A unified iron carbonate solubility expression which accounts for both temperature and ionic strength effects is developed based on the literature data. The predictions made with this unified equation agree well with the published experimental data.
2. The calculated results obtained by the previous kinetics expressions using the traditional dissolved ferrous ion concentration method overestimated the scale retention rate of iron carbonate on the steel surface (using weight change method) by a large margin. Based on the experimental data, a reliable iron carbonate scale retention rate expression for engineering application is developed to predict iron carbonate scale growth.
3. The thermodynamics of hydrogen sulfide and iron sulfides was clarified from the literature data. Reliable solubility expressions of hydrogen sulfide, the first dissociation constant expression of hydrogen sulfide, and the solubility expression of mackinawite are recommended for further use. It is also suggested that the researchers should avoid using the second dissociation constant of hydrogen sulfide to calculate the concentration of species and further to predict the supersaturation of iron sulfides. Data on solubility limits for other types of sulfides were also scattered.
4. Mackinawite is the predominant iron sulfide formed on the steel surface in H_2S/N_2 corrosion, most likely by a solid state reaction. The scale retained on the steel surface depends on both the scale formation rate and the scale damage rate.

The scale formation rate includes both the corrosion rate and precipitation mechanisms. The corrosion rate of carbon steel in H_2S corrosion is affected by H_2S concentration, temperature, velocity, and the protectiveness of the scale. The scale damage rate includes the removal by both mechanical and chemical means. A mechanistic model of H_2S corrosion is developed to accurately predict the pure H_2S corrosion process of mild steel.

5. The source of ferrous ions forming iron carbonate scale includes ferrous ions both released from the steel surface and those provided by the bulk of the solution. However, the source of ferrous ions forming iron sulfide scale mainly comes from the corrosion of the steel.
6. Mackinawite is the predominant scale formed on the steel surface, which protects the steel from corroding in CO_2/H_2S corrosion. The mechanistic model for H_2S corrosion is extended to predict the CO_2/H_2S corrosion process by considering the effect of the presence of CO_2.

Chapter 8: Recommendations and future work

Some recommendations for future work are as follows:

1. Further study the effect of velocity on H_2S corrosion for a better understanding of the iron sulfide scale damage by mechanical means.
2. Further study the mackinawite scale formation in the under-saturated conditions to understand the properties of the thinner tight mackinawite inner layer as well as the iron sulfide scale removal by chemical means.
3. Investigate the iron sulfide scale growth and its effect on corrosion rate by running long – term experiments to better understand the role of iron sulfide precipitation.
4. Investigate the parameters that cause H_2S localized corrosion.

Nomenclature

A and B	the Arrhenius constants, B in J/mol
a and c	the experimentally determined constants for a rotating cylinder flow geometry
A_{CO_2} , B_{CO_2}	the Arrhenius constants for CO_2, A_{CO_2} in mol/(m^{2}s) and B_{CO_2} in J/mol
A_{H^+} , B_{H^+}	the Arrhenius constants for H^+, A_{H^+} in mol/(m^{2}s) and B_{H^+} in J/mol
A_{H_2S} , B_{H_2S}	the Arrhenius constants for H_2S, A_{H_2S} in mol/(m^{2}s) and B_{H_2S} in J/mol
c_{b,CO_2}	the bulk concentration of CO_2 in the liquid phase in mol/m^3
c_{b,H_2S}	the bulk concentration of H_2S in the liquid phase in mol/m^3
c_{b,H^+}	the bulk concentration of H^+ in the liquid phase in mol/m^3
$c_{CO_3^{2-}}$	the concentration of CO_3^{2-}, in mol/L
$c_{Fe^{2+}}$	the concentration of Fe^{2+}, in mol/L
$c_{H_2S_{(g)}}$	the concentration of hydrogen sulfide in the gas phase, in mol/L
$c_{H_2S_{(aq)}}$	the concentration of hydrogen sulfide in the solution, mol/L
$c_{HS^-_{(aq)}}$	the concentration of HS^-, in mol/L
c_{i,CO_2}	the interfacial concentration of CO_2 at the inner scale/film interface in mol/m^3
c_{i,H^+}	the interfacial concentration of H^+ at the inner scale/film interface in mol/m^3
c_{i,H_2S}	the interfacial concentration of H_2S at the inner scale/film interface in mol/m^3
c_{o,CO_2}	the interfacial concentration of CO_2 at the outer scale/solution interface in mol/m^3
c_{o,H^+}	the interfacial concentration of H^+ at the outer scale/solution interface in mol/m^3
c_{o,H_2S}	the interfacial concentration of H_2S at the outer scale/solution interface in mol/m^3
c_{s,CO_2}	the concentration of CO_2 on the steel surface in mol/m^3
c_{s,H^+}	the concentration of H^+ on the steel surface, in mol/m^3
c_{s,H_2S}	the concentration of H_2S on the steel surface, in mol/m^3
D_{CO_2}	the diffusion coefficient for dissolved H_2S in water, in m^2/s
D_{H^+}	the diffusion coefficient for dissolved H^+ in water, in m^2/s
$D_{H_2CO_3}$	the diffusion coefficient of carbonic acid, in m^2/s
D_{H_2S}	the diffusion coefficient for dissolved H_2S in water, in m^2/s

F	Faraday constant (96485 C/mol)
$f_{H_2CO_3}$	the flow factor, including the effect of the reaction diffusion layer on the limiting current.
$Flux_{CO_2}$	the flux of CO_2 in mol/(m^{2}s)
$Flux_{H_2S}$	the flux of H_2S, in mol/(m^{2}s)
$Flux_{H^+}$	the flux of H^+, in mol/(m^{2}s)
H_{H_2S}	the Henry's constant
I	the ionic strength, in mol/L
i_{CO_2}	the corrosion current caused by CO_2, in A/m^2
K_1	the first dissociation constant of H_2S
K_2	the second dissociation constant of H_2S
$K_{eq,FeS}$	the equilibrium constant of the reaction $FeS(s)+H_2S \Leftrightarrow Fe^{2+}+2HS^-$,
K_{H_2S}	the equilibrium constant of H_2S
K_{FeS}	the equilibrium constant of reaction $FeS(s)+2H^+ \Leftrightarrow Fe^{2+}+H_2S(aq)$ in (mol/L)^2
K_{hyd}	the equilibrium constant for the CO_2 hydration reaction
k_{hyd}^f	the forward reaction rate for the CO_2 hydration reaction
k_{m,CO_2}	the mass transfer coefficient for CO_2 in the hydrodynamic boundary layer in m/s
k_{m,H_2S}	the mass transfer coefficient for H_2S in the hydrodynamic boundary layer, in m/s
k_{m,H^+}	the mass transfer coefficient for protons in the hydrodynamic boundary layer, in m/s
k_r	the kinetic constant, which is a function of temperature, in kg^2/(mol m^2 s)
K_{sp}	the solubility limit, in (mol/L)^2
$K_{sp,mck}$	the solubility limit of mackinawite,
$K_{sp,FeS}$	the solubility limit of amorphous iron sulfide
K_{sp,FeS_2}	the solubility limit of pyrite
$m_{FeCO_{3(s)}}$	the mass of iron carbonate, in kg
M_{FeS}	the molar mass of iron sulfide, in kg/mol
m_{os}	the mass of the mackinawite scale, in kg
P_{H_2S}	the partial pressure of hydrogen sulfide, in Pa
PR	the precipitation rate of the scale, in mol/(m^{2}s)
r	the reaction order
R	the gas constant (8.3145 J/mol/K)
S	the surface area, in m^2
SFR	the scale formation rate, in mol/(m^{2}s)

SDR	the scale damage rate, in mol/(m^2s)
SDR_m	the mechanical scale damage rate, in mol/(m^2s)
SRR	the scale retention rate, in mol/(m^2s)
SS	supersaturation
ST	the scaling tendency
S/V	the surface area-to-volume ratio, in m^{-1}
T_c	the temperature, in ^oC
T_k	the temperature, in kelvin
V	the volume of the scale, in m^3
V_{void}	the volume of the void in the scale, in m^3
V_{total}	the total volume of the scale, in m^3
$V_{FeCO_{3(s)}}$	the volume of the iron carbonate scale, in m^3
z	the species charge
$\alpha_{Fe^{2+}}$	the activity of Fe^{2+}, in mol/L
α_{H^+}	the activity of H^+, in mol/L
α_{HS^-}	the activity of HS^-, in mol/L
$\alpha_{H_2S(aq)}$	the activity of aqueous H_2S, in mol/L
ΔH^0	the standard enthalpy of reaction, in J/mol
ΔC	the standard heat capacity of reaction, in J/mol/K
Δt	the time interval in seconds
$\delta_{FeCO_{3(s)}}$	the calculated thickness of the scale, in m
δ_{os}	the thickness of the mackinawite scale $\delta_{os} = m_{os} / (\rho_{FeS}\ A)$ in m
δ_{SEM}	the thickness of the scale obtained by SEM, in m
ε	the outer mackinawite scale porosity
$\rho_{FeCO_{3(s)}}$	the density of iron carbonate, in kg/m^3
σ	the driving force
Ψ	the outer mackinawite scale tortuosity factor

References

1. W. F. Rogers and J. A. Rowe, Jr., Corrosion effects of hydrogen sulfide and carbon dioxide in oil productions, Proceedings of the Fourth World Petroleum Congress, Rome, 479-499, 1955.

2. F. H. Meyer, O. L. Riggs, R. L. McGlasson, and J. D. Sudbury, Corrosion of mild steel in H_2S environments, Corrosion, 14 (1958) 109.

3. E. C. Greco and W. B. Wright, Corrosion of iron in an H_2S-CO_2-H_2O system, Corrosion, 18 (1962) 119-124.

4. M. Bonis, M. Girgis, K. Goerz, and R. MacDonald, Weight loss corrosion with H_2S: using past operations for designing future facilities, Corrosion/2006, paper no. 06122, NACE International, Houston, Texas, 2006.

5. S. N. Smith and M. Joosten, Corrosion of carbon steel by H_2S in CO_2 containing oilfield environments, Corrosion/2006, paper no. 06115, NACE International, Houston, Texas, 2006.

6. S. N. Smith, A proposed mechanism for corrosion in slightly sour oil and gas production, Twelfth International Corrosion Congress, Houston, Texas, September 19 – 24, paper no. 385, 1993.

7. S. N. Smith and E. J. Wright, Prediction of minimum H_2S levels required for slightly sour corrosion, Corrosion/94, paper no. 11, NACE International, Houston, Texas, 1994.

8. A. Anderko and P. J. Shuler, A Computational Approach to Predicting the Formation of Iron Sulfide Species Using Stability Diagrams, Computers & Geosciences, Vol. 23, No. 6, 647-658, 1997.

9. A. Anderko and P. J. Shuler, Modeling the Formation of Iron Sulfide Scales Using Thermodynamic Simulation, Corrosion/98, paper no. 64, NACE International, Houston, Texas, 1998.

10. A. Anderko and R. D. Young, Simulation of CO_2/H_2S Corrosion Using Thermodynamic and Electrochemical Models, Corrosion/99, paper no. 31, NACE International, Houston, Texas, 1999.

11. A. Anderko, Simulation of $FeCO_3$ / FeS scale formation using thermodynamic and electrochemical models, Corrosion/2000, paper no. 00102, NACE International, Houston, Texas, 2000.

12. S. N. Smith and J. L. Pacheco, Prediction of corrosion in slightly sour environments, Corrosion/2002, paper no. 02241, NACE International, Houston, Texas, 2002.

13. K. Videm and A. Dugstad. Corrosion of carbon steel in an aqueous carbon dioxide environment part 2. film formation, Materials Performance, 28 (4):46-50, 1989.

14. A. Dugstad, The importance of $FeCO_3$ supersaturation on the CO_2 corrosion of carbon steels, Corrosion/92, paper no. 14, NACE International, Houston, Texas, 1992.

15. A. Dugstad, Mechanism of protective film formation during CO_2 corrosion of carbon steel. Corrosion/98, paper no. 31, NACE International, Houston, Texas, 1998.

16. M. Nordsveen, S. Nesic, R. Nyborg, and A. Stangeland, A mechanistic model for carbon dioxide corrosion of mild steel in the presence of protective iron carbonate films – part 1: theory and verification, Corrosion, 59 (2003) 443-457.

17. S. Nesic and K.-L. J. Lee, The mechanistic model of iron carbonate film growth and the effect on CO_2 corrosion of mild steel, Corrosion/2002, paper no. 02237, NACE International, Houston, 2002.

18. S. Nesic and K.-L. J. Lee, The mechanistic model for carbon dioxide corrosion of mild steel in the presence of protective iron carbonate films – part 3: film growth model, Corrosion, 59 (2003) 616-628.

19. K. Chokshi, W. Sun, and S. Nesic, Iron carbonate scale growth and the effect of inhibition in CO_2 corrosion of mild steel, Corrosion/2005, paper no. 05285, NACE International, Houston, 2005.

20. M. L. Johnson and M. B. Tomson, Ferrous carbonate precipitation kinetics and its impact on CO_2 corrosion, Corrosion/91, paper no. 268, NACE International, Houston, Texas, 1991.

21. E. W. J. van Hunnik, B.F. M. Pots, and E. L. J. A. Hendriksen, The formation of protective $FeCO_3$ corrosion product layers in CO_2 corrosion, Corrosion/96, paper no. 6, NACE International, Houston, Texas, 1996.

22. R. A. Berner, Thermodynamic stability of sedimentary iron sulfides, Am. J. Sci. 265 (1967) 773-785.

23. P. Taylor, The stereochemistry of iron sulfides – a structural rationale for the crystallization of some metastable phases from aqueous solution, American Mineralogist. 65 (1980) 1026-1030.

24. J. S. Smith and J. D. A. Miller, Nature of sulfides and their corrosive effect on ferrous metals: a review, British Corrosion Journal, 10 (1975) 136-143.

25. D. W. Shoesmith, P. Taylor, M. G. Bailey, and D. G. Owen, The formation of ferrous monosulfide polymorphs during the corrosion of iron by aqueous hydrogen sulfide at 21^{o}C, Journal Electrochemical Society, 125 (1980) 1007-1015.

26. D. W. Shoesmith, Formation, transformation and dissolution of phases formed on surfaces, Lash Miller Award Address, Electrochemical Society Meeting, Ottawa, Nov. 27, 1981.

27. D. Rickard, Kinetics of FeS precipitation: part 1. competing reaction mechanisms, Geochimica et Cosmochimica Acta. 59 (1995) 4367-4379.

28. N. G. Harmandas and P. G. Koutsoukos, The formation of iron sulfides in aqueous solutions, Journal of Crystal Growth, 167 (1996) 719-724.

29. W. Sun and S. Nesic, Kinetics of scale formation in CO_2/H_2S solutions, the internal confidential report at Ohio University Advisory Board Meeting, Athens, Ohio, March 2003.

30. W. Sun and S. Nesic, Kinetics of scale formation in CO_2/H_2S solutions, the internal confidential report at Ohio University Advisory Board Meeting, Athens, Ohio, September 2003.

31. W. Sun and S. Nesic, Kinetics of precipitation of iron carbonate, the internal confidential report at Ohio University Advisory Board Meeting, Athens, Ohio, March 2004.

32. W. Sun and S. Nesic, Kinetics of iron sulfide scale formation in solutions with a small amount of H_2S, the internal confidential report at Ohio University Advisory Board Meeting Report, Athens, Ohio, September 2004.

33. W. Sun and S. Nesic, Kinetics of iron carbonate scale precipitation in CO_2 corrosion, the internal confidential report at Ohio University Advisory Board Meeting Report, Athens, Ohio, April 2005.

34. W. Sun and S. Nesic, Kinetics of iron sulfide scale precipitation in pure H_2S environments, the internal confidential report at Ohio University Advisory Board Meeting Report, Athens, Ohio, April 2005.

35. W. Sun and S. Nesic, Kinetics of iron carbonate and iron sulfide scale precipitation in H_2S/CO_2 environments, the internal confidential report at Ohio University Advisory Board Meeting Report, Athens, Ohio, April 2005.

36. J. Alberch, W. Sun, and S. Nesic, H_2S corrosion electrochemistry, the internal confidential report at Ohio University Advisory Board Meeting Report, Athens, Ohio, October 2005.

37. S. Nesic, W. Sun, and R. Woollam, The effect of temperature and ionic strength on iron carbonate ($FeCO_3$) solubility, the internal confidential report at Ohio University Advisory Board Meeting Report, Athens, Ohio, March 2006.

38. W. Sun and S. Nesic, Kinetics of scale formation, part 1. iron carbonate scale formation in pure carbon dioxide corrosion, the internal confidential report at Ohio University Advisory Board Meeting Report, Athens, Ohio, March 2006.

39. S. Nesic, W. Sun, and R. Woollam, The solubility study of hydrogen sulfide and iron sulfide in hydrogen sulfide corrosion, the internal confidential report at Ohio University Advisory Board Meeting Report, Athens, Ohio, March 2006.

40. W. Sun and S. Nesic, Investigation of the mechanism of H_2S corrosion, the internal confidential report at Ohio University Advisory Board Meeting Report, Athens, Ohio, March 2006.

41. W. Sun and S. Nesic, A mechanistic model of hydrogen sulfide corrosion, the internal confidential report at Ohio University Advisory Board Meeting Report, Athens, Ohio, October 2006.

42. W. Sun and S. Nesic, Basics revisited: kinetics of iron carbonate scale precipitation in CO_2 corrosion, Corrosion/2006, paper no. 06365, NACE International, Houston, Texas, 2006.

43. W. Sun, S. Nesic, and S. Papavinasam, Kinetics of iron sulfide and mixed iron sulfide / carbonate scale precipitation in CO_2/H_2S corrosion, Corrosion/2006, paper no. 06644, NACE International, Houston, Texas, 2006.

44. S. Nesic, W. Sun, and K. Chokshi, Study of scale formation in CO_2 corrosion of mild steel, paper no. 6-21, 16th ICC, Beijing, China, 2005.

45. K. Chokshi, W. Sun, and S. Nesic, The mechanism of inhibitor – scale interaction in carbon dioxide corrosion of mild steel, ECS, Los angles, California, 2005.

46. W. Sun, K. Chokshi, S. Nesic, and D. Gulino, A study of protective iron carbonate scale formation in CO_2 corrosion, AIChE, Austin, Texas, 2004.

47. S. Nesic, W. Sun, K. Chokshi, and O. Nafday, Formation of protective iron carbonates films – some important issues, NACE 2004 RIP symposium, New Orleans, LA, 2004.

48. W. Sun and S. Nesic, A mechanistic model of hydrogen sulfide corrosion,

Corrosion/2007, paper no. 07655, NACE International, Houston, Texas, 2007.

49. D. K. Nordstrom, L. N. Plummer, D. Langmuir, E. Busenberg, H. M. May, B. F. Jones, and D. L. Parkhurst, Revised chemical equilibrium data for major water-mineral reactions and their limitations, ACS Symp. Ser, 1990, 416, 398.

50. C. A. R. Silva, X. Liu, and F. J. Millero, Solubility of sidertie ($FeCO_3$) in NaCl solutions, Journal of Solution Chemistry, 31 (2002) 97-108.

51. H. L. James, Chemistry of the iron-rich sedimentary rocks, U.S. Geol. Surv. Prof., paper 440-W, 1966, 61.

52. Q. J. Fisher, R. Raiswell, and J. D. Marshall, Siderite concretions from nonmarine shales (westphalian A) of the pennines England: controls of their growth and composition, J. Sediment. Res., 68 (1998) 1034-1045.

53. L. Jensen, J. K. Boddum, J. C. Tjell, and T. H. Christensen, The solubility of rhodochrosite ($MnCO_3$) and siderite ($FeCO_3$) in anaerobic aquatic environments, Applied Geochemistry, 17 (2002) 503-511.

54. H. J. Smith, Equilibrium in the system: ferrous carbonate, carbon dioxide and water, J. Am. Chem. Soci. 40 (1918) 879-883.

55. C. J. Ptacek and E. J. Reardon, Solubility of siderite ($FeCO_3$) in concentrated NaCl and Na_2SO_4 solutions at 25^oC, Water-Rock Interaction, 1992, 181-183.

56. P. C. Singer and W. Stumm, The solubility of ferrous iron in carbonate-bearing waters, J. Am. Water Works Assoc. 62 (1970) 198-202.

57. W. M. Latimer, The oxidation states of the elements and their potentials in aqueous solutions. Prentice Hall Chemistry Series, Prentice Hall, Englewood Cliffs, NJ, 1952.

58. J. Greenberg and M. Tomson, Precipitation and dissolution kinetics and equilibria of aqueous ferrous carbonate vs. temperature, Appl. Geochem. 7 (1992) 185-190.

59. J. Bruno, P. Wersin, and W. Stumm, On the influence of carbonate in mineral dissolution: II. The solubility of $FeCO_3$ (s) at 25^oC and 1atm total pressure. Geochim. Cosmochim. Acta. 56 (1992) 1149-1155.

60. R. D. Braun, Solubility of iron (II) carbonate at temperatures between 30 and 80^o, Talanta 38 (1991), 205 – 211.

61. C. J. Ptacek and D. W. Blowes, Influence of siderite on the pore-water chemistry of inactive mine-tailings impoundments. In: C. N. Alpers, D. W. Blowes (Eds.),

Environmental Geochemistry of Sulfide Oxidation. American Chemical Society, Washington, DC, 1994, 172-189. (Chapter 13).

62. W. Preis and H. Gamsjager, Critical evaluation of solubility data: enthalpy of formation of siderite, Phys. Chem. Chem. Phys., 4 (2002) 4014-4019.

63. H. C. Helgeson, Thermodynamics of hydrothermal systems at elevated temperatures and pressures, American Journal of Science, 267 (1969) 729-804.

64. E. Hogfeldt, IUPAC, Stability Constants of Metal-Ion Complexes, Part A: Inorganic Ligands, Pergamon Press, 1982.

65. Personal communication, S. Nesic, IFE (Institute for Energy, Norway), Norway, presently affiliated with Ohio University, 2004.

66. G. M. Marion, D. C. Catling, and J. S. Kargel, Modeling aqueous ferrous iron chemistry at low temperatures with application to Mars, Geochimica et Cosmochimica Acta, 67 (2003) 4251-4266.

67. R. D. Braun, Solubility of iron (II) carbonate at temperatures between 30 and 80^{o}C, Talanta 38 (1991) 205 – 211.

68. Norsok Standard, http://www.nts.no/norsok.

69. W. Daniels and R. A. Alberty, Physical Chemistry, 3rd Edition, John Wiley & Sons Inc., New York, 1996.

70. A. K. Dunlop, H. L. Hassell, and P.R. Rhodes, Advances in CO_2 Corrosion, Ed. R. H. Hausler, H.P. Godard., Houston, Texas, National Association of Corrosion Engineers, 1984.

71. A. Ikeda, M. Ueda, and S. Mukai, Advances in CO_2 Corrosion, Ed. R. H. Hausler, H. P. Godard., Houston, Texas, National Association of Corrosion Engineers, 1984.

72. J. Garside, AIChE Symposium Series, New York, American Institute of Chemical Engineering, Ed. G. R. Youngquist, (1984) 23-38.

73. G. H. Nancollas, Advances in Colloid and Interface Science, 10 (1979) 215.

74. A. E. Neilsen, Treatise on Analytical Chemistry, Ed. I. M. Kolthoff and P. J. Elving, New York, John Wiley and Sons, Inc., 1983.

75. Laboratory Corrosion Tests and Standards, American Society for Testing and Materials, p. 507, 1985.

76. J. W. Mullin, Crystallization, 4th ed., Biddles Ltd, Woburn, Great Britain, 2001.

77. R. W. Doyle, Identification and solubility of iron sulfide in anaerobic lake sediment, Am. J. Sci., 266 (1968) 980-984.

78. R.D. Deshmukh and A.E. Mather, A mathematical model for equilibrium solubility of hydrogen sulfide and carbon dioxide in aqueous alkanolamine solutions, Chemical Engineering Science, 36 (1980) 355-362.

79. J. Vorholz, B. Rumpf, and G. Maurer, Prediction of the vapor-liquid phase equilibrium of hydrogen sulfide and the binary system water-hydrogen sulfide by molecular simulation, Phys. Chem. Chem. Phys. (2002) 4449-4457.

80. D. T. Rickard, The chemistry of iron sulfide formation at low temperatures, Stockholm Cont. Geology, 20 (1969) 67-95.

81. R. F. Weiss, The solubility of nitrogen, oxygen and argon in water and seawater, Deep Sea Research, 17 (1970) 721–735.

82. P. A. A. Douabul and J. P. Riley, The solubility of gases in distilled water and seawater – V. hydrogen sulphide, Deep Sea Research, 26A, 259-268.

83. B. E. Roberts, Vapor liquid equilibrium calculations for dilute aqueous solutions of CO_2, H_2S, NH_3 and NaOH to 300^oC, The Canadian Journal of Chemical Engineering, 63 (1985) 294-300.

84. J. Carroll and A. E. Mather, The solubility of hydrogen sulfide in water from 0 to 90^oC and pressures to 1 MPa, Geochimica et Cosmochimica Acta., 53 (1989) 1163-1170.

85. O. M. Suleimenov and R. E. Krupp, Solubility of hydrogen sulfide in pure water and in NaCl solutions, from 20 to 320^oC and at saturation pressures, Geochimica et Cosmochimica Acta, 58 (1994) 2433-2444.

86. O. M. Suleimenov and T. M. Seward, A spectrophotometric study of hydrogen sulfide ionization in aqueous solutions to 350^oC, Geochimica et Cosmochimica Acta, 61 (1997) 5187-5198.

87. H. A. Flaschka, A. J. Barnard, Jr. and P. E. Starrock, Quantitative Analytical Chemistry, 2nd ed., Willard Grant Press, Boston, MA, 1980.

88. D. A. Day and A. L. Underwood, Quantitative Analysis, 6th ed., Prentice-Hall, Englewood Cliffs, NJ, 1991.

89. T. A. Tumanova, K. P. Mischehenko, and I. E. Flis, Dissociation of hydrogen sulfide in aqueous solutions at different temperatures, Zh. Neorg. Khim., 2 (1957) 1990-1997.

90. H. L. Loy and D. M. Himmelblau, The first ionization constant of hydrogen sulfide in water, J. Phys. Chem., 65 (1961) 264-267.

91. A. Ringborn, Solubility of sulfides, Report to Anal. Sect. of IUPAC, 1953.

92. H. Kubli, Die dissociation von schwefelwas-serstoff, Helv. Chim. Acta, 29 (1946) 1962-1973.

93. Y. S. Su, K. L. Cheng, and Y. C. Jean, Amplified potentiometric determination of pK_{00}, pK_0, pK_1, and pK_2 of hydrogen sulfides with Ag_2S ISE, Talanta, 44 (1997) 1757-1763.

94. L. Bruner and J. Zawadzki, Uber die Gleichgewichte der schwefelwasserstoffallung der metalle, Z. Anorg. Chem., 65, 1909, 136.

95. A. Thiel and H. Gessner, Uber nickelsulfid and kobaltsulfid, Z. Anorg. Chem., 86, 1914, 1-57.

96. E. H. Swift and E. A. Butler, Quantitative measurements and chemical equilibrium, Freeman, 1972.

97. R. C. Weast, Handbook of Physics and Chemistry, 72nd ed., CRC Press, Boca Raton, FL, 1991.

98. A. J. Ellis and R. M. Golding, Spectrophotometric determination of acid dissociation constant of hydrogen sulfide, J. Chem. Soc. (1959) 127-130.

99. D. C. Harris, Quantitative Chemical Analysis, 4th ed., p. AP25, Freeman, New York, 1995.

100. J. R. Goates, M. B. Gordon, and N. D. Faux, Calculated values for the solubility product constants of metal sulfides, Journal of American Chemical Society, 74 (1952) 835-836.

101. R. L. Pecsok, L. Shields, T. Cains and I. G. McWilliam, Modern methods of chemical analysis, 2nd ed., Wiley, New York, 1968.

102. I. M. Kolthoff, E. B. Sandell, E. J. Meehan and S. Bruckenstein, Quantitative Chemical Analysis, 4th ed., Macmillan, London, 1969.

103. A. J. Ellis and W. Giggenbach, Hydrogen sulfide ionization and sulfur hydrolysis in high temperature solution, Geochim Cosmochim. Acta, 35 (1971) 247-260.

104. D. A. Skoog and D. M. West, Fundamental of Analytical Chemistry, 4th ed., Saunders, Philadelphia, PA, 1982.

105. N. Konopik and O. Leberl, Colorimetric pH determination in the range 10 to 15, IV. the second dissociation constant of hydrogen sulfide, Monatsh. Chem., 80 (1949) 781-787.

106. H. A. Pohl, Solubility of iron sulfides, Journal of Chemical Engineering Data, 7 (1962) 295-306.

107. T. R. Blackbarn, Equilibrium, Holt, Rinehart, and Winston, New York, 1969.

108. I. L. Khodakovskii, V. V. Zhogina, and B. N. Ryzenko, Dissociation constants of hydrosulphuric acid at elevated temperatures, Geokhimia, 7 (1965) 827-833.

109. M. B. Goldhaber and I. R. Kaplan, Apparent dissociation constants of hydrogen sulfide in chloride solutions, Mar. Chem., 3 (1975) 83-104.

110. R. H. Wright and O. Maass, The solubility of hydrogen sulfide in water from the vapour pressures of the solutions, Can. J. Res., 6 (1932) 94-101.

111. A. F. Kapustinskii, Solubility product and the solubility of metal sulfides in water, C. R. Acad. Sci., USSR, 28 (1940) 144-147.

112. W. M. Latimer, Oxidation Potentials, Prentice Hall, New York, 2nd ed., 1952.

113. J. A. Barbero, K. G. McCurdy, and P. R. Tremaine, Apparent molar heat capacities and volumes of aqueous hydrogen sulfide and sodium hydrogen sulfide near 25°C: the temperature dependence of H_2S ionization, Can. J. Chem., 60 (1982) 1872-1880.

114. F. J. Millero, The thermodynamics and kinetics of the hydrogen sulfide system in natural waters, Mar. Chem., 18 (1986) 121-147.

115. Y. K. Kharaka, E. H. Perkins, W. D. Gunter, J. D. Debral, and C. H. Bamford, Solmineq 88: a computer program for geochemical modeling of water rock interactions, Menlo Park, CA: Alberta Research Council, 1989.

116. R. J. Myers, The new low value for the second dissociation constant for H_2S, Journal of Chemical Education, 63 (1967) 687.

117. G. Yagil, The effect of ionic hydration on equilibria and rates in concentrated electrolyte solutions III. the H scale in concentrated hydroxide solutions, J. Phys. Chem., 71 (1967) 1034.

118. S. Licht, F. Forouzan, and K. Longo, Differential densometric analysis of equilibria in highly concentrated media: determination of the aqueous second acid dissociation constant of H_2S, Anal. Chem., 62 (1990) 1356-1360.

119. J. Knox, Zur Kenntnis der ionengbildung des schwefels und der komplexionen des quecksilber, Z. Elektrochem., 12 (1906) 477-481.

120. M. Widmer and G. Schwarzenbach, Die sauergrad des hydrogensulfidions, HS^-, Helv. Chim. Acta, 47 (1964) 266-271.

121. A. J. Ellis and N. B. Milestone, The ionization constants of hydrogen sulfide from 20 to 90^oC, Geochim. Cosmochim. Acta, 31 (1967) 615-620.

122. S. S. Muhammad and E. V. Sundarahm, The spectrophotometric determination of the dissociation constants of hydrogen sulfide, J. Aci. Ind. Res., sect. B, 20 (1961) 16-18.

123. G. Maronny, Constants de dissociation de I'hydrogen sulfure, Electrochim. Acta, 1 (1959) 58-69.

124. W. Giggenbach, Optical spectra of highly alkaline sulfide solutions and the second dissociation constant of hydrogen sulfide, Inorganic chemistry, 10 (1971) 1333-1338.

125. A. A. Migdisov, A. E. Williams-Jones, L. Z. Lakshtanov, and Y. V. Alekhin, Estimates of the second dissociation constant of H_2S from the surface sulfidation of crystalline sulfur, Geochimica et Cosmochimica Acta, 66 (2002) 1713-1725.

126. J. W. Morse, F. J. Millero, J. C. Cornwell, and D. Richard, The chemistry of the hydrogen sulfide and iron sulfide systems in natural waters, Earth Science Reviews, 24 (1987) 1-42.

127. L. G. Benning, R. T. Wilkin, and H. L. Barnes, Reaction pathways in the Fe-S below 100^oC, Chemical Geology, 167 (2000) 25-51.

128. K. J. Lee, A mechanistic modeling of CO_2 corrosion of mild steel in the presence of H_2S, PhD dissertation, Ohio University, 2004.

129. P. Marcus and E. Protopopoff, Potential-pH diagrams for adsorbed species, application to sulfur adsorbed on iron in water at 25^oC and 300^oC, J. Electrochemical Society, 137 (1990) 2709-2712.

130. B. Brown, K. J. Lee, and S. Nesic, Corrosion in multiphase flow containing small amount of H_2S, Corrosion/2003, Paper no. 03341, NACE International, Houston, Texas, 2003.

131. M. Schutze, Protective Oxide Scales and Their Breakdown, John Wiley & Sons, Chichester, 1997.

132. K-L J. Lee and S. Nesic, EIS investigation on the electrochemistry of CO_2/H_2S corrosion, paper no. 04728, NACE International, Houston, Texas, 2004.

133. M. Schulte and Michael Schutz, The role of scale stresses in the sulfidation of steels, Oxidation of Metals, 51 (1999) 55-77.

134. A. Dravnieks and C. H. Samans, Kinetics of reaction of steel with hydrogen sulfide/hydrogen mixtures, J. Electrochemical Society, 105 (1958) 183-191.

135. D. N. Tsipas, H. Noguera, and J. Rus, Corrosion behavior of boronized low carbon steel, Materials Chemistry and Physics, 18 (1987) 295-303.

136. B. Brown, Srdjan Nesic and Shilpha Reddy Parakala, CO_2 corrosion in the presence of trace amounts of H_2S, paper no. 04736, NACE International, Houston, Texas, 2004.

137. M. Schutze, Protective Oxide Scales and Their Breakdown, John Wiley & Sons, Chichester, 1997.

138. B. Brown, H_2S/CO_2 corrosion in multiphase flow, Ohio University Advisory Board Meeting Report, Internal report to be published, 2006.

139. S. Nesic, B. F. M. Pots, J. Postlethwaite, and N. Thevenot, Superposition of diffusion and chemical reaction controlled limiting currents – application to CO_2 corrosion, J. Corrosion Science and Engineering, ISSN, 1466-8858, 1995.

Appendix: Experimental techniques

Weight change method

The weight change method was developed as a reliable method to obtain both the corrosion rate of the steel and the retention rate of the scale. The corrosion rate by weight change method is determined as follows:

$$CR = \frac{m_1 - m_3}{MW_{Fe} \times t \times S} \tag{79}$$

$$SRR = \frac{m_2 - m_3}{MW_{FeCO_3 \, or \, FeS} \times t \times S} \tag{80}$$

Where CR = corrosion rate, in mol/(m^{2}h),

SRR = scale retention rate, in mol/(m^{2}h),

m_1 = the weight of coupon prior to running experiments, in g,

m_2 = the weight of coupon which has scale on it after the experiments, in g,

m_3 = the weight of coupon after removing the scale, in g,

MW_{Fe} = the molecular weight of iron atom, in g/mol,

$MW_{FeCO_3 \, or \, FeS}$ = the molecular weight of iron carbonate or iron sulfide, in g/mol,

t = the exposed time, in hour,

S = the exposed coupon surface area, in m^2.

Corrosion rate can also be obtained by using the following equation:

$$\begin{aligned} CR &= \frac{m_1 - m_3}{MW_{Fe} \times t \times S} \quad \left(\frac{mol}{m^2 h} \right) \\ &= \frac{m_1 - m_3}{MW_{Fe} \times t \times S} \times \frac{365 \times 24 \times MW_{Fe}}{\rho} \quad (mm/year) \end{aligned} \tag{81}$$

Where ρ = density of the coupon in kg/m^3.

Electrochemical methods

Linear polarization method was used to measure the corrosion rate of the steel. Potentiodynamic sweep was used to investigate the mechanism of H_2S corrosion. These two techniques are discussed in detail in Lee's dissertation[128].

The linear polarization method is based on the electrochemical theory and the corrosion current can be obtained using the following Equation (82).

$$i_{corr} = \frac{\beta_a \beta_c}{2.303(\beta_a + \beta_c)} \frac{di_{app}}{dE} \tag{82}$$

where i_{app} is the applied current density, E is the applied voltage, β_a is the anodic tafel slope, and β_c is the cathodic tafel slope. The corrosion rate can be obtained by converting the corrosion current density (i_{corr}) to the corrosion rate using Equation (83).

$$Corrosion\ rate\ (mm/year) = 1.16 i_{corr} \tag{83}$$

where i_{corr} is the current density in A/m^2.

The potentiodynamic sweep technique can determine whether the corrosion process is controlled by charge transfer, mass transfer, or chemical reaction; and further determine the exchange current density, tafel slopes and chemical reaction rate. In this project, the cathodic sweep scanned from the corrosion potential to approximately -650 mV below the corrosion potential and then the anodic sweep scanned from the corrosion potential to 200 mV with a sweep rate of 0.2 mV/s.

Gas analysis method

MKS Type 1179A and 2179A mass-flow controllers were used to obtain a certain H_2S concentration. Piston-type H_2S detector was used to measure H_2S concentration.

Solution analysis method

The scale retention rate can obtained through the indirect ferrous ions concentration measurement by using the following equation.

$$SRR = \frac{\Delta m_{Fe}(in\ the\ solution)}{MW_{Fe} \times t \times S} \tag{84}$$

where m_1 = the weight of Fe lost in the solution, in g. The concentration of ferrous ions concentration (Fe^{2+}) in the solution is measured by using a spectrophotometer (Turner SP-870).

Surface analysis method

Optical Microscope, Scanning Electron Microscopy/Energy Dispersive Spectrometry (SEM/EDS), X-ray Diffraction methodology (XRD), X-ray Photoelectron Spectroscopy (XPS), and Electron Microprobe Analysis (EMPA) were used to do surface analysis. Surface analysis is aiming at:

1. Evaluating the properties and the thickness of the corrosion products,
2. Defining the composition of the corrosion products,
3. Evaluating the ratio of iron carbonate and iron sulfide on the specimens.

Morphology

Scanning Electron Microscopy/Energy Dispersive Spectrometry (SEM/EDS) was employed to study the morphology of the scale on the steel surface.

Cross section

For the cross section analyses, cold mounting method was used to mount the samples. Both the samples and epoxy are placed in a vacuum to make sure there is no air on the sample surface. The samples are mounted by the epoxy in the vacuum and then stored in the air for one day in order to dry the epoxy. The cross sections of the samples are polished first with 220 grit sand paper and then with 9 μm, 3 μm, and 1 μm diamond solution for a fine finish.

Composition

The composition of the corrosion product film was examined by using four tools, Energy Dispersive Spectrometry (EDS), X-ray Diffraction methodology (XRD), X-ray Photoelectron Spectroscopy (XPS), and Electron Microprobe Analysis (EMPA).

XRD data of the samples were collected on a SIEMENS D5000 automated diffractometers over the angular range 2 to 72° (2θ) in 0.02° steps. The XRD system operates in the theta: theta geometry, uses Cu (Kα) radiation, 1.5405981 Å, and is equipped with a diffracted-beam graphite monochromator, a scintillation detector and solid state counting electronics. The generator voltage and current settings were 40kV and 30mA, respectively. The following slit arrangement was used for data collection: three 1° beam apertures, one 0.05° detector aperture, and one 0.15° diffracted-beam aperture. The diffraction spectra were processed using the JADE version 6.5 XRD processing software. Identification of the chemical or mineral compounds was performed using the search/match option in JADE.

A PHI-5700-2 X-ray Photoelectron Spectrometer (XPS) was used to determine the bonding state of sulphur to iron in the deposition layer. The tube was lightly doused with propanol prior to being loaded in the ultrahigh vacuum system to prevent outgassing of grease associated with handling (fingerprints). The sample was examined using a broad, low-energy resolution spectral acquisition (survey) to reveal surface elemental composition. The XPS technique only examines the first few atomic layers (~2 nm). The sample was also examined using a high-energy resolution spectral acquisition (multiplex) to determine chemical information about specific elements. The tube was etched using an Ar ion beam. After ion etching, survey and multiplex spectra were again recorded. Finally, spectra were collected during ion etching in a new area, which provided a depth profile.

A CAMECA SX-51 electron probe micro-analyzer (EPMA) equipped with four spectrometers were used to analyze the chemical composition of the deposited Fe-S film. Pure low-carbon steel and $SrSO_4$ were used as Fe and S standards respectively. The acceleration voltage used is 20 kV with a 20 nA beam current with 20 seconds counting time. Fe Kα and S Kα X-ray were used in the measurement.